UNIVERSITÉ DE NEUCHÂTEL

2019

INCREASING THE SIZE OF METALLA-ASSEMBLIES TO TARGET THE EPR-EFFECT OF TUMORS AND SOLID CANCERS

Thèse présentée à la Faculté de Science,
pour l'obtention du grade de Docteur és Science par

VIDYA MANNANCHERRIL

Titulaire d'un Master en Chimie de l'Université de Bâle

Membres du jury:

Prof. Dr. Bruno THERRIEN	Directeur de thèse, Université de Neuchâtel
Prof. Dr. Robert DESCHENAUX	Expert interne, Université de Neuchâtel
Prof. Dr. Catherine HOUSECROFT	Experte externe, Universität Basel

Faculté de Science — Institut de Chimie

Soutenue le 29 avril 2019

UNIVERSITÉ DE NEUCHÂTEL

Faculté des Sciences
Secrétariat-décanat de Faculté
Rue Emile-Argand 11
2000 Neuchâtel – Suisse
Tél : + 41 (0)32 718 21 00
E-mail : secretariat.sciences@unine.ch

IMPRIMATUR POUR THESE DE DOCTORAT

La Faculté des sciences de l'Université de Neuchâtel autorise l'impression de la présente thèse soutenue par

Madame Vidya MANNANCHERRIL

Titre:

"Increasing the Size of Metalla-Assemblies to Target the EPR-Effect of Tumors and Solid Cancers"

sur le rapport des membres du jury composé comme suit:

- Prof. associé Bruno Therrien, directeur de thèse, UniNE
- Prof. Robert Deschenaux, UniNE
- Prof. Catherine Housecroft, Université de Bâle

Neuchâtel, le 10 mai 2019

Le Doyen, Prof. P. Felber

P. Fel

Pour Christophe
et pour ma famille

A scientist in his laboratory is not a mere technician: he is also a child confronting natural phenomena that impress him as though they were fairy tales.

Marie Curie (1867 - 1934)

ACKNOWLEDGEMENT

I would like to express my gratitude to the following people, without whom this thesis would not have been possible:

PROF. BRUNO THERRIEN for giving me the opportunity to do my Ph.D. thesis in your research group and for your support and guidance.

PROF. CATHERINE HOUSECROFT, my former professor in inorganic chemistry from the University of Basel, for accepting to evaluate my thesis and for being my examiner as a chemistry expert.

PROF. ROBERT DESCHENAUX for the co-examination of my thesis and for allowing me to utilize your machines for my analysis.

PROF. PAUL DYSON and his Ph.D. student LUCINDA KATE BATCHELOR from the EPFL for the biological analysis of my metalla-assemblies.

PROF. STEPHAN VON REUSS for your support in all areas.

PROF. EDITH JOSEPH for allowing me to utilize the IR machine for my analysis.

DR. DIEGO CARNEVALE and especially DR. SYLVAIN SUTOUR for your NMR support.

DR. FREDY NYDEGGER and DR. ALBERT RUGGI from the University of Fribourg for the ESI-MS measurements.

The team responsible for the elemental analysis at the ETH Zürich.

DR AURÉLIEN BORNET from EPFL, for the special NMR tests.

Mme LUCIENNE BAZZONI-BOICHAT and DR. JULIETA GRADNINARU for the preparation of the solutions we needed for TP.

HABIB ABDELKHALEK and MATTHIEU BUECHE for your work in La Centrale d'achats produits chimiques (CAPC).

MOHAMED BILLA and MASSIMO DANIELE for your kindness and help.

The former group members: DR. BING SUN, DR. DAVID STIBAL, DR. THOMAS CHEMINEL, DR. BALAZS BREM, MINGHUI YUAN and JOHANNA BURRI for welcoming me into the group and for helping me to get started.

DR. FAN ZHANG, my lab mate, for all the discussions about chemistry and for sharing your knowledge with me, MARIE GASCHARD, who started the Ph.D. thesis on the same day like me, for preparing TP, for helping me out with French whenever I needed it and DR. CRISTINA ALVARIÑO BOUZA, who started a few months after me as a Post-Doc. Thank you all, for the good times we had in Neuchâtel and especially for the great time in Barcelona and Tarragona.

DANY MARQUES, my apprentice who worked with me during my first year. Thank you for your effort.

CYRIL HELBLING and PIERRE BENA, who did their traveaux de maturité with me. You both did a great job and showed great interest and I am proud of you that you have chosen a scientific study subject.

LEONARDO PALAFERRI, MANUEL GALLARDO VILLAGRAN and CHRYSANTHI PAPADIMOU, the new Ph.D. students in our group, DIOGO DA SILVA BORGES and BASTIAN GUERRY the apprentices that worked with Marie in our labs and WASSILA ABOURA and FARZANEH NEHZAT, who did an internship during a few months in our group, it was nice to meet you and have you around.

HOANG-GIAU LE, with you I always had a good time. Whenever you were around, there were a lot of reasons to laugh, nevertheless you have a great knowledge about chemistry and never hesitated to help.

ROCÌO DE LAS NIEVES RIVERA SÁNCHEZ, we shared a lot of laughter in and outside the institute and you were my go-to friend here in Neuchâtel and I am very grateful for your friendship and the good times we had together.

DR. SYLVAIN ROGER AIMÉ SUTOUR, I think every Ph.D. student here in Neuchâtel who uses the NMR is very grateful for you. But besides your work in the institute as NMR specialist, you became also a very good friend to me.

AURÉLIEN SÉBASTIEN PIERRE BILLOT, you know a lot about chemistry and you were always ready to help me with my chemistry problems. Even though you are so many years younger than me, we get each other and you also, became a very good friend to me.

CÉLIA BERGAME and AHMED YASSINE CHADI, you both are totally crazy, but nevertheless very kind people. It was great to have at least one person to speak German to and another person to be weird with.

MAGDALENA ALBELDA BERENGUER and MATHILDE MONACHON, thank you for the good times during lunch and for organizing the group meetings, the Halloween party, the Christmas party the Secret Santa and so much more.

DR. SIVA BANDI, LIDIA MATHYS and NAÏMA GUTKNECHT, even though we did not have the time to know each other better, I would like to thank you for being part of my journey in Neuchâtel.

PATRICK FALLET and JOHNNY WING MOREIRA, I will never forget new year's eve 2018 and I will keep those beautiful pictures for ever. Thank you for this awesome memory.

My friends from the University of Basel RAHEL HINKELMANN and KATHRIN HÖNERLAGE who always supported me mentally when I needed it.

A big thanks goes to my parents DIAS and MATHEW MANNANCHERRIL, without whom none of this would have been possible.

My brother SOOREJ, my sister-in-law DEEPA and their wonderful daughters SOPHIYA and MIYA for supporting me and for believing in me.

Last but not least I would like to thank my fiancé DR. CHRISTOPHE ALEXANDRE DAEPPEN. All these years, you have been my strongest support, not only in chemistry but in every aspect of my life. You were there when I felt weak and you were there when I felt strong. The only reason I felt strong was because of you! Thank you for everything. I love you!

ABSTRACT

Cancer, a malignant disease, is one of the leading causes of mortality and morbidity among humans. However, selective targeting of cancerous tissue remains challenging. The enhanced permeability and retention effect (EPR-effect), a naturally occurring phenomenon in solid cancerous tissue, is a suitable treatment pathway to selectively target cancerous tissues, whereas healthy tissue remains untouched, and therefore side effects are reduced. This effect is observed for large and heavy molecular structures. Ruthenium has shown to possess anti-cancer activity, and is able to form macromolecular assemblies that could potentially exploit the EPR-effect and selectively accumulate on the tumor site to fight the disease locally. The goal of this thesis is to prepare macromolecular and multi-nuclear arene ruthenium metalla-assemblies to target the EPR-effect.

Le cancer, une maladie maligne, est l'une des principales causes de mortalité et de morbidité chez l'homme. Cependant, le ciblage sélectif des tissus cancéreux reste un défi. L'effet de perméabilité et de rétention accrue (effet EPR) est un phénomène naturel dans les tissus cancéreux solides qui est observé pour les structures moléculaires grandes et lourdes. Il constitue donc une voie de traitement appropriée pour cibler de manière sélective les tissus cancéreux, laissant intacts les tissus sains et réduisant les effets secondaires. Le ruthénium possède une activité anticancéreuse et est capable de former des assemblages macromoléculaires susceptibles d'exploiter l'effet EPR et de s'accumuler de manière sélective sur le site de la tumeur pour lutter localement contre la maladie. Le but de cette thèse est de préparer des métalla-assemblages

KEYWORDS

EPR-effect
Tumors
Drug delivery
Passive tumor targeting
Ruthenium complexes
Nanomedicine
Supramolecular chemistry
Anti-cancer activity

MOTS-CLÉS

Effet EPR
Tumeurs
Administration de médicaments
Ciblage tumoral passif
Complexes de Ruthénium
Nano-médecine
Chimie Supramoléculaire
Activité anticancéreuse

ABBREVIATIONS

4-tpt	2,4,6-tri(pyridin-4-yl)-1,3,5-triazine
6-MP	6-mercaptopurine
Å	ångström
A2780	ovarian cancer cell line
A2780cisR	cisplatin resistant ovarian cancer cell line
Akt	AKT8 virus oncogene cellular homolog
ALL	acute lymphoblastic leukaemia
aq.	aqueous
BCR-ABL	breakpoint cluster region - abelson tyrosine kinase
BuOH	butanol
CAN	ceric ammonium nitrate
cisplatin	*cis*-diamminendichloridoplatinum(II)
CML	chronic myeloid leukaemia
DCC	*N,N'*-dicyclohexylcarbodiimide
DCM	dichloromethane
DDQ	2,3-dichloro-5,6-dicyano-*p*-benzoquinone
dhbq	dihydroxybenzoquinone
DIPEA	*N,N*-diisopropylethylamine
DMAP	4-dimethylaminopyridine
DMF	dimethyl formamide
DMSO	dimethylsulfoxide
DNA	deoxyribonucleic acid
DOSY	diffusion-ordered spectroscopy
DPTS	4-(dimethylamino)pyridinium *p*-toluenesulfonate
dsmz	Deutsche Sammlung von Mikroorganismen und Zellkulturen
DTPA	diethylene triamine pentaacetic acid
EA	elemental analysis
EDHF	endothelium derived hyperpolarizing factor
EGFR	epidermal growth factor receptor
EMA	European Medicines Agency
en	ethylenediamine

EPFL	École Polytechnique Fédéral de Lausanne
EPR	enhanced permeability and retention
equiv	equivalent
ERK	extracellular signaling-regulated kinase
ESI-MS	electrospray ionization - mass spectrometry
ET-1	endothelin
Et_2O	diethyl ether
EtOAc	ethyl acetate
EtOH	ethanol
FDA	Food and Drug Administration
h	hour
HATU	1-[bis(dimethylamino)methylene]-1*H*-1,2,3-triazolo[4,5-*b*]pyridinium 3-oxid hexafluorophosphate
HD	hydrodynamic diameter
HEK	human embryonic kidney cell line
Hz	hertz [s^{-1}]
IC_{50}	drug concentration necessary to inhibit 50% of cell survival
ICG	indocyanine green
IGF	insuline-like growth factor
IL	interleukin
*i*Pr	isopropyl
*iPr*OH	isopropanol
IR	infrared spectroscopy
IUPAC	international union of pure and applied chemistry
Jak	Janus-family tyrosine kinase
kDa	kilodalton
KIT	tyrosine kinase
M	molarity [$mol \cdot L^{-1}$]
MAPK	mitogen-activated protein kinase
MeCN	acetonitrile
MeOH	methanol
MsCl	methanesulfonyl chloride

mTOR	mammalian target of rapamycin
MTT assay	3-(4,5-dimethyl-2-thiazolyl)-2,5-diphenyl-2*H*-tetrazolium bromide assay
NBS	*N*-bromosuccinimide
NCI	National Cancer Institute
NCS	neocarzinostatin
NEt_3	triethylamine
NF-kB	nuclear factor-kappa B
NMR	nuclear magnetic resonance
NO	nitric oxide
NSCLC	non-small cell lung cancer
$Pd(II)(dppf)Cl_2$	[1,1'-bis(diphenylphosphino)ferrocene] dichloropalladium(II)
PDGFRβ	platelet derived growth factor receptor-β
PDT	photodynamic therapy
PEG	polyethylene glycol
PGI_2	prostacyclin
PI3K	phosphoinositide 3-kinase
pin	pinacol
POMP	purinethol, oncovin, methotrexate and prednisone
ppm	parts per million
PTA	1,3,5-triaza-7-phosphaadamantane
quant.	quantitative
ROESY	rotating frame overhause effect spectroscopy
RT	room temperature
sat.	saturated
SBTI	soybean trypsin inhibitor
SC	selectivity coefficient
SMA	poly(styrene-co-maleic acid anhydride)
SMANCS	styrene maleic acid conjugated NCS
SOD	superoxide dismutase
Stat	signal transducer and activator of transcription
TGF	transforming growth factor

THF	tetrahydrofuran
TLC	thin layer chromatography
tpp	5,10,15,20-tetra(pyridin-4-yl)porphyrin
tris-pvb	1,3,5-tris((*E*)-2-(pyridin-4-yl)vinyl)benzene
TXA_2	thromboxane
UV-VIS	ultraviolet-visible spectroscopy
WHO	World Health Organization
Wnt	wingless/integral
XPhosPdG2	2nd generation XPhos precatalyst, chloro(2-docyclohexylphospino-2',4',6'-triisopropyl-1,1'-biphenyl)[2-(2'-amino-1,1'-biphenyl)]palladium(II)
δ	chemical shift [ppm]
η^x	hapticity: × is the number of atoms of the ligand bound to the metal center
μ_x	bridging ligand: × is number of metal atoms bridged to the ligand

TABLE OF CONTENT

1. INTRODUCTION

Cancers are among the leading causes for mortality worldwide. It describes a group of diseases that are able to affect any part of the body and spread and invade into healthy tissues or organs. Other terms for cancers are malignant tumors. Any abnormal proliferation of cells is referred to as tumor which may be distinguished between malignant and benign. Benign tumors remain in their original location. They do not spread nor invade to other body parts and can be removed by surgery. However, malignant tumors are able to spread beyond their usual boundaries and throughout the whole body *via* the circulatory and lymphatic systems. Only malignant tumors are referred to as cancers. With their ability to metastasize, they are often resistant to local treatments like surgery which makes them dangerous and life-threatening.[1,2]

Approximately 14.1 million new cancer cases and 8.2 million cancer related deaths were reported in 2012 and these numbers are expected to rise by around 70% over the next twenty years. In 2012, 32.6 million cancer patients over the age of 15 were estimated who had had a cancer diagnosed in the previous five years. In 2015, 8.8 million cancer related deaths were reported, which makes a sixth of all deaths globally.[1] In 2018, the number of death rose to 9.6 million.[3] Therefore, there is an urgent need for cancer research to cure cancer.

To date there are more than a hundred different types of cancers known. They can alternate significantly in their behavior and their respond to treatments. All tumors are classified according to their origin. Most cancers can be categorized into three main groups: carcinomas, sarcomas and leukaemias/lymphomas. Carcinomas, which are malignancies of epithelial cells, represent with approximately 90% the largest group of human cancers. Sarcomas are with around 2% rare in humans. They represent solid tumors of connective tissues, such as muscles, bones, cartilages and fibrous tissues. Leukaemias and lymphomas stand for 8% of human cancers. They originate from blood-forming cells or from cells of the immune system, respectively.[2] In 2018 the most common cancers were: lung (18.3%), colorectal (9.0%), stomach (8.2%), liver (8.1%) and breast (6.5%).[1] For an effective cancer treatment a correct diagnosis is necessary because every type of cancer requires a specific treatment. Some cancers have high cure rates if detected at an early stage. Otherwise the primary goal is to prolong life of patients and to improve their quality of life.[1]

1.1. CANCER DEVELOPMENT AND PROGRESSION

Cancers arise from one single mutated cell that is transformed to a tumor cell in a process containing multiple steps involving mutation and selection for those cells with capacity for proliferation, survival, invasion and metastasis.[2,4] Characteristic for cancer cells are their abnormal rapid growth and proliferation, owning to the excessive angiogenesis, which supports nutrition and oxygen uptake. They divide uncontrolled and invade into healthy tissues and organs and eventually they spread throughout the whole body. Figure 1 shows the oversimplified illustration of cancer progression. Before cancer cells are formed, a hyperplasia is observed, where the number of cells in certain organs increase abnormally. Those cells may or may not become cancers.[5] The formation of carcinoma *in situ* is also called stage 0 disease. It describes a group of abnormal cells that are only found in one place and do not spread. Also these cells may or may not become cancers.[6] In case of cancer development, angiogenesis will lead to cell growth and cell proliferation and the carcinoma *in situ* will turn into an invasive carcinoma, that spreads beyond its place of origin and grows into its surroundings.[7] Cancer cell migration, intravasation of cancer cells into the circulatory system, dissemination of a cancer cell to a distant organ and extravasation of those cells out of the blood stream lead to the development of metastasis.[8,9] Dormant tumor cell is the term for cancer cells that lack of the ability for proliferation until the conditions are favorable for successful proliferation and only then macro-metastases are formed.[10,11]

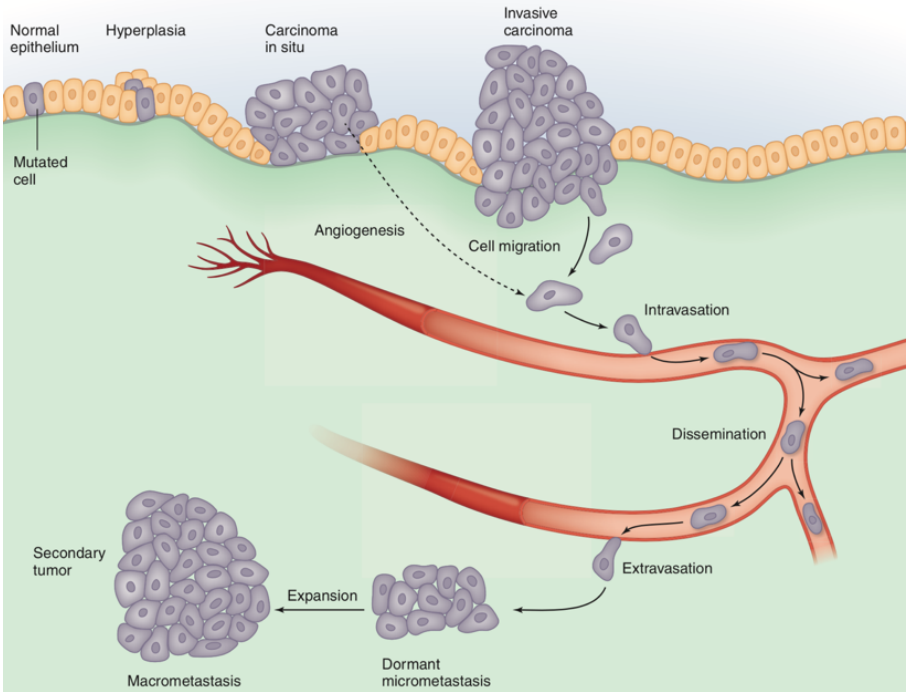

Figure 1: Cancer progression.[12]

Reasons for cancer cells to develop can be diverse and are a result of the interaction between genetics and external carcinogens. External carcinogens may be of physical nature such as UV light and radiation, or of chemical nature like tobacco smoke, drinking water/food contaminants and air pollution or of biological nature such as infections from viruses, bacteria and parasites. Some carcinogens act by damaging DNA and inducing mutations. These carcinogens are known as inducing agents, since the induction of mutations in genes is assumed to be the initial event leading to cancer development. Compounds that contribute to tumor cell proliferation rather than inducing mutations are referred to as tumor promoters. Examples for molecular tumor promoters are phorbol esters and their derivatives which are able to stimulate tumor cell proliferation, phenobarbital and 2,3,7,8-tetrachlorodibenzo-*p*-dioxin (TCDD) are shown in figure 2.[13–15]

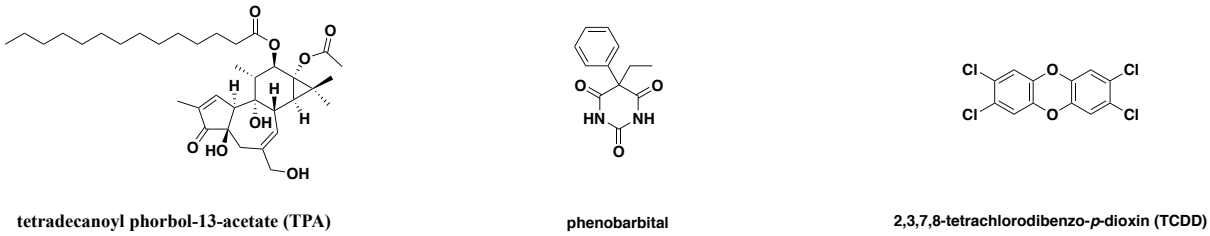

Figure 2: Structures of tumor promoters tetradecanoyl phorbol-13-acetate (TPA), phenobarbital, 2,3,7,8-tetrachlorodibenzo-p-dioxin (TCDD).[13,15]

However, the development of cancer cannot be affiliated to one single cause, but many factors are playing a part. The risk of cancer can be reduced by regular physical activity and avoiding tobacco, alcohol and unhealthy food with low fruit and vegetable intake.[1] Cancer cell development is connected to signal transduction between biomolecules within a cell. Not only cancer cells, but also healthy cells communicate *via* those signals, in order to know whether they have to grow, divide, survive, or undergo apoptosis. All cellular processes within a body are controlled and managed by signal transduction in signaling pathways. They control and coordinate cell growth of all eukaryotic cells with the supply of nutrients in their environment. Signaling pathways are complex networks, where signals are transducted between many biomolecules to regulate cellular processes, such as cell survival and cell migration. Figure 3 shows a very simplified illustration of such a complex network within a cell, where proteins and biomolecules and their upstream and downstream targets are interlinked. Such signaling pathways are composed of numerous components which interact with each other. Mutations in components of those complex signaling networks, caused for example by tumor inducing agents might have severe consequences, as wrong signals are sent and received. This might cause activation or inhibition of undesired components in the signaling pathway, leading to undesired

cell responses. Such undesired cell responses might lead to the survival, migration and proliferation of undesired cells. Mutations of signaling pathways that control cellular processes, such as PI3K (phosphoinositide 3-kinase), Ras (*Rat sarcoma*) and their downstream factors are observed in many human cancers.[12,16,17] In figure 3 a cell is depicted with several signaling pathways and the genes that are known to be functionally altered in solid cancers are highlighted in red. Deregulated processes involve growth factor pathways: EGFR (epidermal growth factor receptors), TGF (transforming growth factor), IGF (insuline-like growth factor) and further signaling pathways: Wnt pathways (wingless/integrated)[18], Hedgehog pathway, Akt/mTOR (mammalian target of rapamycin)[19], Jak/Stat pathway (Janus-family tyrosine kinase/signal transducer and activator of transcription), MAPK pathway (mitogen-activated protein kinase), PI3K pathway (phosphoinositide 3-kinase), ERK pathway (extracellular signaling-regulated kinase), NF-kB (nuclear factor-kappa B) and IL pathway (interleukin). All listed pathways can be regarded as targets for cancer research.

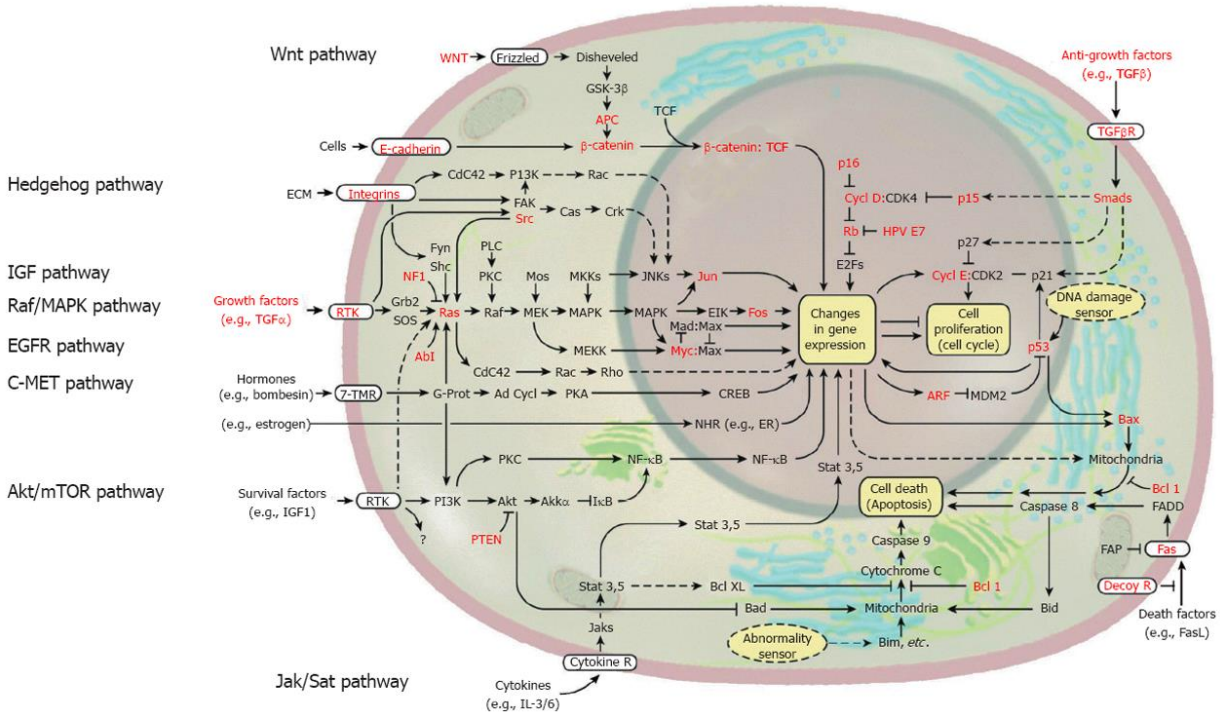

Figure 3: Signal transduction in solid cancer cells. Genes that are known to be functionally altered are highlighted in red.[20]

Once cancer cells have developed they do not respond appropriately to the signals arising from those networks, which may lead to over-proliferation and migration of those cells. If propagation of these cells is not kept under control, this might result in death.[1,2]

1.2. CANCER THERAPIES

Every cancer type needs a dedicated treatment. The type of treatment depends on the type of cancer and on its state of development. Mostly, there will be a combination of different treatment types.[21] The different types of treatments are:

- Surgery, where the tumor can be fully or partly removed by excise.[22,23] There are methods of surgery that do not involve cuts: cryosurgery[24], lasers[25], hyperthermia[26] and photodynamic therapy (PDT).[27]
- Radiation therapy with high doses of radiation to destroy cancer cells.[28]
- Immunotherapy, since cancers are not recognized as a threat by the immune system certain immunotherapies boost the immune system, others label the cancer cells so the immune system is able to find and destroy them.[29]
- Targeted therapy, where biomolecules and proteins that are responsible or involved in cancer development, growth and proliferation of cancer cells are targeted to inhibit their function using small molecule drugs or monoclonal antibodies.[30,31]
- Hormone therapy is a type of targeted therapy, which is used to treat tumors that need hormones to grow. Two types of hormone therapy are applied: one type prevents the body from making them, and the other type prevents the hormones from acting on the cells.[32]
- Stem cell transplant can be administered to fight certain types of cancers, like multiple myeloma and some types of leukaemia. The treatment works *via* the graft-versus-tumor effect, which occurs when white blood cells from the donor (graft) attack cancer cells in the patients' body (tumor).[33]
- Precision medicine, where the treatment for each patient is specific depending on their tumors' genetic changes. Same cancer types can act and develop differently depending on the patients' genetics. Furthermore, patients can respond differently to the same treatment. Therefore, a biopsy is needed for the further cancer treatment evaluation and application.[34]
- Chemotherapy, where cells that grow and divide quickly are attacked by chemical drugs to inhibit their growth. Numerous and severe side effects are often observed, because not only cancer cells are attacked, but also healthy cells that grow and divide quickly. Chemotherapy is generally used in combination with other treatments and applied to different kind of cancers.[35]

1.3. THE MODERN ERA OF CHEMOTHERAPY

Origins of cancer treatments are found in ancient documents such as the Ebers papyrus, the Edwin Smith papyrus and in the Ramayana, to only name very few examples.[36] Nevertheless, most treatments were ineffective until the 19th century. At the starting point cancer treatment was dominated by removal by surgery or radiology. However, due to formation of metastases in some cancer types, surgery or radiology were not always suitable and hence, small molecule drugs came into the focus of researchers.

The beginning of the modern era of chemotherapy was in the 1940s with the discovery of nitrogen mustard and antifolate drugs (figure 4).[37] In 1942, Goodman and Gilman proposed that nitrogen mustard might destroy lymphoid tumor, according to examinations of soldiers dying of exposure to sulfur mustard gas during the first World War, as the victims had profound lymphoid hypoplasia and myelosuppression.[38] Shortly after the Second World War, in 1950 Sydney Farber examined the effects of folic acid and its synthetic analogues on patients with leukaemia. Antifolates were able to suppress proliferation of malignant cells, and therefore became the first compounds to successfully induce remission in children with acute lymphoblastic leukaemia (ALL).[37] Furthermore, in 1958, Hertz and Li discovered that methotrexate, an antifolate analogue, was the first compound to cure a solid cancer.[39]

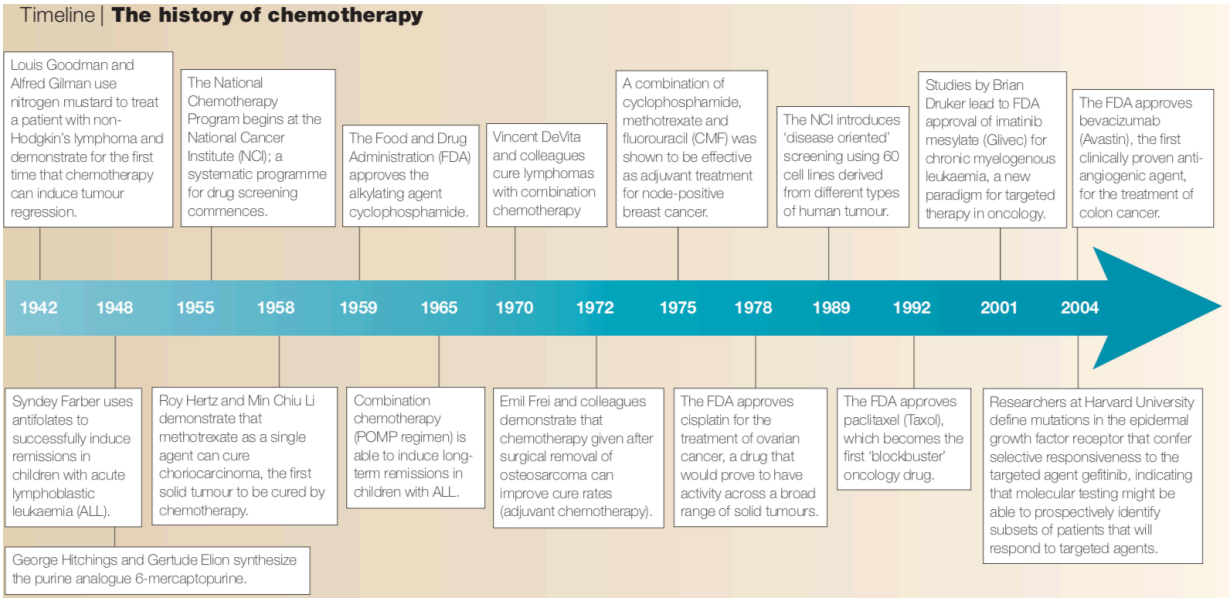

Figure 4: The history of chemotherapy.[37]

In the following years, other interesting properties, activities and the mode of action of antifolates were investigated by other researchers.[40–43] Modern chemotherapy began with the development of purine analogues such as 6-mercaptopurine (6-MP) and the discovery of *Vinca* alkaloids which were able to inhibit the growth of tumor cells and to block tumor cell proliferation (figure 5). Most interestingly in this era, POMP (purinethol, oncovin, methotrexate and prednisone) was realized, which is a combination of methotrexate, vincristine (*Vinca* alkaloid), 6-MP and prednisone, which was able to induce long-term remission in children with ALL.[44–48]

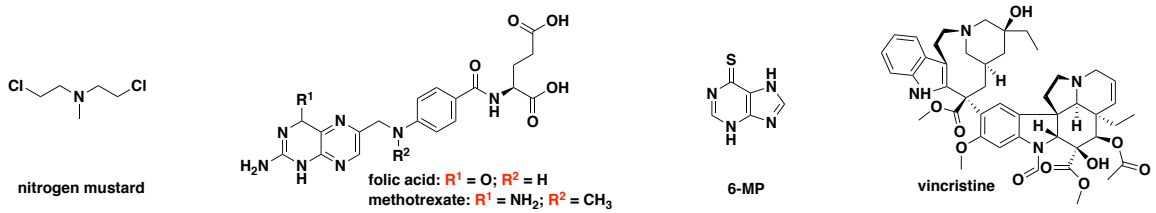

Figure 5: Beginning of the modern era of chemotherapy.

Systematic drug screening began at the National Cancer Institute (NCI) in 1955. Each year 15'000 new drugs and natural products were screened.[49] The years from 1960 - 1970 can be regarded as the golden era of chemotherapy with the discovery of cisplatin, a cell division inhibitor in *Escherichia coli*, in 1965 by Rosenberg.[50] Subsequently a derivative of cisplatin named carboplatin was developed with a broad antitumor activity and less nephrotoxicity.[51] Meanwhile, other organometallics were developed and their behavior is later discussed in this thesis. Around the same time, nitrosoureas were found to alkylate and crosslink DNA at the O6 position of guanine, which was effective against malignant gliomas.[52] This finding was interesting, since cisplatin crosslinks DNA at the N7 position of guanine (scheme 2.[53] This demonstrated that totally different compounds can undergo a similar mode of action. In figure 6 the structure of guanine is depicted with the respective positions.

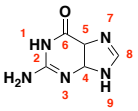

Figure 6: Structure of nucleobase guanine with the respective positions.

Despite the success of anticancer drug development, researchers repeatedly encountered problems due to the acute and long-term toxicities of chemotherapies, which affected every organs of the body. These drawbacks were accepted as the price for controlling a fatal disease.[37] In the 1980s, the development of cancer research stagnated due to long-term trials resulting in minor gains against tumors. Additionally, mouse models only poorly predicted the outcome of

clinical trials. Thus, screening of numerous drug analogues, random chemicals and natural products did not show the expected results against tumors and the costs exploded. Therefore, the NCI started to use human tumor xenografts in mice, covering a broad range of tumor types with 60 cell lines.[37] However, success did not come, since large screening did not lead to the identification of any novel anticancer agent. Despite the unsuccessfulness of new anticancer drug development, there were significant improvements in screening methodology, suggesting a need to change strategies.

Investigations on molecular and biological mechanisms of cell biology and cancers have led to the identification of new signaling networks that regulate and control cellular processes, like proliferation and survival. Many mutations and alterations were found in the signaling networks of cancer cells. Here began the era of targeted therapy. Researchers began the attempt to repair those mutations by targeting affected biomolecules and proteins within cells.[54] Research in the area of targeted therapy in connection with cell biology grew rapidly resulting in the identification of a large number of target molecules, which transformed cancer cell development from a low-budget, government-supported research to a multi-billion dollar industry.[37] Numerous inhibitors of specific targets were identified due to new technology and thousands of potential drugs were designed by means of combinatorial chemistry. Their properties concerning specificity and bioavailability were then optimized using computer simulations.[55] New standards for drug administration were established in respect to drug compatibility, metabolic stability, well-absorption after oral administration and favorable toxicity profiles at biologically effective doses.[37] The development of imatinib mesylate was a significant milestone in the research of targeted cancer therapy. Imatinib mesylate is an inhibitor of the kinase BCR-ABL, a fusion gene responsible for the development of chronic myeloid leukaemia (CML).[56] Moreover, it inhibits the KIT tyrosine kinase and platelet derived growth factor receptor-β (PDGFRβ) tyrosine kinase which is effective against gastrointestinal stromal tumors and other neoplasms.[57] Gefitinib, an inhibitor of the epidermal growth factor receptor (EGFR) was able to cause remissions in 10-15% of patients with non-small cell lung cancer (NSCLC).[58] The structure of imatinib and gefitinib are shown in figure 7.

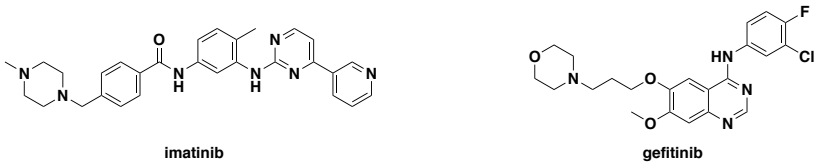

Figure 7: Targeted cancer drugs imatinib and gefitinib.

Despite successes, there were also disappointments in targeted therapy research, and it still remains a challenge to create the perfect anti-cancer drug due to many reasons. Animal models can only poorly simulate the effects of a drug in humans because of their more rapid metabolism, greater tolerance to side effects and differences in protein binding. Even with the use of human xenografts in mice, the results are not totally reliable for humans. In addition, cancers are heterogeneous diseases and differ in molecular diversity in same organs or among different individuals.[59] Furthermore, sub-clones present in human cancers can develop resistance or respond differently to drugs. Resistant cancer cells are able to survive treatment which might lead to a relapse of the disease.[60] Resistance mechanisms might involve mutations or amplification of the target enzyme, overexpression of drug transporters or mutations in cell death pathways. Combination therapy is therefore essential to overcome this problem since clinical trials have demonstrated great synergy between targeted molecules and traditional chemotherapy.[37] Thus, it is crucial to continue investigations in all areas of cancer research.

2. ENHANCED PERMEABILITY AND RETENTION EFFECT

The previous chapter dealt with methods of cancer treatment, and herein, a different approach to cure the disease is presented. As mentioned previously, to fight this disease it is necessary to know its behavior and to learn about the events that take place therein.

Most solid tumors show unique characteristics which are not observed in healthy tissues and organs, such as increased production of a number of vascular permeability mediators, defective vascular architecture, impaired lymphatic drainage and impaired recovery system and extensive angiogenesis which lead to hypervasculature. All these features comprise the enhanced permeability and retention effect (EPR-effect) which is a natural phenomenon that is observed in most if not all solid tumors and most importantly also in metastatic tumors.[61–63]

Angiogenesis plays an important role in many physiological and vital processes such as embryonic development, female reproductive cycle, wound healing and organ and tissue regeneration. But it can also support the development of unwanted tumors and hypervasculature can be observed even when tumor nodules are smaller than 0.2 mm.[64,65] The connection between angiogenesis and tumor proliferation and the formation of metastases was demonstrated by Folkman in 1971.[66] The elevated blood flow in tumors also supports angiogenesis.[67] The excessive production of vascular mediators causes an excessive extravasation of macromolecules from the blood vessel into the tumor tissue, providing nutrients and oxygen for a rapid tumor growth. This excessive uptake of macromolecules is a useful feature, which could be exploited for drug delivery. Additionally, tumor blood vessels do not have a fixed, compact structure like in healthy tissues. The endothelial cells are disorganized and irregularly shaped with large gaps between each other, which makes them leaky and permeable.[68] The size of those gaps can be from 100 nm to 2 μm, whereas in normal tissue the gaps are < 6 nm (continuous endothelial cells in striated muscles), 10 up to 100 nm in diameter (fenestrated endothelial cells in renal medula, endocrine glands, renal glomerulus, choroid plexus in the brain, intestinal villus) or even larger (discontinuous endothelial cells in sinusoid vessels, liver, spleen, bone marrow, extraneous particles from the blood) depending on the tissue type.[65,68–70] Due to this fenestration they lack of the normal barrier function, therefore small and large substances are able to enter into tissues. High molecular weight compounds such as nanoparticles, macro molecular drugs, polymeric drugs and lipid particles enter into tumor tissue rather than into normal tissue, so there is a selectivity. In other words,

an enhanced permeability in tumors, which is useful for drug delivery. The lymphatic drainage which is responsible for the elimination of foreign substances is found to be damaged in tumors, therefore those substances remain in the tissue for a prolonged time (retention). Currently only a small number of drugs are effective against metastatic cancers, thus the EPR-effect offers a great advantage in nanomedicine therapy.

2.1. DISCOVERY OF THE EPR-EFFECT

The EPR-effect was first described in 1986 by Maeda and is believed to be a promising element for cancer-selective drug delivery.[61,62] Maedas' research around 1978 focused on developing an anticancer drug to target metastatic tumors and particularly the lymphatic system. Amongst other things he worked with the anticancer protein neocarzinostatin (NCS). NCS is an antitumor antibiotic that is obtained from *Streptomyces carzinostaticus var.* F-41 and was first isolated in 1965.[71] NCS was a widely used anticancer agent, but most interestingly for Maeda, it showed a predominant accumulation in regional lymph nodes. This discovery was highly important, due to the fact that the lymphatic system was often the route by which cancer cells metastasize and metastases are the main reason why many treatments failed. Therefore, targeting the lymphatic system more effectively could bring significant advances in cancer research. However, NCS showed an extremely short half-life with $t_{1/2}$ = 1.8 min *in vivo* and *in vitro*, therefore in its native form, it was not very effective. In 1979, Maeda reported on the synthesis of its protein conjugate SMANCS (styrene maleic acid conjugated NCS), where styrene maleic acid forms a synthetic polymer, which is soluble in both, water and organic solvents.[72] Various tests were performed by different research groups to determine the plasma clearance time of a number of polymer conjugates or modified proteins and the results are summarized in table 1. The tests with NCS and SMANCS (table 1, entries 1-2) were performed by Maeda.

entry	*protein*	*type of polymer modification*	*molecular mass (kDa)*	$t_{1/2}$	*test animal*
1.	*NCS*	*none*	*12*	*1.8 min*	*mouse*
2.	*SMANCS*	*poly(styrene-comaleic acid)-NCS*	*16*	*19 min*	*mouse*
3.	*ribonuclease*	*none*	*13.7*	*5 min*	*mouse*
4.	*ribonuclease dimer*	*cross-linked*	*27*	*18 min*	*mouse*
5.	*soybean trypsin inhibitor (SBTI)*	*none*	*20*	*< 2.0 min*	*rabbit*
6.	*dextran–SBTI*	*dextran*	*127*	*≃ 20 min*	*rabbit*
7.	*ovomucoid*	*diethylene triamine pentaacetic acid (DTPA)/NH_2/^{51}Cr*	*29*	*5 min*	*mouse*
8.	*Cu^{2+}, Zn^{2+} superoxide dismutase (SOD)*	*none*	*30*	*4 min*	*rat*
9.	*SOD–SMA*	*SMA conjugate*	*40*	*> 300 min*	*rat*
10.	*bilirubin oxidase*	*none*	*50*	*< 10 min*	*rat*
11.	*PEG –bilirubin oxidase*	*PEG*	*70*	*5.0 min*	*rat*
12.	*serum albumin, mouse*	*none*	*68*	*3-4 days*	*mouse*
13.	*serum albumin, mouse*	*evans blue dye*	*-*	*2 h*	*mouse*
14.	*formaldehyde-conjugated human serum albumin*	*formaldehyde/^{125}I*	*-*	*25 min*	*rat*
15.	*L-asparaginase*	*none*	*65 × (2-8)*	*1.5-3.4 h*	*rat*
16.	*L-asparaginase–PEG*	*PEG_2-linked*	*-*	*56 h*	*mouse*
17.	*immunoglobin G, mouse*	*DTPA*	*150*	*60 h*	*rat*
18.	*α_2-macroglobulin, human*	*iodination/^{125}I*	*180 × 4*	*140 h*	*mouse*
19.	*α_2-macroglobulin–plasmin complex*	*iodination/^{125}I*	*180 × 2*	*2.5 min*	*mouse*

Table 1: Plasma clearance time of various proteins and their polymer conjugates or modified proteins.[73]

As shown in the list, in most cases the plasma clearance time increases in the presence of a polymer conjugate. Generally, the obtained data indicate that a molecular weight of around or above 50 kDa, neutral or negative electric charge and biocompatibility are important parameters for a prolonged plasma half-time. However, some proteins, such as albumin, can have a shorter $t_{1/2}$ value after chemical modification or denaturation.

In order to increase the half-life $t_{1/2}$ of NCS, Maeda synthesized poly(styrene-co-maleic acid anhydride (SMA), a copolymer to modify NCS to increase its lipophilicity and stability. It seemed ideal due to the anhydride groups, that would react with the amino groups of NCS and the styrene groups which would add a hydrophobicity to the compound. Smaller or larger sized SMA were used and the conjugate was just as effective to bind plasma albumin. As shown in table 1, $t_{1/2}$ was increased by a factor of ten (table 1, entries 1-2; figures 8 and 9).[73]

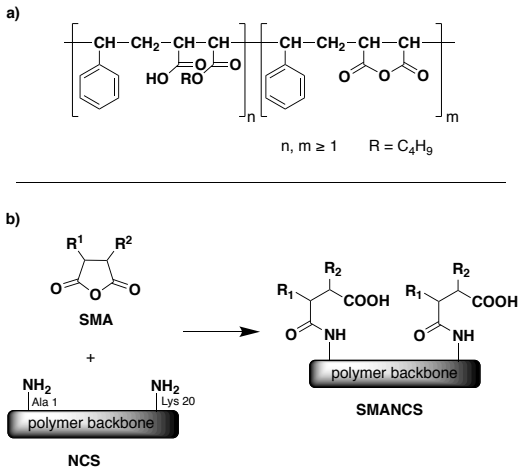

Figure 8: a) Structure of SMA; b) reaction with NCS to produce the conjugate SMANCS. [73]

This compound was the very first polymer-conjugated macromolecular anticancer agent, furthermore it was the first macromolecular anticancer drug possessing anti-metastatic activities and was used against different solid tumors in humans.[73] Moreover, SMANCS' further interesting property was its effect against the multidrug resistance of tumor cells.[74] Even though SMANCS is a relatively small protein with 16 kDa, it can bind non-covalently to albumin *in vivo* and behaves therefore like a large protein of about 80 kDa.[75] Figure 9 illustrates that NCS traces are found in the blood plasma after 240 minutes, whereas SMANCS showed improve stability in the same time range.

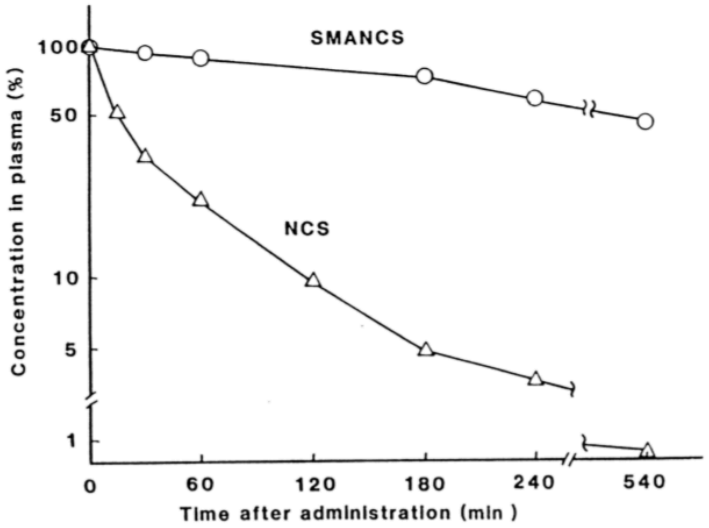

Figure 9: Plasma concentration of NCS and SMANCS in human after intravenous injection. The concentration was measured by radioimmunoassay for NCS and immunological assay for SMANCS.[73]

Generally, macromolecules with a molecular weight of 50 kDa are retained in the blood stream and do not leak out of the vascular endothelial compartment into normal tissue. However, macromolecules behave differently in inflammatory tissue and more importantly in tumor tissues. Tests have shown that SMANCS and other macromolecules preferentially accumulate in solid tumors and granulomas than in normal organs or tissues. Most interestingly in tumors, these substances are unlikely recovered by the lymphatic system, as it is the case in healthy tissue, as a result these macromolecules are retained in the tumor tissue more effectively. This natural behavior, named the EPR-effect, takes place in solid tumors and can be exploited to our benefit.[73]

In 1986, Maeda investigated on the accumulation of proteins with different weight (M_w 12'000 to 160'000) on tumors in mice. He used ^{51}Cr-labelled proteins and dye-complexed serum albumin to visualize protein accumulation in tumors.[63]

Figure 10 illustrates the selectivity of the EPR-effect. Albumin, a serum protein with an approximate molecular weight of 68 kDa and Evans blue, an azo dye with a high affinity for albumin, were administered on tumors. In figure 10a a homogenous uptake is depicted, whereas in 10b the heterogeneity of a tumor causes uptake only at the tumor periphery. It is nicely shown that only the tumor tissue is colored and the healthy tissue remains untouched. Human tumors are highly heterogeneous. They possess widely different structures and their size can vary from less than 1 mm to over 10 cm. Different stages of tumors show different vascular densities. Furthermore, different etiologies of tumors increase the heterogeneity between tumors.[76]

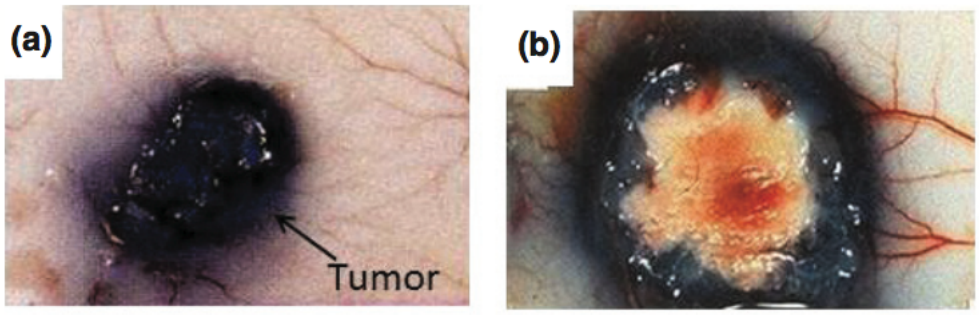

Figure 10: Selective treatment with EPR-effect. (a) A S180 tumor on the skin of a mouse. Relatively homogenous uptake of Evans blue/albumin is shown, but normal skin in the background contains no blue color. (b) Heterogeneity of EPR-effect is shown. Only the tumor periphery took up Evans blue/albumin.[74]

The development of the perfectly selective low-molecular weight drug able to prevent tumor cell growth without causing side effects was challenging to realize in practice. Therefore, tumor targeting and synthetic macromolecular therapeutics using drug delivery systems and nano-sized vectors made a crucial contribution to cancer therapy in recent times.[77] This offers a wide range of methods: biodegradable polymers containing entrapped drugs can be placed in the body and can be used for localized and therefore more selective and targeted drug delivery. In this manner, a controlled release of a drug over a period of months is possible as well.[77]

2.2. MECHANISM OF THE EPR-EFFECT

The key mechanism for the EPR-effect was found to be retention of high-molecular weight substances in the tumor environment, whereas low-molecular weight substances were returned to the blood circulatory system by diffusion.[29] Retention is caused by the impaired lymphatic drainage. An intact lymphatic drainage ensures that ectopic substances are removed from the tissues. However, in a damaged lymphatic drainage, only low-molecular weight substances are removed and high-molecular weight substances remain in the tissue. After administration of such high-molecular weight compounds it was shown that their concentration are 10 - 200 times higher in tumors than in normal tissues.[65]

A promising drug in general has to fulfill certain requirements. The candidate has to be water soluble, stable over time as well as biologically stable, biocompatible, inert and non-toxic and must show no interactions with blood components or blood vessels. Further, it has to be cytotoxic against certain cells and it must demonstrate no antigenicity, limited clearance by the reticuloendothelial system and no cell lysis. Moreover, it needs to be long-circulating in the blood system. The perfect drug to exploit the EPR-effect acquires a certain size (> 6 nm but

variable depending on tissue type) to pass the membrane and to avoid excretion by the renal clearance threshold. Thereby, passive targeting can be converted into the EPR-effect.[77] However, researchers disagree about the perfect size.

To investigate the molecular weight dependence Jain and coworkers examined in 1995 compounds between 25 and 160 kDa in a mice transplanted human colon adenocarcinoma using intravital fluorescence microscopy technique.[78] The permeability increased by a factor of two in the range of 25 to 160 kDa molecular weight. This confirmed that tumor vessels are less permselective than healthy vessels, which is caused by the large pores in the vessel wall arising from the large gaps (~1 μm)[65] between the single endothelial cells. The transport of macromolecular size compounds appears by diffusion through these porous structures. Experiments on tumors with liposomes performed by the same group suggest that the cutoff size of the pores lies between 400 and 600 nm in diameter.[78] Yet, tumor microvascular permeability depends on tumor size and growth rate, but in general it is always higher than in normal tissues. In the year 2000 Maeda stated that the EPR-effect was observed at a molecular weight of 60 kDa, whereas later he stated that accumulation was observed already at a weight of 40 kDa.[61,62,79,80] In 2006, Haag und Kratz observed an EPR-effect at a molecular weight of 20 kDa, but they also stated that the renal clearance occurs at a molecular weight of 30 - 50 kDa.[81] In 2014, Kobayashi estimated a needed size of over 6 nm in diameter, which is approximately the pore size of a glomerulus of the kidney, to avoid excretion thus for the drugs to be effective, a prolonged retention being mandatory.[82] Caliceti stated in 2003 that renal clearance can be avoided from a molecular weight of 70 kDa, but molecules that exceed this size can be eliminated from the body by other pathways such as liver uptake, proteolytic digestion and clearance by the immune system.[83] Expressed in nm, it means that the threshold for rapid renal clearance is 5.5 nm and molecules larger than 8 nm in hydrodynamic diameter (HD) are excreted *via* hepatobiliary clearance (figure 11).[84] According to Choi and co-workers, molecules can undergo the EPR-effect when they possess an hydrodynamic diameter comprised between 10 nm and 200 nm.[84]

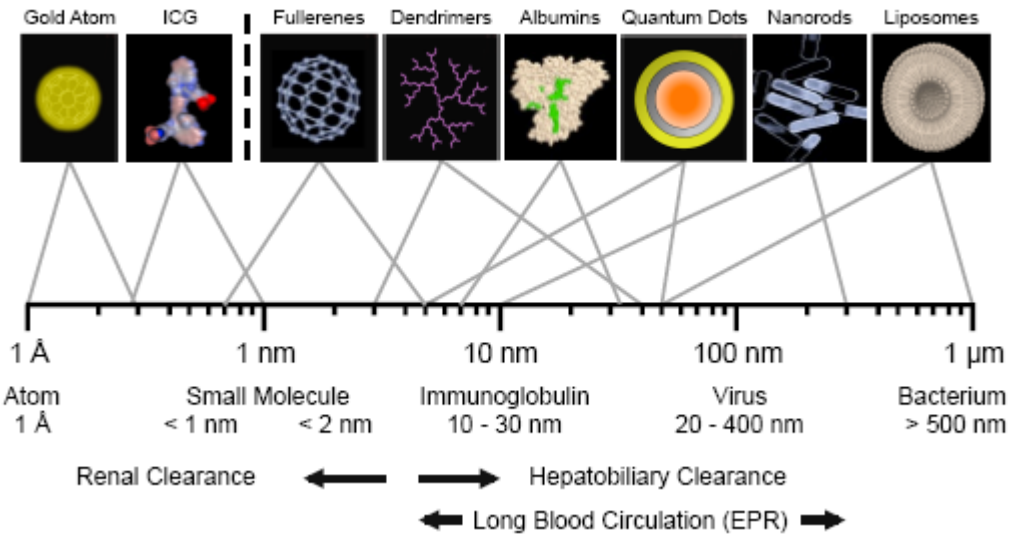

Figure 11: Biomedical imaging (top row) and naturally occurring materials (bottom row). ICG = indocyanine green. [84]

But one thing is certain: As molecular size increases, systematic clearance decreases. The surface charge of a drug should be weakly negative to near neutral to avoid any interactions with endogenous substances. Positively charged molecules will be filtered more efficiently by the kidney than negatively charged compounds.[82] However, a positive charge shows also advantages as for some drugs interaction with endogenous substances is mandatory to be effective. For example, some biomolecules like DNA have a negative overall charge.[85] Therefore positively charged compounds are able to bind DNA. Mitochondria as well has an overall negative charge and other biomolecules like proteins have a partly negative charge, which gives them the ability to attract positively charged molecules.[86] Furthermore, charged compounds have a better water solubility, which is also essential for administration.

In figure 12 a simplified illustration of the EPR-effect is depicted. In the upper part the healthy tissue is shown where the endothelial cells (red) and the normal cells (yellow) are compact. This prevents macromolecules from entering the tissue. Only small molecular-weight molecules like nitric oxide (NO), prostacyclin (PGI_2), endothelium derived hyperpolarizing factor (EDHF) or vasoconstrictive factors such as thromboxane (TXA_2) and endothelin-1 (ET-1) are able to enter, which are removed after a while by the lymphatic drainage.[87] The lower part of figure 12 shows damaged cancerous tissue with large gaps between the single cell units. As a consequence, macromolecules are able to enter into this tissue and due to the poor lymphatic drainage those macromolecules are not removed from the tissue. Macromolecular anti-cancer drugs could fight the tumors locally.

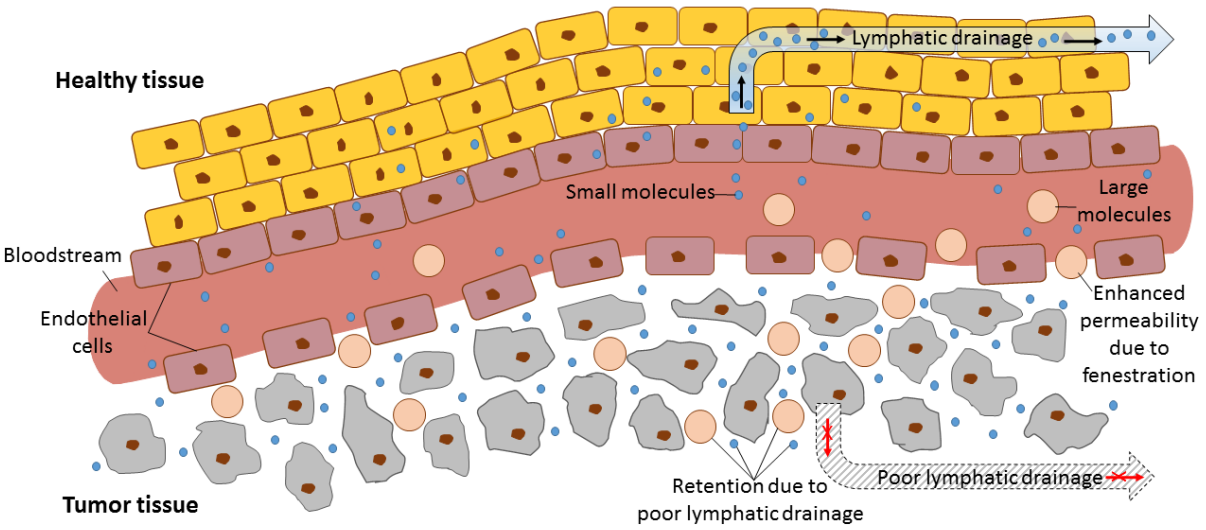

Figure 12: Illustration of a blood - top: healthy tissue - bottom: tumor tissue.[88]

Many macromolecular drugs including liposomes, polymers, micelles, nanoparticles and conjugates containing an active small molecular drug which is linked to biologically relevant enzymes or proteins were developed and have passed clinical and preclinical trials. Active components were taken and modified to obtain large conjugates with elevated stability and pharmacokinetic properties. Some examples of the active components are shown in figure 13 below.

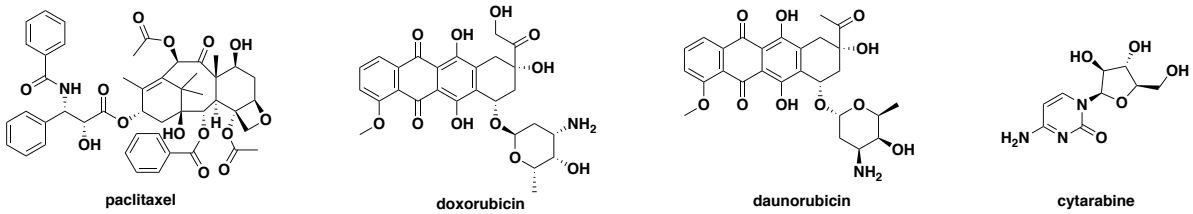

Figure 13: Anti-cancerous active components used to make large conjugates.

The structures shown in figure 13 possess anti-cancerous activity and all of them are also administered as single agents or as a component in combination therapy without their conjugates. Generally, their mode of action lies in inhibiting cell division. But as cell division belongs to the most important cellular processes in our body, its inhibition also brings numerous side effects. A way to reduce the number of side effects is the formulation of large conjugates which are able to exploit the EPR-effect and therefore fight cancer more selectively by doing less harm to healthy cells. Furthermore, conjugates can increase the water solubility of those drugs and therefore the effectiveness of the drug is increased as well. Polymer conjugation alters the bio-distribution of low molecular weight drugs enabling tumor-specific targeting.[77] Some of the polymer-anti-tumor-conjugates are listed in table 2:

entry	*drug*	*active component*	*conjugate*	*mode of action*
1	***DaunoXome®***	*daunorubicin (anthracycline)*	*daunorubicin citrate liposome*	*prevention of DNA replication, inhibition of protein synthesis, conjugate decreases side effects* [89]
2	***Abraxane®***	*paclitaxel (taxanes)*	*paclitaxel bound to albumin*	*blocks mitosis and one stade of cell divison.* [90]
3	***DepoCyt®***	*cytarabine*	*cytarabine encapsulated in multivesicular lipid particles for sustained release (DepoFoam)*	*antimetabolite that are similar to normal substances in the cell. When they are incorporated into the cellular metabolism the cells are unable to divide.* [91]
4	***Doxil®***	*doxorubicin (anthracycline)*	*PEGylated liposomal doxorubicin hydrochloride*	*prevention of DNA replication, inhibition of protein synthesis, conjugate improves drug penetration into tumors and decreases drug clearance* [92]
5	***Myocet®***	*doxorubicin (Anthracycline)*	*doxorubicin hydrochloride packed in liposomes*	*prevention of DNA replication, inhibition of protein synthesis, conjugate decreases side effects* [93]
6	***Genexol-PM®***	*paclitaxel*	*paclitaxel-loaded polymeric micelle*	*antineoplastic activity, interferes with mitosis, conjugate increases water-solubility* [94]
7	***Oncaspar®*** *-Pegaspargase*	*L-asparginase*	*PEG conjugated with L-asparginase*	*L-aspargine depletion blocks protein synthesis and cell proliferation.* [77,95]
8	***Oncaspar®*** *-Calaspargase Pegol*	*L-asparginase*	*E. coli-derived L-asparginase II conjugated with succinimidyl carbonate monoethylene glycol*	*antineoplastic activity, L-aspargine depletion blocks protein synthesis and cell proliferation.* [77,95]

Table 2: Macromolecular anti-cancer drugs that passed clinical trials or preclinical trials.[88]

Conjugates in table 2 were designed to follow the passive tumor targeting by the EPR-effect. In the case of DaunoXome®, Abraxane®, DepoCyt®, Doxil®, Myocet®, Genexol-PM® a small molecule active component was taken and modified to increase the size and efficiency and to decrease the toxicity and number of side effects. In the case of Oncaspar® the active component is the already large enzyme L-asparaginase which causes an L-asparagine depletion that prevents protein synthesis and cell proliferation. The drug was further modified by PEGylation which has proven to be useful for a variety of reasons:[77,96]

- increases protein solubility and stability and reduces protein immunogenicity.
- prevents the rapid clearance of small proteins.
- known to be non-toxic and non-immunogenic, therefore more attractive than other water-soluble polymers.
- increases plasma residence of the drug.
- can increase the therapeutic index, so the dose can be elevated without being toxic.
- its high degree of hydration provides a water shell which supports protein masking.

All these features of PEG can be used to create a conjugate which could be a potential anti-cancer candidate.

As previously discussed, there are great diversities among tumors and the grade of EPR-effect observed can differ tremendously. Some tumors show a strong EPR-effect whereas others only a poor, which can be demonstrated by arterial angiography using an X-ray lipid contrast agent.[62] Vascular permeability and the grade of EPR-effect may depend on tumor type and may increase with tumor size and growth rate and it might be higher in the periphery than in the central regions of tumors.[78] Therefore, there is no uniform treatment of solid cancers exploiting the EPR-effect, which ensures sufficient drug delivery to all tumor regions.[97] The over production of vascular mediators such as bradykinin, nitric oxide (NO), vascular endothelial growth factor (VEGF) and carbon monoxide (CO) can further enhance the permeability of tumors and can be used for the augmentation of EPR based tumor targeting, achieving more tumor accumulation of macromolecular drugs.[65] NO production is inevitable for tumor growth to maintain the supply of nutrients and oxygen. In the presence of a NO-scavengers the extravasation was significantly inhibited. CO is involved in many biological functions including vascular regulation, anti-apoptosis, anti-inflammation and angiogenesis. CO was found to increase vascular permeability, blood flow and augment the EPR-effect. Usage of CO donors can increase the grade of EPR-effect.[65] Another strategy to augment the EPR-effect is the elevation of systolic

blood pressure *via* slow angiotensin II infusion.[79] Infusion of angiotensin II, a peptide hormone, leads to a tremendous increase of the blood flow in tumor tissue without increasing blood flow in normal tissue.[98]

However according to recent statements the EPR-effect might not be valid in humans but only in rodents. Models that are used to investigate the EPR-effect might not be accurate enough, as the murine tumor differs from that of the human in regards to the rate of development, the size relative to host, metabolic rates and host lifespan.[99] Nevertheless, further tests have to be done to confirm this assumption.

Other promising candidates for exploiting the EPR-effect are large organometallic assemblies, such as platinum containing substances which are already known to possess anti-cancer activity and are also administered on patients suffering from cancer.[100,101] In this project we are aiming to create large organometallic assemblies containing ruthenium. Ruthenium-based anti-cancer drugs are very attractive as they have shown to cause less side effects than platinum-containing anti-cancer drugs.[102] The size of the assembly can be increased by the usage of different ligands or by functionalizing the building blocks.

3. RUTHENIUM AND THE PLATINUM FAMILY

Karl Karlovitch Klaus may be regarded as a pioneer of the chemistry of the platinum metals. He discovered a new platinum metal in 1844 at the University of Kazan, Russia and he named it ruthenium, after Ruthenia, the latinized name for Russia, in honor of his motherland.[103]

Platinum was recovered and extracted from the Ural placer deposits in Russia and the insoluble residues, containing the other platinoids rhodium, iridium and osmium, were collected but not further used. During this time platinum was of great interest in Russia, which might be the reason Klaus started his research on the platinoids. He developed a method to extract the platinum from the residue he was investigating. Klaus studied the platinum metals in his own way, using a microscope and by smelling and tasting the preparations and next to platinum he found osmium, iridium, palladium and a new 'body' he could not assign. As shown in scheme 1 he found ways to extract the ruthenium from the residue. It depends on the precipitation of double salts of ruthenium and potassium (K_2RuCl_6, K_3RuCl_6, $K_4Ru_2OCl_{10} \cdot H_2O$ etc.) and the precipitation of ruthenium from its chloride solution by zinc. Furthermore, he discovered that when treating chloride salts of ruthenium with hydrogen sulfide (H_2S) a dense sapphire-blue formed, which was not observed with any of the other metals. His discovery and his general conclusion about the studies on the residue of the Ural platinum deposits were published.[104] He described in detail all the characteristics, properties and behavior of ruthenium and assigned to it the atomic weight of 104.2 u.

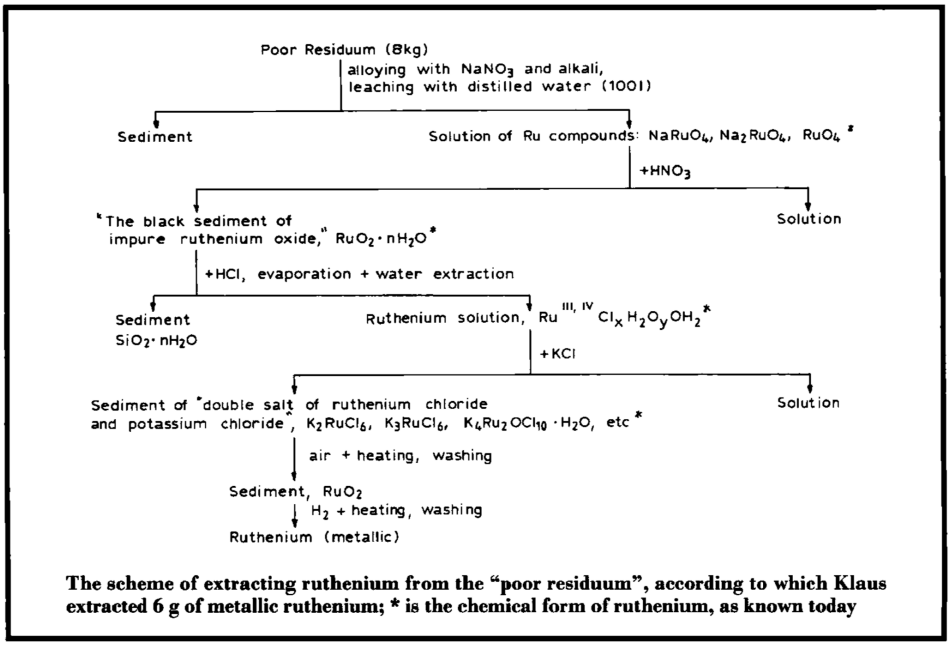

Scheme 1: Extraction of ruthenium.[103]

Not only was Klaus an excellent experimental worker but his interest and ability in investigating theories in depth was as well outstanding. He stated that platinum metals have a number of properties in common and can be grouped in pairs (platinum and palladium; iridium and rhodium; osmium and ruthenium according to their likeness and can be further arranged in two super-imposed groups of three forming triads, composed of the secondary series containing ruthenium, rhodium, palladium and the principal series containing osmium, iridium and platinum.[105] He observed that osmium, iridium and platinum had approximately the same weight and that ruthenium, rhodium, palladium had approximately half their weight, which implies that they are closely connected by similar properties and morphologies. This observation about the similarities and differences within the elements of the triads Ru-Rh-Pd, Os-Ir-Pt led to Dimitri Ivanovich Mendeleevs' conclusion that the platinum metals belonged in one group (VIII) of his periodic table.[103] This discovery can be regarded as an early categorization of elements which led to todays' periodic table by Dimitri Ivanovich Mendeleev and Lothar Meyer.[106]

3.1. PROPERTIES OF THE PLATINUM METALS

Figure 14 shows the position of the platinum family elements in the periodic table highlighted in red.

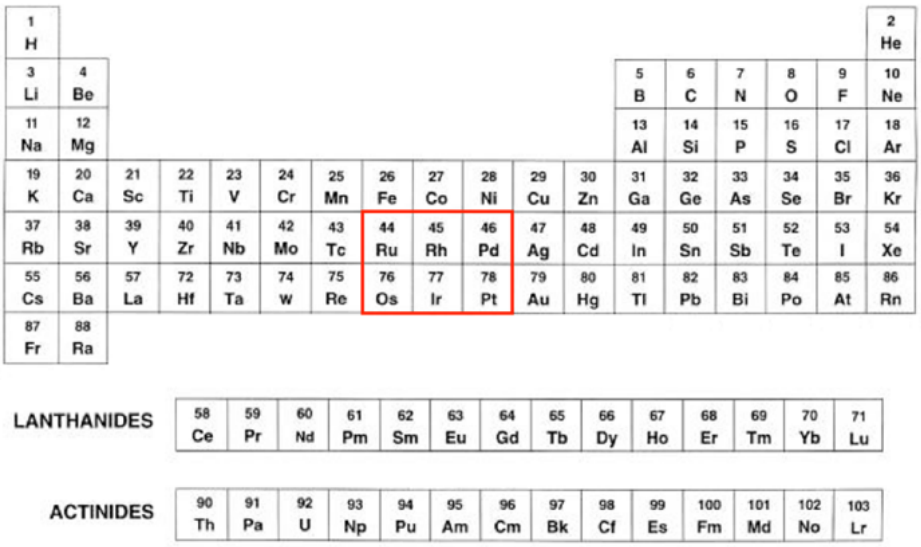

Figure 14: Elements of the platinum family in the periodic table highlighted in red. [107]

Ru, Rh and Pd which belong to the upper row of the periodic table represent the 'light' elements of the platinum family and Os, Ir and Pt which are respectively in the lower row represent their 'heavy' counterparts. In table 3 the atomic and physical properties of the metals of the platinum family is summarized.

	Ru	Rh	Pd	Os	Ir	Pt
Atomic properties						
Atomic number	44	45	46	76	77	78
Atomic weight	101.07	102.905	106.42	190.2	192.22	195.08
Crystal structure	hcp	fcc	fcc	hcp	fcc	fcc
Lattice constant, Å	$a = 2.701$ $c = 4.275$ $c/a = 1.583$	3.803	3.887	$a = 2.735$ $c = 4.319$ $c/a = 1.579$	3.839	3.924
Atomic radius, Å	1.325	1.345	1.376	1.377	1.357	1.377
Mechanical properties						
Density (20 °C), g/cm^3	12.45	12.41	12.02	22.59	22.56	21.45
Density liquid at melting point, g/cm^3	10.90	10.70	10.49	20.1	19.39	18.91
Hardness (HV), Kg/mm^2	250 – 500[a]	130	50	300 – 680[a]	200	48
Young's modulus, GPa	485	386	124	570	538	173
Modulus of rigidity, MPa	172	153	51	220	214	67
Poisson's ratio	0.29	0.26	0.39	0.25	0.26	0.39
Coefficient of compressibility	0.31	0.36	0.52	0.28	0.28	0.36
Thermal properties						
Melting point, °C	2310	1966	1554	3045	2410	1772
Vapor pressure at *mp*, mbar	5.5	3.5	20	20	4	0.1
Boiling point, °C	3900	3700	2970	5000	4130	3827
Thermal conductivity (20 °C), W m^{-1} K^{-1}	117	150	75	87	147	73
Coeff. of linear expansion (0 – 100 °C), 10^{-6} K	9.5	8.5	11.1	6.5	6.8	9.0
Electrical properties						
Specific electrical resistance (0 °C), μΩcm	6.7	4.34	9.725	8.2	4.7	9.825
Temperature coefficient of electrical resistance (0 – 100 °C), 10^{-3} K	4.0	4.6	3.8	4.2	4.3	3.92
Transition temperature of superconductivity	0.47	0.9	0.71	0.11		
Thermoelectric voltage against Pt (0 – 100 °C), mV	0.684	0.70	− 0.570		0.660	0
Work function	4.52	4.8	4.97	4.55	5.40	5.27

[a] Depending on crystal orientation

Table 3: Atomic and physical properties of the platinum group metals.[108]

In general, the elements of the platinum family have high melting points, low vapor pressures, high temperature coefficients of electrical resistivity and low coefficients of thermal expansion. The atomic radius of all six metals are very close, which is explained by the fact that the 'heavy' elements possess fully occupied $4f^{14}$ orbitals, which leads to a more compact electron shell. Due to the small energy differences between the electron shells many oxidation states are possible which are depicted in table 4.

Ru	*- 2*		*0*		***+ 2***	***+ 3***	*+ 4*	*+ 5*	*+6*	*+7*	*+8*
Rh		*- 1*	*0*	*+ 1*	*+ 2*	*+* ***3***	*+ 4*	*+ 5*	*+ 6*		
Pd			*0*		*+* ***2***	*+ 3*	*+ 4*				
Os	*- 2*		*0*	*+ 1*	*+ 2*	*+ 3*	*+* ***4***	*+ 5*	*+ 6*	*+ 7*	*+ 8*
Ir		*- 1*	*0*	*+ 1*	*+ 2*	*+ 3*	*+* ***4***	*+ 5*	*+ 6*		
Pt			*0*		*+* ***2***		*+* ***4***	*+ 5*			

Table 4: Possible oxidation states and principal oxidation states in bold.[108]

Additionally, as transition metals they possess other properties like their catalytic activity due to their inconsistent valence structure and their ease to change it, their ability to form intermediate compounds with different reagents, color, para-magnetism due to unpaired electrons and their strong tendency to form complexes. In the periodic table the elements within a group have similar chemical and physical characteristics. However, in the group of platinum metals also neighboring elements show similarities.[108] Nowadays ruthenium is used in different fields, such as catalysis, solar cells and most importantly for our research also in biological applications.[109–111]

3.2. CISPLATIN AS METAL-BASED ANTI-CANCER AGENT

Cisplatin belongs to the most known metal-based anti-cancer drugs.[53,112] It was first synthesized by Peyrone in 1844 and its chemical structure was first elucidated by Werner in 1893.[112] Its activity as a cell division inhibitor was discovered serendipitously by Rosenberg in the 1960s.[113]

Scheme 2 shows the mode of action of cisplatin upon activation. The neutral cisplatin is believed to be biologically inactive and it is activated by an aquation reaction which involves the exchange of the two chlorides as leaving groups with two water molecules. The activation is prevented if there is a high concentration of chlorides. The concentration of chlorides in intracellular fluids is approximately one-thirteenth compared to the concentration in extracellular fluids, hence under these conditions cisplatin is activated leading to DNA damage. Once cisplatin is activated it will bind two sites of DNA. There are two possible ways of binding. A DNA adduct is formed when the two binding sites are on the same DNA strand (scheme 2) or a DNA cross-link is formed when the two binding sites are on two different strands. Cisplatin is able to bind all nucleobases but it has a higher affinity for the N-7 positions of adenine and guanine due to the high nucleophilicity of the N-7 positions of purine bases. Both DNA adducts and DNA cross-links are able to inhibit DNA replication in mammalian cells and as a result cell division is inhibited as well.[53]

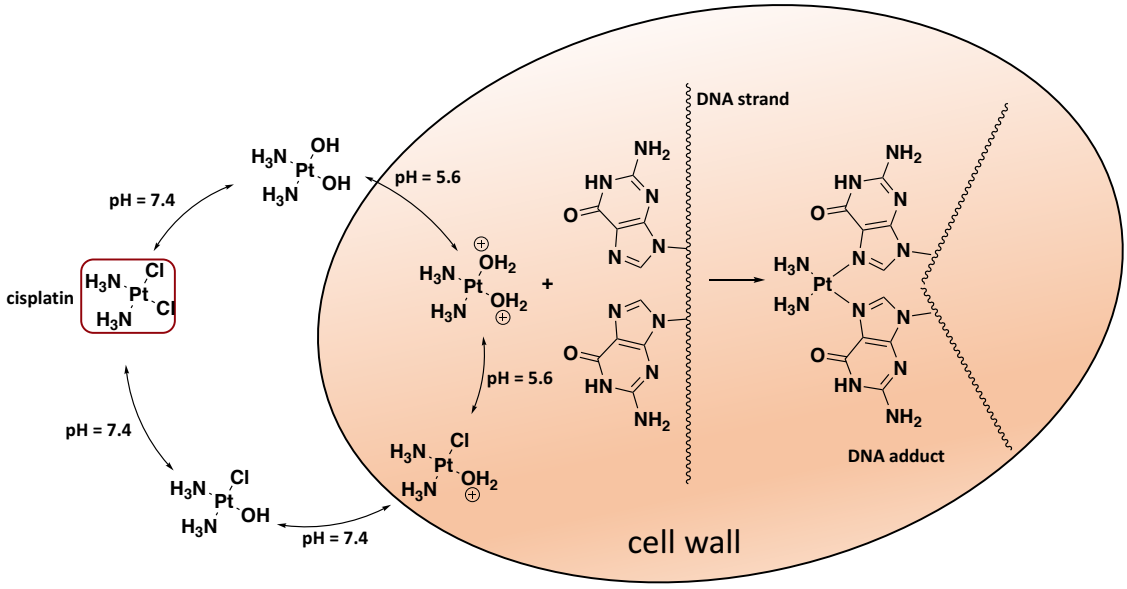

Scheme 2: Aquation reaction of cisplatin and adduct formation at the N-7 position of guanine on two sites of DNA, which results in DNA damage, leading to cell death.[53,114]

Cisplatin entered phase I clinical trials in 1971 and was approved for the treatment of testicular and ovarian cancer in 1978.[100] It also shows highly curative effects on many solid malignancies. Since its discovery many inorganic chemists have been working on developing new platinum-based anti-cancer drugs. However, after numerous clinical candidates only two more platinum-containing anti-cancer drugs were approved worldwide: carboplatin (1993) and oxaliplatin (2002), which are both analogues of cisplatin and their structures are shown in figure 15. In all three square planar structures of the top row of figure 15 platinum is present as Pt(II). Pt(IV) containing structures are octahedral and are prodrugs that require activation *via* reduction.[115]

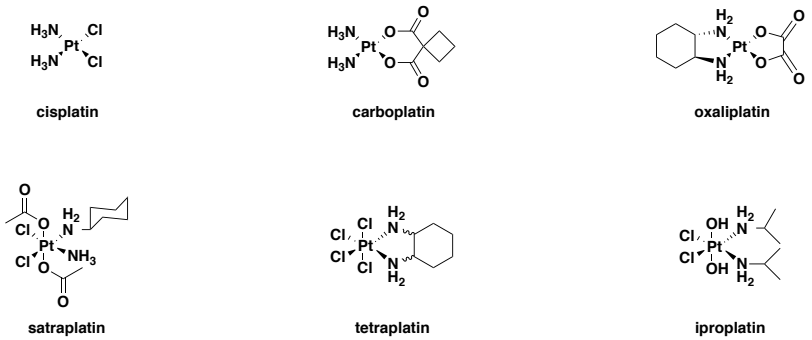

Figure 15: Pt(II) complexes (top) and Pt(IV) complexes (bottom).[115]

Platinum-containing drugs show effectiveness in chemotherapeutical cancer treatments but there are also limitations. Many common types of cancers cannot be cured, also drug resistance was observed and a treatment includes a number of side effects like nerve damage, hair loss, nausea, nephrotoxicity, gastrointestinal toxicity and ototoxicity. To overcome these limitations

other metal-based drugs were developed and tested on their anti-cancerous activity. Other metals, such as gallium, ruthenium and titanium were recognized for their antineoplastic potential more than two decades ago, but the development of non-platinum containing drugs was not pursued because of the clinical success of cisplatin.[101]

3.3. RUTHENIUM AS ANTI-CANCER AGENT

Ruthenium and iron containing drugs seemed to be good alternatives to platinum considering that they are well tolerated *in vivo* and show fewer and less severe side effects. Ruthenium complexes exhibit an excellent cytotoxicity and low general toxicity.[116] The fewer side effects of ruthenium can be partly explained by the fact that ruthenium and the essential iron are in the same group. Therefore, ruthenium has the ability to mimic iron in binding within minutes to biological molecules like human serum albumin and transferrin. It is also known that the anti-cancer activity is significantly higher for apotransferrin-bound complexes compared to the albumin-bound or free species.[101,117,118] This leads to the assumption that apotransferrin acts as a natural carrier of such drugs to the tumor due to numerous transferrin receptors on the surface of tumors.[118] Ruthenium containing drugs are able to use the iron detoxification paths inside the body which also explains why less harm is done to healthy tissue.[119]

The lower toxicity can also be explained by the fact that ruthenium is accessible in different oxidation states. For example, ruthenium (III) complexes are inactive compared to ruthenium (II) complexes. In other words, ruthenium can be activated by reduction. The inactive Ru(III) enters the reductive environment of cancers, where it is reduced to Ru(II) and thereby activated. The low oxygen level and the lower extracellular pH and the presence of cellular reducing agents like glutathione provides good conditions for a selective reduction of the drug exploiting the Ru(III)/Ru(II) redox potential.[101,102] Furthermore, ruthenium drugs are less prone to resistance mechanism than platinum drugs.[119] Complexes of such kind bind non-covalently to DNA by electrostatic or van der Waals forces and the mode of interaction depends on the structure of the complex and can involve intercalation, cross-linking and ionic interactions.[119] The majority of the known ruthenium-containing drugs act by causing DNA damages in cancer cells.[119] Furthermore, ruthenium complexes have mainly an octahedral coordination chemistry, which implies a reactivity and mode of function different from the square-planar platinum(II)-complexes. Additionally, ruthenium is stable when exposed to air and shows relatively slow *in vivo* ligand exchange.[102]

Figure 16 shows the ruthenium(III)-containing anti-cancer candidates NAMI-A and KP1019 and the Ru(II)-arene containing RAPTA-C.[120,121] NAMI-A and KP1019 are Ru(III) containing prodrugs that need to be activated by reduction.[122] NAMI-A reduces the formation of metastases and inhibits their growth. However, it has only little impact on primary tumors. Furthermore, it interferes with the interactions of tumor cells with the extracellular matrix, increases cell dependent cell adhesion, inhibits matrix degradation, reduces cell invasiveness and migration which results in a less malignant cell phenotype.[101] However, clinical trials for NAMI-A were terminated due to insufficient effects and elevated side effects.[123]

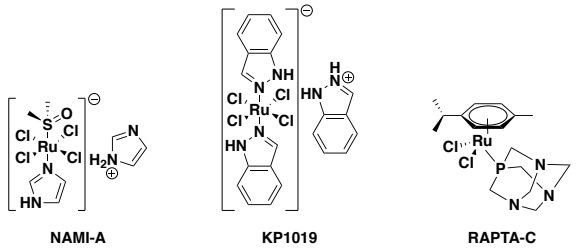

Figure 16: Chemical structures of NAMI-A, KP1019 and RAPTA-C.

RAPTA-C shows great potential for clinical applications. It is proposed that the RAPTA-C treatment triggers the mitochondrial apoptotic pathway. Furthermore, its 1,3,5-triaza-7-phosphaadmantane (PTA) ligand has shown moderate anti-cancerous activity in various cell lines and excellent activity in reducing the number of weight of solid metastases.[124] RAPTA-C remains the best anti-cancerous compound of the series of Ru(II)-series drugs, nonetheless the molecular mechanism and the signaling pathways remains to be elucidated.

KP1019 is currently under clinical investigations. It is suggested that the mechanism of KP1019 involves interaction with mitochondria due to rutheniums similarity with iron.[101,125] However, its precise mechanism of action remains poorly understood.[126] Mitochondria use and accumulate a large amount of iron, and mitochondrial iron is mainly used in three metabolic pathways: heme synthesis, iron-sulphur cluster biogenesis and mitochondrial iron storage.[127] Heme is a non-protein, crucial for every organism since it is one of the constituents of hemoglobin, chlorophyll, myoglobin and cytochrom.[128] There are many different kinds of iron-sulphur clusters ([2Fe-2S]; [3Fe-4S]; [4Fe-4S] etc.) and depending on the cluster type they interact with different proteins being responsible for many biological processes. An excess of iron is stored in ferritin, which is a multimeric protein composed of 24 subunits and is able to store around 4500 iron atoms. Mitochondrial ferritin serves as additional iron storage.[129] In cancer, for example in lung carcinoma, approximately 20% of total cellular iron was present in mitochondria. Another example are hepatocytes in rats, where in mitochondria the

concentration of metabolic iron was twice as much as in the cytosol. However, the role of mitochondrial iron in cancer development is only poorly elucidated.[127]

With the development of compounds like NAMI-A, KP1019 and RAPTA-C ruthenium was established as a potential anti-cancer agent. Therefore, in this project we would like to combine rutheniums' potential anti-cancer activity with the EPR-effect. As mentioned before, for the EPR-effect macromolecules are required which cannot be removed from cancerous tissue because of their large size.

4. STRATEGIES TO INCREASE THE MOLECULAR WEIGHT OF ARENE RUTHENIUM ASSEMBLIES TO EXPLOIT THE EPR-EFFECT

To date there are no ruthenium-containing compounds known to exploit the EPR-effect. With the knowledge about the anti-cancer activity of ruthenium complexes and their ability to form supramolecular structures the development of ruthenium containing anti-cancer drugs to exploit the EPR-effect presents an interesting field of research. In this chapter the preparation of diverse ruthenium complexes is discussed starting from small mono-nuclear compounds to large multi-nuclear compounds. The goal of this project is to develop a suitable arene ruthenium based anti-cancer agent with the ability to exploit the EPR-effect.

In figure 16 three examples of ruthenium containing drugs are shown which have been in clinical trials. They carry different ligands and therefore, they differ in weight, size and shape. With DMSO and imidazole NAMI-A has rather small ligands, whereas KP1019 with indazoles carries clearly larger ligands, which results in larger weight and size. RAPTA-C belongs to the piano stool family, where one ligand is a cyclic polyhapto ligand. In the case of RAPTA-C the cyclic polyhapto ligand is *p*-cymene. Furthermore, the cyclic polyhapto ligands or arenes are known to stabilize the Ru(II) centers, which is the active form of such complexes. Furthermore, the arene provides a hydrophobic surface, allowing cellular diffusion through the lipophilic plasma membrane.[130] For these reasons, arene-ruthenium complexes as anti-cancer drugs have been extensively investigated in recent years.

Arenes are defined as hydrocarbons with a conjugated monocyclic molecular structure according to IUPAC.[131] They are strong electron donors and are able to form strong bonds with *d*-metals. *d*-Elements possess an incomplete *d* shell and an empty last *p*-shell and therefore they accept and share electrons from ligands to increase their stability.[132] Since arenes are strong electron donors they present an interesting group of ligands for organometallic chemistry. A depletion of π-electron density is observed in arenes when bound to a transition metal, which supports the theory that strong bonds are formed between an arene and a *d*-metal.[133]

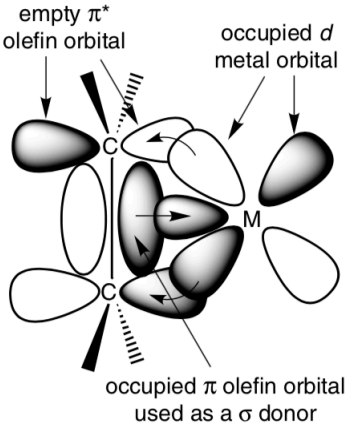

Figure 17: Dewar-Chatt-Duncanson model π-bonding and π-antibonding for a π-accepting alkene ligand with a transition metal.*[132]

Figure 17 illustrates how π-electron donors, in this case an olefin, form a σ-bond by donating electrons in a coaxial manner from the filled *p*-orbitals of the ligand to the empty *d*-orbitals of the metals. Furthermore, there is a lateral π-type backbonding from a filled *d*-orbital to a vacant antibonding orbital of the alkene ligand forming a π-bond.[132] The π-bond point in the opposite direction to the σ-bond. This partly compensates the σ-bond and allows the metal to return part of the excess of electron density and therefore it is able to exist in a low or negative oxidation state.[132] Using this molecular orbital theory the stabilisation of Ru(II) centers using arenes can be explained.

As already mentioned, ruthenium can possess an octahedral geometry. For the metal to form the desired assembly, some of the coordination sites at the metal center must be occupied. In this manner the accessibility of the coordination sites can be controlled. This can be done with the use of η^5 or η^6 ligands. In this thesis η^6 ligands are discussed. The use of such aromatic ligands brings advantages as three of the six coordination sites are occupied by the aromatic ligands, hence there is a better control in the synthesis of the desired assemblies. Furthermore, the strongly bonded aromatic ligand can be further modified to enhance the size, mass and solubility or to add new properties to the assemblies.[134]

4.1. MONONUCLEAR PIANO STOOL COMPLEXES

Half-sandwich compounds possess a piano stool geometry, meaning the metal center is coordinated to an arene or a cyclopentadienyl ligand on one site. The general structure of such a compound as well as the structure of [(η^6-benzene)Ru(II)(metronidazole)Cl_2] is comparable to the geometry of a piano stool as illustrated in figure 18.

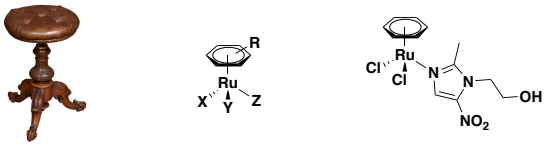

Figure 18: General structure of piano stool complexes and [(η^6-benzene)Ru(II)(metronidazole)Cl_2] synthesized by Dale and co-workers in 1992.[122,135]

The first biologically inspired compound of this kind was prepared by Dale and co-workers. He used metronidazole (1-β-hydroxyethyl-2-methyl-5-nitro-imidazole), a known anti-cancer drug to coordinate to a Ru(II) benzene dichloride fragment. [(η^6-benzene)Ru(II)(metronidazole)Cl_2] has shown to have a better activity than metronidazole alone.[122]

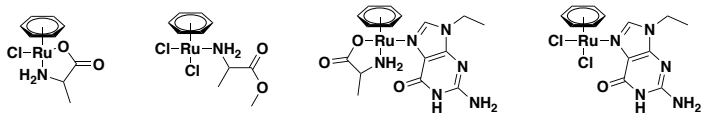

Figure 19: Structures of [(η^6-benzene)Ru(II)(L-alanine)Cl], [(η^6-benzene)Ru(II)(L-alanine methyl ester)Cl_2], [(η^6-benzene)Ru(II)(L-alanine)(ethylguanine] and [(η^6-benzene)Ru(II)(ethylguanine)Cl_2]show how different ligands can be used to prepare a variety of piano stool complexes.[136]

Later, Sheldrick and co-workers reported the synthesis of [(η^6-arene)Ru(II)(LL)Cl_x] half-sandwich compounds (figure 19), where the amino acids L-alanine, guanine and their derivatives are used as ligands. These examples show how different ligands can be used to prepare a variety of piano stool complexes.

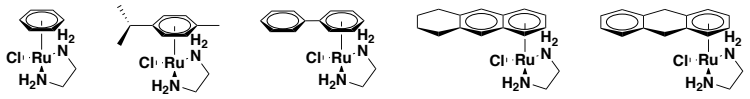

Figure 20: Half-sandwich complexes using different arenes and ethylenediamine [(η^6-arene)Ru(II)(en)Cl].[137]

Sadler and co-workers prepared half-sandwich complexes using different arenes as illustrated in figure 20 and ethylenediamine (en) to establish structure-activity relationships.[137] In this manner it is possible as well to prepare a variety of complexes. In table 5 the impact of the different arenes in respect to their IC_{50} values are depicted:

arene-Ru drug	*IC_{50} [µM]*
benzene	*17*
p-cymene	*10*
biphenyl	*5*
tetrahydroanthracene	*0.5*
dihydroanthracen	*2*

Table 5: Arene-ruthenium complexes with respective IC_{50} values in human ovarian A2780 cancer cells after 24 h drug exposure.[137]

Dyson and co-workers prepared a series of half-sandwich complexes using modified arene ligands and PTA (1,3,5-triaza-7-phosphaadamantane) to develop a structure-activity relationship (figure 21). These structures were considered to be the prototypes of the Ru(II) anti-cancer drug RAPTA-C.

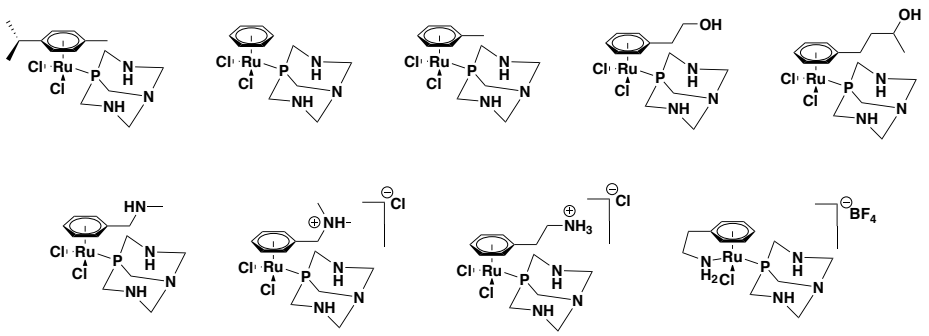

Figure 21: [(η^6-arene)Ru(II)(PTA)Cl_2] half-sandwhich complexes with different arenes. [138]

Half-sandwich piano stools are mono-nuclear complexes with only one metal center. However, complexes can also be formed with multiple metal centers. The following chapter deals with multi-nuclearity and its link to supramolecular chemistry. Furthermore, it describes how the choice of the ligand and its denticity is crucial for the final shape and size of the desired assembly.

4.2. CONCEPTS OF MULTI-NUCLEAR ASSEMBLIES

Maverick and co-workers were the first to report the synthesis of a copper based M_2L_2-type rectangular structure in 1984.[139] Shortly after in 1986, they reported on the synthesis of a second macrocycle.[140] He used a Cu(II) metal center and β-diketones as ligands. Both macrocylces are shown in figure 22.

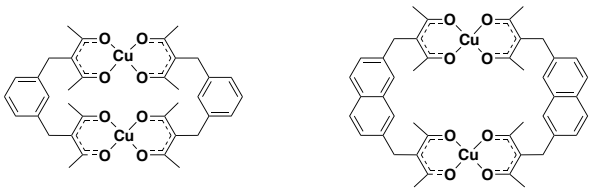

Figure 22: First macrocylces synthesized by Maverick.

A few years later, Fujita reported the preparation of a polynuclear Pd(II) complex, $[(en)Pd(4,4'\text{-bpy})]_4(NO_3)_8$, where the *cis* position of the square-planar Pd atoms were occupied by ethylenediamine ligands and the remaining coordination sites linked to each other by bridging 4,4'-bipyridine spacer ligands (figure 23).[141]

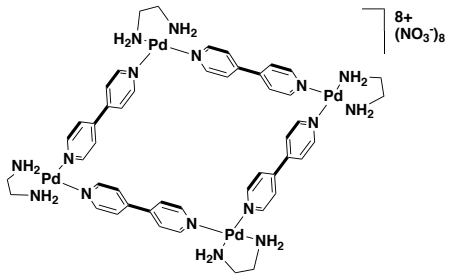

Figure 23: Polynuclear Pd(II) complex synthesized by Fujita, in 1990.[141]

Hereafter, many other groups have also developed similar supramolecular structures.[142–148] In 2001 Stang and co-workers developed a strategy to generate supramolecular rectangles from so called 'molecular clips'. Molecular clips are dinuclear building blocks with two 90 ° angles as shown in scheme 3. In order to form a rectangle, he combined two molecular clips by introducing a bidentate bridging ligand to connect the platinum metal centers with each other. Stang recognized that it was necessary for the molecular clip to possess a rigid backbone, to avoid formation of complex mixtures.[142]

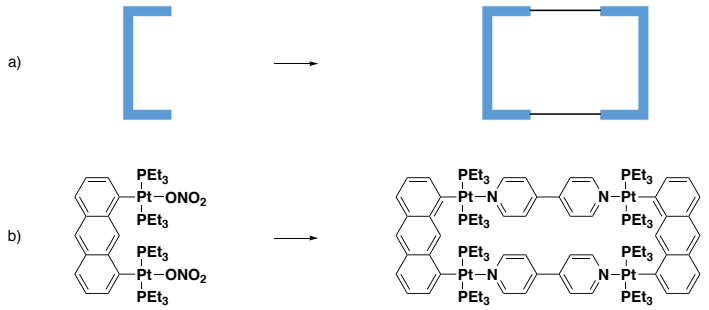

Scheme 3: a) Simplified illustration of molecular clip (left) and resulting rectangle (right) b) molecular clip 1,8-bis(trans-Pt(PEt$_3$)$_2$-(NO$_3$))anthracene (left) and resulting rectangle cyclobis[1,8-bis(trans-Pt(PEt$_3$)$_2$)anthracene)(4,4'-dipyridyl] (right) by Stang and co-workers.[142]

Stang further increased the size of this rectangle shown in figure 24 by exchanging the 4,4'-bypyridine with larger bidentate ligands. He interlinked 1,2-di(pyridin-4-yl)ethene and 1,4-bis(pyridin-4-ylethynyl)benzene between the two molecular clips.

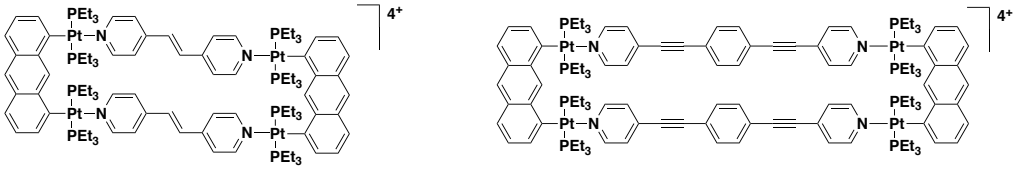

Figure 24: Rectangles by Stang with 1,2-di(pyridin-4-yl)ethene (left) and 1,4-bis(pyridin-4-ylethynyl)benzene (right) between two molecular clips.[142]

When comparing the rectangle containing 4,4'-bypyridine (scheme 3b) and 1,4-bis(pyridin-4-ylethynyl)benzene (figure 24, right) as ligands, we can see that the size increased. It seems obvious that the choice of an even larger ligand results in the formation of an even larger rectangle. In these examples each bidentate bridging ligand possesses two donor groups to undergo coordination to the metal center. In the cases shown herein, the nitrogen heteroatom acts as donor group *via* its lone pair.[132] Now it seems possible to use ligands of a higher denticity to make different kinds of supramolecular structures. This strategy will be discussed in the following section based on ruthenium containing assemblies.

4.3. ARENE-RUTHENIUM BASED MULTINUCLEAR ASSEMBLIES

As discussed before arene-ruthenium complexes possess interesting anti-cancer properties and some examples of mononuclear compounds were shown. In 1997, Süss-Fink and co-workers used a similar approach to synthesize tetra-nuclear rectangles containing ruthenium.[142,149]

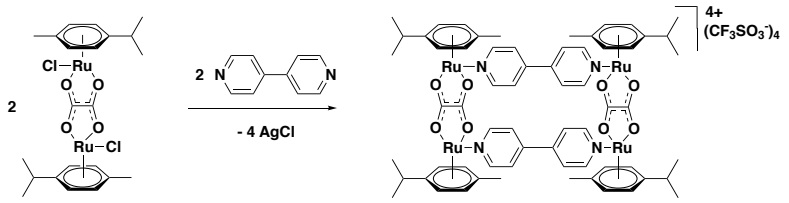

Scheme 4: Molecular clip $[Ru_2(\mu\text{-}\eta^4\text{-}C_2O_4)(Cl)_2((\eta^6\text{-}p\text{-}cymene)_2]$ (left) and the resulting rectangle $[Ru_4(\mu\text{-}\eta^4\text{-}C_2O_4)_2(\mu_2\text{-}\eta^4\text{:}\eta^4\text{-}bipy)_2\text{-}(\eta^6\text{-}p\text{-}cymene)_4]_4$.

The molecular clip (scheme 4, left) is a dinuclear arene-ruthenium complex, where the two metal centers are linked by a spacer ligand. In this manner the molecular clip possesses a rigid structure in order to avoid formations of polymers or other complex structures in the following step. Likewise to Stang (schemes 3 and figure 24) it is possible to connect two rigid molecular clips by introducing bridging ligands. The spacer ligand used in scheme 4 to connect the two metal centers is oxalate, which is a chelating bidentate ligand. However, in this case, since one ligand is coordinating to two different Ru centers it is called a bis-bidentate ligand. Keppler and co-workers have shown that anti-cancer activity is as well observed in dinuclear ruthenium complexes. Furthermore, they have also demonstrated that the anti-cancer activity is further increased the longer the distance between the two metal centers is.[150,151] A method to further augment the distance between the metal centers is the use of a different spacer ligand.

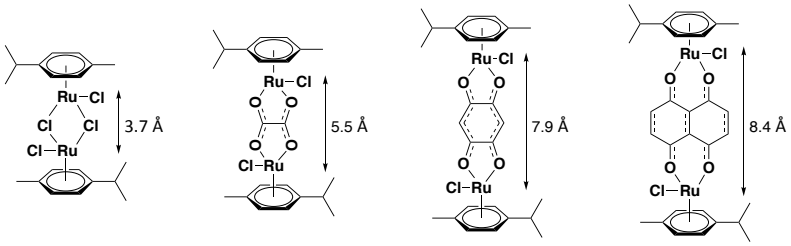

Figure 25: Dinuclear arene ruthenium precursor and metalla-clips with respective spacer length. Precursor: $[Ru_2(p\text{-}cymene)_2(\mu\text{-}Cl)_2Cl_2]$ and clips: $[Ru_2(p\text{-}cymene)_2(\mu\text{-}C_2O_4)Cl_2]$, $[Ru_2(p\text{-}cymene)_2(\mu\text{-}dhbq)Cl_2]$ and $[Ru_2(p\text{-}cymene)_2(\mu\text{-}dhnq)Cl_2]$ (from left to right).[134,152]

In figure 25 dinuclear ruthenium species are illustrated and the influence of the spacer ligands on the size of the molecular clips is shown. $[Ru_2(p\text{-cymene})_2(\mu\text{-Cl})_2Cl_2]$, the first molecule shown in figure 25, is the ruthenium precursor which is prepared from $RuCl_3 \cdot nH_2O$ and α-phellandrene in EtOH. It is used for the preparation of dinuclear metalla-clips by introducing

the spacer ligands. The precursor possesses two chlorine atoms which act as bridging ligands to connect the two ruthenium metal centers. The length from one ruthenium to the other ruthenium amounts 3.7 Å. By introducing oxalate as a spacer ligand the size increases to 5.5 Å. In the last two examples of figure 25 dihydroxybenzoquinone (dhbq) and dihydroxynaphtoquinone (dhnq) were used as spacer ligands and the distances were increased to 7.9 Å and 8.4 Å respectively. All spacer ligands illustrated in figure 25 are bis-bidentate ligands. It is shown that spacer ligands need certain properties to be suitable for the formation of such clips. In the example of oxalic acid and dhbq, there are two hydroxy groups within the ligand and in their α-position there are carbonyl functions. In the example of dhnq there are as well two hydroxy groups and in their β-position there are carbonyl functions. The deprotonated hydroxy groups form a bond to the metal centers and the carbonyl functions further coordinate with their lone pairs to the metal centers. In this manner a bis-bidentate chelating mode is possible.

Once, the molecular clip is synthesized, two of them can be combined by introducing another ligand, so called panel ligands. In schemes 3 and 4 and figure 24 rectangles are formed using bidentate linkers, which act as bridging ligands. In all cases two linkers were required to connect two clips to form a rectangle and therefore a tetra-nuclear metalla-assembly.

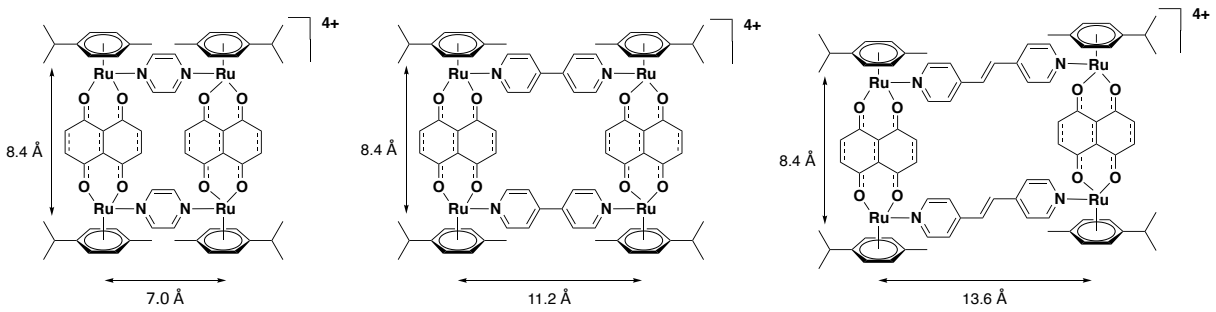

Figure 26: Tetra-nuclear ruthenium rectangles with respective length of panel ligands: $[Ru_4(p\text{-cymene})_2(\mu\text{-prz})_2(\mu\text{-dhnq})_2]^{4+}$, $[Ru_4(p\text{-cymene})_2(\mu\text{-bpy})_2(\mu\text{-dhnq})_2]^{4+}$ and $[Ru_4(p\text{-cymene})_2(\mu\text{-bpe})_2(\mu\text{-dhnq})_2]^{4+}$.[152,153]

The linkers used for the formation of the rectangles shown in figure 26 are the bidentate pyrazine, 4,4'-bipyridine and (*E*)-1,2-di(pyridine-4-yl)ethene. Like before the distance between the ruthenium metal centers can be increased using diverse panel ligands. Depending on the choice of the connector the final assembly can possess a different structure as illustrated in figure 27.

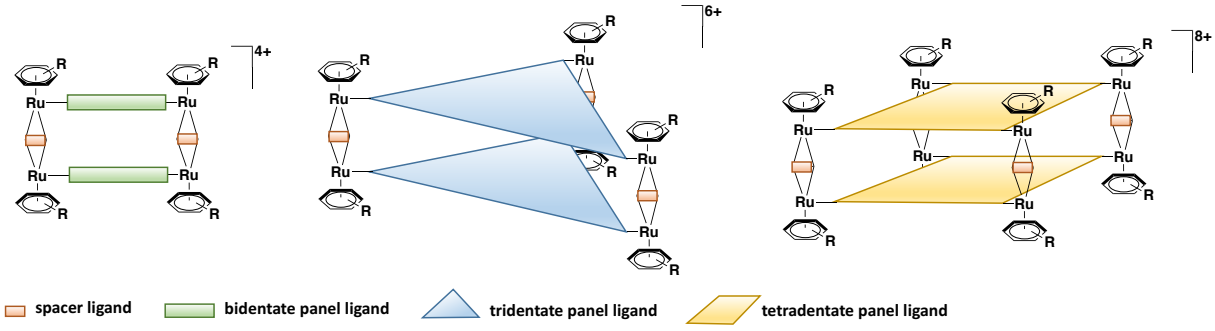

Figure 27: Preparation of different kinds of assemblies with the right choice of ligands. Tetra-nuclear rectangle (left), hexa-nuclear prism (center) and octa-nuclear prism (right).

Polypyridyl derivatives are suitable panel ligands for the preparation of cage-like structures. They possess several position to coordinate to a metal center. In figure 28 some examples of tridentate polypyridyl derivatives are shown.

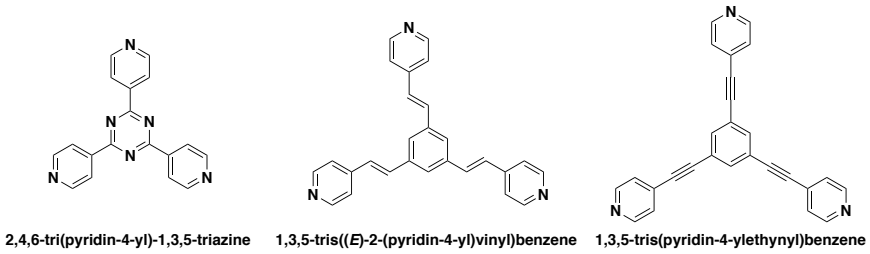

Figure 28: Tri-dentate polypyridyl panel ligands to form hexa-nuclear ruthenium prisms.[154–157]

2,4,6-tri(pyridin-4-yl)-1,3,5-triazine is prepared from isonicotinonitrile and NaOH.[155] Three pyridyl moieties are directly attached to the triazine ring in the center at 2, 4 and 6 position. In this thesis 2,4,6-tri(pyridin-4-yl)-1,3,5-triazine will be referred to as 4-tpt. 1,3,5-Tris((*E*)-2-(pyridin-4-yl)vinyl)benzene is prepared from 1,3,5-tribromobenzene and 4-vinylpyridine in a Heck reaction and will be referred to as tris-pvb.[156] In this case the pyridyl moiety is connected to the aromatic ring in the center *via* an olefin. 1,3,5-Tris(pyridin-4-ylethynyl)benzene is prepared from 1,3,5-triethynylbenzene and bromobenzene in a Sonogashira cross-coupling reaction to form a triple bond between the three pyridyl moieties and the aromatic ring in the center.[157] A triple bond is shorter than a double bond, however, since a triple bond possesses a linear structure, the overall size is increased. Using these ligands, it is possible to synthesize hexa-nuclear prism-like structures, as shown in figure 29.

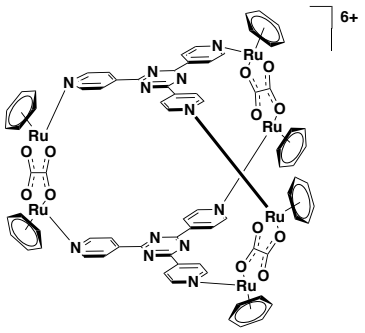

Figure 29: Structure of a hexa-nuclear prism using a tri-dentate panel ligand.

In figure 30 some other structural motifs of polypyridyl derivatives are shown. In particular, tetra-dentate ligands that are able to coordinate four ruthenium centers.

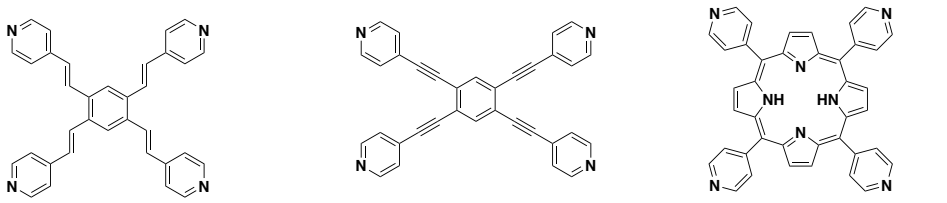

Figure 30: Tetra-dentate polypyridyl panel ligands to form octa-nuclear ruthenium assemblies.[158,159]

1,2,4,5-Tetrakis((*E*)-2-(pyridin-4-yl)vinyl)benzene is prepared in a Wittig-Horner reaction starting from 4-pyridinecarboxaldehyde and 1,2,4,5-tetrakis(bromomethyl)benzene which is converted to the respective phosphonate.[158] 1,2,4,5-tetrakis(pyridin-4-ylethynyl)benzene is synthesized in a Sonogashira cross-coupling reaction starting from 1,2,4,5-tetraiodobenzene and 4-ethynylpyridine.[159] The length of the ligand was increased by replacing the double bond with a triple bond, due to its linear structure. The last example shown in figure 30 is a polypyridyl porphyrin derivative and in this theses it is referred to as tpp. It is prepared from isonicotinaldehyde and 1*H*-pyrrole.[160,161] The molecular weight was increased significantly for the porphyrin derivative compared to the other two tetra-pyridyl ligands. As mentioned in chapter 2, not only the size but also the molecular weight matters for the EPR-effect. Using these tetradentate ligands the formation of octa-nuclear assemblies is possible.

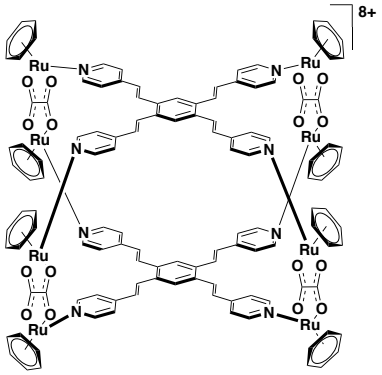

Figure 31: Structure of octa-nuclear cube using a tetra-dentate panel ligand.

Figure 31 shows an octa-nuclear cube using 1,2,4,5-tetrakis((*E*)-2-(pyridin-4-yl)vinyl)benzene as panel ligand, which has the ability to coordinate four ruthenium metal centers.

4.4. AIM OF THIS THESIS

The aim of this project is to synthesize macromolecular multi-nuclear arene-ruthenium metalla-assemblies with anti-cancer activity to target cancer cells *via* the EPR-effect. This study should provide access to novel arene-ruthenium assemblies with an increased mass and size to exploit the discrepancy between cancerous and healthy tissues. Moreover, encapsulation of anti-cancerogenic guest molecules into the metalla-assembly will be tested. The biological activity of the herein synthesized complexes will be examined by the group of Prof. Paul Dyson at the EPFL in Lausanne, Switzerland.

5. SYNTHETIC STRATEGY

The synthesis of arene-ruthenium assemblies starts with the preparation of a ruthenium precursor which is obtained from $RuCl_3 \cdot n\ H_2O$ and a cyclic diene. Two of the four chlorine atoms of the precursor act as bridging ligands to connect the two ruthenium metal centers and the cyclic diene becomes the arene that coordinates to the metal center with a hapticity of 6. In the second step of the synthetic pathway, the spacer ligand is introduced. In scheme 5 the spacer ligand is illustrated as an orange square and its corners represent heteroatoms that are able to undergo coordination with the metal center. Spacer ligands are for example bis-bidentate ligands with the ability to bind two metal centers. In the last step the panel ligand, which is depicted as blue triangles is inserted. It is able to coordinate several clips to form a hexa-nuclear prism.

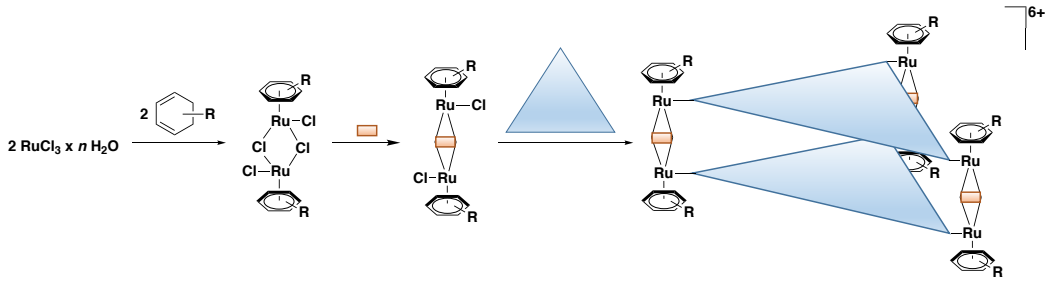

Scheme 5: Simplified synthesis of an hexa-nuclear arene-ruthenium prism. Orange bar: spacer ligand; blue triangle: tridentate panel ligand.

In this project, we mainly focused our attention on the preparation of spacer ligands, in view to increase the size and molecular weight of the metalla-assemblies.

5.1. MODIFICATION OF SPACER LIGANDS

5.1.1. Oxalamides

Oxalamides are structurally similar to oxalate, which have already presented to be suitable spacer ligands as shown in figure 25. Like oxalate, they possess four heteroatoms on two neighboring carbons, which allows coordination to two metal centers by creating a chelating complex (molecular clip). The advantage of oxalamides as compared to oxalate is their facility to be functionalized. In both cases the spacer ligands must be doubly deprotonated in order to be able to undergo coordination with the metal centers. The oxalate possesses no substituents other than the carboxylic acid functions on both carbons. Therefore, there is no possibility to further modify this ligand. Oxalamides on the other hand, are easily functionalized, owning to

the presence of the nitrogen atoms. Therefore, there is room for a substituent on the nitrogen atom. Once the ligand is deprotonated, the negative charge is delocalized between the heteroatoms, which will result in a coordination between the ligand and the metal center to form a stable chelate complex. Oxalamides have already been used for the formation of molecular clips.[162] Figure 32 illustrates two molecular clips that were synthesized previously, [(η^6-*p*-cymene)$_2$Ru$_2$(μ_4-N^1,N^2-bis(2-hydroxyethyl)oxalamide)Cl$_2$] (**1**) and [(η^6-*p*-cymene)$_2$Ru$_2$(μ_4-N^1,N^2-bis(2-(2-hydroxyethoxy)ethyl)oxalamide)Cl$_2$] (**2**). Oxalamides are bis-(bidentate ligands) and they are symmetrical ligands.

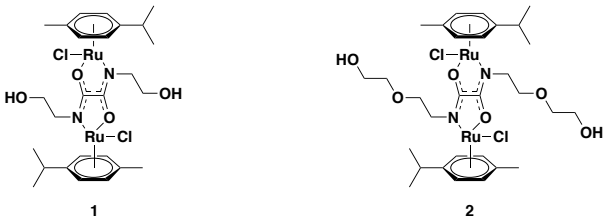

Figure 32: Molecular clips synthesized by our group using oxalamides as spacer ligands.[162]

Scheme 6 depicts the synthesis of four oxalamides (**3** - **6**), which are easily prepared in a one-step reaction starting from oxalyl chloride and the commercially available amine.[163] The ligands N^1,N^2-dihexyloxalamide (**3**) and N^1,N^2-dioctyloxalamide (**4**) were synthesized in excellent yields, whereas N^1,N^2-didecyloxalamide (**5**) and N^1,N^2-ditetradecyloxalamide (**6**) were isolated in lower yields. It was shown that the yields decreased with longer alkyl chains. This can be explained by the presence of the long alkyl chains that reduce solubility. To resolve this issue, hydrophilic functions were added to the structure.

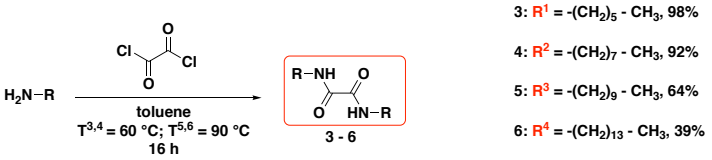

*Scheme 6: Oxalamides ligands **3** - **6**.*[163]

5.1.2. Pegylated Oxalamides

As mentioned on page 21, PEG chains possess many features that are interesting in biological applications. PEG chains are known to be non-toxic and non-immunogenic, therefore the therapeutic index can be increased. Furthermore, they increase the overall solubility and stability of the compound, prevent rapid clearance of small molecules and can increase the plasma residence of certain drugs.[77,96,164,165] Therefore, in the second series of ligands, PEG chains are introduced, similar to those shown in figure 32.

As presented in scheme 7, the synthetic pathway started with the commercially available 2-(2-(2-chloroethoxy)ethoxy)ethan-1-ol (**PEG 1**). First, the chloride is converted into the azide, and then reduced in a Staudinger reaction into the corresponding amine. This pegylated amine (**PEG 2**) then allowed to react with oxalyl chloride to obtain the desired ligand N^1,N^2-bis(2-(2-(2-hydroxyethoxy)ethoxy)ethyl)oxalamide (**7**). Separation of this ligand from $NEt_3 \cdot HCl$ was challenging, however, in earlier reports of similar compounds, the presence of $NEt_3 \cdot HCl$ was also observed in the final product.[162] The yield is rather poor with 14%, which might be explained by the possible formation of polymers.

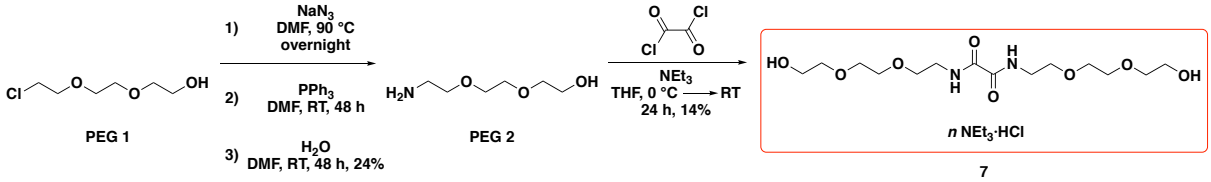

*Scheme 7: Synthesis of pegylated ligands N^1,N^2-bis(2-(2-(2-hydroxyethoxy)ethoxy)ethyl)oxalamide (**7**).*[166]

5.1.3. Diazene Dicarboxylates and Hydrazine Dicarboxylates

The synthesis of a diazene carboxylate derivative as spacer ligand for the formation of a molecular clip has been reported.[162] Diethyldiazene-1,2-dicarboxylate was used as spacer ligand to form the molecular clip $[(\eta^6\text{-}p\text{-cymene})_2Ru_2(\mu_4\text{-diethyl diazene-1,2-dicarboxylate})Cl_2]$ (**8**) (figure 33).

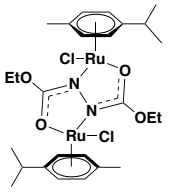

*Figure 33:Molecular clip **8** formed from diazene carboxylate or hydrazine dicarboxylates as spacer ligand.*[162]

Diazene dicarboxylates are synthesized in a two-step reaction starting from hydrazine and the commercially available chloroformate to form the hydrazine dicarboxylates (**9** and **10**). Then, they are oxidized to the desired diazene dicarboxylate ligands **11** and **12** with NBS. A shorter analog of such ligands is used to form clip **8**, however the ligands **9** and **10** might also be interesting for the formation of molecular clips. Therefore, they were considered as potential spacer ligands as well (scheme 8).

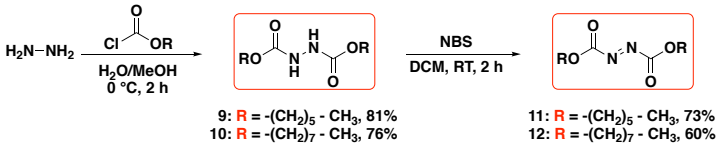

*Scheme 8: Hydrazine dicarboxylates (**9**, **10**) and diazene dicarboxylates (**11**, **12**) as spacer ligands.*[167]

5.1.4. Diazenes Diacyls and Hydrazines Diacyls

The next type of ligands is very similar to those shown in scheme 8. However, in this case, the dicarboxylate functions next to the hydrazine and diazene function are replaced by carbonyl functions in order to obtain molecular clips such as **13** (figure 34).

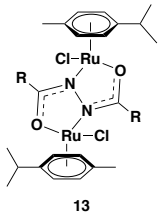

13

Figure 34: Molecular clips obtained from diazene diacyls or hydrazine diacyls.

Scheme 9 shows the synthesis of the ligands starting from hydrazine. Two synthetic pathways are depicted. The top pathway involves an anhydride and the bottom pathway involves an acid chloride. Both pathways provide the same hydrazine derivatives **14** and **15** in excellent yields, which might be potential ligands. In the second step, the hydrazine derivatives are oxidized using $Pb(OAc)_4$ to form the respective diazene compounds **16** and **17**. Diazenes **16** and **17** are structurally similar to **12**, of which the diethyl analog has already demonstrated to be a suitable ligand for the formation of clip **8**.[162]

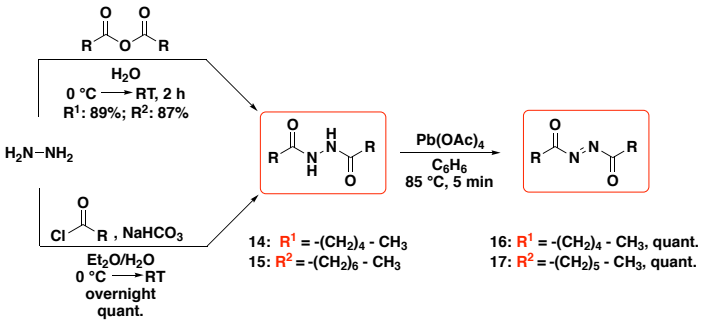

Scheme 9: Diazene diacyls or hydrazine diacyls as spacer ligands.[168–171]

5.1.5. Dihydroxybenzoquinones

2,5-Dihydroxybenzoquinones (dhbq) are another type of spacer ligands to form clip-like complexes. They possess two hydroxy groups in a *para* position and two carbonyl functions as well in a *para* position to each other. Therefore, they are able to coordinate two metal centers

to form a chelating complex. Accordingly, functionalized dhbq derivatives can be exploited to increase the size of molecular clips. As illustrated in figure 35, several dinuclear ruthenium complexes [(η^6-*p*-cymene)$_2$Ru$_2$(μ_4-R-dhbq-R')Cl$_2$] (**18**) have already been synthesized and reported.[172]

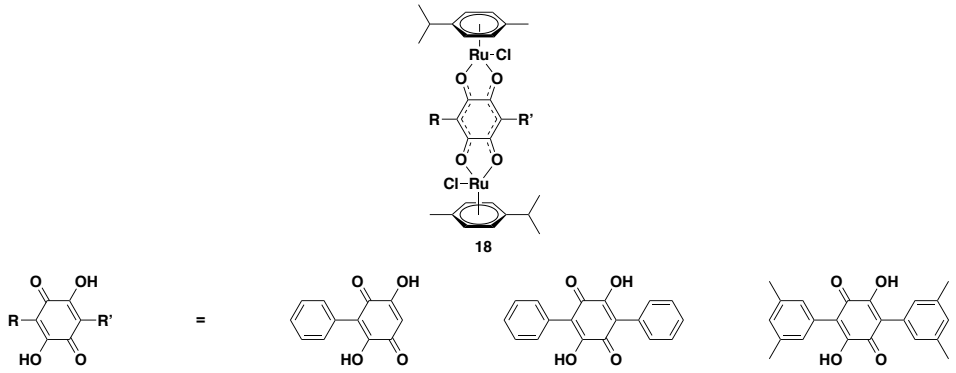

Figure 35: Molecular clips containing a variety of dhbq derivatives as spacer ligands.[172]

5.1.5.1. Preparation of dhbq Ligands via Cross-Coupling Reactions

An approach to obtain modified dhbq ligands is *via* a Suzuki cross-coupling reaction. As illustrated in scheme 10, 3-bromo-2,5-dimethoxycyclohexa-2,5-diene-1,4-dione (**20**) and 2,5-dibromo-3,6-dimethoxycyclohexa-2,5-diene-1,4-dione (**21**) are two suitable candidates for a Suzuki cross-coupling reaction in view to increase the size and weight of molecular clips. Furthermore, **20** and **21** are prepared in a straightforward two step reaction from dhbq *via* 2,5-dimethoxycyclohexa-2,5-diene-1,4-dione (**19**). The Suzuki cross-coupling is performed once or twice on these molecules. Such cross-coupling reactions on **20** and **21** have already been reported.[173] Then after deprotection, the dhbq derivatives are obtained and ready to react with the arene ruthenium complexes.

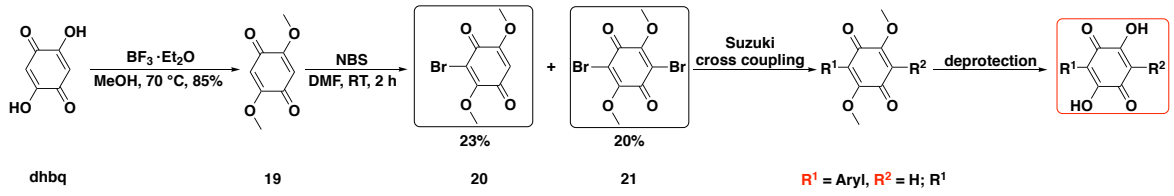

*Scheme 10: Synthesis of 3-bromo-2,5-dimethoxycyclohexa-2,5-diene-1,4-dione (**20**) and 2,5-dibromo-3,6-dimethoxycyclohexa-2,5-diene-1,4-dione (**21**).*[174]

Figure 36 depicts the general structure of the dhbq derivatives and ligands after functionalization of intermediates **20** or **21**. The basic scaffold is shown in blue and will remain the same during the reaction sequences shown in this chapter. The R^1 substituent represents the aryl moiety from the Suzuki cross-coupling reaction. If the dibromobenzoquinone **21** is used for the Suzuki cross-coupling, R^2 is identical to R^1 whereas, if the monobromobenzoquinone

20 is used R^2 represents a hydrogen atom. R^3 represents a methyl group for the protected hydroxy groups and hydrogen atom for the free hydroxy groups. This general structure is valid for the following sequence and the substituents are not outlined again in the figures.

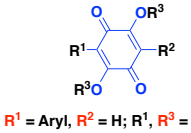

Figure 36: General structure of dhbq derivatives and dhbq ligands after Suzuki cross-coupling.

PEG is known to possess numerous beneficial properties from the biological and medicinal point of view, therefore the preparation of PEG containing ligands are of special interest in this project. Furthermore, by increasing the size, solubility is often an issue, however, PEG chains can counteract this effect.

Scheme 11 illustrates the retrosynthesis of the functionalized dhbq **22**. The proposed retrosynthesis of **22** involves a four steps reaction sequence. As depicted, the desired dhbq ligand was modified at its 3 and 6 positions and its dhbq-coordination sites are maintained, which are crucial for the formation of the clip. Two different methods for the synthesis of **22** are shown in scheme 11. Route A suggests 4-bromobenzamide (**26**) as starting material, whereas in route B 4-bromobenzoyl chloride (**27**) is used as starting material. In both cases a PEG chain is added to form the amide bond, while in route A, the PEG acts as electrophile and in route B the PEG acts as nucleophile to obtain intermediate **25**. In the second step the boronic ester (**24**) is prepared *via* Miyaura borylation. In the following step the Suzuki cross-coupling is performed between the boronic ester **24** and monobromo- **20** or dibromobenzoquinone **21** (scheme 10) to form **23** and in the final step the hydroxy groups are deprotected in order to obtain **22**.

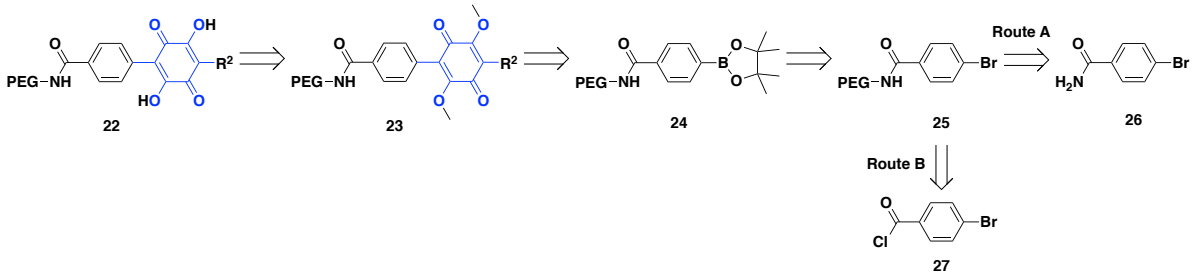

*Scheme 11: Retrosynthesis of dhbq derivative as potential ligand starting from 4-bromobenzamide (**26**) or 4-bromobenzoyl chloride (**27**), R^2 = H; R^1.*

Route A of scheme 12 shows the synthetic attempt to prepare ligand **25**[a,b,c] from **26**. NaH was used as a base to deprotonate amide **26**. The commercially available 2-(2-(2-

chloroethoxy)ethoxy)ethanol (**PEG 1**) was used as the first electrophile with chlorine as leaving group to form amide **25**[a]. However, the desired product was not obtained and only starting material was recovered. Therefore, the reactivity of the PEG was increased by replacing the chlorine with iodine (**PEG 3**) in a Finkelstein reaction. Since there was still no conversion observed, a *tert*-butyldimethylsilyl protected (**PEG 4**) and a methyl protected (**PEG 6**) electrophile were used. However, the preparation of the desired amides **25**[b] and **25**[c] was also unsuccessful. The deprotonation of the amide group might have been the problem causing the failure of this reaction.

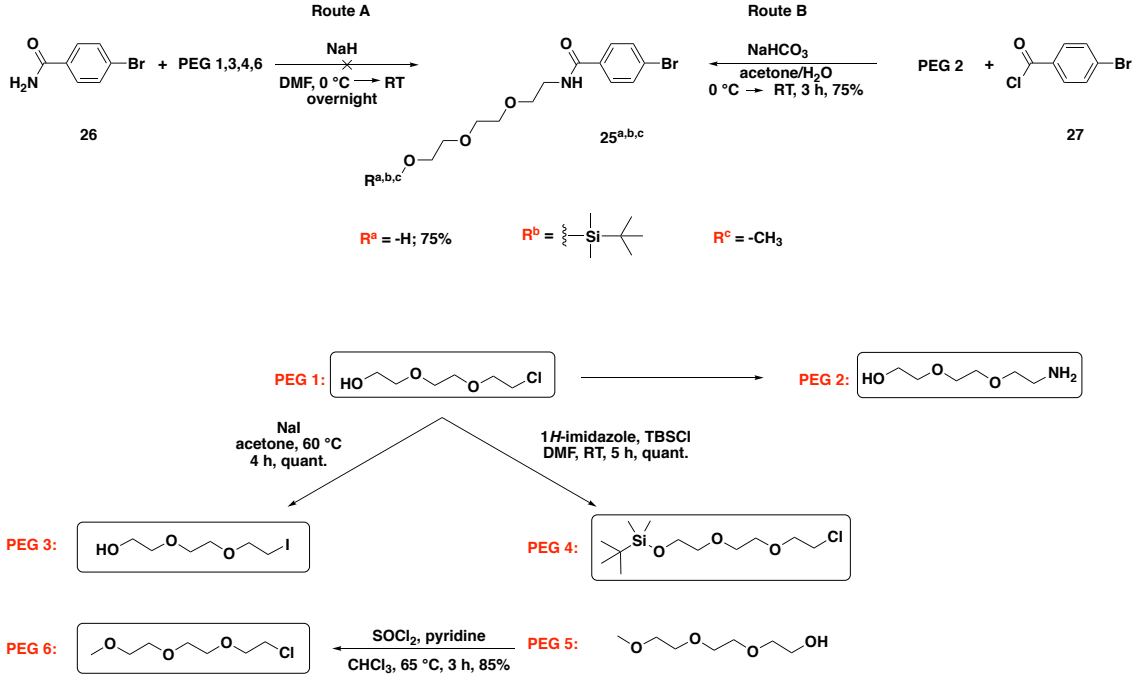

*Scheme 12: Route a): Attempts to prepare 4-bromo-N-(PEG)benzamide (**25**[a,b,c]) from 4-bromobenzamide (**26**) using commercially available 2-(2-(2-chloroethoxy)ethoxy)ethan-1-ol (**PEG 1**), and the prepared 2-(2-(2-iodoethoxy)ethoxy)ethan-1-ol (**PEG 3**),[175] 12-chloro-2,2,3,3-tetramethyl-4,7,10-trioxa-3-siladodecane (**PEG 4**)[176] and 1-chloro-2-(2-(2-methoxyethoxy)ethoxy)ethane (**PEG 6**).[177] Route b) Synthesis of **25**[a] from 4-bromobenzoyl chloride (**27**) and 2-(2-(2-aminoethoxy)ethoxy)ethan-1-ol (**PEG 2**).[166]*

As shown in route B of scheme 12 the reaction was repeated with 4-bromobenzoyl chloride (**27**) as starting material and the previously synthesized 2-(2-(2-aminoethoxy)ethoxy)ethan-1-ol (**PEG 2**) (scheme 7) was used as nucleophile. The reaction was performed under basic conditions in a mixture of acetone and dist. H_2O at RT according to a patent[178] for a similar reaction and amide **25**[a] was obtained in a good yield of 75%.

In the next step the Miyaura borylation was performed using **25**[a] according to another patent in 1,4-dioxane at 80 °C in the presence of KOAc and Pd(II)(dppf)Cl_2.[179] However, the boronic

ester **24[a]** was not obtained under these conditions even after extended reaction time and the utilization of various bases and different Pd-catalysts (scheme 13). NMR analysis of the reactions showed a complex mixture containing the product of proto-demetalation, unreacted starting materials and unidentified byproducts.

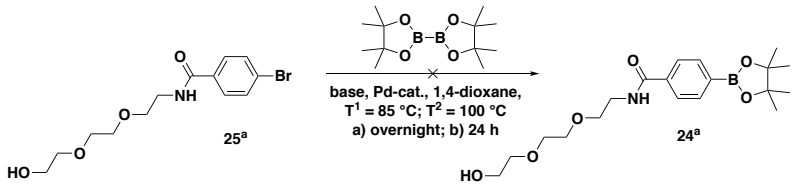

*Scheme 13: Attempt to prepare N-(2-(2-(2-hydroxyethoxy)ethoxy)ethyl)-4-(4,4,5,5-tetramethyl-1,3,2-dioxaborolan-2-yl)benzamide (**24[a]**). Pd-cat: Pd(II)(dppf)Cl_2, Pd(0)$(PPh_3)_4$, XPhosPdG2; base: KOAc, NaOAc.*

Since the preparation of the boronic ester **24[a]** was not successful, in the next example commercially available boronic esters are used and the Suzuki cross-coupling reaction is carried out in the first step with **20** or **21** as shown in scheme 14. In route A the boronic ester (4-(methoxycarbonyl)phenyl)boronic acid (**28**) is used to form ester **29**. The ester group of **29** could then be converted to the acid chloride and the nucleophilic attack of **PEG 2** would result in an amide bond to obtain **23[a]**. The Suzuki cross-coupling reaction was tested in 1,4-dioxane using nickel and palladium catalysts in combination with different bases, however compound **29** was not obtained under these conditions, even after extended reaction times and higher temperatures. Route B describes the Suzuki cross-coupling reaction using (4-hydroxyphenyl)boronic acid (**31**) to form the phenol **32**. The nucleophilic attack of the deprotonated phenol **32** on the electrophilic PEGs **1**, **3**, **4**, **6** would result in the formation of **33[a]** or **33[b,c]**. The same conditions like for the preparation of **29** were tested, however, also in this case the reaction was not successful and intermediate **32** was not obtained.

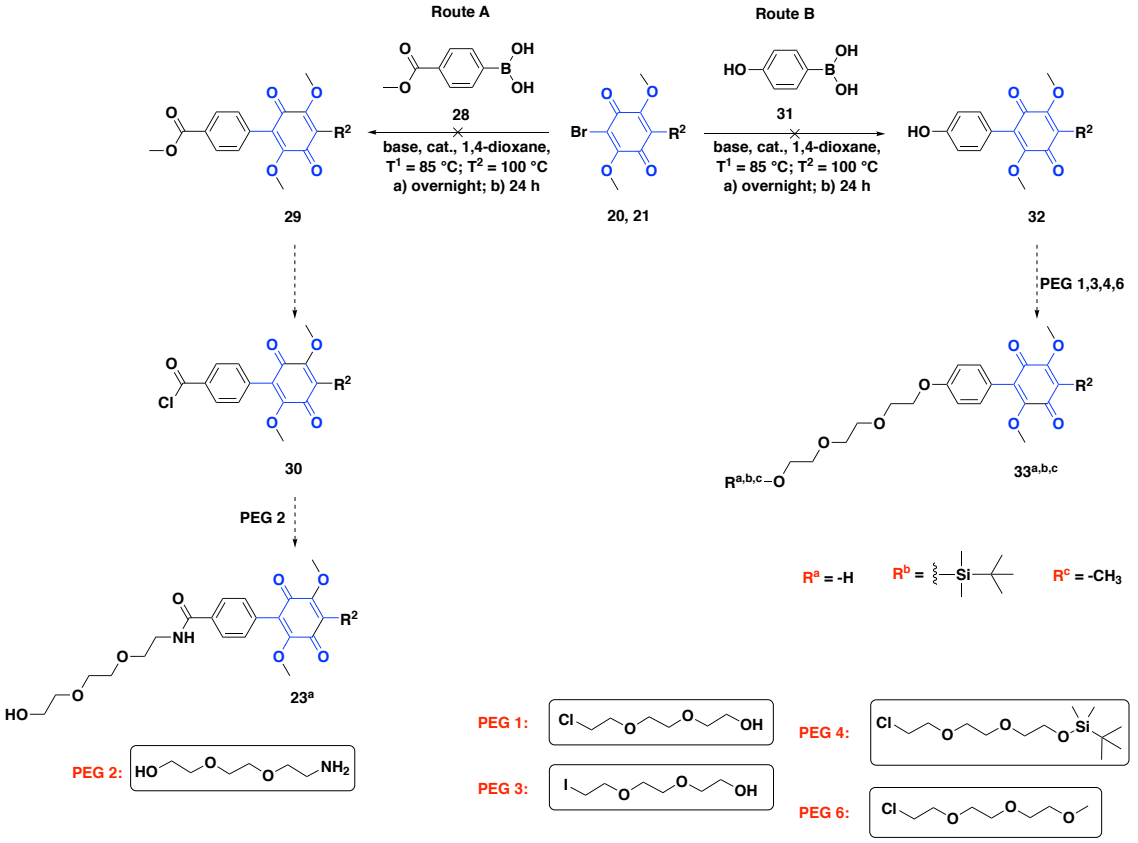

*Scheme 14: Suzuki cross-coupling reaction of **20** and **21** with boronic esters (4-(methoxycarbonyl)phenyl)boronic acid (**28**) and (4-hydroxyphenyl)boronic acid (**31**). Cat: $Ni(II)(PPh_3)_2Cl_2$, $Pd(0)(PPh_3)_4$, $Pd(II)(dppf)Cl_2$, XPhosPdG2; base: K_2CO_3, Na_2CO_3, CsF; R^2 = H; R^1.*

NMR analysis of the crude products showed a complex mixture containing the product of proto-demetalation, unreacted starting materials and unidentified byproducts. Furthermore, NMR analysis of the commercially available starting materials showed several impurities, which might have caused the failing of the reaction.

5.1.5.2. Embelin Derivatives as dhbq Ligands

Embelin as well, is a derivative of 2,5-dihydroxybenzoquinone (dhbq) with a $-C_{11}H_{23}$ alkyl chain attached at the three position of the six-membered ring (figure 37). Its IUPAC name is 2,5-dihydroxy-3-undecylcyclohexa-2,5-diene-1,4-dione and as a dhbq derivative it is also a potential ligand to form arene-ruthenium metalla-assemblies. Embelin is isolated from the fruit of *Embelia ribes* that grows in India and was used for the treatment of fever, inflammatory and gastrointestinal diseases for centuries.[180] Embelin derivatives were of special interest for this project, as embelin has shown further interesting biological activities like analgesic, anti-inflammatory, anti-diabetic effects and it also possesses anti-tumor properties.[181–185]

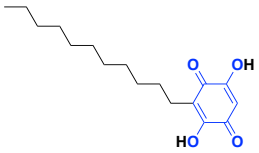

Figure 37: Structure of embelin.

For this project, we were interested in enlarging the structure of embelin by attaching a longer chain and the combined procedures for the synthesis of embelin published by Chen and co-workers and Filosa and co-workers were used to synthesize a new derivative, as shown in scheme 15 below.[186,187] The synthetic pathway starts with dhbq, which is converted to 2,5-dimethoxybenzoquinone under acidic condition and in the presence of MeOH. This intermediate is then reduced to 2,5-dimethoxybenzene-1,4-diol (**34**) using $Na_2S_2O_4$. In the following step the resulting hydroxy groups were converted to methoxy groups using MeI to obtain 1,2,4,5-tetramethoxybenzene (**35**). *n*-BuLi was used to deprotonate the aromatic proton, followed by a lithium-halogen exchange with 1-bromoicosane to form icosane derivative **36**. This reaction was followed by the oxidation with CAN to form the quinone 3-icosyl-2,5-dimethoxycyclohexa-2,5-diene-1,4-dione **37**. In the last step both methoxy groups were converted into free alcohols to obtain the desired ligand (**38**) in an overall yield of 17%.

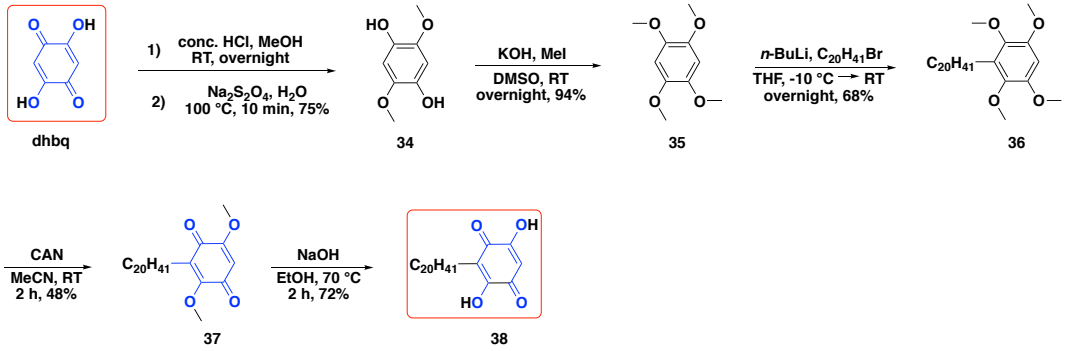

Scheme 15: Synthesis of the icosyl derivative of embelin.[186,187]

The synthesis of **36**, **37** and **38** were the critical steps in this reaction sequence, nevertheless all three compounds were successfully prepared. The published yields for the undecan analogues to form embelin were 70%, 60% and 80%, respectively, resulting in an overall yield of 24%. This implies that a chain of almost twice the size does not interfere significantly in the reaction process.

After the successful synthesis of 2,5-dihydroxy-3-icosylcyclohexa-2,5-diene-1,4-dione (**38**), the preparation of other derivatives was attempted using the same procedure. Scheme 15 shows that compound 1,2,4,5-tetramethoxybenzene (**35**) is the key intermediate in this reaction. The

reaction with *n*-BuLi and a suitable electrophile allows the formation of the monosubstituted tetramethoxybenzene analouges **38**. Subsequent oxidation and deprotection reestablish the dihydroxy quinone functionality, required for clip formation. Therefore, several PEG-molecules were tested as potential electrophiles under the same conditions as illustrated for the preparation of **36** in scheme 15. The electrophiles **PEG 4** and **PEG 6** were previously synthesized and used for the attempt to synthesize amides **25**^{b} and **25**^{c} as shown in route A of scheme 12. The bromine **PEG 7** was prepared from the respective alcohol **PEG 5** using molecular bromine and triphenylphosphine. **PEG 7** possesses a higher electrophilic character than **PEG 6** owning to the bromine, which is a better leaving group than chlorine. The reaction to attach a PEG chain was performed in dry THF, where *n*-BuLi was added at - 10 °C and the reaction was allowed to warm to RT. However, under these conditions the monosubstituted tetramethoxybenzene derivatives **39**^{a,b} were not obtained, therefore the reaction was repeated and the reaction was heated to 65 °C. The reaction to attach a PEG chain was not successful and the attempt to further functionalize 1,2,4,5-tetramethoxybenzene (**35**) with PEG moieties failed.

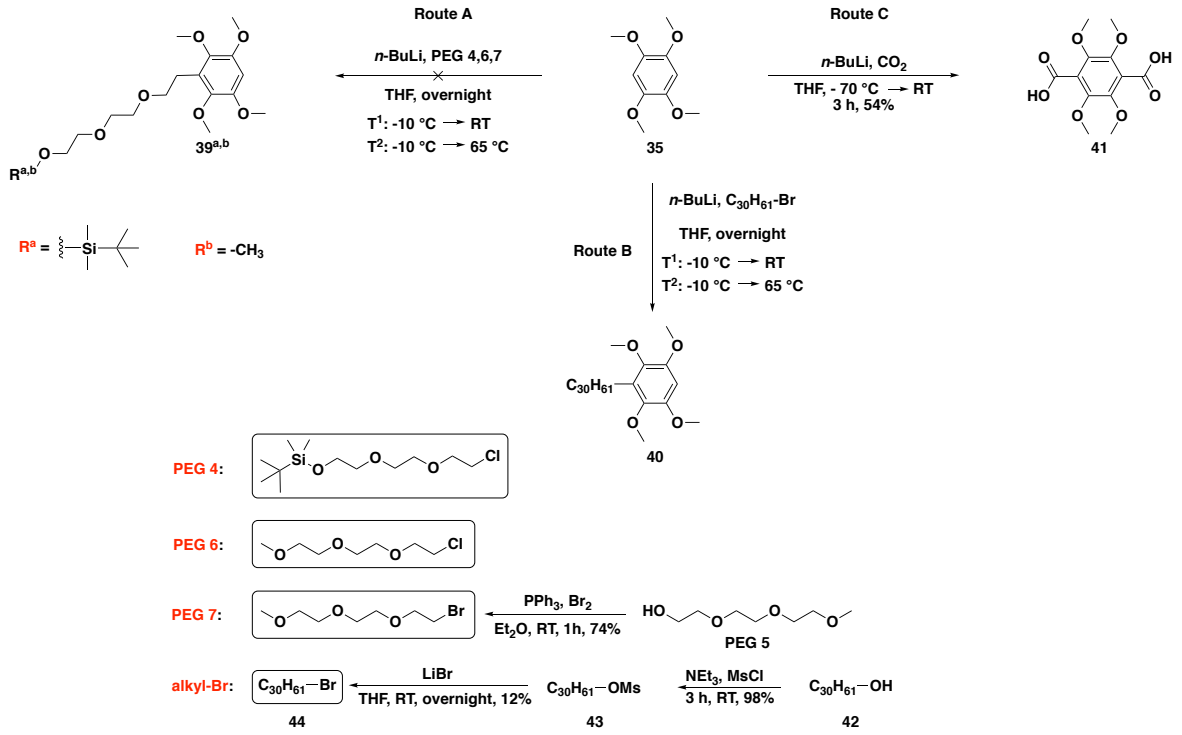

*Scheme 16: Attempt to attach different substituents to key intermediate **35** using various PEG chains: 12-chloro-2,2,3,3-tetramethyl-4,7,10-trioxa-3-siladodecane (**PEG 4**), 1-chloro-2-(2-(2-methoxyethoxy)ethoxy)ethane (**PEG 6**) and 1-bromo-2-(2-(2-methoxyethoxy)ethane (**PEG 7**)[188] (Route A); alkyl chains: 1-bromotriacontane[189] (Route B); and the synthesis of 2,3,5,6-tetramethoxyterephtalic acid (**41**)[190] (Route C).*

Since the introduction of the icosyl alkyl chain, using 1-bromoicosane worked under these conditions, in the next attempt, 1-bromotriacontane (**44**) was used as an electrophile to insert a triacontyl chain, containing 30 carbons (Route B). Bromine **44** was synthesized from the respective alcohol **42**, *via* mesylate intermediate **43**. The reaction was performed at RT and at 65 °C, however, **40** was not obtained. In this case the alkyl chain might be too long, causing solubility problems, which resulted in the failure of this reaction. Nevertheless, as shown in route C of scheme 16, the introduction of CO_2 using dry ice under similar conditions, to synthesize 1,2,4,5-tetramethoxyterephtalic acid (**41**) was successful.[190] Since the direct attachment of PEG chains was unsuccessful, dicarboxylic acid **41** offers a useful intermediate to introduce PEG chains *via* amide bond formation.

The synthesis of **41** was accomplished according to published methods of Mathison and co-workers.[190] To perform the amide coupling, 2-(2-(2-methoxyethoxy)ethoxy)ethan-1-amine (**PEG 8**) was synthesized from the previously used **PEG 6** (scheme 12 and 16), which was first converted to the respective azide and then reduced in a Staudinger reduction to the desired amine **PEG 8**, as shown in scheme 17 and several published conditions were tested to synthesize **45**. In a first attempt, a one pot reaction using thionyl chloride was performed to convert the dicarboxylic acid into acid chlorides to increase the reactivity, but the desired diamide **45** was not obtained. In a second attempt, the coupling was performed using dicyclohexylcarbodiimide (DCC), which is a very popular coupling reagent for the formation of amide bonds, but here again, the reaction was not successful. The coupling with DCC was repeated under two different conditions (b, c). Conditions d) and e) are normally used for esterifications. First, 4-dimethylaminopyridine (DMAP) was added as catalyst and second, 1,4-dimethylpyridinium *p*-toluenesulfonate (DPTS) was added as catalyst. However, the coupling failed. At last, the amide coupling was performed in the presence of 1-[bis(dimethylamino)methylene]-1*H*-1,2,3-triazolo[4,5-*b*]pyridinium 3-oxid hexafluorophosphate (HATU), which is also a known coupling reagent (condition f). However also here, the coupling failed and only starting materials were isolated.

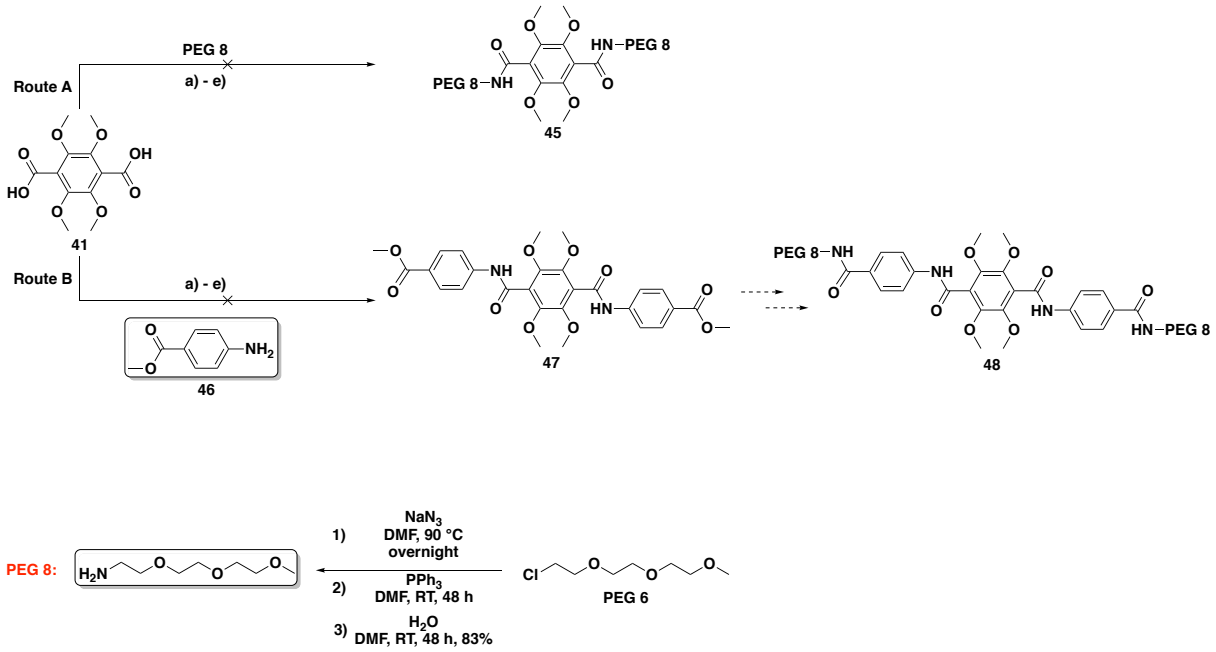

*Scheme 17: Attempt to prepare 2,3,5,6-tetramethoxy-N^1,N^4-bis(2-(2-(2-methoxyethoxy)ethoxy)ethyl)terephthalamide (**45**) and attempt to synthesize dimethyl 4,4'-((2,3,5,6-tetramethoxyterephthaloyl)bis(azanediyl))dibenzoate (**47**) from 2,3,5,6-tetramethoxyterephtalic acid **41** and 2-(2-(2-methoxyethoxy)ethoxy)ethan-1-amine (**PEG 8**) according to published methods.[191–196] a) $SOCl_2$, DCM, RT, overnight; b) DCC, $CHCl_3$, 60 °C, overnight; c) DCC, DMAP, $CHCl_3$, 60 °C, overnight; d) DCC, DMAP, DCM, RT, overnight; e) DCC, DPTS, DCM, RT, overnight f) HATU, DIPEA, DMF, RT, overnight.*

Since the direct attachment of a PEG chain failed again, in the next attempt methyl 4-aminobenzoate (**46**) was added as linker, in order to link dicarboxylic acid **41** with a PEG chain as shown in Route B of scheme 17. Also in this case, the amide bond is formed between the dicarboxylic acid **41** and the commercially available amide **46** to obtain the intermediate **47**. The ester group of **47** can then be converted to the acid chloride, which could form another amide bond with **PEG 8** to obtain **48**. However, previously used conditions a) - f) did not lead to the formation of the desired product **47**, only starting materials were recovered. There is no report of syntheses and isolations of similar compounds, which leads to the assumption that this synthetic approach is very challenging.

5.2. PREPARATION OF MOLECULAR CLIPS

Molecular clips are building blocks of the multi-nuclear prisms, cubes and rectangles, which consist of two arene ruthenium metal centers that are bridged by a spacer ligand. The syntheses of thirteen potential spacer ligands (**3 - 6**, **9 - 12**, **14 - 17, 38**) were illustrated in the previous chapter and their ability to form a molecular clip has been tested. Before the preparation of the molecular clip, a precursor (**49**) must be synthesized.

5.2.1. Molecular Clip with Oxalamide **3**

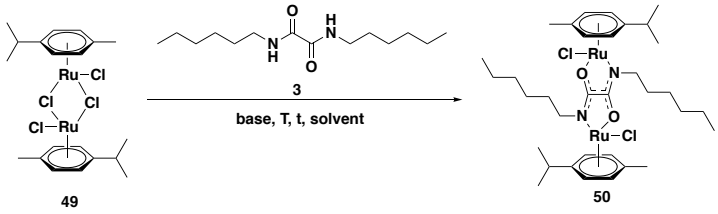

*Scheme 18: Preparation of molecular clip [(η^6-p-cymene)$_2$Ru$_2$(μ_4-N^1,N^2-dihexyloxalamide)Cl$_2$] (**50**).*

In figure 32 two examples of molecular clips prepared by our group, containing oxalamides as spacer ligands are shown.[162] That reaction was performed in MeOH under reflux and NaOAc was used as base. The same condition were tested for the preparation of clip **50 (**scheme 18). However, the molecular clip was not formed, even after extended reaction time. Therefore, different conditions were tested, which are summarized in table 6.

entry	*solvent*	*T [°C]*	*t [h]*	*base*	*yield [%]*
1	*MeOH*	*60*	*15*	*NaOAc*	*0*
2	*MeOH*	*60*	*24*	*NaOAc*	*0*
3	*MeOH*	*60*	*15*	*NEt_3*	*0*
4	*MeOH*	*60*	*24*	*NEt_3*	*0*
5	*EtOH*	*90*	*15*	*NaOAc*	*0*
6	*EtOH*	*80*	*24*	*NaOAc*	*0*
7	*EtOH*	*80*	*15*	*NEt_3*	*low*
8	*EtOH*	*80*	*24*	*NEt_3*	*low*
9	*EtOH*	*80*	*15*	*DIPEA*	*16*
10	*EtOH*	*80*	*24*	*DIPEA*	*25*
11	*EtOH*	*80*	*72*	*DIPEA*	*27*

*Table 6: Tested conditions for the synthesis of molecular clip [(η^6-p-cymene)$_2$Ru$_2$(μ_4-N^1,N^2-dihexyloxamide)Cl$_2$] (**50**).*

NEt_3, a stronger base was used, however there was no formation of the desired clip. Next, the solvent was changed from MeOH to EtOH (entry 5) and the reaction was performed at 90 °C. After 15 h the residue had decomposed and a black precipitate was observed, suggesting that the temperature was too high. So the reaction was repeated at 80 °C using first NaOAc and then NEt_3 as bases. No conversion was observed with NaOAc, but low conversion was observed for the reaction with NEt_3, but the purification of the crude product was not successful. To achieve better conversion, the base was exchanged from NEt_3 to DIPEA (entry 9) and the reaction was successful. The molecular clip [(η^6-*p*-cymene)$_2$Ru$_2$(μ_4-N^1,N^2-dihexyloxalamide)Cl$_2$] (**50**) was

prepared in EtOH at 80 °C with a low yield of 16%. Reaction time of 24 h yielded in 25% of conversion (entry 10) and further extended reaction times have only a small impact on the yield as shown in entry 11. The ^{1}H-NMR shows both *p*-cymene moieties and the hexyl chains with diastereomeric protons. Furthermore, the success of this synthesis was confirmed by ^{13}C-NMR IR, UV-VIS, ESI-MS and elemental analysis.

5.2.2. Molecular Clip with Oxalamide **4**

Then N^1,N^2-dioctyloxalamide (**4**) was used as bridging ligand and molecular clip [(η^6-*p*-cymene)$_2$Ru$_2$(μ_4-N^1,N^2-dioctyloxalamide)Cl$_2$] (**51**) was formed. At 80 °C, only traces of the desired clip were observed by ^{1}H-NMR analysis, therefore, the reaction was repeated at a higher temperature. At 90 °C the desired molecular clip **51** was obtained with a rather moderate yield of 21% (scheme 19). It seems, the longer the aliphatic chains, the higher the required temperature to achieve a conversion into the molecular clip. In contrast higher temperatures seem to promote decomposition of the molecule, this might be the reason for the low yield.

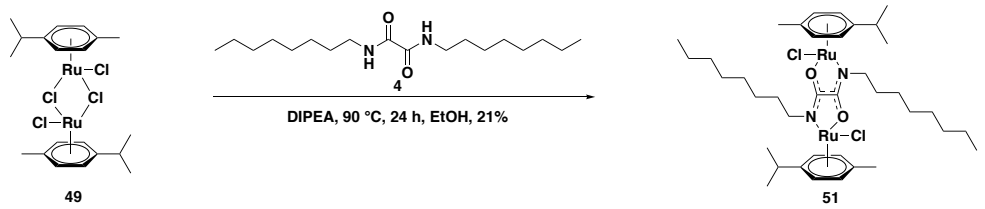

*Scheme 19: Synthesis of molecular clip [(η^6-p-cymene)$_2$Ru$_2$(μ_4-N^1,N^2-dioctyloxamide)Cl$_2$] (**51**).*

The ^{1}H-NMR spectra of both clips **50** and **51** look very similar, with only differences in the integrals of the aliphatic area. Figure 38 shows the ^{1}H-NMR spectra of molecular clip **51** recorded in $CDCl_3$. The signals for the aromatic hydrogens of *p*-cymene are shown as a multiplet at around 5.3 ppm and a doublet at 5.0 ppm with an integral of 6 and 2, respectively. The singlet at 2.12 ppm and the two doublets at 1.20 ppm and 1.16 ppm with an integral of six for each signal belong to the methyl groups and the *i*Pr groups of *p*-cymene. The two single protons of the *i*Pr groups of *p*-cymene are observed with a multiplicity of seven at 2.68 ppm. At around 4.0 ppm and 3.3 ppm two multiplets are shown with an integral of two for each. They belong to the CH_2 groups in the α-position to the nitrogen atom of the oxalamide moiety. An integral of two indicates that the hydrogen atoms are diastereotopic. The shape of the signal at about 1.6 ppm with an integral of four implies two overlying multiplets. This signal belongs to the CH_2 in β-position to the nitrogen. The remaining CH_2 groups of the chains arise as a

multiplet at around 1.3 ppm with an integral of 20 and the CH_3 groups is observed at around 0.9 ppm.

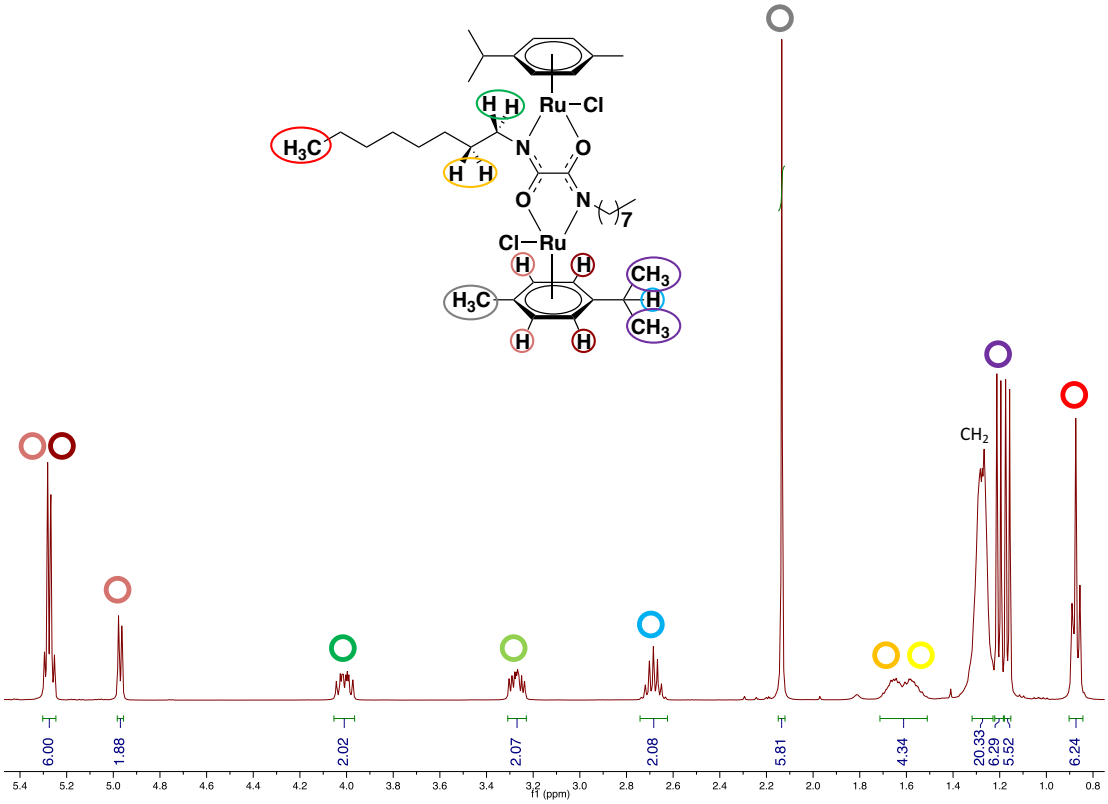

*Figure 38: ^{1}H-NMR spectra of molecular clip **51** (400 MHz, $CDCl_3$, RT).*

In Figure 39 the ^{13}C-NMR of clip **51**, recorded in $CDCl_3$ at RT is shown. The signal at 170.1 ppm belongs to the acyl group of the oxalamide moiety of the spacer ligand. The CH_2 group in the α-position of the nitrogen is observed at 51.7 ppm and the CH_3 group of the chains at 14.3 ppm. The remaining protons of the CH_2 chains are in the aliphatic area. The quaternary carbons of *p*-cymene are seen at 100.7 ppm and 94.4 ppm and the remaining aromatic carbons are observed between 82.5 and 79.5 ppm. The methyl groups of the *p*-cymene moieties are also detected at 22.6 and 22.2 ppm in the aliphatic area and all signals were assigned using 2D-NMR analysis.

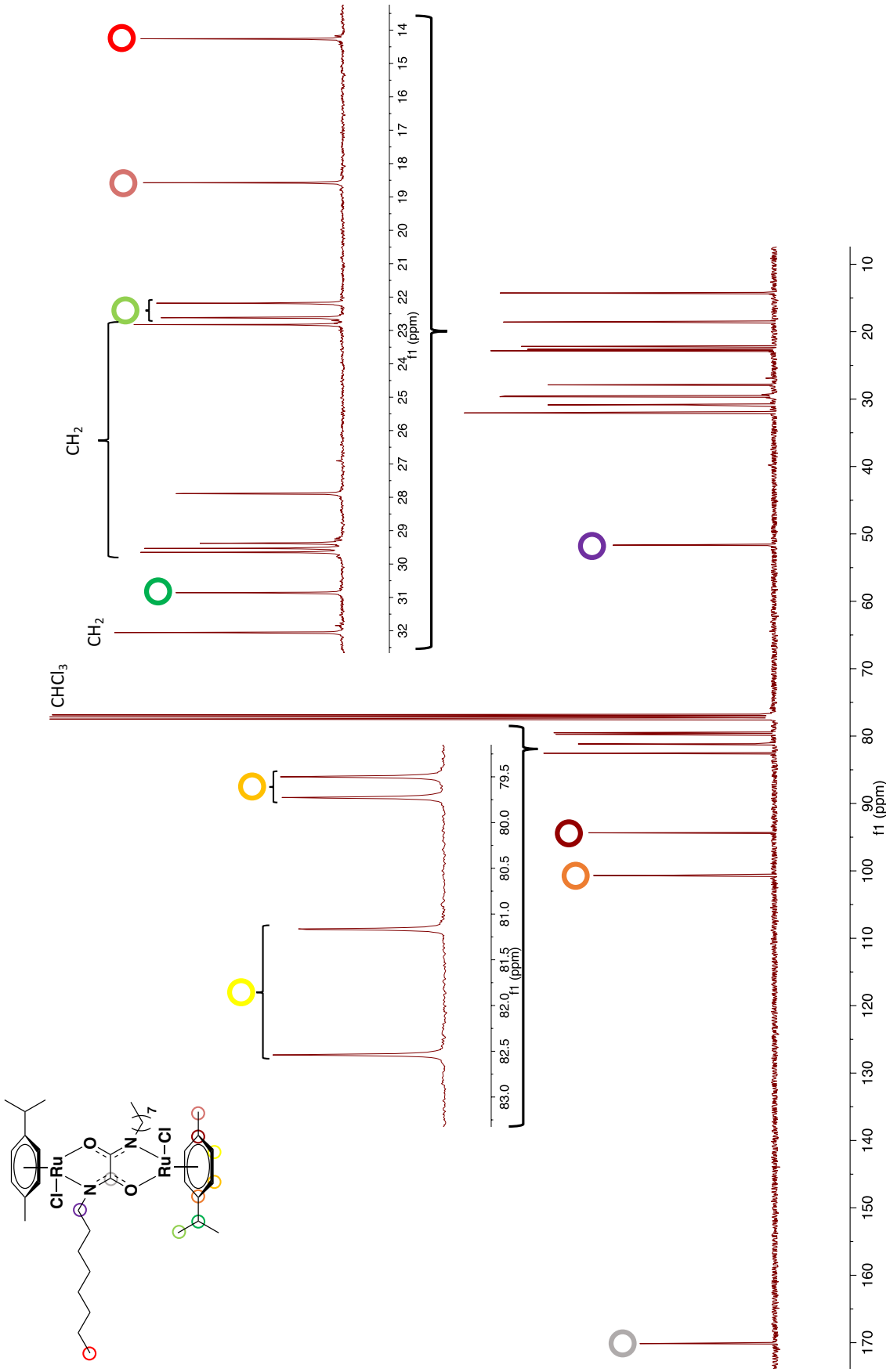

*Figure 39: ^{13}C-NMR spectra of molecular clip **51** (101 MHz, $CDCl_3$, RT).*

Figure 40 shows the crystal structure of molecular clip **51** with omitted hydrogen atoms for increased clarity. Both *p*-cymene moieties, both chlorines, as well as the octyl chains point in opposite directions. The distance between the two ruthenium metal centers is 5.6 Å, which is slightly longer when compared to the oxalate analogue with 5.5 Å. ESI-MS analysis showed the same peak ($[M - Cl]^+$) for both molecular clips **50** and **51** at m/*z* = 761.1 and 817.3, respectively and the elemental analysis proved the purity of the compounds.

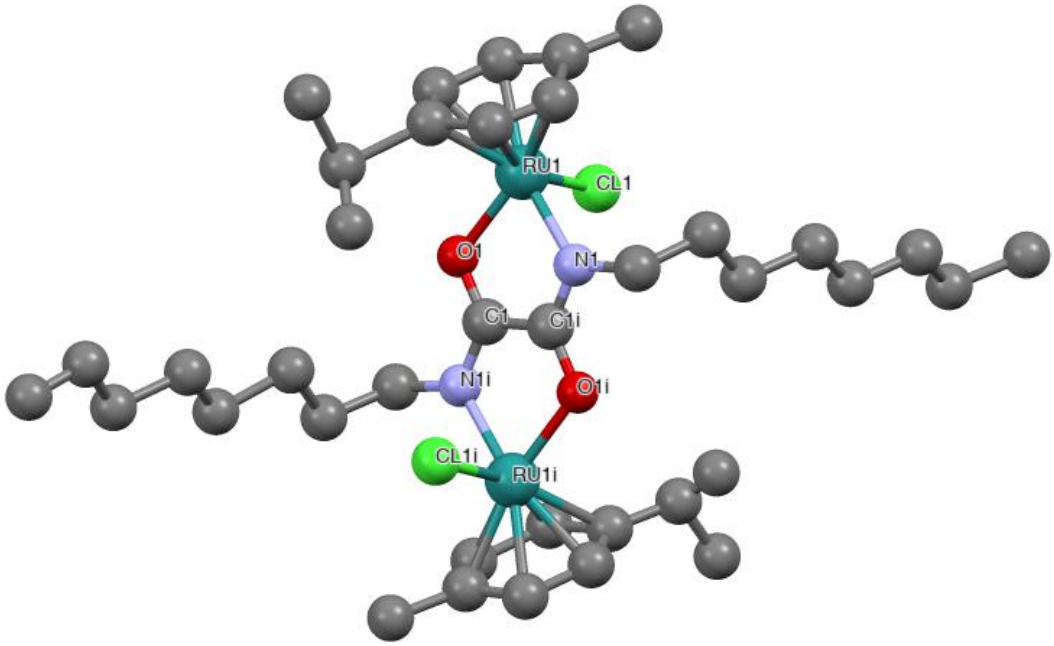

*Figure 40: Molecular structure of clip **51** with omitted hydrogen atoms for clarity. Selected bond lengths/(Å) and angles/(°): Ru(1)-Ru(1i) 5.556(2), Ru(1)-O(1) 2.114(5), Ru(1)-N(1) 2.089(4), Ru(1)-Cl(1) 2.400(2), O(1)-C(1) 1.297(1), N(1)-C(1i) 1.329(7), C(1)-C(1i) 1.459(1); O(1)-Ru(1)-N(1) 76.5(6), O(1)-Ru(1)-Cl(1) 85.6(0), N(1)-Ru(1)-Cl(1) 85.0(9), Ru(1)-N(1)-C(1i) 114.9(1), O(1)-C(1)-C(1i) 115.3(0), N(1)-C(1i)-C(1) 116.3(5), i = -X; -Y; -Z.*

Comparison of the IR spectra of the ligands **3** and **4** with the IR spectra of the respective clips **50** and **51** further proves the success of the reaction. The spectra of the ligands show clearly the bands representing the N-H stretching of secondary amines at around 3300 cm^{-1} which have disappeared in the spectra of the clips (experimental section).[197]

5.2.3. Molecular Clips with Oxalamide **5** and **6**

Molecular clips **50** and **51** were successfully synthesized with the oxalamides **3** and **4**. Herein, compounds **5** and **6** (scheme 6) are tested for their ability to act as spacer ligands for the formation of molecular clips. The same conditions as for the preparation of molecular clips **50** and **51** were applied (table 7), however only starting materials were isolated.

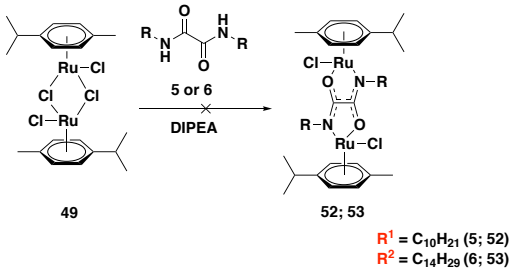

entry	*solvent*	*T [°C]*	*t [h]*	*base*	*yield [%]*
1	*EtOH*	*80*	*24*	*DIPEA*	*0*
2	*EtOH*	*90*	*24*	*DIPEA*	*0*
3	*BuOH*	*100*	*24*	*DIPEA*	*0*
4	*BuOH*	*110*	*24*	*DIPEA*	*0*

*Table 7: Attempt to synthesize molecular clips [(η^6-p-cymene)$_2$Ru$_2$(μ_4-N^1,N^2-didecyloxalamide)Cl$_2$ (**52**) and [(η^6-p-cymene)$_2$Ru$_2$(μ_4-N^1,N^2-ditetradecyloxalmide)Cl$_2$ (**53**) containing oxalamides **5** or **6**.*

The formation of **51** required a higher temperature than **50** due to the longer alkyl chain. In these cases, the chains are even longer, therefore, BuOH with a higher boiling point was used as solvent and the reaction was performed at 100 °C and 110 °C, however the desired clips **52** and **53** were not obtained, but decomposition of the starting material was observed at these temperatures.

5.2.4. Molecular Clip with PEGylated Oxalamide **7**

The syntheses of very similar clips, with PEG-monomers or PEG-dimers on each side of the oxalamide was realized in our group (figure 32).[162] Herein, an attempt to prepare a molecular clip from an oxalamide consisting of PEG-trimers on each side (**7**) was performed according to the published method for shorter chains; MeOH at RT, overnight and NaOAc as a base (scheme 20).[162] However, molecular clip **54** was not obtained, even after extended reaction time. Like previous examples, several conditions were systematically tested by changing the base, the solvent or the temperature. The stronger bases NEt_3 and DIPEA were used in order to deprotonate the oxalamide functionality. Since it failed, the reaction was carried out in MeOH under reflux, retesting all three bases, but the reaction was also unsuccessful. Therefore, MeOH was replaced with EtOH and the reaction was repeated at 80 °C and 90 °C. Again no molecular clip **54** was obtained. (scheme 20). The PEG chains are very flexible, which might cause interactions between the electronegative oxygen-atoms and the electropositive metal center, blocking the coordination site for the oxalamide functionality in order to form the clip.

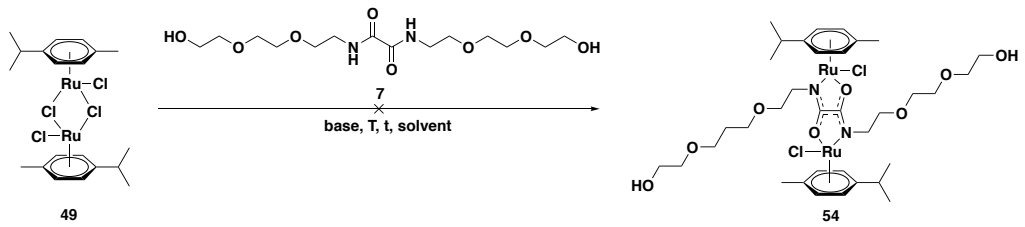

*Scheme 20: Attempt to synthesize molecular clip [(η^6-p-cymene)$_2$Ru$_2$(μ_4-N^1,N^2-bis(2-(2-(2-hydroxyethoxy)ethoxy)ethyl)oxalamide)Cl$_2$ (**54**). Base: NaOAc, NEt$_3$, DIPEA; T: RT, 65 °C, 80 °C, 90 °C; t = 15 h, 24 h; solvent: MeOH, EtOH.*

5.2.5. Molecular Clips from Diazene Dicarboxylates and Hydrazine Dicarboxylates

In this section the preparation of another type of molecular clips are shown using different spacer ligands. As shown in figure 33 molecular clip **8** is formed using the diethyldiazene-1,2-dicarboxylate as ligand. Herein we use derivatives of that diazene dicarboxylates **11** and **12** in order to form the larger molecular clips **55** and **56** (Route A, scheme 21). The chlorines of the precursor **49** are abstracted using $AgCF_3SO_3$, to create a coordination site in order to form the molecular clip with **11** and **12** as spacer ligands. Another possibility to synthesize the same molecular clips **55** and **56** is *via* the hydrazine dicarboxylates **9** and **10** (Route B). In the latter example, inorganic and organic bases are used to deprotonate the ligands.

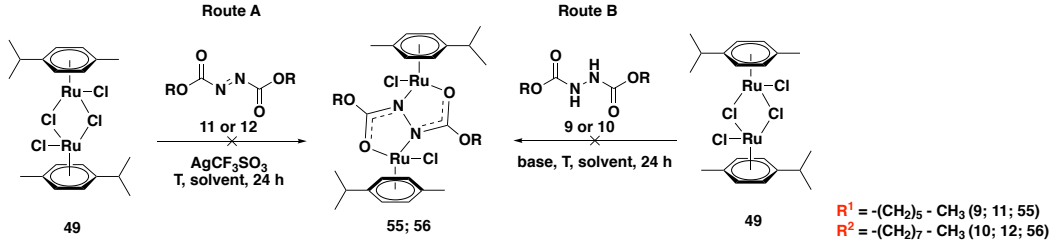

*Scheme 21: Attempt to synthesize molecular clips [(η^6-p-cymene)$_2$Ru$_2$(μ_4-dihexyl hydrazine-1,2-dicarboxylate)Cl$_2$ (**55**) and [(η^6-p-cymene)$_2$Ru$_2$(μ_4-dioctyl hydrazine-1,2-dicarboxylate)]Cl$_2$ (**56**) using diazene dicarboxylates **11** and **12** and hydrazine dicarboxylates **9** and **10** as spacer ligands. Base: NaOAc, NEt$_3$, DIPEA; solvent (T): MeOH (RT; 65 °C), EtOH (RT; 80 °C; 90 °C), DCM (RT; 40 °C), MeCN (RT; 80 °C), MeNO$_2$ (RT, 100 °C).*

To find the optimal conditions for the reaction, the conditions were systematically changed in respect of base, solvent and temperature (scheme 21). In Route A, all tested conditions were in the presence of $AgCF_3SO_3$ in MeOH, EtOH, DCM, MeCN or $MeNO_2$ as solvent. For each solvent the reactions were performed at RT and under reflux, additionally also at 80 °C for EtOH. However, clips **55** and **56** were not obtained. Route B starts from the hydrazine derivatives **9** and **10**. Herein, the same conditions as in route A were tested, in combination with the inorganic base NaOAc and the organic bases NEt_3 and DIPEA. But the reaction was unsuccessful and the synthesis of clips **55** and **56** was not observed. No reaction was observed

at RT, 40 °C and 65 °C. The formation of a complex mixture was observed for the reactions at 80 °C and decomposition occurred at higher temperatures.

5.2.6. Molecular Clips from Diazene and Hydrazines Diacyls

As discussed previously, molecular clip **8** (figure 33) is synthesized using diethyldiazene-1,2-dicarboxylate. The atoms involved in the bonding to the metal centers are the centered nitrogen atoms and the oxygen atoms of the carbonyl functions. These four atoms are as well present in diazene derivatives (**16** and **17**) and hydrazine derivatives (**14** and **15**), therefore they are potential ligands for the formation of molecular clips (scheme 22).

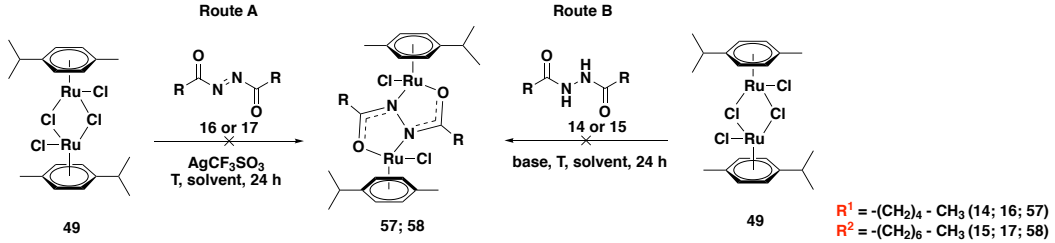

*Scheme 22: Attempts to synthesize molecular clips [(η^6-p-cymene)$_2$Ru$_2$(μ_4- N'-hexanoylhexanehydrazide)]Cl$_2$ (**57**) and [(η^6-p-cymene)$_2$Ru$_2$(μ_4- N'-octanoyloctanehydrazide)]Cl$_2$ (**58**) using diazene derivatives **16** and **17** and hydrazine derivatives **14** and **15** as spacer ligands. Base: NaOAc, NEt$_3$, DIPEA; solvent (T): MeOH (RT; 65 °C), EtOH (RT; 80 °C; 90 °C), DCM (RT; 40 °C), MeCN (RT; 80 °C), MeNO$_2$ (RT, 100 °C).*

Similarly, route A starts from the diazene derivatives **16** and **17** and the reaction is performed in the presence of $AgCF_3SO_3$ to abstract the chlorine of precursor **49**, while in route B, the hydrazine derivatives **14** and **15** are deprotonated using bases NaOAc, NEt_3 or DIPEA (scheme 22). The same conditions were tested, as for the preparation of clips **55** and **56** from spacer ligands **11**, **12** or **9** and **10** (scheme 21), and again the synthesis of clips **57** and **58** failed. Like in the examples before, no reaction was observed at RT or 65 °C, at 80 °C a complex mixture of unidentified byproduct was isolated, which were not possible to separate, and decomposition occurred at high temperatures.

5.2.7. Molecular Clips from dihydroxybenzoquinone derivatives

In this section, the preparation of the molecular clip **59** using the dhbq derivative **38** is shown. As mentioned before on page 37, the formation of clips using simple dhbq or its derivatives as spacer ligands have already been demonstrated.[134]

Scheme 23 shows the condition for the synthesis of clip **59** using ligand **38**. The synthesis was performed according to published methods for the dhbq spacing ligand.[198] EtOH was used as

solvent in the presence of NaOAc as the base and the reaction was performed at 80 °C and the desired clip was successfully synthesized with a good yield (77%).

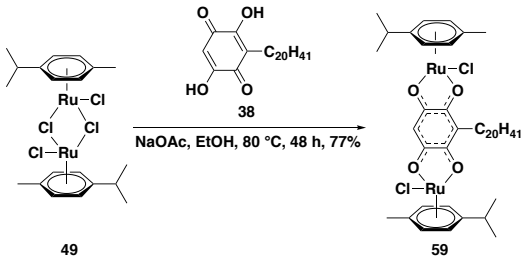

*Scheme 23: Synthesis of molecular clip [(η^6-p-cymene)$_2$Ru$_2$(μ_4-3-icosyl-dihydroxybenzoquinone]Cl$_2$ (**59**).*

In figure 41, the ^{1}H-NMR for molecular clip **59** shows at 5.69 ppm a singlet with an integral of 1 for the single proton of dhbq, next to two multiplets for the eight aromatic protons of the *p*-cymene moieties at around 5.6 ppm and 5.4 ppm with an integral of four for each signal. The single proton of the *i*Pr groups are represented by a septet with an integral of two at 2.90 ppm and the methyl groups of the *i*Pr groups as a multiplet with an integral of twelve at around 1.4 ppm. The remaining methyl groups of the *p*-cymene moieties are shown as a singlet with six protons at 2.91 ppm. The CH_2 and CH_3 groups corresponding to the icosyl chain are as well observed in the aliphatic area as a multiplet with 36 protons at around 1.3 ppm and a triplet with three protons at around 0.9 ppm, respectively.

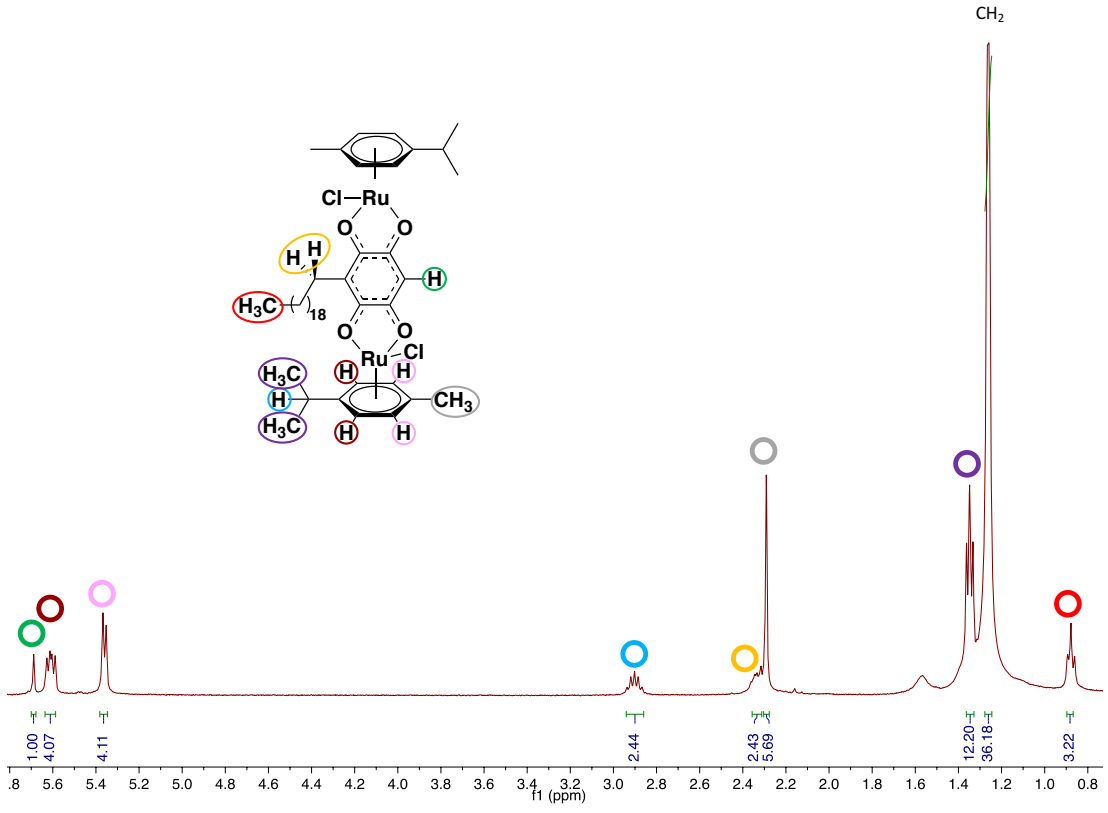

*Figure 41: ^{1}H-NMR spectrum of molecular clip **59** (400 MHz, $CDCl_3$, RT).*

In figure 42 the ^{13}C-NMR of molecular clip **59** is shown and the signal assignment was done using 2D-NMR techniques. The signals for the aromatic carbons of the *p*-cymene are observed between 100.6 ppm and 79.1 ppm. The *i*Pr groups of the *p*-cymene are detected at 31.5 and at 22.7 ppm, respectively. The remaining methyl groups of the *p*-cymene moiety arise at 18.7 ppm. The carbonyl group of the spacer ligand **38** are observed at 184.4 ppm and 181.1 ppm, respectively. The CH group of the dhbq ring moiety is observed at 115.5 and the quaternary carbon, where the chain is attached is detected at 100.7 ppm. All the CH_2 groups of the chain are shown in the aliphatic area and the terminal CH_3 group of the chain arises at 14.3 ppm.

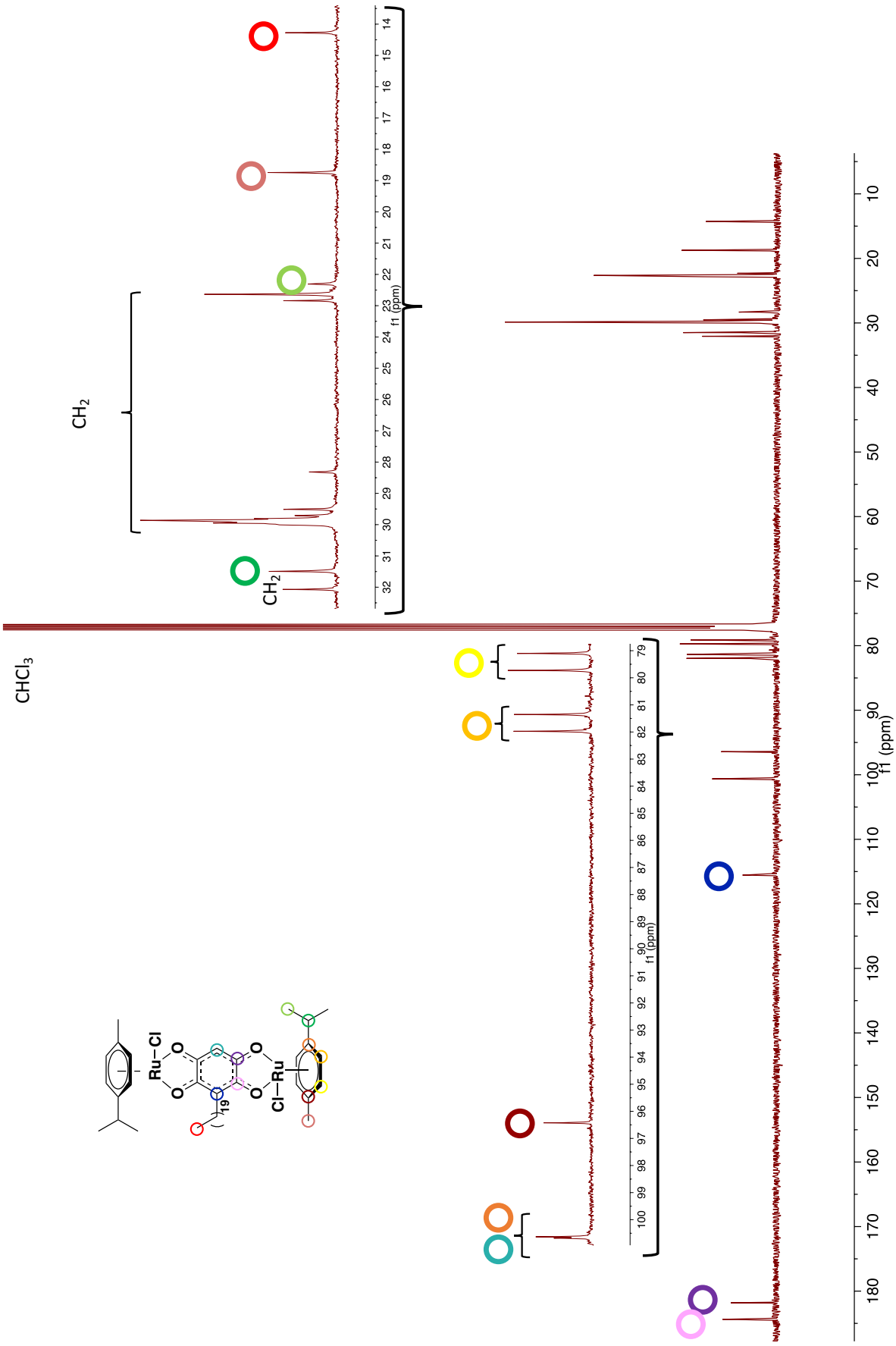

*Figure 42: ^{13}C-NMR spectrum of molecular clip **59** (101 MHz, $CDCl_3$, RT).*

The ESI-MS analysis of clip **59** shows a peak for $[M - Cl]^+$ at m/*z* = 925.3. The success of the reaction and the purity of the compound was further confirmed by elemental analysis. The IR spectrum of ligand **38** showed the band representing intramolecular O-H stretching at around 3300 cm^{-1} which is not observed anymore in the IR spectrum of the clip **59**.[197]

5.2.8. Molecular Clips with Precursor **60**

Until this point, molecular clips consisting of *p*-cymene as arene moiety were discussed. Herein a different precursor consisting of another arene moiety is shown. Precursor **60** was prepared by Süss-Fink and co-workers in 2004.[199] Like in the case of precursor **49** the bridging chlorines can be replaced by a spacer ligand to form a molecular clip.

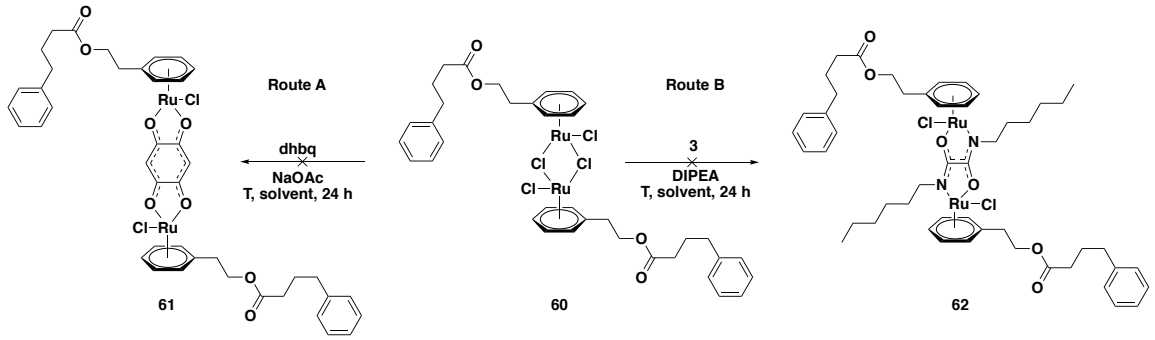

*Scheme 24: Attempts to synthesize molecular clips [(η^6-phenethyl 4-phenylbutanoate)$_2$Ru$_2$(μ_4-dihydroxybenzoquinone)]Cl$_2$ (**61**) (route A) and [(η^6-phenethyl 4-phenylbutanoate)$_2$Ru$_2$(μ_4- N^1,N^2-dioctyloxalamide)]Cl$_2$.(**62**) (route B) from precursor [Ru$_2$(η^6-phenethyl 4-phenylbutanoate)$_2$(μ_2-Cl)$_2$Cl$_2$] (**60**).* [199] *Solvent (T): MeOH (65 °C), EtOH (80 °C, 90 °C), DCM (40 °C), MeCN (80 °C), MeNO$_2$ (100 °C).*

In route A of scheme 24, the commercially available dhbq was used as spacer ligand, in order to synthesize molecular clip **61**. NaOAc was used as the base, since it has already proven to deprotonate dhbq and its derivatives. However, the reaction to insert dhbq was not successful. In route B, the previously synthesized N^1,N^2-dihexyloxalamide (**3**) is used as spacer ligand in the presence of DIPEA as a base, which has demonstrated to be able to deprotonate oxalamides. The reaction was tested in several solvents and at different temperatures, but the desired clip **62** was not obtained. The ^{1}H-NMR showed a complex mixture, nevertheless the expected mass was detected in ESI-MS analysis. Nonetheless, it was not possible to isolate the desired clip for further tests. The substituent of the arene moiety are large and flexible and are therefore able to interfere with the metal centers. This might be the reason for the formation of numerous byproducts, which could not be identified.

5.3. PREPARATION OF METALLA-ASSEMBLIES

In this section the final step for the formation of the multi-nuclear assemblies is discussed. As explained previously in chapter 4, the connecting ligand, according to its denticity and therefore ability to combine a number of molecular clips, is responsible for the formation of such structures. Three molecular clips **50**, **51** and **59** were successfully synthesized and in this section their ability to form a molecular assembly is tested.

5.3.1. Preparation of Metalla-Prisms from Oxalamide-Clips

First the tridentate 4-tpt panel ligand is used to prepare a prism. In the first step, $AgCF_3SO_3$ is used to abstract the chlorines of the clip to obtain the twofold positively charged intermediate. Then the panel ligand is added and the assembly is allowed to form by coordination. Scheme 25 shows the synthesis of prisms **63** and **64** from the clips **50** and **51**. Similar prisms have been previously prepared by our group in MeOH under reflux.[162]

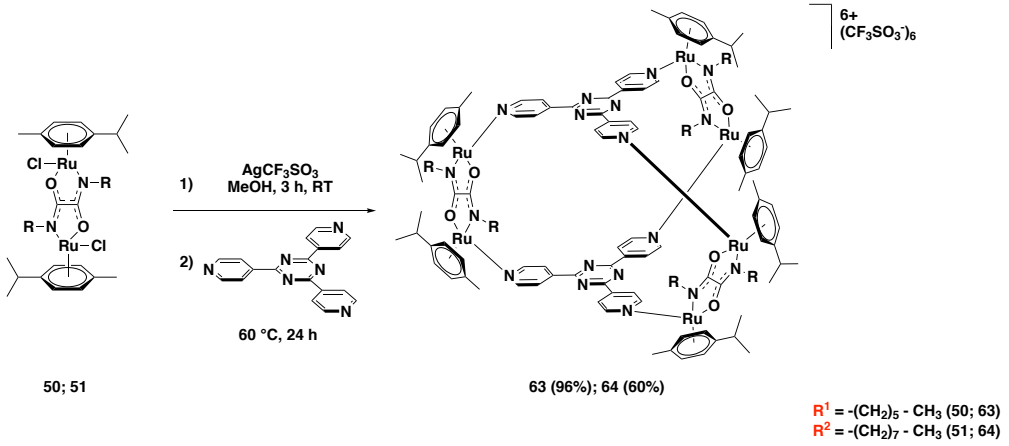

*Scheme 25: Synthesis of hexa-nuclear molecular prism [(η^6-p-cymene)$_6$Ru$_6$(μ_4-N^1,N^2-dihexyloxalamide)$_3$(μ_3-4-tpt)$_2$][CF_3SO_3]$_6$ (**63**) and [(η^6-p-cymene)$_6$Ru$_6$(μ_4-N^1,N^2-dioctyloxalamide)$_3$(μ_3-4-tpt)$_2$][CF_3SO_3]$_6$ (**64**).*

Prism **63** was obtained in an excellent yield of 96%, while **64** was obtained with 60% yield, which is comparable to similar assemblies.[162] Figure 43 shows the ^{1}H-NMR spectra of clip **51** (top) and prism **64** (bottom). The ^{1}H-NMR spectra of the clip **51** was discussed previously on page 57.

The ^{1}H-NMR spectrum of prism **64** (bottom) shows very similar chemical shifts to those in the ^{1}H-NMR spectrum of the clip **51** (top) except for the signals associated to 4-tpt arising at around 8.5 ppm. Three clips are combined by two panel ligands, increasing rigidity to the structure of the prism, this results in broad signals in the ^{1}H-NMR. Despite a slight shift and broadening, the signals of clip **51** are clearly seen and the integrals correspond to three clips in

relation to the 4-tpt panels. The 4-tpt panels possess 24 protons in total, which are represented by a broad multiplet at around 8.5 ppm. The aromatic protons of six *p*-cymene moieties are observed as two multiplets with an integral of 12 each at around 5.5 ppm. The diastereotopic protons of the octyl chains and the single proton of the *i*Pr groups are observed as broad multiplets at around 4.3 ppm, 3.5 ppm and 2.8 ppm, respectively and with an integral of six for each signal. The six CH_3 groups of the octyl chains are seen at 0.9 ppm and correspond to 18 protons. The *i*Pr and methyl groups of the *p*-cymene moieties and the CH_2 groups of the octyl chains appear in the aliphatic area, causing overlying signals, nevertheless they are clearly visible.

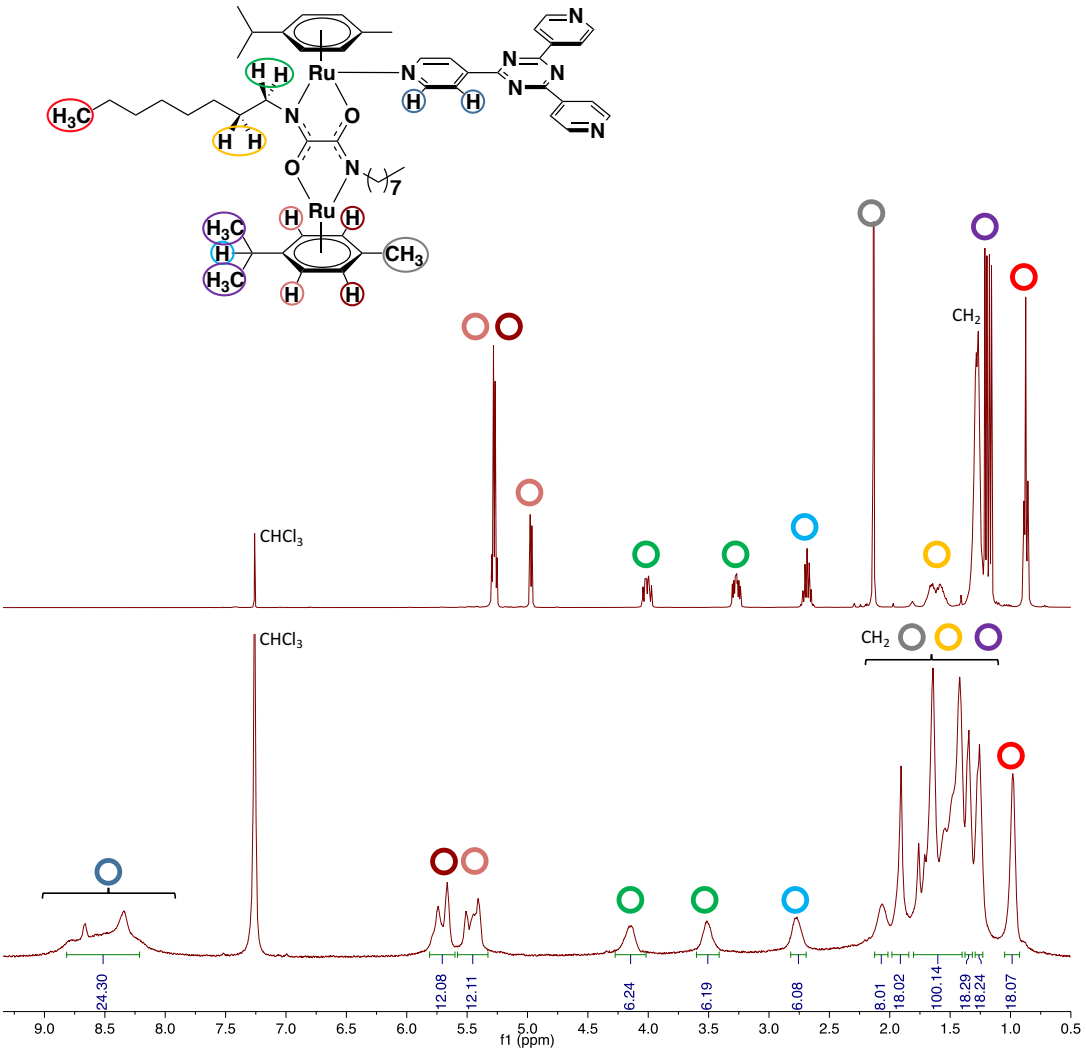

*Figure 43: ^{1}H-NMR spectra of molecular clip **51** (top) and molecular prism **64** (bottom). Only relevant structural motives of prism **64** represented for clarity (400 MHz, $CDCl_3$, RT).*

In figure 44 the ^{13}C-NMR spectra of clip **51** (top) and prism **64** (bottom) are presented. All the signals present in the spectrum of the clip are as well observed for the prism. Additionally, all four carbons of the panel ligand 4-tpt are observed between 172 ppm and 120 ppm.

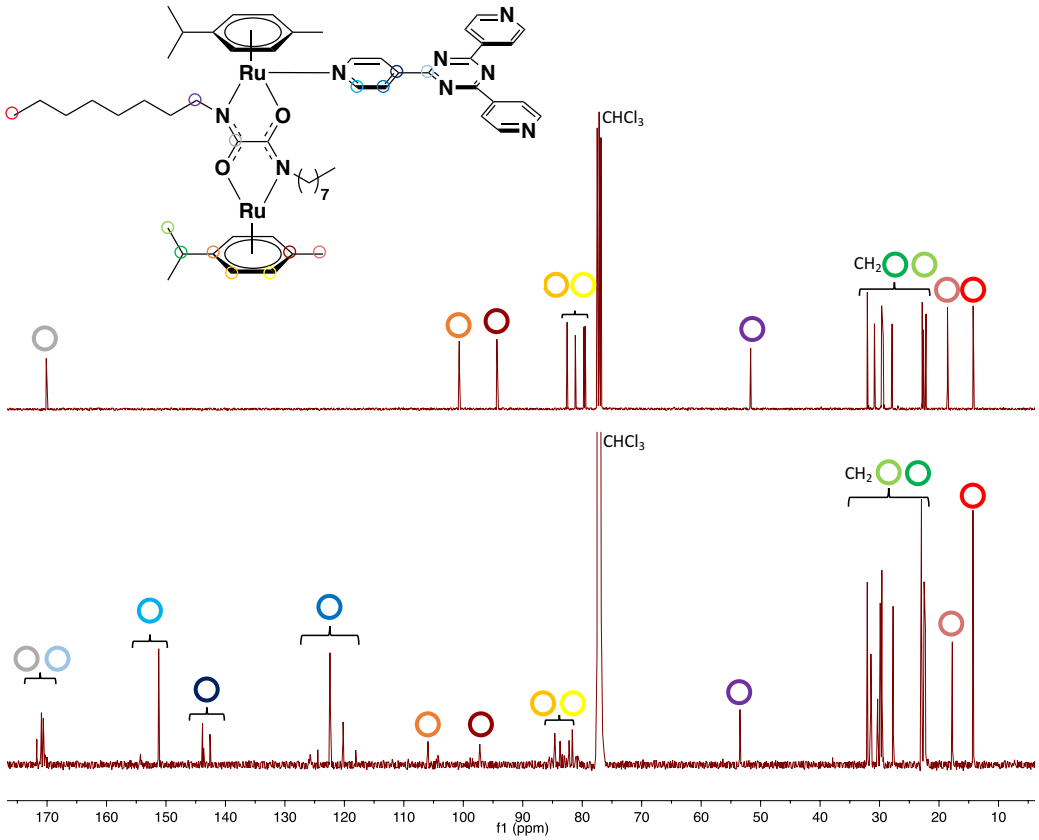

*Figure 44: ^{13}C-NMR spectra of molecular clip **51** (top, 101 MHz, $CDCl_3$, RT) and hexa-nuclear prism **64** (bottom, 151 MHz, $CDCl_3$, 45 °C). Only relevant structural motives of prism **64** represented for clarity.*

Figure 45 shows the DOSY (diffusion ordered NMR spectroscopy) spectrum of prism **64**. The 2D-DOSY NMR experiment is a method developed by Morris and Johnson in 1992. This method allows molecular components of mixtures to be identified and simultaneously characterize the size of aggregates.[200] Molecular motion of compounds in solution occur in rotational as well as in translational manner. The translational motion is also known as Brownian molecular motion and is simply called diffusion or self-diffusion. The diffusion coefficient *D* can be estimated using the Stokes-Einstein equation, when assuming a spherical shape for the molecule.

$$D = \frac{KT}{6\pi\eta r}$$

D: diffusion coefficient [$m^2 \cdot s^{-1}$]

K: Boltzmann constant [$1.38064852 \times 10^{-23} \cdot m^2 \cdot kg \cdot s^{-2} \cdot K^{-1}$]

T: absolute temperature [K]

η: viscosity of solvent [$kg \cdot m^{-1} \cdot s^{-1}$]

r: hydrodynamic radius [m]

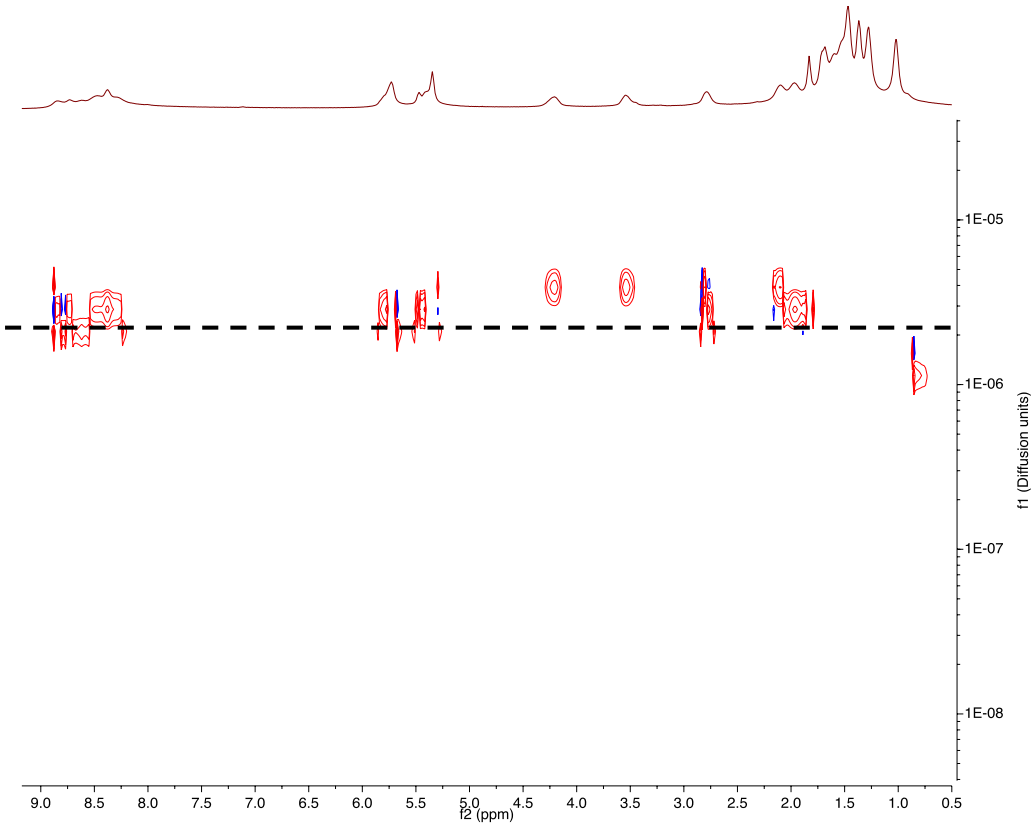

*Figure 45: DOSY spectrum of prism **64** (400 MHz, $CDCl_3$, RT).*

The DOSY experiment was recorded in $CDCl_3$, at RT and the spectrum shown in figure 45 was obtained. The F2 axis of the spectrum shows the chemical shift in ppm and the F1 axis shows the diffusion constant of the corresponding site. The signals belonging to prism **64** are diffusing at a rate of 2.52 x 10^{-10} $m^2 \cdot s^{-1}$ and the hydrodynamic radius amounts 16.4 x 10^{-10} m. However, the detected signals do not arise perfectly linear, suggesting that there might be more than one species present. Further indications for this assumption is seen in the ^{13}C-NMR spectrum in figure 44, where too many peaks are observed for the panel ligand 4-tpt. Furthermore, the ESI-MS spectrum shows a signal at m/*z* = 317.3 for $[Clip - Cl]^+$, which means that not all chlorines of the clips were successfully abstracted and therefore the presence of other species is possible. Nevertheless, the characteristic peaks for $[M - 2\ CF_3SO_3]^{2+}$ and $[M - 3\ CF_3SO_3]^{3+}$ of both prisms **63** and **64** were detected and the elemental analysis showed good purity.

5.3.2. Preparation of Molecular Prism from dhbq-Clip

Herein, the previously synthesized molecular clip **59** was used for the formation of the prism. Clip **59** includes **38** as spacer ligands, an analog to embelin, a natural product known to possess numerous biological activities.[181]

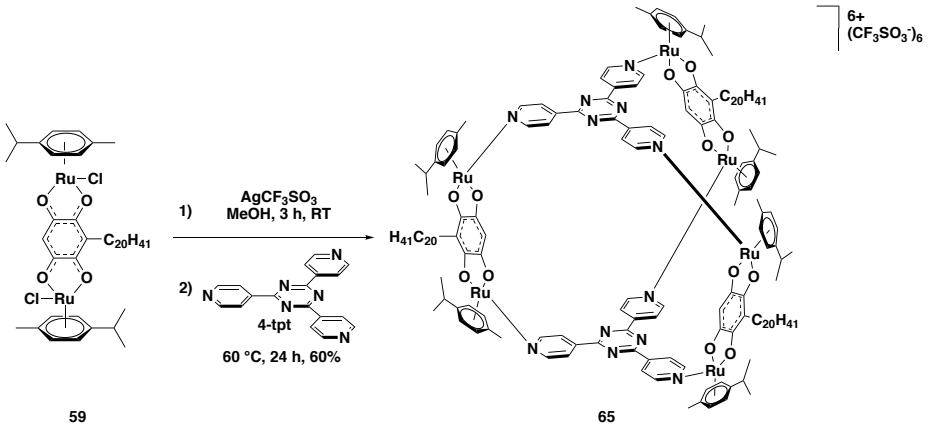

*Scheme 26: Synthesis of molecular prism [(η^6-p-cymene)$_6$Ru$_6$(μ_4-3-icosyl-dihydroxybenzoquinone)$_3$(μ_3-4-tpt)$_2$][CF_3SO_3]$_6$ (**65**).*

Scheme 26 shows the synthesis of the hexa-nuclear prism **65**. The synthesis was performed under the exact same conditions as the previous prisms, where first the chlorines are abstracted using $AgCF_3SO_3$ and then the panel ligand 4-tpt is added to allow the formation of the prism in MeOH under reflux. **65** was isolated with a good yield 60%.

In figure 46 the ^{1}H NMR spectra of the clip **59** (top) and the respective prism **65** (bottom) are presented. The ^{1}H-NMR spectra of **59** was previously discussed, and like before the ^{1}H-NMR spectrum of the prism **65** shows very similar shifts to the respective clip **59**. In addition, the signals of the panel ligands are observed. In the bottom spectrum the shapes of the signals are broader and less clear, nevertheless all the characteristic signals for clip **59** are well observed with integrals corresponding to a prism. The signals for the panel ligands 4-tpt arise between 9.0 and 8.5 ppm representing two different protons with an integral of twelve for each signal. The aromatic protons of three **59** moieties and the aromatic protons of six *p*-cymene moieties appear in the aromatic region as overlying signals integrating for 27 protons. The methyl groups of the *p*-cymene moieties are observed at around 2.1 ppm, the single proton of the *i*Pr groups with an integration of six at around 2.8 ppm is observed as a broad multiplet, while the methyl groups are observed around 1.4 ppm. The CH_2 groups of the icosyl chains appear between 1.3 ppm and 1.2 ppm as a large and broad peak. The CH_3 group of the icosyl chains is clearly seen at 0.8 ppm with an integral of 9.

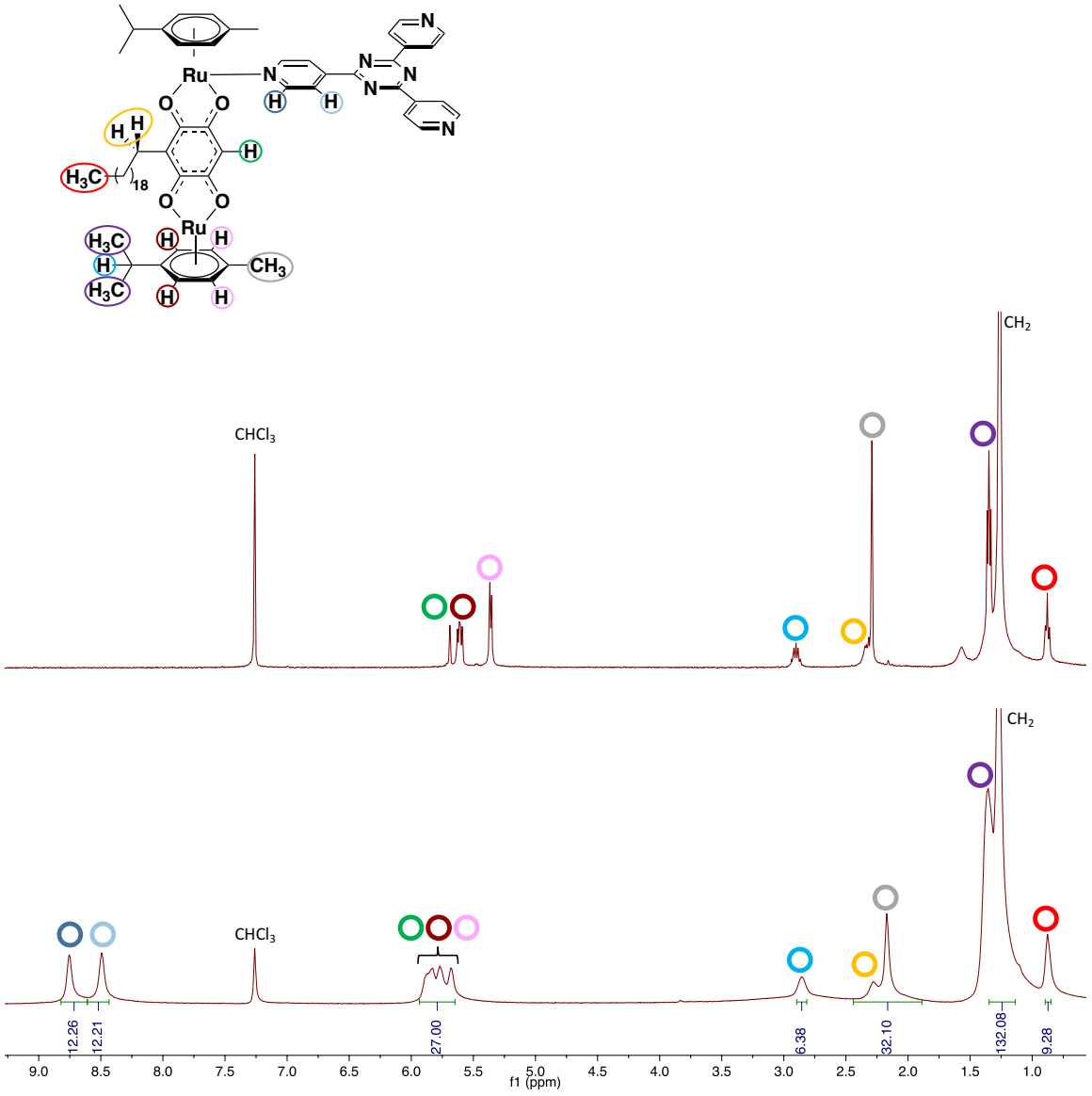

*Figure 46: [1]H-NMR spectra of molecular clip **59** (top) and metalla-prism **65** (bottom). Only relevant structural motives of prism **65** represented for clarity (400 MHz, $CDCl_3$, RT)*

In figure 47 the ^{13}C-NMR spectra of clip **59** (top) and prism **65** (bottom) are shown. All signals observed for the clip are as well present in the prism. In addition, signals corresponding to the panel ligands are observed between 170 and 140 ppm for the prism.

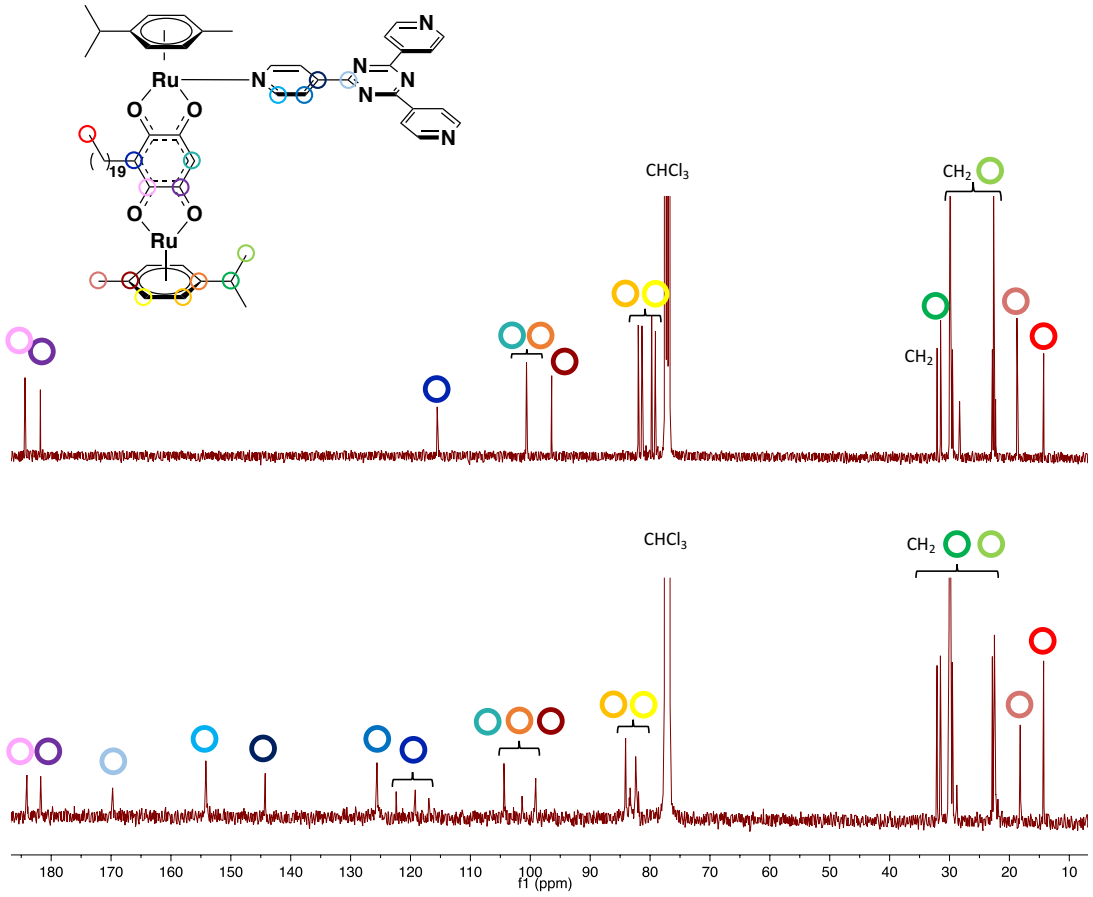

*Figure 47: ^{13}C-NMR spectra of molecular clip **59** (top) and hexa-nuclear metalla-prism **65** (bottom). Only relevant structural motives of prism **65** represented for clarity (101 MHz, $CDCl_3$, RT).*

Figure 48 shows the DOSY spectrum of prism **65**. The diffusion constant shows that all arising signals belong to prism **65** apart from the signal at 7.26 ppm belonging to $CHCl_3$. The signals belonging to prism **65** are diffusing at a rate of $2.47 \times 10^{-10} m^2 \cdot s^{-1}$, which corresponds to a hydrodynamic radius of 16.7×10^{-10} m.

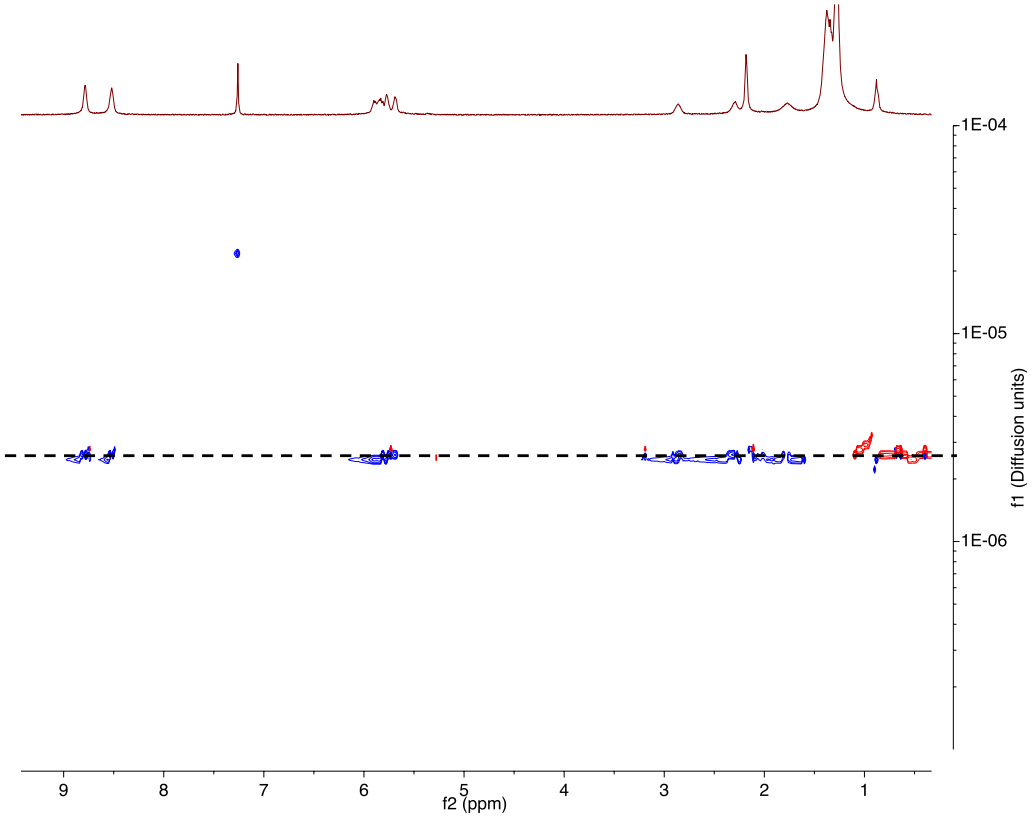

*Figure 48: DOSY spectra of hexa-nuclear prism **65** (400 MHz, $CDCl_3$, RT).*

All 1D- and 2D-NMR experiments showed the success of the preparation of prism **65**. Furthermore, the ESI-MS showed the characteristic peaks $[M - 2\ CF_3SO_3]^{2+}$ and $[M - 3\ CF_3SO_3]^{3+}$ and the purity of the compound was further confirmed by elemental analysis.

5.3.3. Preparation of Molecular Cubes from Oxalamide-Clips

Herein, preparation of octa-nuclear molecular cubes is presented. As in the synthesis of hexa-nuclear prisms, the first step is also the abstraction of the chlorines of the clips **50** and **51** using $AgCF_3SO_3$. Then the tetra-dentate panel ligand tpp is added to allow the formation of the cube. In the first attempt the synthesis was performed in DCM at RT for 15 h, following standard procedures.[201] However, the cubes were not obtained, only starting materials were isolated even after extended reaction times and higher temperature, therefore the reaction was repeated using MeOH, EtOH, MeCN or $MeNO_2$ at RT and under reflux for 72 h. As depicted in scheme 27, the reaction was successful in MeCN for clips **50** and **51** and the molecular cubes **66** and **67** were successfully isolated with a yield of 73% and 71%, respectively.

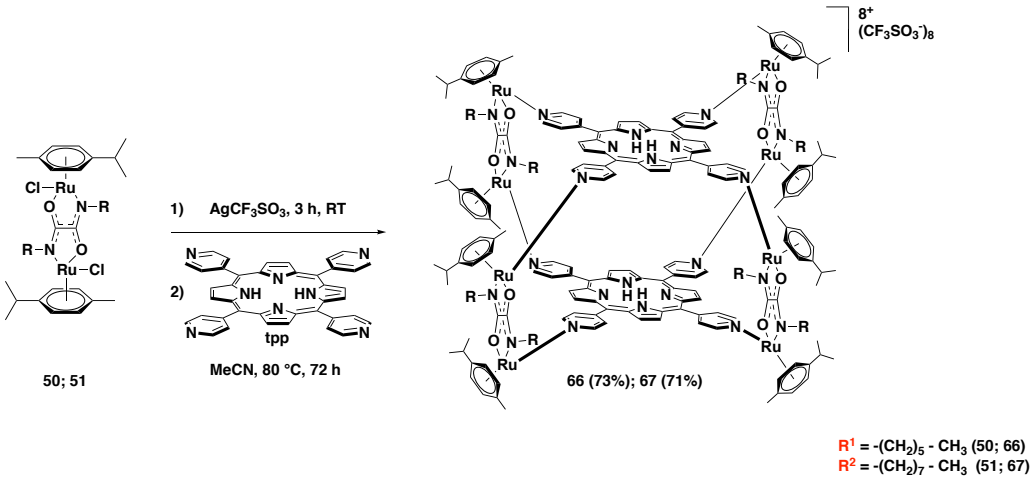

*Scheme 27: Synthesis of molecular cubes [(η^6-p-cymene)$_8$Ru$_8$(μ_4-N^1,N^2-dihexyloxalamide)$_4$(μ_4-tpp)][CF_3SO_3]$_8$ (**66**) and [(η^6-p-cymene)$_8$Ru$_8$(μ_4-N^1,N^2-dioctyloxalamide)$_4$(μ_4-tpp)$_2$][CF_3SO_3]$_8$ (**67**).*

The difficulty of finding the appropriate synthetic conditions was linked to the poor solubility of the building blocks. Similarly, recording the NMR spectra was challenging, due to the insolubility of cubes **66** and **67**. It was not possible to obtain a useful ^{1}H-NMR at RT, therefore high temperature experiments were carried out. Figure 49 shows the ^{1}H-NMR spectrum of molecular cube **67** recorded in $MeNO_2$-d_3 at 65 °C with a field strength of 800 MHz (recorded by Dr. Aurélien Bornet at the EPFL in Lausanne).

Despite using a high field strength, the multiplicity of the signals was not clearly distinguished: The rigidity of the structure being probably responsible. Nevertheless, the significant signals of the tpp, the arene, the diastereotopic protons of the octyl chains and the terminal CH_3 groups of the chains are clearly detected with their corresponding integrals. All remaining protons of the cube appear in the aliphatic region, leading to overlying signals. The

tpp panels are observed as multiplets between 9.5 ppm to 8.0 ppm and account for 52 protons. The aromatic protons of the *p*-cymene moieties are detected around 6.0 ppm with an integral of 32 protons. The diastereotopic protons of the octyl chains are observed around 4.1 ppm and 3.1 ppm with an integral of eight and the terminal CH_3 group of the chain is observed at around 1.0 ppm with an integral of 24.

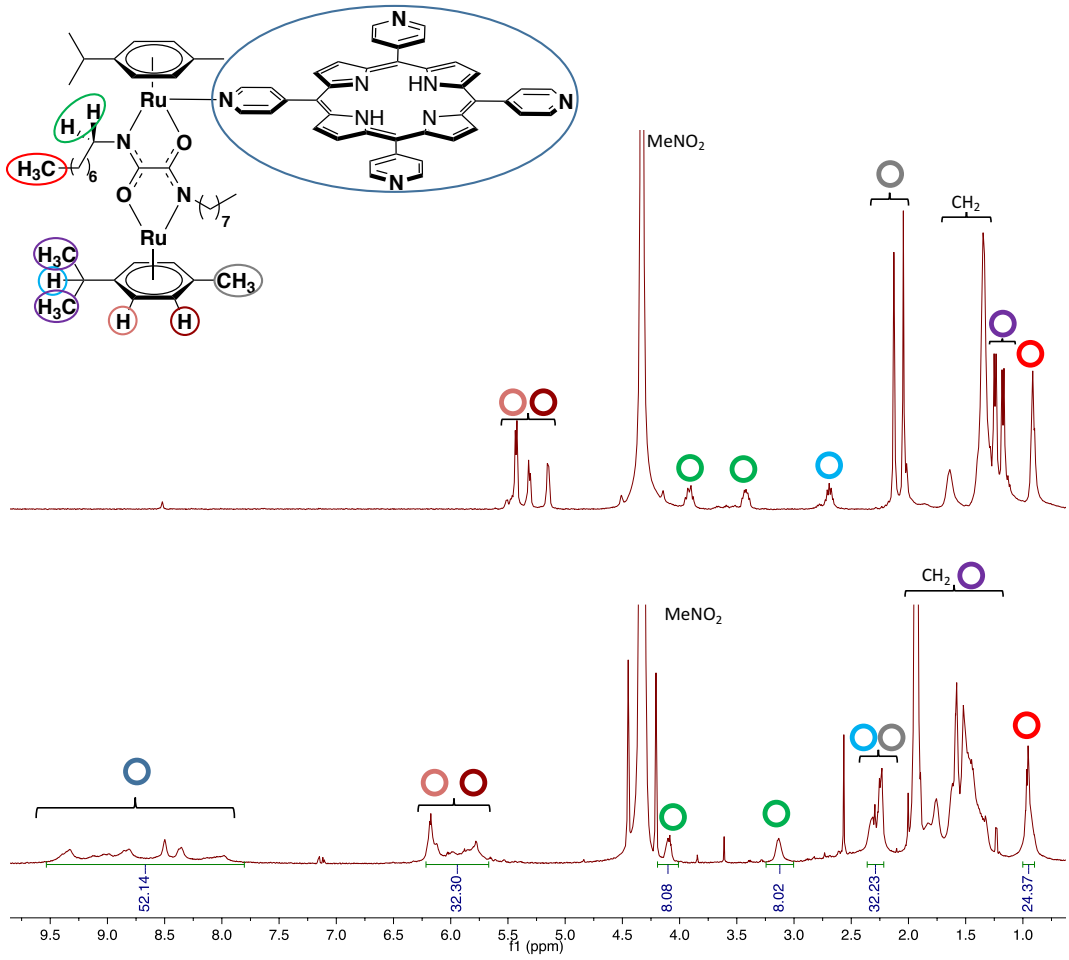

*Figure 49: ^{1}H-NMR spectra of molecular clip **51** (top, 400 MHz, $MeNO_2$-d_3, RT) and molecular cube **67** (bottom, 600 MHz, $MeNO_2$-d_3, 65 °C). Only relevant structural motives of cube **67** represented for clarity.*

In figure 50 the ^{13}C-NMR spectra of clip **50** (top) and cube **66** (bottom) is depicted. The signals for the oxalamide function, the protons of the aromatic and aliphatic protons of the *p*-cymene and the hexyl chains appear at similar positions in both spectra. In addition, the signals for the tpp is also observed.

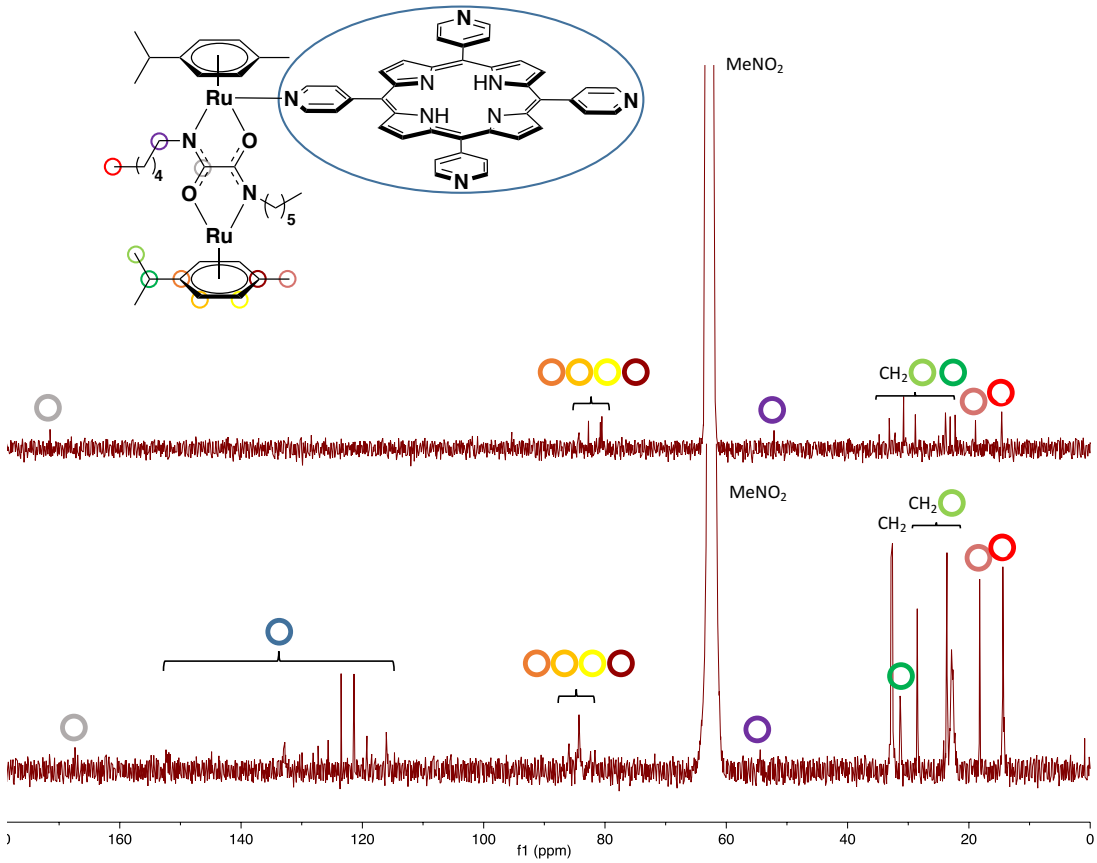

*Figure 50: ^{13}C-NMR spectra of molecular clip **50** (top, 101 MHz, $MeNO_2$-d_3, RT) and molecular cube **66** (bottom, 151 MHz, $MeNO_2$-d_3, 65 °C). Only relevant structural motives of cube **67** represented for clarity.*

Figure 51 illustrates the DOSY NMR spectrum of cube **67**. The experiment shows that the signals belonging to cube **67** are diffusing at a rate of 2.3 x 10^{-10} $m^2 \cdot s^{-1}$. The diffusion constant can be read from the spectrum and the hydrodynamic radius (17.9 x 10^{-10} m) can be calculated using the Stokes-Einstein equation.

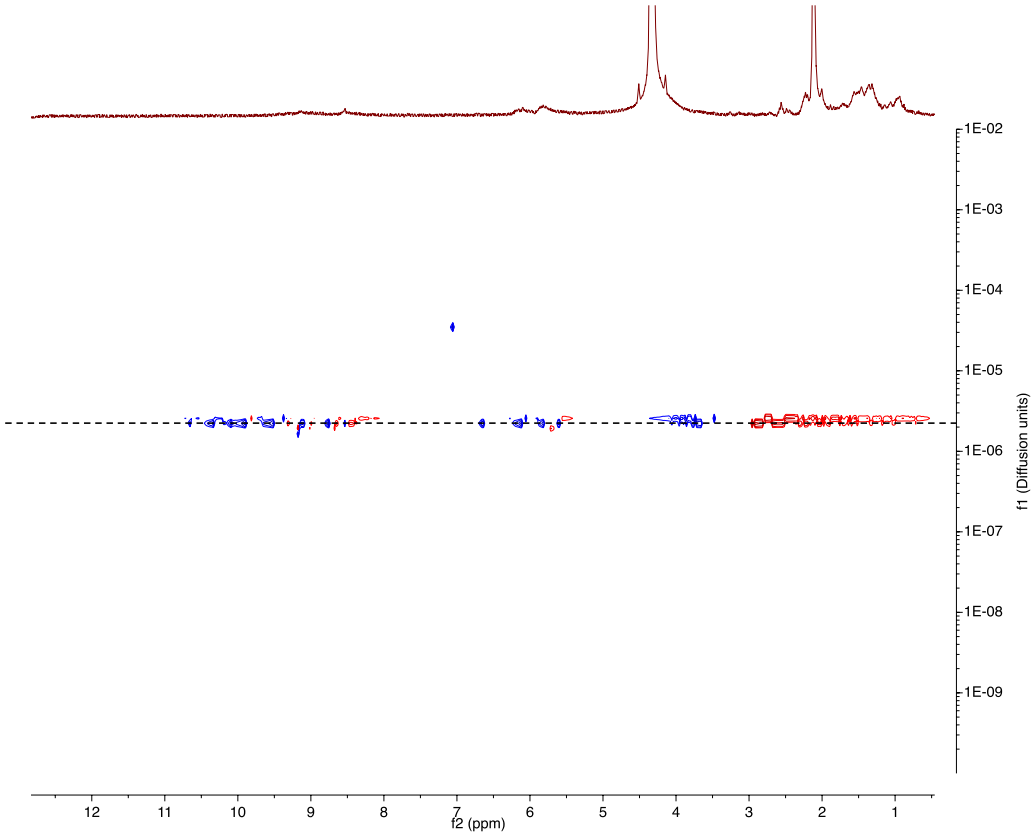

*Figure 51: DOSY NMR spectrum of octa-nuclear cube **67** (400 MHz, $MeNO_2$-d_3, RT).*

The formation of the cube was further confirmed by ESI-MS analysis. Both cubes **66** and **67** show the characteristic peaks at $[M- 4\ CF_3SO_3]^{4+}$ and $[M- 3\ CF_3SO_3]^{3+}$. The nature of the salts was also confirmed by elemental analysis.

5.3.4. Preparation of Molecular Cube from dhbq-Clips

In this section, an attempt to prepare a molecular cube from clip **59** is described. Like in the case of the oxalamide-clips **50** and **51** various conditions were tested, however, the preparation of the molecular cube **68** from dhbq-clip **59** failed, see 28.

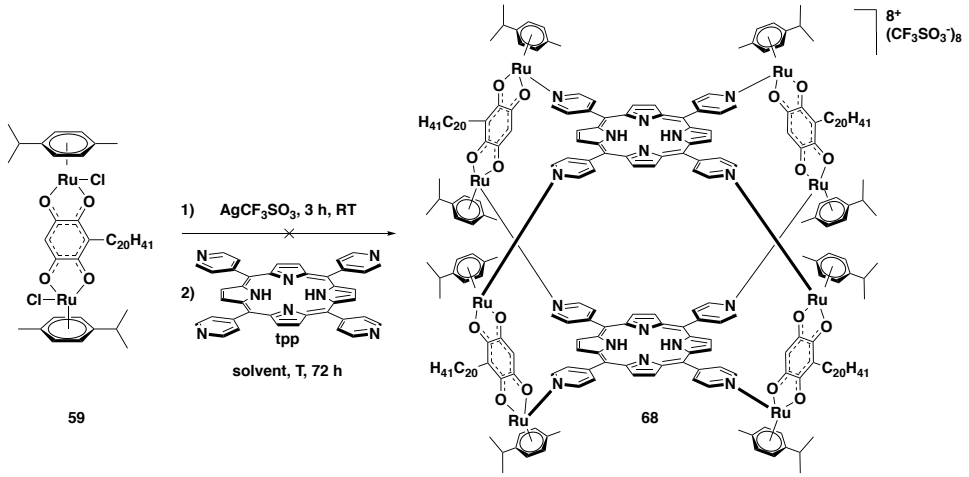

*Scheme 28: Attempt to synthesize molecular cube [(η^6-p-cymene)$_8$Ru$_8$(μ_4-3-icosyl-dihydroxybenzoquinone)$_8$(μ_4-tpp)$_2$][CF_3SO_3]$_8$ (**68**). Solvent (T): DCM (RT, 40 °C), MeOH (RT, 65 °C), EtOH (RT, 80 °C, 90 °C), MeCN (80 °C), $MeNO_2$ (100 °C).*

5.3.5. Preparation of Molecular Prism with Guest Molecule

Most assemblies presented in the previous sections possess a cavity, which can be used to encapsulate guest molecules. Guest molecules can further increase the weight of the assembly, which is beneficial for the EPR-effect. Moreover, small molecules with anti-cancer property could be encapsulated and guided to the cancer *via* the EPR-effect. Synthetically, the procedure of encapsulation is straightforward. The guest molecule is added simultaneously during the synthesis of the assembly. Non-covalent interactions, including hydrogen-bonding, π-π stacking, electrostatic interactions, van der Waals force, and hydrophobicity of the guest molecule provide stability to the entire complex.[202]

Scheme 29 depicts the synthesis of host-guest systems using arene-ruthenium assemblies. In the first step, both chlorines are abstracted using $AgCF_3SO_3$ in order to be able to form the final assembly by coordinating the pyridyl functions of the 4-tpt panel ligand. The guest molecule is added simultaneously with the panel ligands and due to various interactions, the guest is encapsulated in the cavity. Several guest molecules were successfully encapsulated previously in our group using this strategy. All guest molecules possess an aromatic character or delocalized electrons, as well as a favorable size which allows them to fit within the cavity of the host.[203]

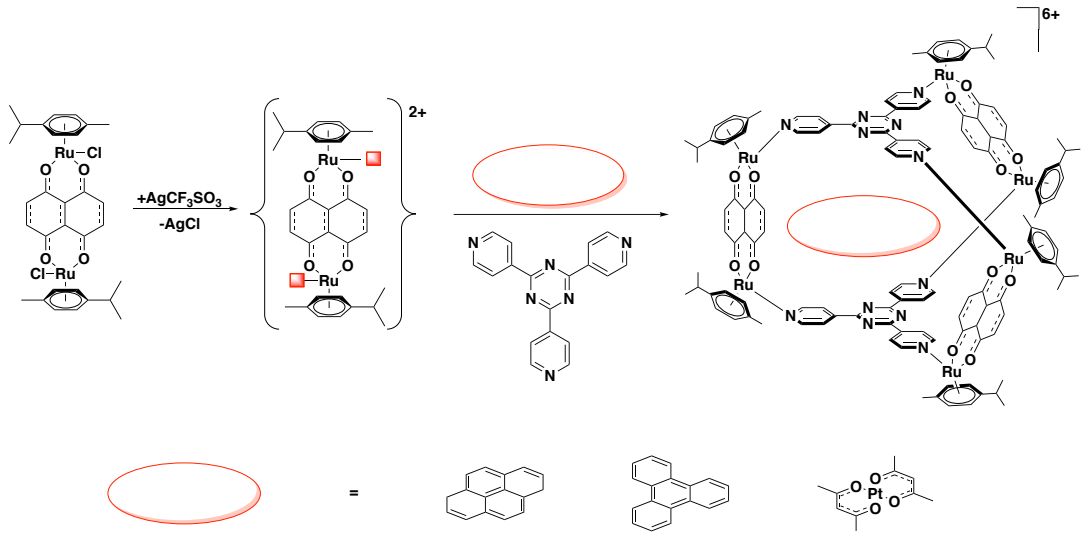

Scheme 29: Formation of a host-guest system with an arene-ruthenium metalla-assembly using various guests.[198]

Herein, two guest molecules with large functional groups (figure 52) were used as guest molecules. The potential guest molecules **Guest 1** and **Guest 2** are triphenylene derivatives and were synthesized by Dr. Franck Camerel from the University of Rennes.

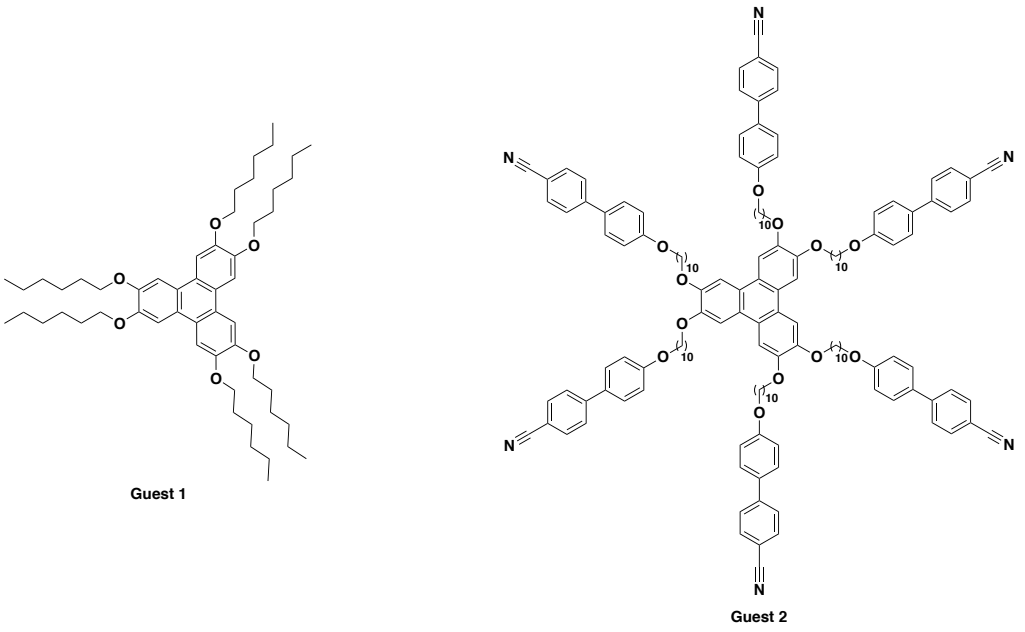

*Figure 52: Potential guest molecules **Guest 1** and **Guest 2** synthesized by Dr. Franck Camerel from the University of Rennes.*

The reason a guest molecule is encapsulated, can be explained by its behavior in a certain environment. In order for an encapsulation to take place, the choice of solvent is crucial. Supposing the solubility of the guest molecule is high in the chosen solvent, there is no necessity for it to be encapsulated, since it undergoes stable non-covalent interactions with the surrounding solvent molecules and it is therefore not driven into the cavity of a host system. In order to be encapsulated the interaction with the solvent molecules must be low or repulsive, consequently, there is a driving force compelling the guest into the host. An aromatic guest is likely to be found inside the hydrophobic cavity of the assembly. In general, aromatic and hydrophobic compounds such as perylene, anthracene, pyrene or coronene showed such host-guest behavior for ruthenium metalla-assemblies. Methods to verify the success of an encapsulation are DOSY, ROESY and fluorescence spectroscopy.[203] To find the optimal solvent, solubility tests with **Guest 1** and **Guest 2** were carried out and summarized in table 8.

	H_2O	MeOH	EtOH	iPrOH	BuOH
Guest 1	– –	– –	– –	– –	– –
Guest 2	– –	–	–	– –	–

	pentane	hexane	petrol ether	cyclohexane	toluene
Guest 1	++	++	+	+	++
Guest 2	– –	– –	– –	– –	–

	Acetone	EtOAc	DMF	DMSO	MeCN
Guest 1	–	++	–	– –	– –
Guest 2	– –	–	–	–	– –

	$CHCl_3$	DCM	Et_2O	$MeNO_2$
Guest 1	++	++	+	–
Guest 2	++	++	– –	–

*Table 8: Solubility of **Guest 1** and **Guest 2** in various solvents to find optimal condition for encapsulation: high = ++; good = +; poor = –; no = – –. (Row 1: polar, protic, hydrophilic; row 2: apolar, aprotic, hydrophobic; row 3: polar, aprotic, hydrophilic; row 4: chlorinated ($CHCl_3$, DCM), polar, aprotic, hydrophilic (Et_2O) and polar, protic,hydrophilic ($MeNO_2$).*

The solubility of a compound is divided in four levels (high solubility, good solubility, low solubility and no solubility). In this case, a compound is declared as well soluble if it is dissolved at RT and it is described as highly soluble, if it is dissolved at RT without the requirement of stirring. A compound is characterized as poorly soluble, if it requires higher temperature to be dissolved and no solubility is observed when the compound remains undissolved despite stirring and high temperature. For this experiment the guest molecule must show poor solubility in a certain solvent. The solvents were categorized depending on their properties. As shown in table 8, guest molecule **Guest 1** shows poor solubility in acetone, DMF and $MeNO_2$, therefore they were tested for the encapsulation. **Guest 2** is poorly soluble in MeOH, which was already used as solvent for the encapsulation of guest molecules.[204]

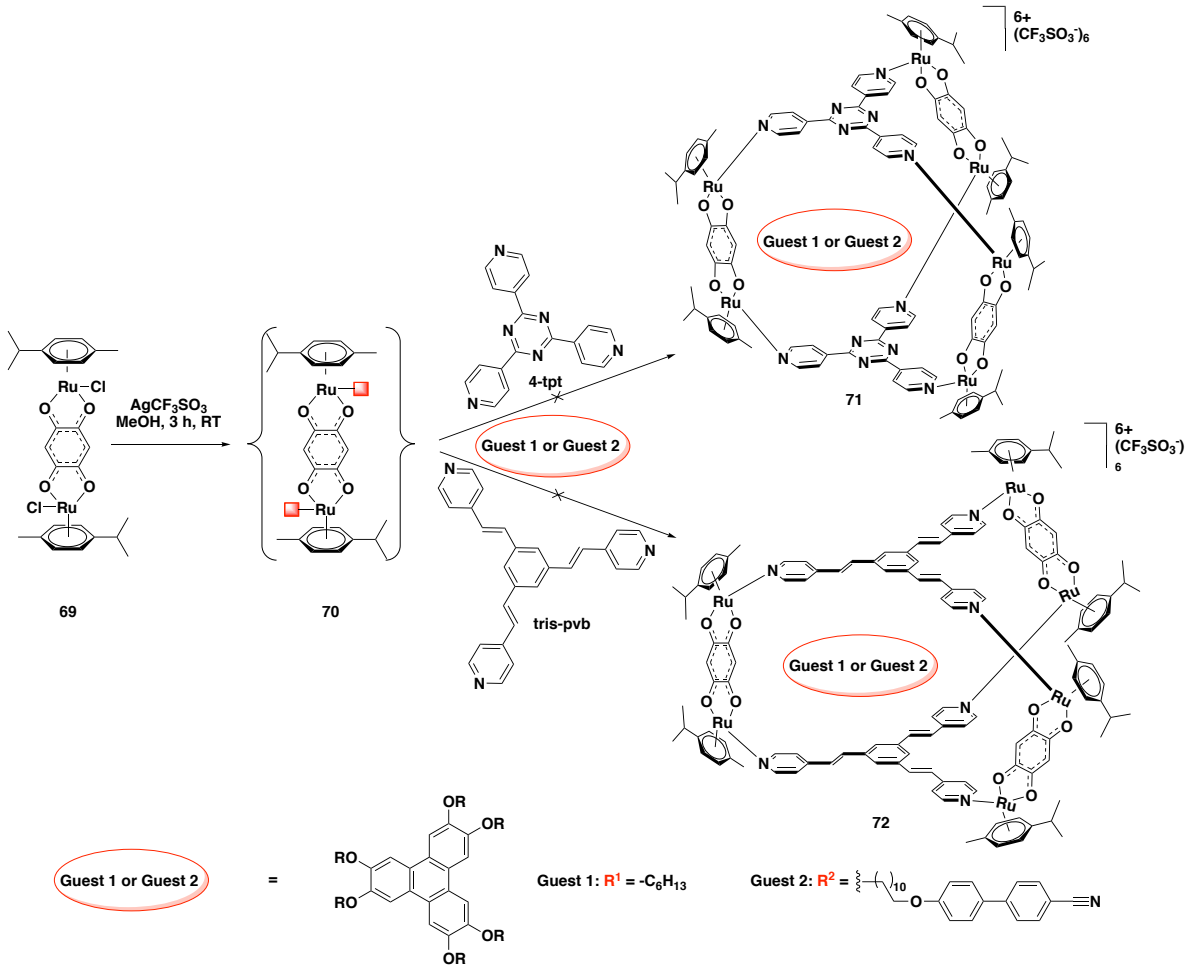

*Scheme 30: Attempt to encapsulate guest molecules **Guest 1** and **Guest 2** in the cavity of prisms **71** and **72**.*

Hexa-nuclear prisms **71** and **72** were chosen as host molecules for the encapsulation of guest molecules **Guest 1** and **Guest 2** as shown in scheme 30.[205,206] The conditions used to test the encapsulation of the guest molecules in the prisms **71** and **72** are listed in table 9. In these solvents (acetone, DMF, $MeNO_2$, DCM and MeOH) the hosts showed a good solubility.

entry	*guest*	solvent	T [°C]	panel ligand	observation
1	***Guest 1***	acetone	55	4-tpt	no reaction
2	***Guest 1***	DMF	90	4-tpt	no reaction
3	***Guest 1***	$MeNO_2$	90	4-tpt	decomposition of clip **69**
4	***Guest 1***	DCM	40	4-tpt	no reaction
5	***Guest 1***	MeOH	65	4-tpt	prism formation without guest encapsulation
6	***Guest 2***	MeOH	65	4-tpt	prism formation without guest encapsulation
7	***Guest 1***	MeOH	65	tris-pvb	no reaction
8	***Guest 2***	MeOH	65	tris-tvb	no reaction

*Table 9: Tested conditions for the encapsulation of guest molecules **Guest 1** and **Guest 2.***

For **Guest 1** the reaction was first performed in acetone and DMF (entries 1 - 2), where the guest was poorly soluble, however in both cases the prisms were not formed, but only starting materials were isolated. In $MeNO_2$, where the guest is as well poorly soluble, decomposition of clip **69** was observed (entry 3). This might be due to coordination of the solvent molecules with the metal centers of the clip. The reaction was further performed in DCM, where the guest showed high solubility, however in this case as well, no reaction was observed (entry 4). Since the encapsulation of various guest molecules was successfully performed in MeOH, MeOH was also tested to encapsulate **Guest 1**, however in this case only the empty prism **71** was isolated (entry 5).[204] The reaction in MeOH was repeated with the second guest molecule, which showed poor solubility in MeOH, however no encapsulation was observed (entry 6). To enlarge the size of the resulting prism, tris-tvb was used as panel ligands and the encapsulation was tested in MeOH (entries 7 - 8) for both guests. However, in both cases the prism formation was not observed, only starting materials being isolated. A reason for the failure of this encapsulation might be the substituents which results in a rather large size of **Guest 1** and **Guest 2**, preventing them from being encapsulated into the host systems.

6. BIOLOGICAL ACTIVITIES

The antiproliferative activities of the DMSO soluble metalla-prisms **28 - 30** were obtained using the 3-(4,5-dimethyl-2-thiazolyl)-2,5-diphenyl-2*H*-tetrazolium bromide (MTT) assays.[207] Cisplatin and RAPTA-C were used as reference and the results are summarized in table 10. The metalla-cubes **66** and **67** were not tested due to insolubility issues.

As shown in table 10, all three prisms possess a much better activity in the ovarian cancer cell line (A2780) than the mono-nuclear arene-ruthenium complex RAPTA-C, however they are not as active as cisplatin. Amongst the tested compounds, the oxal amide containing prisms **28** and **29** show the best activities. They are also active in the cisplatin resistant cancer cell line (A2780cisR), which indicates that they possess a different mode of action from cisplatin. Furthermore, their activities are lower in the non-cancerous human embryonic kidney cell line (HEK).

compound	***A2780***	***A2780cisR***	***HEK***	***SC***
28	*4.5 ± 0.5*	*5.9 ± 0.3*	*10.2 ± 0.7*	*2.3*
29	*3.9 ± 0.2*	*6.1 ± 0.4*	*10.8 ± 1.0*	*2.8*
30	*10.1 ±0.6*	*12.4 ± 0.6*	*10.9 ± 0.8*	*1.1*
cisplatin	*2.0 ± 0.2*	*18.1 ± 2.1*	*8.1 ± 1.3*	*4.0*
RAPTA-C	*<200*	*<200*	*<200*	*-*

*Table 10: IC_{50}-values in µmol for metalla-prisms **28 - 30** in A2780 (ovarian cancer cell line); A2780cisR (cisplatin resistant ovarian cancer cell line); HEK (human embryonic kidney cell line); SC (selectivity coefficient [HEK/A2780]). Data obtained from the group of Paul Dyson (EPFL).*

The selectivity coefficients (SC = IC_{50}-values on HEK / IC_{50}-values on A2780) of prisms **28** and **29** are > 1, which means that their cytotoxicity towards cancer cells is higher than towards non-cancerous cells, however the values are rather low and therefore the compounds are only poorly selective.

7. CONCLUSION AND PERSPECTIVES

The goal of this thesis entitled, *"Increasing the Size of Metalla-Assemblies to Target the EPR-Effect of Tumors and Solid Cancers"* was the development of macromolecular and multi-nuclear arene-ruthenium metalla-assemblies with anti-cancer activity and the ability to exploit the EPR-effect of solid cancers. Therefore, dinuclear arene-ruthenium complexes, so called molecular clips, were synthesized from the dinuclear arene-ruthenium precursor $[Ru_2(\eta^6\text{-}p\text{-cymene})_2(\mu_2\text{-}Cl)_2Cl_2]$ in combination with a spacer ligand. Several clip moieties were connected by two multi-dentate panel ligands in order to create supramolecular multi-nuclear assemblies, as shown in figure 53. Such an assembly offers four possibilities to increase the overall size and weight of assemblies: the arene, the spacer ligand, the panel ligand and the guest molecule.

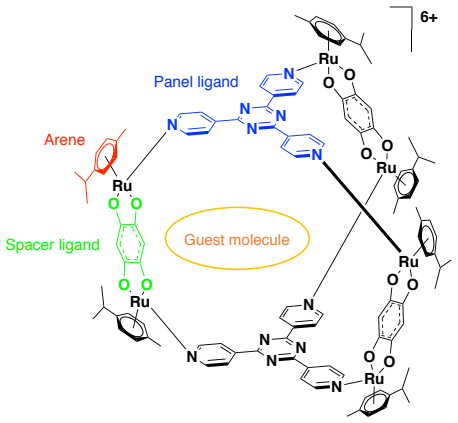

Figure 53: Typical molecular prism built from arene ruthenium clips and tridentate panels offering the possibility of guest encapsulation.

This project mainly focused on the modification of the spacer ligands. The spacer ligands shown in this work possess bis-bidendate chelating properties, in order to combine two ruthenium metal centers to form a molecular clip. Four different types of spacer ligands were synthesized: oxalamides, hydrazines, diazenes and dihydroxybenzoquinones (figure 54).

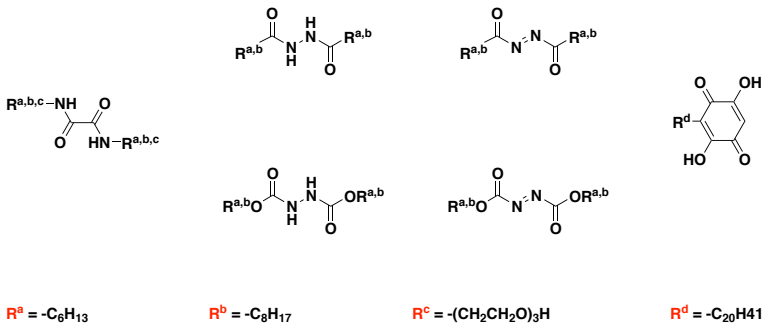

Figure 54: Synthesized bis-bidentate chelating ligands for clip formation, (from left to right: oxalamides, hydrazine derivatives, diazene derivatives, dihydroxybenzoquinone derivatives).

The functionalization of oxalamides was straightforward. Oxalyl chloride and a primary amine were used as starting materials. Four oxalamides with alkyl chains (N^1,N^2-dihexyloxalamide, N^1,N^2-dioctyloxalamide, N^1,N^2-didecyloxalamide and N^1,N^2-ditetradecyloxalamide) as well as one PEGylated oxalamide derivative (N^1,N^2-bis(2-(2-(2-hydroxyethoxy)ethoxy)ethyl)oxalamide) were successfully synthesized.
For the preparation of hydrazine and diazene derivatives, hydrazine monohydrate was used as starting material, which was allowed to react with an acid chloride or a chloroformate to yield hydrazine diacyl or hydrazine dicarboxylate, respectively. After oxidation, the diazene analogues were obtained. The hexyl and octyl derivatives of hydrazine diacyl, hydrazine dicarboxylate, diazene diacyl and diazene dicarboxylate were successfully synthesized.

Another goal of this thesis was the functionalization of dhbq and two methods were tested (scheme 31). Methylation and bromination of dhbq yield the mono- and dibromo compounds 3-bromo-2,5-dimethoxycyclohexa-2,5-diene-1,4-dione and 2,5-dibromo-3,6-dimethoxycyclohexa-2,5-diene-1,4-dione, which are potential intermediates for further functionalization *via* Suzuki-cross coupling reactions. However, neither the Suzuki-cross coupling nor the Miyaura borylation were successful. In the next attempt dhbq was converted to 1,2,4,5-tetramethoxybenzene *via* oxidation followed by methylation. *n*-BuLi was used to deprotonate the aromatic ring at three position in order to react with electrophilic alkyl halides or PEG halides.

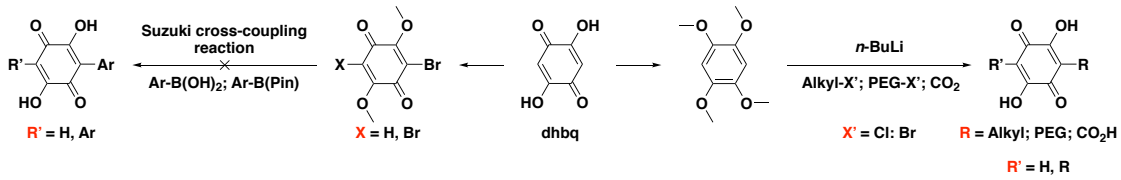

Scheme 31: Possible methods to functionalize dhbq.

The derivative of the bioactive natural product embelin, 2,5-dihydroxy-3-icosylcyclohexa-2,5-diene-1,4-dione, was successfully synthesized. The attempt to attach longer alkyl chains or PEGylated chains failed with this method. Therefore, intermediate 1,2,4,5-tetramethoxybenzene was converted to 2,3,5,6-tetramethoxyterephthalic acid in the presence of *n*-BuLi and CO_2, to attach a PEGylated chain *via* amide bond formation. However, introduction of PEGylated chains was also unsuccessful. Nevertheless, 14 spacer ligands were successfully synthesized during the Ph.D. thesis.

Three new molecular clips were presented in this work (figure 55) that were used to form five multi-nuclear assemblies. The spacer ligands N^1,N^2-dihexyloxalamide, N^1,N^2-dioctyloxalamide and 2,5-dihydroxy-3-icosylcyclohexa-2,5-diene-1,4-dione were successfully used for the preparation of the respective molecular clips with a yield of 25%, 21% and 77%, respectively.

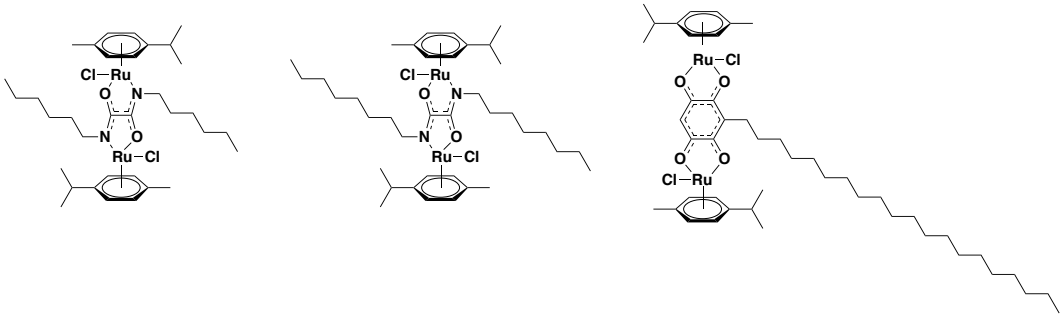

Figure 55: Successfully synthesized molecular clips consisting of oxalamides and dhbq derivatives.

The corresponding hexa-nuclear prism using the tri-dentate panel 4-tpt resulted in the formation of three prisms $[(\eta^6\text{-}p\text{-cymene})_6Ru_6(\mu_4\text{-}N^1,N^2\text{-dihexyloxalamide})_3(\mu_3\text{-4-tpt})_2][CF_3SO_3]_6$, $[(\eta^6\text{-}p\text{-cymene})_6Ru_6(\mu_4\text{-}N^1,N^2\text{-dioctyloxalamide})_3(\mu_3\text{-4-tpt})_2][CF_3SO_3]_6$ and $[(\eta^6\text{-}p\text{-cymene})_6Ru_6(\mu_4\text{-3-icosyl-dihydroxybenzoquinone})_3(\mu_3\text{-4-tpt})][CF_3SO_3]_6$. These prisms were isolated in good yields, 96%, 60% and 60%, respectively. The biological activities of the metalla-prisms were investigated in the group of Prof. Paul Dyson at the EPFL. The oxal amide containing hexa-nuclear prisms show IC_{50}-values in the low micromolar range on ovarian cancer cell lines.

Similarly, the three molecular clips were used for the preparation of octa-nuclear cubes using the tetra-dentate panel tpp. The reaction was successful with the clips containing oxalamides but failed with the clip made from the dhbq derivative. Two octa-nuclear cubes $[(\eta^6\text{-}p\text{-cymene})_8Ru_8(\mu_4\text{-}N^1,N^2\text{-dihexyloxalamide})_4(\mu_4\text{-tpp})][CF_3SO_3]_8$ and $[(\eta^6\text{-}p\text{-cymene})_8Ru_8(\mu_4\text{-}N^1,N^2\text{-dioctyloxalamide})_4(\mu_4\text{-tpp})_2][CF_3SO_3]_8$ were prepared with 73% and 71% yield, respectively. The weight of these multi-nuclear assemblies ranged from 3.7 kDa to 5.6 kDa (figure 56). Synthetic limitations regarding solubility and reactivity were observed when increasing the size and apolarity of the compound. Attempts to introduce PEGylated functionalities to increase solubility failed, due the low reactivity of the starting materials or due to interference of the oxygen rich PEG-groups with the metal moieties.

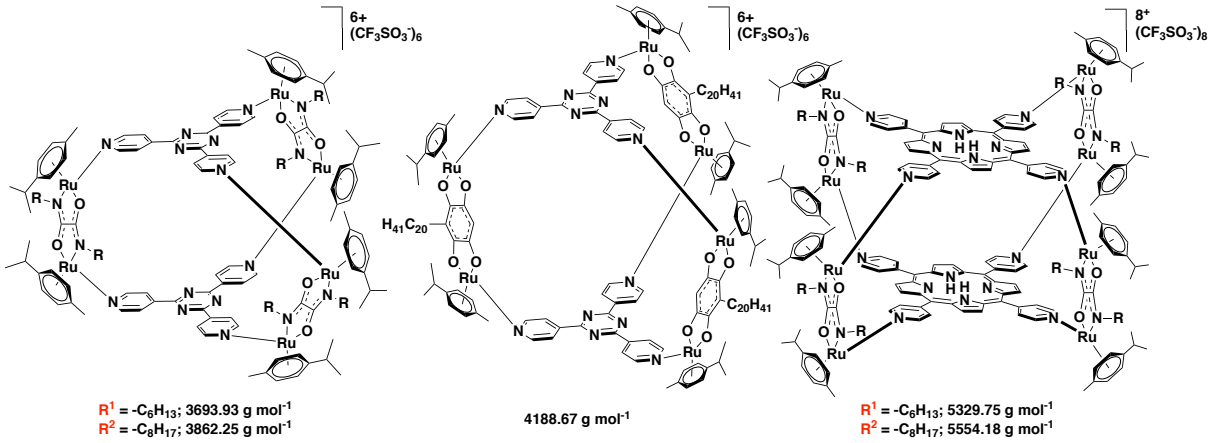

Figure 56: Molecular weights of the successfully synthesized molecular prisms and cubes.

Limitations regarding size enlargement and solubility were encountered during the thesis. Therefore, in the future, modification of the panel ligand can be proposed in order to combine a higher number of clips to increase significantly the size and molecular weight. Figure 57 shows the structure of 1,2,3,4,5,6-hexakis(pyridin-4-ylethynyl)benzene, a hexa-dentate ligand, that was used to coordinate Zn-centered porphyrin derivatives.[208] This ligand can be used as hexa-dentate panel ligand to combine six clips in order to synthesize a dodeca-nuclear assembly. A dodeca-nuclear *p*-cymene-ruthenium assembly consisting of this panel ligand and 2,5-dihydroxy-3-icosylcyclohexa-2,5-diene-1,4-dione, the largest spacer ligand synthesized in this project, and twelve triflate counterions would result in an overall molecular weight of around 8.5 kDa.

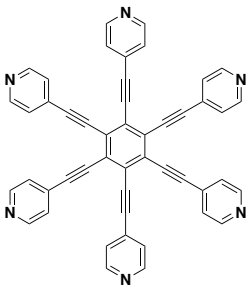

Figure 57: Possible hexa-dentate panel for the preparation of dodeca-nuclear assemblies.[208]

Porphyrin derivatives are ideal panel ligands for the preparation of metalla-assemblies and the modification of porphyrins is well described in the literature.[161] As presented in a review article of Tanaka,[209] several porphyrin units can be linked by triple bonds. However, this results in a 90° angle between adjacent units, which makes an assembly improbable. To overcome this problem, two triple bonds can be interlinked between the porphyrin units to obtain flat structures, ideal for the preparation of discrete assemblies.[209] Figure 58 shows the porphyrin derivative synthesized by Osuka and co-workers. In order to serve as a panel ligand, the aryl

moiety has to be replaced by pyridyl substituents for coordination. In this manner, multiple porphyrin units can be fused and the simplest two singly-linked porphyrin, should already result in a dodeca-nuclear ruthenium assembly.

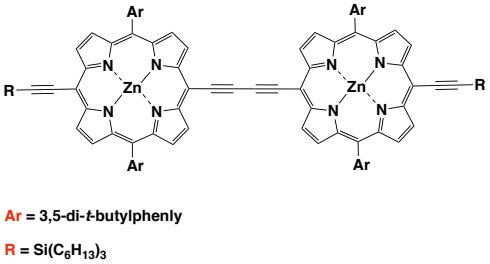

Figure 58: Porphyrin derivative linked by two triple bonds synthesized by Osuka and co-workers.[209]

Scheme 32 presents a different approach to synthesize multi-nuclear arene-ruthenium assemblies using porphyrin derivatives as panel ligands. The macromolecular structure shown in scheme 32 was also synthesized by Osuka and co-worker and demonstrates a method to combine up to 128 porphyrin units. However, the geometry of the resulting oligomer is not suitable for the assembly using arene-ruthenium molecular clips. He developed a strategy to triply fuse the single porphyrin units with each other to obtain a flat macromolecular structure and could connect up to 24 porphyrin units in this manner, as confirmed by mass spectroscopy. Furthermore, the number of units in such an oligomer can be controlled using Osuka's technique. The coordinating Zn^{2+} in the center is crucial to increase the solubility of the porphyrin oligomer.[210–212]

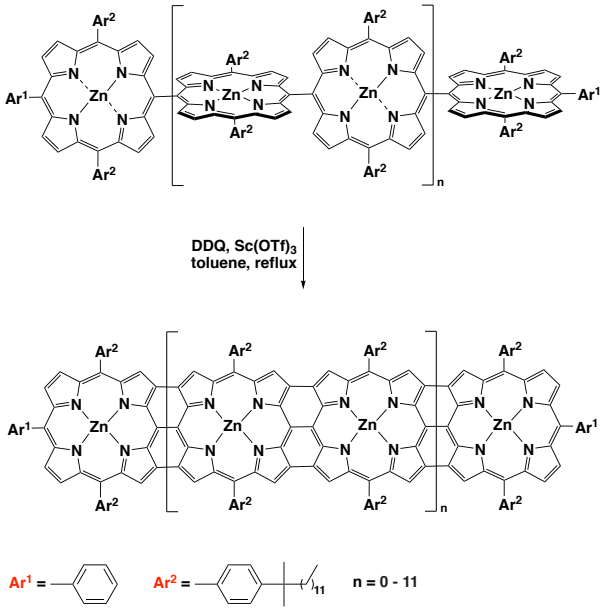

Scheme 32: Triply fused porphyrin derivatives to obtain oligomeric structures as described by Osuka.[212]

Replacement of the aryl moieties with pyridyl substituents would offer a potential multi-dentate ligand with the ability to combine 50 clips. For our purpose, the di-pyridyl and tri-pyridyl derivatives of porphyrin are used and their preparation was described by Sanders and co-workers in 2006.[213] Moreover, highly water soluble and smaller spacer ligands could be used for clip formation to avoid solubility problems. Two of such 24mer panel ligands in combination with 50 molecular clips derived from oxalate and *p*-cymene with 100 triflate counter ions would result in an overall weight of approximately 65 kDa. Using this strategy, the resulting metalla-assembly exceeds by far the minimal requirement of 20 kDa, and can therefore be ideal to exploit the EPR-effect. Osuka and co-workers were able to fully characterize the porphyrin oligomer consisting of four units, without encountering solubility issues.[212] Therefore, the preparation of a molecular metalla-assembly, consisting of a 24mer panel ligand, might be challenging. Nevertheless, a porphyrin panel ligand consisting of seven units, in combination with a counter ion and the PEG-containing molecular clip, which was prepared and published previously by our group,[162] would yield an overall assembly of over 20 kDa (figure 59).

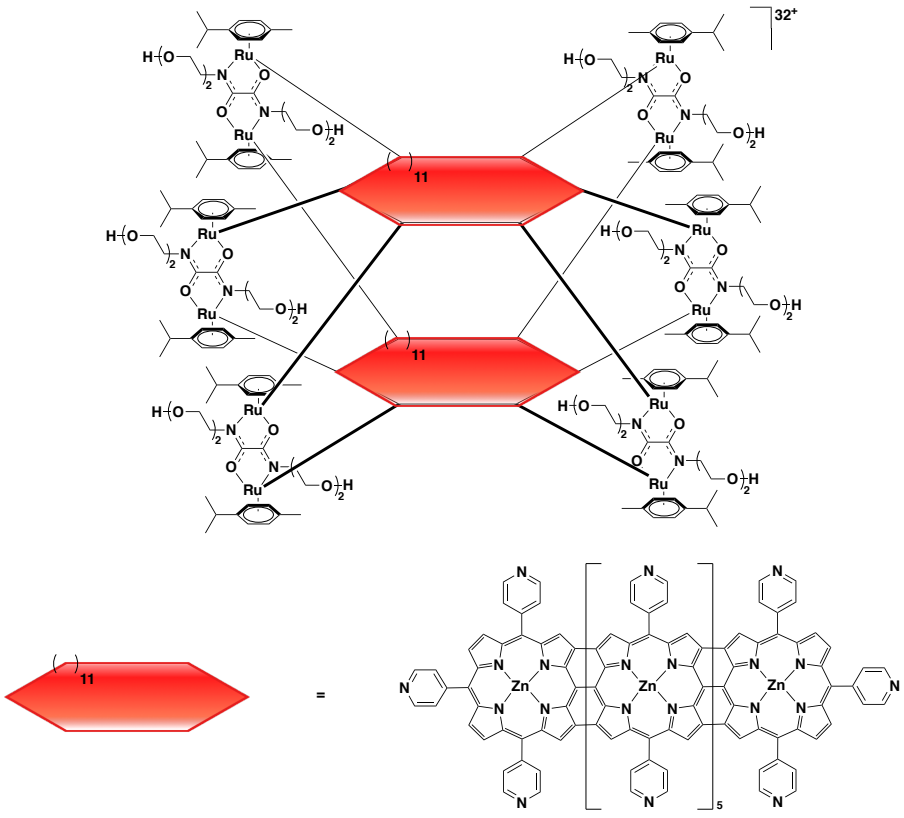

Figure 59: Simplified illustration of a multi-nuclear PEG-containing p-cymene ruthenium metalla-assembly connected by two 7mer of pyridyl porphyrin derivatives to reach a mass of over 20 kDa in order to exploit the EPR-effect and to counteract solubility issues.

8. EXPERIMENTAL PART

Materials and Methods: Commercially available reagents were purchased from Sigma-Aldrich and Brunschwig and were used as received. All reactions were carried out in abs. solvents, which were dried before use according to standard procedures and all reactions were performed under an inert atmosphere. Column chromatographic purifications were performed on silica gel 60 Å (32 - 63 mesh) under positive pressure of air and with technical grade eluents without further purification. Concentration was performed by rotary evaporation at 40 °C under reduced pressure and products were dried under high vacuum (~ 1 mbar) at RT.

Thin layer Chromatography (TLC) plates were obtained from Merck (TLC Silica gel 60 F_{254} aluminium sheets, with fluorescence indicator). UV light (254 nm) or a basic aqueous $KMnO_4$ - K_2CO_3 solution were used to visualize the respective compounds.

Nuclear magnetic resonance (NMR) spectroscopy was performed on a Bruker Avance II 400 spectrometer at 400 MHz for ^{1}H-NMR and at 101 MHz for ^{13}C-NMR at the University of Neuchâtel. ^{1}H- and ^{13}C-NMR of molecular cubes **65** and **66** and ^{13}C-NMR of molecular prisms **62** and **63** were recorded by Dr. Aurélien Bornet from EPFL in Lausanne and were acquired on a Bruker AV3HD 600 MHz spectrometer (14.1 T) equipped with a 5 mm BBO N_2 cooled cryoprobe at 600 MHZ (^{1}H-NMR) and 151 MHz (^{13}C-NMR). Chemical shifts (δ-values) are reported in parts per million (ppm). Spectra were calibrated related to the deuterated solvents[214,215] residual proton chemical shifts: 7.26 ppm (^{1}H-NMR) and 77.16 (^{13}C-NMR) for $CDCl_3$; 2.50 ppm (^{1}H-NMR) and 39.52 (^{13}C-NMR) for $(CD_3)_2SO$; 4.33 (^{1}H-NMR) and 62.80 (^{13}C-NMR) for CD_3NO_2. ^{13}C-NMR spectra were recorded ^{1}H-decoupled. Multiplets are assigned as: s (singlet), d (doublet), t (triplet), q (quartet), sept (septet) and m (multiplet).

Infrared spectra were recorded with a Thermoscientific Nicolet iS5 spectrometer. Peaks were defined as: s (strong), m (medium) and w (weak).

Electrospray ionization mass spectrometry (ESI-MS) spectra were obtained in positive or negative mode with a LCQ Finnigan mass spectrometer recorded at the University of Fribourg by Dr. Fredy Nydegger and Dr. Albert Ruggi.

UV-VIS absorption spectra were recorded with a Perkin–Elmer UV-VIS spectrophotometer.

Elemental analyses were carried out by the Mikroelementaranalytisches Laboratorium, ETH Zürich (Zürich, Switzerland).

The ruthenium precursor $[Ru_2(\eta^6\text{-}p\text{-cymene})_2(\mu_2\text{-}Cl)_2Cl_2]$[216], the spacer ligands **3** - **6**[163], **9**[167] and **11**[167] and the panel ligands 4-tpt[155] and tris-pvb[156] were prepared according to published methods.

Ligands that were used for the formation of the final assembly are fully characterized, others are characterized by NMR or ESI-MS for identification. All complexes are fully characterized.

8.1. Synthesis of N^1,N^2-Dihexyloxalamide (**3**)

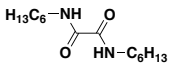

To a solution of hexylamine (5.0 mL, 37.85 mmol, 4.0 eq) in toluene (10 mL) was slowly added a solution of oxalyl chloride (0.8 mL, 9.46 mmol, 1.0 eq) in toluene (15 mL) at RT. The mixture was heated to 60 °C to become a clear solution and was stirred overnight. The reaction was allowed to cool to RT and the precipitate was filtered and washed with cold toluene (3 × 10 mL) and dried to yield the desired amide **3** as a white solid (2.38 g, 98%). **^{1}H-NMR** ($CDCl_3$, 400 MHz) δ/ppm: 7.48 (s, 2H, N*H*), 3.30 (q, $^3J_{HH}$ = 6.9 Hz, 4H, NCH_2), 1.58 - 1.51 (m, 4H, CH_2), 1.37 - 1.27 (m, 12H, CH_2), 0.90 - 0.86 (m, 6H, CH_3). **^{13}C-NMR** ($CDCl_3$, 101 MHz): 160.0 (2C, *C*O), 39.8 (2C, N*C*H_2), 31.5 (2C, *C*H_2), 29.3 (2C, *C*H_2), 26.6 (2C, *C*H_2), 22.7 (2C, *C*H_2), 14.1 (2C, *C*H_3). **IR** (cm^{-1}): 3299 (s), 2956 (m), 2919 (m), 2854 (m), 1644 (s), 1507 (s), 1474 (s), 1464 (s), 1383 (m), 1291 (w), 1241 (w), 1208 (m), 1156 (w), 1131 (w), 890 (w), 799 (w), 784 (m), 718 (s), 575 (w), 566 (w), 557 (w), 548 (w), 539 (w), 538 (m), 531 (w), 509 (w), 501 (w), 493 (w), 485 (w), 475 (w), 467 (w), 458 (w), 449 (w), 441 (w), 432 (w), 424 (w). **ESI-MS$^+$** Calcd for $C_{14}H_{29}N_2O_2$ ($[M + H]^+$): m/*z* 257.2. Found: m/*z* 257.3. **UV-VIS** (1.0×10^{-4} M, CH_2Cl_2): λ_{max} 229 nm ($\varepsilon = 5.6 \times 10^3$ $M^{-1}cm^{-1}$). **EA**: Calcd for $C_{14}H_{28}N_2O_2$ (256.4): C, 65.59; H, 11.01; N, 10.93; Found: C, 65.84; H, 11.22; N, 10.97.

8.2. Synthesis of N^1,N^2-Dioctyloxalamide (**4**)

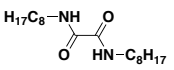

To a solution of octylamine (1.28 mL, 7.74 mmol, 4.0 eq) in toluene (10 mL) was slowly added a solution of oxalyl chloride (0.17 mL, 1.93 mmol, 1.0 eq) in toluene (15 mL) at RT. The mixture was heated to 60 °C and became a clear solution. The mixture was stirred at 60 °C for 15 h and then allowed to cool to RT. The white precipitate was filtered and washed with hot dist. H_2O (3 × 20 mL) and toluene (3 × 20 mL) to yield the desired amide **4** as a white solid (555 mg, 92%). **^{1}H-NMR** ($CDCl_3$, 400 MHz) δ/ppm: 7.56 (s, 2H, N*H*), 3.31 - 3.26 (m, 4H, NCH_2), 1.58 - 1.51 (m, 4H, CH_2), 1.33 - 1.24 (m, 22H, CH_2), 0.86 (t, $^3J_{HH}$ = 6.5 Hz, 6H, CH_3). **^{13}C-NMR** ($CDCl_3$, 101 MHz) δ/ppm: 160.0 (2C, *C*O), 39.8 (2C, N*C*H_2), 31.9 (2C, *C*H_2), 29.34 (2C, *C*H_2), 29.30 (2C, *C*H_2), 29.27 (2C, *C*H_2), 27.0 (2C, *C*H_2),

22.7 (2C, *C*H_2), 14.2 (2C, *C*H_3). **IR** (cm^{-1}): 3301 (s), 2918 (s), 2849 (m), 1644 (s), 1505 (s), 1467 (s), 1381 (m), 1266 (w), 1224 (w), 1205 (w), 785 (m), 718 (s), 582 (w), 539 (w), 516 (w), 502 (w), 462 (w), 447 (w). **ESI-MS**$^+$ Calcd for $C_{18}H_{37}N_2O_2$ ($[M + H]^+$): m/*z* 313.3. Found: m/*z* 313.3. **UV-VIS** (1.0×10^{-4} M, CH_2Cl_2): λ_{max} 229 nm ($\varepsilon = 5.14 \times 10^3$ $M^{-1}cm^1$). **EA**: Calcd for $C_{18}H_{36}N_2O_2$ (312.5): C 69.18; H 11.61; N 8.96; Found: C 68.89; H 11.53; N 8.84.

8.3. Synthesis of *N*^{1},*N*^{2}-didecyloxalamide (**5**)

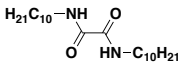

Oxalyl chloride (0.11 mL, 1.25 mmol, 1.0 eq) was dissolved in toluene and the mixture was cooled to 0 °C and decylamine (1.0 mL, 5.00 mmol, 4.0 eq) was added slowly. After the addition, the mixture was heated to 90 °C and stirred overnight and then allowed to cool to RT and the resulting solid was filtered and washed with toluene and Et_2O. The product was dried under high vacuum to yield the desired amide **5** as a white solid (295 mg, 64%). **^{1}H-NMR** ($CDCl_3$, 400 MHz) *δ*/ppm: 7.45 (s, 2H, N*H*), 3.30 (q, $^3J_{HH}$ = 6.8 Hz, 4H, N*C*H_2), 1.58 - 1.51 (m, 4H, C*H*$_2$), 1.35 - 1.24 (m, 28H, C*H*$_2$), 0.89 - 0.86 (m, 6H, C*H*$_3$). **^{13}C-NMR** (101 MHz, $CDCl_3$) *δ*/ppm: 160.0 (2C, *C*O), 39.9 (2C, N*C*H_2), 32.0 (2C, *C*H_2), 29.7 (2C, *C*H_2), 29.6 (2C, *C*H_2), 29.42 (2C, *C*H_2), 29.36 (4C, *C*H_2) 27.0 (2C, *C*H_2), 22.8 (2C, *C*H_2), 14.2 (2C, *C*H_3).

8.4. Synthesis of *N*^{1},*N*^{2}-ditetradecyloxalamide (**6**)

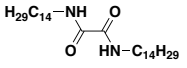

Oxalyl chloride (0.1 mL, 1.17 mmol, 1.0 eq) was dissolved in toluene (10 mL) and cooled to 0 °C. Then a solution of tetradecylamine (1.0 g, 4.69 mmol, 4.0 eq) in toluene (40 mL) was added and the white mixture was heated at 90 °C overnight. The solution was allowed to cool to RT to give a white suspension. The mixture was concentrated, washed with hot dist. H_2O (2 × 50 mL) and redissolved in DCM (50 mL), dried over $MgSO_4$, filtered and concentrated to give a white solid. The solid was recrystallized over propylene carbonate (15 mL, 240 °C) to obtain the desired amide **6** as a colorless solid (319 mg, 39%). **^{1}H-NMR** ($CDCl_3$, 400 MHz) *δ*/ppm: 7.43 (s, 2H, N*H*), 3.30 (q, 4H, $^3J_{HH}$ = 7.0 Hz, NC*H*$_2$), 1.60 - 1.61 (m, 12H, C*H*$_2$), 1.31 - 1.21 (m, 36H, C*H*$_2$), 0.92 - 0.85 (m, 6H, C*H*$_3$).

8.5. Synthesis of *N*^{1},*N*^{2}-bis(2-(2-(2-hydroxyethoxy)ethoxy)ethyl)oxalamide (**7**)

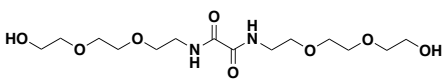

2-(2-(2-aminoethoxy)ethoxy)ethan-1-ol (**PEG 2**) (138 mg, 928 *μ*mol, 2.0 eq) was dissolved in dry THF (5 mL) and cooled to 0 °C. NEt_3 (0.07 mL, 1.02 mmol, 1.1 eq) was added dropwise and the mixture

was stirred for 10 min. Oxalyl chloride (0.04 mL, 464 μmol, 1.0 eq) was added slowly and the ice bath was removed and the yellow mixture was stirred 16 h. The white solid was filtered off, the mixture was concentrated and suspended in THF (20 mL) and the resulting white solid was filtered off. The mixture is concentrated and the desired amide **7** is obtained with traces of $HNEt_3Cl$ salt as yellowish oil (22.9 mg, 14%). **^{1}H-NMR** ($CDCl_3$, 400 MHz) δ/ppm: 4.48 - 4.45 (m, 4H, HOCH_2), 3.85 - 3.77 (m, 8H, CH_2), 3.73 - 3.71 (m, 8H, CH_2), 3.68 - 3.65 (m, 4H, NCH_2). **^{13}C-NMR** ($CDCl_3$, 101 MHz) δ/ppm: 160.6 (2C, *C*O), 69.6 (2C, HO*C*H$_2$), 31.4 (2C, *C*H$_2$), 28.5 (2C, *C*H$_2$), 25.4 (2C, *C*H$_2$), 22.6 (2C, *C*H$_2$), 14.1 (2C, N*C*H$_2$). **ESI-MS$^+$** Calcd for $C_{24}H_{29}N_2O_8$ ([M + H]$^+$): m/*z* 353.2. Found: m/*z* 353.1.

8.6. Synthesis of dihexyl hydrazine 1,2-dicarboxylate (**9**)

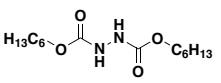

A solution of hydrazine monohydrate (0.5 mL, 6.65 mmol, 1,0 eq) in MeOH (5.0 mL) and dist. H_2O (5.0 mL) was placed in an ice bath and hexyl chloroformate (2.2 mL, 13.7 mmol, 2.0 eq) was added slowly. The mixture was stirred for 2 h at 0 °C until a colorless solid was formed. The mixture was extracted with EtOAc (3 x 10 mL) and washed with brine (1 x 10 mL), dried over $MgSO_4$, filtered and concentrated. The crude product was purified by flash column chromatography (SiO_2, pentane/EtOAc 14:1) to yield the desired dicarboxylate **9** as a colorless solid (1.55 g, 81%). **^{1}H-NMR** ($CDCl_3$, 400 MHz) δ/ppm: 6.86 (s, 2H, N*H*), 4.09 (t, 4H, $^3J_{HH}$ = 6.8 Hz, OCH_2), 1.63 - 1.56 (m, 4H, CH_2), 1.34 - 1.22 (m, 12H, CH_2), 0.87 - 0.80 (m, 6H, CH_3). **^{13}C-NMR** ($CDCl_3$, 101 MHz) δ/ppm: 157.1 (2C, *C*O), 66.4 (2C, OCH_2), 31.5 (2C, *C*H$_2$), 28.8 (2C, *C*H$_2$), 25.4 (2C, *C*H$_2$), 22.6 (2C, *C*H$_2$), 14.0 (2C, *C*H$_3$).

8.7. Synthesis of dioctyl hydrazine 1,2-dicarboxylate (**10**)

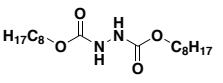

A solution of hydrazine monohydrate (0.22 mL, 4.60 mmol, 1,0 eq) in MeOH (5.0 mL) and dist. H_2O (5.0 mL) was placed in an ice bath and octyl chloroformate (1.8 mL, 9.20 mmol, 2.0 eq) was added slowly. The mixture was stirred for 2 h at 0 °C until a colorless solid was formed. The mixture was extracted with EtOAc (3 x 10 mL) and washed with brine (1x 10 mL), dried over $MgSO_4$, filtered and concentrated. The crude product was purified by flash column chromatography (SiO_2, pentane/EtOAc 14:1) to yield the desired dicarboxylate **10** as a colorless solid (1.16 g, 73%). **^{1}H-NMR** ($CDCl_3$, 400 MHz) δ/ppm: 6.45 (s, 2H, N*H*), 4.13 (t, $^3J_{HH}$ = 6.6 Hz, 4H, NCH_2), 1.63 (t, $^3J_{HH}$ = 7.2 Hz, 4H, CH_2), 1.35 - 1.26 (m, 20H, CH_2), 0.88 (t, $^3J_{HH}$ = 6.2 Hz, 6H, CH_3). **^{13}C-NMR** ($CDCl_3$, 101 MHz) δ/ppm:

156.9 (2C, *C*O), 66.6 (2C, O*C*H_2), 31.9 (2C, *C*H_2), 29.3 (2C, *C*H_2), 19.3 (2C, *C*H_2), 29.0 (2C, *C*H_2), 25.9 (2C, *C*H_2), 22.8 (2C, *C*H_2), 14.2 (2C, *C*H_3).

8.8. Synthesis of dihexyl azodicarboxylate (**11**)

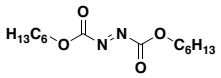

The hydrazine derivative **9** (50.0 mg, 192 μmol, 1.0 eq) was dissolved in DCM (5 mL) and NBS (34.2 mg, 192 μmol, 1.0 eq) was added at RT and the mixture was stirred for 2 h. After TLC showed full conversion of starting materials the mixture was diluted by DCM (20 mL) and the organic layer was washed by dist. H_2O and brine, dried over $MgSO_4$, filtered and concentrated. The crude product was further purified by flash column chromatography (SiO_2, pentane/EtOAc 14:1) to yield the desired azodicarboxylate **11** a yellow oil (40.1 mg, 73%). **^{1}H-NMR** ($CDCl_3$, 400 MHz) δ/ppm: 4.43 (t, 4H, $^3J_{HH}$ = 6.7 Hz, O*C*H_2), 1.82 - 1.75 (m, 4H, CH_2), 1.44 - 1.38 (m, 4H, CH_2), 1.35 - 1.27 (m, 8H, CH_2), 0.90 (m, 6H, CH_3). **^{13}C-NMR** ($CDCl_3$, 101 MHz) δ/ppm: 160.6 (2C, *C*O), 69.7 (2C, O*C*H_2), 31.4 (2C, *C*H_2), 28.5 (2C, *C*H_2), 25.4 (2C, *C*H_2), 22.6 (2C, *C*H_2), 14.1 (2C, *C*H_3).

8.9. Synthesis of dioctyl azodicarboxylate (**12**)

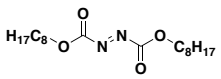

The hydrazine derivative **10** (1.0 g, 3.50 mmol, 1.0 eq) was dissolved in DCM (20 mL) and NBS (623 mg, 3.50 mmol, 1.0 eq) was added at RT and the clear solution turned yellow-orange and then red. After 2 h the mixture was diluted with DCM, washed with dist. H_2O (3 × 40 mL) and brine (1 × 40 mL) and concentrated. The crude product was purified by flash column chromatography (SiO_2, pentane/EtOAc 5:1 → 5:2) to obtain the desired azodicarboxylate **12** as yellow oil (720 mg, 60%). **^{1}H-NMR** ($CDCl_3$, 400 MHz) δ/ppm: 4.44 (t, $^3J_{HH}$ = 7.0 Hz, 4H, NCH_2), 1.79 (q, $^3J_{HH}$ = 7.1 Hz, 4H, CH_2), 1.44 - 1.37 (m, 4H, CH_2), 1.34 - 1.23 (m, 16H, CH_2), 0.90 - 0.86 (m, 6H, CH_3). **^{13}C-NMR** ($CDCl_3$, 101 MHz) δ/ppm: 160.6 (2C, *C*O), 69.6 (2C, O*C*H_2), 31.9 (2C, *C*H_2), 29.2 (4C, *C*H_2), 28.6 (2C, *C*H_2), 25.7 (2C, *C*H_2), 22.8 (2C, *C*H_2), 14.2 (2C, *C*H_3).

8.10. Synthesis of *N'*-hexanoylhexanehydrazine (**14**)

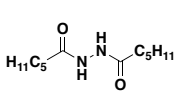

A solution of hydrazine monohydrate (0.07 mL, 1.14 mmol, 1.0 eq) in dist. H_2O (5.0 mL), was cooled to 0 °C and hexanoic anhydride (1.08 mL, 4.67 mmol, 3.3 eq) was added dropwise while stirring. The mixture was stirred for 2 h and the formed precipitate was filtered and washed with dist. H_2O and Et_2O and dried under high vacuum to obtain the desired hydrazine derivative **14** as a white solid (232 mg, 89%). **^{1}H-NMR** ($CDCl_3$,

400 MHz) δ/ppm: 8.97 (s, 2H, N*H*), 2.26 (t, $^{3}J_{HH}$ = 7.5 Hz, 4H, OCC*H*$_2$), 1.68 - 1.63 (m, 4H, C*H*$_2$), 1.34 - 1.29 (m, 8H, C*H*$_2$), 0.91 - 0.86 (m, 6H, C*H*$_2$). **^{13}C-NMR** ($CDCl_3$, 101 MHz) δ/ppm: 169.9 (2C, *C*O), 34.2 (2C, *C*H$_2$), 31.5 (2C, *C*H$_2$), 25.2 (2C, *C*H$_2$), 22.5 (2C, *C*H$_2$), 14.0 (2C, *C*H$_3$).

8.11. Synthesis of *N'*-octanoyloctanehydrazine (**15**)

Octanoyl chloride (5.2 mL, 30.3 mmol, 3.2 eq) was dissolved in Et_2O (40 mL) and dist. H_2O (4.0 mL) and $NaHCO_3$ (2.52 g, 30.0 mmol, 3.0 eq) was added. The mixture was cooled to 0 °C, hydrazine monohydrate (0.5 mL, 10.0 mmol, 1.0 eq) was added slowly and the mixture was stirred at RT overnight. The resulting colorless solid was filtered, washed with dist. H_2O and dried under high vacuum to obtain the desired hydrazine derivative **15** as colorless solid (2.85 g, quant.). **^{1}H-NMR** ($SO(CD_3)_2$, 400 MHz) δ/ppm: 9.59 (s, 2H, N*H*), 2.09 - 2.05 (m, 4H, OCC*H*$_2$), 1.51 - 1.46 (m, 4H, C*H*$_2$), 1.25 - 1.24 (m, 16H, C*H*$_2$), 0.88 - 0.83 (m, 6H, C*H*$_3$). **^{13}C-NMR** ($SO(CD_3)_2$, 101 MHz) δ/ppm: 171.0 (2C, *C*O), 33.1 (2C, OC*C*H$_2$), 31.1 (2C, *C*H$_2$), 28.5 (2C, *C*H$_2$), 28.4 (2C, *C*H$_2$), 25.0 (2C, *C*H$_2$), 22.0 (2C, *C*H$_2$), 13.9 (2C, *C*H$_3$). **^{1}H-NMR** ($CDCl_3$, 400 MHz) δ/ppm: 8.29 (s, 2H, N*H*), 2.25 (t, $^{3}J_{HH}$ = 7.6 Hz, 4H, OCC*H*$_2$), 1.66, (q, $^{3}J_{HH}$ = 7.2 Hz, 4H, C*H*$_2$), 1.32 - 1-25 (m, 16H, C*H*$_2$), 0.88 (t, $^{3}J_{HH}$ = 6.6 Hz, 6H C*H*$_3$). **^{13}C-NMR** ($CDCl_3$, 101 MHz) δ/ppm: 169.8 (2C, *C*O), 34.4 (2C, OC*C*H$_2$), 31.8 (2C, *C*H$_2$), 29.3 (2C, *C*H$_2$), 29.0 (2C, *C*H$_2$), 25.5 (2C, *C*H$_2$), 22.8 (2C, *C*H$_2$), 14.2 (2C, *C*H$_3$).

8.12. Synthesis of 1,1'-(diazene-1,2-diyl)bis(hexan-1-one) (**16**)

Hydrazine derivative **14** (688 mg, 3.02 mmol, 1.0 eq) was suspended in DCM (50 mL), cooled to 0 °C and a solution of $Pb(OAc)_4$ (1.48 g, 3.32 mmol, 1.1 eq) in DCM (20 mL) was added dropwise. The ice bath was removed and the reaction was stirred for 1 h at 30 °C. The resulting solid was filtered off and the organic layer was washed with brine (2 × 100 mL) and aq. sat. $NaHCO_3$ (1 × 100 mL) and again with brine (1 × 100 mL). The organic layer was dried over $MgSO_4$, filtered and dried under high vacuum to obtain the desired diazene **16** as an orange oil (682 mg, quant.). **^{1}H-NMR** ($CDCl_3$, 400 MHz) δ/ppm: 2.61 (t, $^{3}J_{HH}$ = 7.3 Hz, 4H, OCC*H*$_2$), 1.77 - 1.68 (m, 4H, C*H*$_2$), 1.40 - 1.30 (m, 8H, C*H*$_2$), 0.93 - 0.89 (m, 6H, C*H*$_3$). **^{13}C-NMR** ($CDCl_3$, 101 MHz) δ/ppm: 190.3 (2C, *C*O), 33.5 (2C, *C*H$_2$), 31.3 (2C, *C*H$_2$), 22.8 (2C, *C*H$_2$), 22.4 (2C, *C*H$_2$), 14.0 (2C, *C*H$_3$).

8.13. Synthesis of 1,1'-(diazene-1,2-diyl)bis(octan-1-one) (**17**)

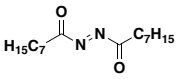

The hydrazine derivative **15** (250 mg, 885 µmol, 1.0 eq) was dissolved in benzene (75 mL), heated to reflux at 80 °C and $Pb(OAc)_4$ (393 mg, 879 µmol, 1.0 eq) was added at once. The mixture was stirred at 80 °C for 15 s and filtered. The orange-red solution was allowed to cool to RT and the solvent was removed under reduced pressure to yield an orange solid which decolored over time. The crude product was purified by recrystallization from DCM/*n*-hexane (2:1) at 40 °C to obtain the diazene **17** as a yellowish solid (249 mg, quant.). **^{1}H-NMR** ($SO(CD_3)_2$, 400 MHz) δ/ppm: 4.18 - 4.10 (m, 4H, OCCH_2), 3.01 - 2.80 (m, 4H, CH_2), 2.17 - 1.99 (m, 16H, CH_2), 1.72 - 0.59 (m, 6H, CH_3). **^{13}C-NMR** ($SO(CD_3)_2$, 101 MHz) δ/ppm: 178.2 (2C, *C*O), 31.6 (2C, OCCH_2), 28.9 (2C, *C*H_2), 27.4 (6C, *C*H_2) , 22.5 (2C, *C*H_2), 14.4 (2C, *C*H_3).

8.14. Syntheses of 4-bromo-*N*-(2-(2-(2-hydroxyethoxy)ethoxy)ethyl)benzamide-(**25^a**)

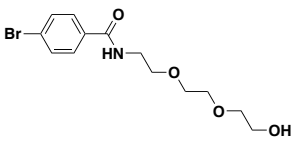

PEG 2 (214 mg, 1.43 mmol, 1.05 eq) was dissolved in dist. H_2O (2.0 mL) and acetone (1.0 mL) and $NaHCO_3$ (123 mg, 1.46 mmol, 1.07 eq) was added. The mixture was cooled to 0 °C and 4-bromobenzoyl chloride (**27**) (299 mg, 1.36 mmol, 1.0 eq) dissolved in acetone (1.2 mL) was added slowly and the formation of a colorless solid was observed. Acetone was removed under reduced pressure, dist. H_2O (15 mL) was added and the mixture was extracted with EtOAc (4 × 15 mL). The combined organic layers were washed with aq. sat. $NaHCO_3$ (1 × 20 mL) and dist. H_2O (1 × 20 mL), dried over $MgSO_4$, filtered and concentrated. The crude product was purified by flash column chromatography (SiO_2, DCM/MeOH 95:5) to yield the desired bromobenzamide **25^a** as a yellow oil (341 mg, 75%). **^{1}H-NMR** ($CDCl_3$, 400 MHz) δ/ppm: 7.70 (d, $^3J_{HH}$ = 8.5 Hz, 2H, C*H*), 7.57 (d, $^3J_{HH}$ = 8.5 Hz, 2H, C*H*), 6.86 (s, 1H, N*H*), 3.73 - 3.70 (m, 2H, CH_2), 3.68 - 3.63 (m, 10H, CH_2), 3.60 - 3.58 (m, 2H, CH_2). **^{13}C-NMR** ($CDCl_3$, 101 MHz) δ/ppm: 166.7 (1C, *C*O), 133.4 (1C, *C*C), 131.8 (2C, *C*H), 128.9 (2C, *C*H), 126.2 (1C, *C*Br), 72.6 (1C, *C*H_2), 70.5 (2C, *C*H_2), 70.0 (1C, *C*H_2), 61.8 (1C, *C*H_2), 39.4 (1C, *C*H_2).

8.15. Synthesis of 3-Icosyl-1,2,4,5-tetramethoxybenzene (**36**)

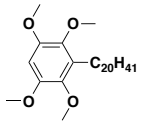

1,2,3,4-Tetramethoxybenzene (**35**) (430 mg, 2.20 mmol, 1.0 eq) was dissolved in THF (10 mL) and the solution was cooled to -10 °C and *n*-BuLi (2.5 M in hexane, 1 mL, 2.42 mmol, 1.1 eq) was slowly added. The mixture was stirred at -10 °C for 30 min, and 1-bromoicosane (904 mg, 2.42 mmol, 1.1 eq) was slowly added. The

mixture was stirred at -10 °C for 10 min and then allowed to warm to room temperature overnight. After completion of the reaction, aqueous saturated NH_4Cl (2 mL) was added to the solution, and the mixture was extracted with Et_2O (3 × 50 mL), washed with brine (1 × 50 mL), dried over $MgSO_4$, filtered, and concentrated under reduced pressure. The crude product was purified by flash column chromatography (SiO_2, pentane/EtOAc 40:1) to yield the desired alkylated tetramethoxybenzene **36** as a colorless solid (710 mg, 68%). **^{1}H-NMR** ($CDCl_3$, 400 MHz) δ/ppm: 6.41 (s, 1H, C*H*), 3.84 (s, 6H, OC*H*), 3.76 (s, 6H, OC*H*), 2.62 - 2.59 (m, 2H, CH_2), 1.56 - 1.49 (m, 2H, CH_2), 1.37 - 1.35 (m, 2H, CH_2), 1.25 (s, 32H, CH_2), 0.88 (t, $^3J_{HH}$ = 6.2 Hz, 3H, CH_3). **^{13}C-NMR** ($CDCl_3$, 101 MHz): δ/ppm: 149.0 (2C, CH_3OC), 141.3 (2C, CH_3OC), 131.3 (1C, $CC_{20}H_{41}$), 96.9 (1C, *C*H), 61.1 (2C, OCH_3), 56.4 (2C, OCH_3), 32.1 (1C, *C*H_2), 30.9 (1C, *C*H_2), 30.2 (1C, *C*H_2), 29.9 (10C, *C*H_2), 29.8 (1C, *C*H_2), 29.7 (1C, *C*H_2), 29.6 (1C, *C*H_2), 29.5 (1C, *C*H_2), 24.8 (1C, *C*H_2), 22.8 (1C, *C*H_2), 14.3 (1C, *C*H_3). **IR** (cm^{-1}): 2957 (w), 2916 (m), 2849 (m), 1594 (w), 1467 (m), 1408 (m), 1367 (w), 1343 (w), 1306 (w), 1244 (w), 1203 (w), 1117 (m), 1066 (w), 1044 (m), 1024 (w), 954 (m), 899 (w), 868 (w), 854 (w), 831 (W), 811 (w), 721 (w), 639 (w). **ESI-MS$^+$** Calcd for $C_{30}H_{54}O_4Na$ ([M + Na]$^+$): m/*z* 501.4. Found: m/*z* 501.4. **UV-VIS** (1.0 × 10^{-4} M, CH_2Cl_2): λ_{max} 229 nm (ε = 0.7 × 10^3 M^{-1} cm^{-1}); λ_{max} 284 nm (ε = 1.7 × 10^3 M^{-1} cm^{-1}). **EA**: Calcd for $C_{30}H_{54}O_4$ (478.4): C, 75.26; H, 11.37. Found: C, 75.40; H, 11.39.

8.16. Synthesis of 3-Icosyl-2,5-dimethoxycyclohexa-2,5-diene-1,4-dione (**37**)

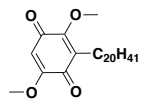

Alkylated tetramethoxybenzene **36** (177 mg, 370 μmol, 1.0 eq) was suspended in MeCN (3 mL), ceric ammonium nitrate (CAN) (510 mg, 930 μmol, 2.51 eq) was added, and the yellow suspension turned into an orange suspension. The mixture was stirred at RT for 2 h. After completion of the reaction, the mixture was extracted with EtOAc (3 × 15 mL). The combined organic layers were washed with brine (1 × 20 mL), dried over $MgSO_4$, filtered and concentrated under reduced pressure. The crude product was purified by flash column chromatography (SiO_2 and 20:1 pentane/EtOAc) to yield the desired benzoquinone **37** as a colorless solid (80.2 mg, 48%). **^{1}H-NMR** ($CDCl_3$, 400 MHz) δ/ppm: 5.72 (s, 1H, C*H*), 4.04 (s, 3H, OCH_3), 3.80 (s, 3H, OCH_3), 2.42 (t, $^3J_{HH}$ = 7.5 Hz, 2H, CH_2), 1.41 - 1.35 (m, 2H, CH_2), 1.25 (s, 34 H, CH_2), 0.88 (t, $^3J_{HH}$ = 6.6 Hz, 3H, CH_3). **^{13}C-NMR** ($CDCl_3$, 101 MHz) δ/ppm: 183.7 (1C, *C*O), 182.6 (1C, *C*O), 158.9 (1C, CH_3OC), 156.0 (1C, CH_3OC), 130.9 (1C, $CC_{20}H_{41}$), 105.5 (1C, *C*H), 61.5 (1C, OCH_3), 56.5 (1C, OCH_3), 32.1 (1C, *C*H_2), 29.81 (8C, *C*H_2), 29.75 (4C, *C*H_2), 29.7 (1C, *C*H_2), 29.6 (1C, *C*H_2), 29.5 (1C, *C*H_2), 28.8 (1C, *C*H_2), 23.2

(1C, *C*H_2), 22.8 (1C, *C*H_2), 14.3 (1C, *C*H_3). **IR** (cm^{-1}): 2916 (m), 2849 (m), 1649 (w), 1597 (w), 1467 (w), 1324 (w), 1206 (w), 1154 (w), 1046 (w), 928 (w), 835 (w), 797 (w), 720 (w), 500 (w), 483 (w), 469 (w), 401 (w), 453 (w), 433 (w), 429 (w). **ESI-MS**$^+$ Calcd for $C_{28}H_{48}O_4Na$ ($[M + Na]^+$): m/*z* 471.4. Found: m/*z* 471.3. **UV-VIS** (1.0×10^{-4} M, CH_2Cl_2): λ_{max} 286 nm (ε = 5.6×10^3 M^{-1} cm^{-1}). **EA**: Calcd for $C_{28}H_{48}O_4$ (448.4): C, 74.95; H, 10.78. Found: C, 75.21; H, 10.85.

8.17. Synthesis of 2,5-dihydroxy-3-icosylcyclohexa-2,5-diene-1,4-dione (**38**)

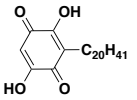

The benzoquinone derivative **37** (116 mg, 259 μmol, 1.0 eq) and EtOH (10 mL) were mixed to give an orange suspension. NaOH (2 M, 5 mL) was added, and the suspension turned into a violet solution. The solution was heated to 70 °C and stirred until thin-layer chromatography showed full conversion of the starting material. The reaction was allowed to cool to RT, HCl (2 M, 25 mL) was added, and the solution turned into an orange suspension. The mixture was extracted with EtOAc (3 × 30 mL). The combined organic layers were dried over $MgSO_4$, filtered, concentrated, and dried under high vacuum to yield the desired dihydroxybenzoquinone **38** as a light brown solid, which was used without further purification (73 mg, 72%). **^{1}H-NMR** ($SO(CD_3)_2$, 400 MHz) δ/ppm: 11.17 (s, 2H, O*H*), 5.77 (s, 1H, C*H*), 2.27 (t, $^3J_{HH}$ = 7.5 Hz, 2H, CH_2), 1.34 (m, 2H, CH_2), 1.22 (m, 34H, CH_2), 0.84 (t, $^3J_{HH}$ = 6.6 Hz, 3H, CH_3). **IR** (cm^{-1}): 3304 (m), 2917 (m), 2847 (m), 1612 (m), 1462 (w), 1325 (m), 1187 (m), 860 (w), 768 (w), 708 (w). **ESI-MS**$^-$ Calcd for $C_{26}H_{43}O_4$ ($[M - H]^-$): m/*z* 419.3. Found: m/*z* 419.3. **UV-VIS** (1.0×10^{-4} M, CH_2Cl_2): λ_{max} 282 nm (ε = 1.4×10^4 M^{-1} cm^{-1}); λ_{max} 290 nm (ε = 1.4×10^4 M^{-1} cm^{-1}). **EA**: Calcd for $C_{26}H_{44}O_4 \cdot EtOH \cdot H_2O$ (420.6 + 18.0 + 46.1): C, 69.38; H, 10.81; N, 0.00. Found: C, 69.87; H, 10.57; N, 0.01.

8.18. Syntheses of 1-(methylsulfonyl)triacontane (**43**)

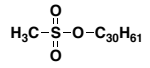

A two-necked flask under nitrogen atmosphere was charged with 1-triacontalol (**42**) (200 mg, 460 μmol, 1.0 eq) and suspended in dry DCM (20 mL) and NEt_3 (148 μL, 1.06 mmol, 2.3 eq). To solubilize the mixture was heated until it turned into a solution. The mixture was stirred at RT for 30 min and MsCl (84.4 mg, 736 μmol, 1.6 eq) was added and the mixture was stirred at RT for 24 h. The mixture was diluted with DCM (20 mL) and the organic phase was washed with dist. H_2O, HCl (2M), aq. sat. $NaHCO_3$ and dist. H_2O, dried over $MgSO_4$, filtered and concentrated to yield the desired sulfonyl **43** as a colorless solid. (229 mg, 96%). **^{1}H-NMR** ($CDCl_3$, 400 MHz) δ/ppm: 4.22 (t, $^3J_{HH}$ = 6.6 Hz, 2H, OCH_2), 3.00 (s, 3H,

SC*H*$_3$), 1.78 - 1.71 (m, 2H, C*H*$_2$), 1.60 - 1.54 (m, 2H, C*H*$_2$), 1.41 - 1.35 (m, 2H, C*H*$_2$), 1.30 - 1.25 (m, 50H, C*H*$_2$), 0.88 (t, $^3J_{HH}$ = 6.7 Hz, 3H, C*H*$_3$).

8.19. Synthesis of Molecular Clip [(η^6-p-Cymene)$_2$Ru$_2$(μ_4- N^1,N^2-dihexyloxalamide)Cl$_2$] (**50**)

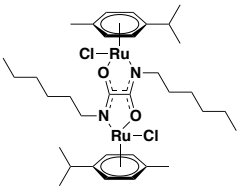

N^1,N^2-Dihexyloxalamide (**3**) (200 mg, 780 μmol, 1.0 eq) was suspended in EtOH (15 mL), and DIPEA (0.3 mL, 1.73 mmol, 2.2 eq) was added dropwise at RT. The mixture was heated to 50 °C until the solid was dissolved, and the solution was stirred at that temperature for 30 min. The dinuclear complex [(η^6-*p*-cymene)$_2$Ru$_2$(μ_2-Cl)$_2$Cl$_2$] (**49**) (500 mg, 816 μmol, 1.05 eq) was added, and the mixture was stirred at 80 °C overnight. The mixture was allowed to cool to RT, filtered, washed with EtOH, acetone, H_2O, Et_2O, and pentane, and then dissolved in CH_2Cl_2, before being filtered over Celite and concentrated under reduced pressure to yield the desired dinuclear clip **50** as an orange solid (156 mg, 25%). **^{1}H-NMR** ($CDCl_3$, 400 MHz) δ/ppm: 5.31 - 5.26 (m, 6H, C*H*, *p*-cymene), 4.99 (d, $^3J_{HH}$ = 5.9 Hz, 2H, C*H*, *p*-cymene), 4.06 - 3.99 (m, 2H, C*H*H, hexyl$_{chain}$), 3.32 - 3.26 (m, 2H, CH*H*, hexyl$_{chain}$), 2.69 (sept, $^3J_{HH}$ = 6.9 Hz, 2H, C*H*, *p*-cymene), 2.15 (s, 6H, C*H*$_3$, *p*-cymene), 1.71 - 1.56 (m, 4H, C*H*$_2$, hexyl$_{chain}$), 1.38 - 1.27 (m, 12H, C*H*$_2$, hexyl$_{chain}$), 1.22 (d, $^3J_{HH}$ = 6.9 Hz, 6H, C*H*$_3$, *p*-cymene), 1.18 (d, $^3J_{HH}$ = 6.9 Hz, 6H, C*H*$_3$, *p*-cymene), 0.92 - 0.87 (m, 6H, C*H*$_3$, hexyl$_{chain}$). **^{13}C-NMR** ($CDCl_3$, 101 MHz) δ/ppm: 170.2 (2C, *C*O, oxalamide), 100.7 (2C, *C*CH(CH$_3$)$_2$, *p*-cymene), 94.4 (2C, *C*CH$_3$, *p*-cymene), 82.6 (2C, *C*H, *p*-cymene), 81.2 (2C, *C*H, *p*-cymene), 79.8 (2C, *C*H, *p*-cymene), 79.6 (2C, *C*H, *p*-cymene), 51.7 (2C, N*C*H$_2$, hexyl$_{chain}$), 31.9 (2C, *C*H$_2$, hexyl$_{chain}$), 30.9 (2C, H*C*(CH$_3$)$_2$, *p*-cymene), 29.4 (2C, *C*H$_2$, hexyl$_{chain}$), 27.6 (2C, *C*H$_2$, hexyl$_{chain}$), 22.9 (2C, *C*H$_2$, hexyl$_{chain}$), 22.6 (2C, HC(*C*H$_3$)$_2$, *p*-cymene), 22.2 (2C, HC(*C*H$_3$)$_2$, *p*-cymene), 18.6 (2C, *C*H$_3$, *p*-cymene), 14.3 (2C, *C*H$_3$, hexyl$_{chain}$). **IR** (cm^{-1}): 2923 (w), 1596 (s), 1458 (w), 1333 (m), 1051 (w), 872 (w), 532 (w), 524 (w), 511 (w), 501 (w), 494 (w), 485 (w), 475 (w), 467 (w), 458 (w), 450 (w), 441 (w), 433 (w). **ESI-MS$^+$** Calcd for $C_{34}H_{54}ClN_2O_2Ru_2$ ([M - Cl]$^+$): m/*z* 761.2. Found: m/*z* 761.1. **UV-VIS** (1.0×10^{-5} M, CH_2Cl_2): λ_{max}, 228 nm ($\varepsilon = 2.1 \times 10^5$ M^{-1} cm^{-1}); λ_{max}, 281 nm ($\varepsilon = 1.1 \times 10^4$ M^{-1} cm^{-1}); λ_{max}, 331 nm ($\varepsilon = 1.1 \times 10^4$ M^{-1} cm^{-1}). **EA**: Calcd for $C_{34}H_{54}Cl_2N_2O_2Ru_2$ (795.9): C, 51.31; H, 6.84; N, 3.52. Found: C, 51.32; H, 6.85; N, 3.72.

8.20. Synthesis of Molecular Clip [(η^6-p-Cymene)$_2$Ru$_2$(μ_4- N^1,N^2-dioctyloxalamide)]Cl$_2$ (**51**)

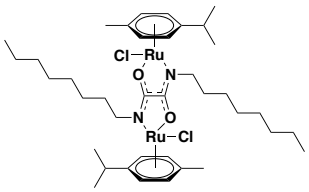

N^1,N^2-Dioctyloxalamide (**4**) (500 mg, 1.60 mmol, 1.0 eq) was suspended in EtOH (30 mL), and DIPEA (0.6 mL, 3.44 mmol, 2.1 eq) was added slowly and stirred at RT for 30 min. The dinuclear precursor **49** (1.03 g, 1.68 mmol, 1.05 eq) was added, and the mixture was stirred at 90 °C overnight. The reaction was allowed to cool to RT, the volume was reduced to half, and the mixture was stored in the refrigerator for 1 h. The orange residue was filtered and washed with EtOH, H_2O, acetone, Et_2O, and pentane. The residue was dissolved in CH_2Cl_2, filtered over Celite, and concentrated under reduced pressure to yield the desired dinuclear clip **51** as red crystals (280 mg, 21%). **^{1}H-NMR** ($CDCl_3$, 400 MHz) δ/ppm: 5.30 - 5.25 (m, 6H, C*H*, *p*-cymene), 4.97 (d, $^3J_{HH}$ = 5.8 Hz, 2H, C*H*, *p*-cymene), 4.04 - 3.97 (m, 2H, C*H*H, octyl$_{chain}$), 3.30 - 3.24 (m, 2H, CH*H*, octyl$_{chain}$), 2.68 (sept, $^3J_{HH}$ = 6.9 Hz, 2H, C*H*, *p*-cymene), 2.12 (s, 6H, CH_3, *p*-cymene), 1.70 - 1.52 (m, 4H, CH_2, octyl$_{chain}$), 1.33 - 1.25 (m, 20H, CH_2, octyl$_{chain}$), 1.20 (d, $^3J_{HH}$ = 6.8 Hz, 6H, CH_3, *p*-cymene), 1.16 (d, $^3J_{HH}$ = 6.9 Hz, 6H, CH_3, *p*-cymene), 0.89 - 0.86 (m, 6H, CH_3, octyl$_{chain}$). **^{13}C-NMR** ($CDCl_3$, 101 MHz) δ/ppm: 170.1 (2C, *C*O, oxalamide), 100.7 (2C, *C*CH(CH$_3$)$_2$, *p*-cymene), 94.4 (2C, *C*CH$_3$, *p*-cymene), 82.5 (2C, *C*H, *p*-cymene), 81.2 (2C, *C*H, *p*-cymene), 79.7 (2C, *C*H, *p*-cymene), 79.5 (2C, *C*H, *p*-cymene), 51.7 (2C, N*C*H$_2$, octyl$_{chain}$), 32.1 (2C, H*C*(CH$_3$)$_2$, *p*-cymene), 30.7 (2C, *C*H$_2$), 29.7 (2C, *C*H$_2$), 29.5 (2C, *C*H$_2$), 29.4 (2C, *C*H$_2$), 27.9 (2C, *C*H$_2$), 22.8 (2C, *C*H$_2$), 22.6 (2C, HC(*C*H$_3$)$_2$, *p*-cymene) , 22.2 (2C, HC(*C*H$_3$)$_2$, *p*-cymene), 18.6 (2C, *C*H$_3$, *p*-cymene), 14.3 (2C, *C*H$_3$, octyl$_{chain}$). **IR** (cm^{-1}): 2954 (m), 2914 (m), 2849 (m), 1645 (w), 1604 (s), 1531 (w), 1510 (w), 1466 (w), 1373 (w), 1349 (w), 1324 (m), 1200 (w), 1153 (w), 1080 (w), 1055 (w), 1025 (w), 996 (w), 857 (m), 800 (m), 724 (m), 594 (w), 496 (w), 463 (w), 445 (w), 429 (w). **ESI-MS$^+$** Calcd for $C_{38}H_{62}ClN_2O_2Ru_2$ ([M - Cl]$^+$): m/*z* 817.3. Found: m/*z* 817.2. **UV-VIS** (1.0×10^{-4} M, CH_2Cl_2): λ_{max} 228 nm ($\varepsilon = 2.3 \times 10^4$ M^{-1} cm^{-1}); λ_{max} 274 nm ($\varepsilon = 1.3 \times 10^4$ M^{-1} cm^{-1}); λ_{max} 313 nm ($\varepsilon = 1.6 \times 10^4$ M^{-1} cm^{-1}). **EA**: Calcd for $C_{38}H_{62}N_2O_2Cl_2Ru_2$ (852.2): C, 53.57; H, 7.33; N, 3.29. Found: C, 53.61; H, 7.48; N, 3.24.

8.21. Synthesis of Molecular Clip [(η^6-p-Cymene)$_2$Ru$_2$(μ_4-3-icosyl-dihydroxybenzoquinone]Cl$_2$ (**59**)

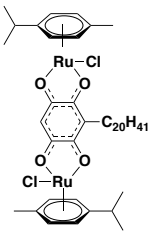

2,5-dihydroxy-3-icosylcyclohexa-2,5-diene-1,4-dione (**38**) (158 mg, 375 μmol, 1.0 eq) was suspended in EtOH (50 mL), and CH_3COONa (64.7 mg, 789 μmol, 2.1 eq) was added. The yellow suspension turned into a red solution. The mixture was allowed to stirr for 1 h at RT, then **49** (225 mg, 367 μmol, 0.98 eq) was added, and the reaction was stirred at 80 °C for 48 h. The reaction was allowed to cool to RT, the volume was reduced to half, and the mixture was stored in the refrigerator overnight. The violet precipitate was filtered and washed with cold dist. H_2O to obtain the desired dinuclear clip **59** as a violet solid (267 mg, 77%). **^{1}H-NMR** ($CDCl_3$, 400 MHz) δ/ppm: 5.69 (s, 1H, C*H*, dhbq), 5.63 - 5.59 (m, 4H, C*H*, *p*-cymene), 5.36 (d, $^3J_{HH}$ = 5.8 Hz, 4H, C*H*, *p*-cymene), 2.90 (sept, $^3J_{HH}$ = 6.9 Hz, 2H, C*H*, *p*-cymene), 2.36 - 2.32 (m, 2H, CH_2, icosyl$_{chain}$), 2.91 (s, 6H, CH_3, *p*-cymene), 1.36 - 1.33 (m, 12H, (CH_3)$_2$, *p*-cymene), 1.27 - 1.26 (m, 36H, CH_2, icosyl$_{chain}$), 0.88 (t, $^3J_{HH}$ = 6.6 Hz, 3H, CH_3, icosyl$_{chain}$). **^{13}C-NMR** ($CDCl_3$, 101 MHz) δ/ppm: 184.4 (2C, *C*O, dhbq), 181.8 (2C, *C*O, dhbq), 115.5 (1C, *C*$C_{20}H_{41}$, dhbq), 100.7 (1C, *C*H, dhbq), 100.6 (2C, *C*CH(CH_3)$_2$, *p*-cymene), 96.4 (2C, *C*CH_3, *p*-cymene), 82.0 (1C, *C*H, *p*-cymene), 81.4 (1C, *C*H, *p*-cymene), 79.7 (1C, *C*H, *p*-cymene), 79.1 (1C, *C*H, *p*-cymene), 32.1 (1C, *C*H_2, icosyl$_{chain}$), 31.5 (1C, *C*(CH_3)$_2$, *p*-cymene), 30.01 (1C, *C*H_2, icosyl$_{chain}$), 29.95 (2C, *C*H_2, icosyl$_{chain}$), 29.93 (2C, *C*H_2, icosyl$_{chain}$), 29.91 (2C, *C*H_2 icosyl$_{chain}$), 29.89 (2C, *C*H_2, icosyl$_{chain}$), 29.86 (4C, *C*H_2, icosyl$_{chain}$), 29.8 (2C, *C*H_2, icosy$_{chain}$), 29.7 (1C, *C*H_2, icosyl$_{chain}$), 29.5 (1C, *C*H_2, icosyl$_{chain}$), 28.3 (1C, *C*H_2, icosyl$_{chain}$), 22.8 (1C, *C*H_2, icosyl$_{chain}$), 22.7 (4C, (*C*H_3)$_2$, *p*-cymene), 18.7 (2C, *C*H_3, *p*-cymene), 14.3 (1C, *C*H_3, icosyl$_{chain}$). **IR** (cm^{-1}): 2918 (m), 2849 (m), 1509 (s), 1495 (s), 1469 (m), 1363 (s), 1315 (w), 1236 (w), 1225 (w), 1165 (w), 1086 (w), 1030 (w), 874 (w), 834 (w), 805 (w), 788 (w), 722 (w), 502 (w), 487 (w), 464 (w), 453 (w), 449 (w), 445 (w), 433 (w), 430 (w). **ESI-MS$^+$** Calcd for $C_{46}H_{70}ClO_4Ru_2$ ([M - Cl]$^+$): m/*z* 925.3. Found: m/*z* 925.3. **UV-VIS** (1.0×10^{-5} M, CH_2Cl_2): λ_{max} 228 nm ($\varepsilon = 3.7 \times 10^4$ M^{-1} cm^{-1}); λ_{max} 317 (1.5×10^4 M^{-1}cm^{-1}); λ_{max} 500 nm ($\varepsilon = 2.0 \times 10^4$ M^{-1} cm^{-1}). **EA**: Calcd for $C_{46}H_{70}O_4Cl_{12}Ru_2$ (960.3): C, 57.55; H, 7.35; N, 0.00. Found: C, 58.08; H, 7.56; N, 0.01.

8.22. Syntheses of Molecular Prism [(η^6-p-cymene)$_6$Ru$_6$(μ_4-N^1,N^2-dihexyloxalamide)$_3$(μ_3-4-tpt)][CF_3SO_3]$_6$ (**63**)

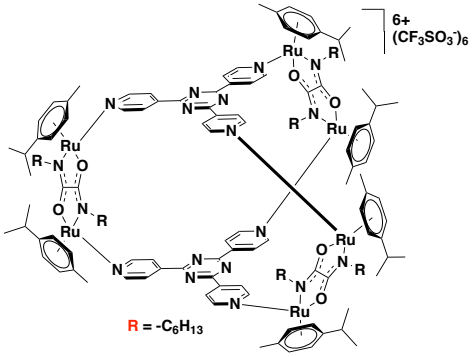

Molecular clip [(η^6-*p*-cymene)$_2$Ru$_2$(μ_4-N^1,N^2-dihexyloxalamide)Cl$_2$] (**50**) (100 mg, 128 μmol, 1.0 eq) was dissolved in MeOH (20 mL), and $AgCF_3SO_3$ (64.0 mg, 249 μmol, 1.95 eq) was added. The mixture was stirred at RT for 3 h. AgCl was filtered off, 4-tpt (44.0 mg, 141 μmol, 1.1 eq) was added to the solution, and the mixture was stirred at 60 °C for 24 h. The reaction was allowed to cool to RT, and the solvent was removed under reduced pressure. CH_2Cl_2 (2 mL) and pentane (100 mL) were added to induce precipitation. The dark-green precipitate was filtered and washed with cold EtOH (3 × 20 mL) to yield the desired hexa-nuclear prism **63** as a dark-green solid. (152 mg, 96%). **^{1}H-NMR** ($CDCl_3$, 400 MHz) δ/ppm: 8.99 - 8.20 (m, 24H, C*H*, 4-tpt), 5.83 - 5.69 (m, 12H, C*H*, *p*-cymene), 5.56 - 5.44 (m, 12H, C*H*, *p*-cymene), 4.20 - 4.13 (m, 6H, NCH_2, hexyl$_{chain}$), 3.62 - 3.55 (m, 6H, CH_2, hexyl$_{chain}$), 2.86 - 2.75 (m, 6H, C*H*, *p*-cymene), 2.14 - 2.07 (m, 6H, CH_2, hexyl$_{chain}$), 1.96 (s, 18H, CH_3, *p*-cymene), 1.82 - 1.66 (m, 22H, CH_2, hexyl$_{chain}$), 1.61 - 1.52 (m, 20H, CH_2, hexyl$_{chain}$), 1.40 - 1.37 (m, 18H, (CH_3)$_2$, *p*-cymene), 1.32 - 1.26 (m, 18H, (CH_3)$_2$, *p*-cymene), 1.07 - 1.03 (m, 18H, CH_3, hexyl$_{chain}$). **^{13}C-NMR** ($CDCl_3$, 151 MHz, 45 °C) δ/ppm: 171.0 (NC_{quart}N, 4-tpt), 170.7 (*C*O, oxalamide), 154.3 (N*C*H, 4-tpt), 151.2 (N*C*H, 4-tpt), 143.9 (CC_{quart}C, 4-tpt), 142.4 (CC_{quart}C, 4-tpt), 122.4 (C*C*H, 4-tpt), 120.2 (C*C*H, 4-tpt), 106.0 (*C*CH(CH$_3$)$_2$, *p*-cymene), 97.2 (*C*CH$_3$, *p*-cymene), 84.6 (*C*H, *p*-cymene), 83.7 (*C*H, *p*-cymene), 82.3 (*C*H, *p*-cymene), 81.7 (*C*H, *p*-cymene), 53.5 (NCH$_2$, hexyl$_{chain}$), 32.1 (*C*H$_2$, hexyl$_{chain}$), 32.0 (*C*H$_2$, hexyl$_{chain}$), 31.5 (*C*(CH$_3$)$_2$, *p*-cymene), 31.4 (*C*(CH$_3$)$_2$, *p*-cymene), 30.3 (*C*H$_2$, hexyl$_{chain}$), 29.9 (*C*H$_2$, hexyl$_{chain}$), 29.5 (*C*H$_2$, hexyl$_{chain}$), 27.4 (*C*H$_2$, hexyl$_{chain}$), 22.9 (*C*H$_2$, hexyl$_{chain}$), 22.8 (*C*H$_2$, hexyl$_{chain}$), 22.5 ((*C*H$_3$)$_2$, *p*-cymene), 22.3 ((*C*H$_3$)$_2$, *p*-cymene), 17.8 (*C*H$_3$, *p*-cymene), 14.3 (*C*H$_3$, hexyl$_{chain}$). **IR** (cm^{-1}): 2928 (w), 1596 (s), 1516 (s), 1371 (m), 1257 (s), 1222 (m), 1149 (m), 1056 (w), 1028 (s), 811 (m), 670 (w), 636 (s), 496 (w), 480 (w), 445 (w). **ESI-MS$^+$** Calcd for $C_{141}H_{186}F_9N_{18}O_{15}Ru_6S_3$ ([M - 3CF_3SO_3]$^{3+}$): m/*z* 1083.3. Found: m/*z* 1082.4. Calcd for $C_{142}H_{186}F_{12}N_{18}O_{18}Ru_6S_4$ ([M - 2CF_3SO_3]$^{2+}$): m/*z* 1699.4. Found: m/*z* 1697.3. **UV-VIS** (1.0 × 10^{-5} M, CH_2Cl_2): λ_{max} 249 nm (ε = 1.7 × 10^5 M^{-1} cm^{-1}). **EA**: Calcd for $C_{144}H_{186}F_{18}N_{18}O_{24}Ru_6S_6$ (3696.6): C, 46.82; H, 5.08; N, 6.83. Found: C, 46.71; H, 5.12; N, 7.30.

8.23. Syntheses of Molecular Prism [(η^6-p-cymene)$_6$Ru$_6$(μ_4-N^1,N^2-dioctyloxalamide)$_3$(μ_3-4-tpt)][CF_3SO_3]$_6$ (**64**)

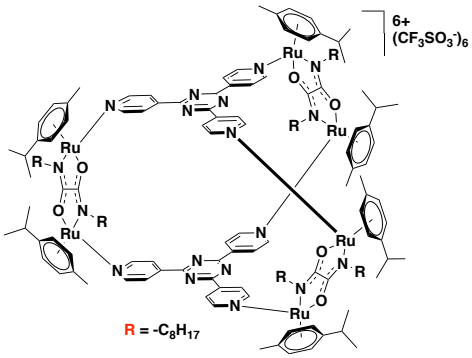

Molecular clip [(η^6-*p*-cymene)$_2$Ru$_2$(μ_4- N^1,N^2-dioctyloxalamide)Cl_2] (**51**) (150 mg, 176 μmol, 1.0 eq) was dissolved in MeOH (20 mL), and $AgCF_3SO_3$ (88.1 mg, 343 μmol, 1.95 eq) was added. The mixture was stirred at RT for 3 h. AgCl was filtered off, 4-tpt (60.4 mg, 194 μmol, 1.1 eq) was added to the mixture, and the solution was stirred at 60 °C for 24 h. The reaction was allowed to cool to RT, and MeOH was removed under reduced pressure. CH_2Cl_2 (2 mL) was added, and pentane (100 mL) was added to induce precipitation. The dark-green-black precipitate was filtered and washed with EtOH (3 × 20 mL) to yield the desired hexa-nuclear prism **64** as a dark green solid (129 mg, 60%). **^{1}H-NMR** ($CDCl_3$, 400 MHz) δ/ppm: 8.78 - 8.21 (m, 24H, C*H*, 4-tpt), 5.77 - 5.65 (m, 12H, C*H*, *p*-cymene), 5.51 - 5.39 (m, 12H, C*H*, *p*-cymene), 4.26 - 4.07 (m, 6H, NC*H*H, octyl$_{chain}$), 3.60 - 3.42 (m, 6H, NCH*H*, octyl$_{chain}$), 2.85 - 2.69 (m, 6H, C*H*, *p*-cymene), 2.13 - 2.00 (m, 8H, CH_2, octyl$_{chain}$), 1.96 - 1.86 (m, 18H, CH_3, *p*-cymene), 1.79 - 1.39 (m, CH_2, 100H, octyl$_{chain}$), 1.34 - 1-31 (m, 18H, (CH_3)$_2$, *p*-cymene), 1.25 - 1.21 (m, 18H, (CH_3)$_2$, *p*-cymene), 1.06 - 0.92 (m, 18H, CH_3, octyl$_{chain}$). **^{13}C-NMR** ($CDCl_3$, 151 MHz, 45 °C) δ/ppm: 171.7 (NC_{quart}N, 4-tpt), 170.9 (*C*O, oxalamide), 170.6 (*C*O, oxalamide), 154.3 (N*C*H, 4-tpt), 151.2 (N*C*H, 4-tpt), 143.9 (CC_{quart}C, 4-tpt), 143.7 (CC_{quart}C, 4-tpt), 142.6 (CC_{quart}C, 4-tpt), 122.4 (C*C*H, 4-tpt), 122.3 (C*C*H, 4-tpt), 120.2 (C*C*H, 4-tpt), 118.1 (C*C*H, 4-tpt), 105.9 (*C*CH(CH$_3$)$_2$, *p*-cymene), 97.2 (*C*CH$_3$, *p*-cymene), 84.6 (*C*H, *p*-cymene), 83.7 (*C*H, *p*-cymene), 82.2 (*C*H, *p*-cymene), 81.7 (*C*H, *p*-cymene), 53.5 (N*C*H$_2$, octyl$_{chain}$), 32.08 (*C*H$_2$, octyl$_{chain}$), 32.06 (*C*H$_2$, octyl$_{chain}$), 31.5 (*C*H, *p*-cymene), 31.5 (*C*H, *p*-cymene), 30.3 (*C*H$_2$, octyl$_{chain}$), 29.9 (*C*H$_2$, octyl$_{chain}$), 29.6 (*C*H$_2$, octyl$_{chain}$), 27.7 (*C*H$_2$, octyl$_{chain}$), 22.9 (*C*H$_2$, octyl$_{chain}$), ((*C*H$_3$)$_2$, *p*-cymene), 22.3 ((*C*H$_3$)$_2$, *p*-cymene), 17.8 (*C*H$_3$, *p*-cymene), 17.8 (*C*H$_2$, octyl$_{chain}$), 14.3 (CH$_3$, octyl$_{chain}$). **IR** (cm^{-1}): 2926 (w), 1596 (s), 1517 (s), 1466 (w), 1371 (m), 1332 (w), 1257 (s), 1222 (m), 1149 (m), 1056 (w), 1028 (s), 871 (w), 811 (m), 753 (w), 670 (w), 658 (w), 635 (s), 572 (w), 487 (w), 467 (w), 439 (w). **ESI-MS$^+$** Calcd for $C_{153}H_{210}F_9N_{18}O_{15}Ru_6S_3$ ([M - $3CF_3SO_3$]$^{3+}$): m/*z* 1139.3. Found: m/*z* 1138.4. Calcd for $C_{154}H_{210}F_{12}N_{18}O_{18}Ru_6S_4$ ([M - $2CF_3SO_3$]$^{2+}$): m/*z* 1782.5. Found: m/*z* 1780.7. **UV-VIS** (1.0 ×

10^{-5} M, CH_2Cl_2) λ_{max} 251 nm ($\varepsilon = 1.3 \times 10^5$ M^{-1} cm^{-1})]. **EA**: Calcd for $C_{156}H_{210}F_{18}F_{18}O_{24}Ru_6S_6$ (3864.8): C, 48.51; H, 5.48; N, 6.53. Found: C, 48.31; H, 5.42; N, 7.76.

8.24. Synthesis of Molecular Prism [(η^6-p-cymene)$_6$Ru$_6$(μ_4-3-icosyl-dihydroxybenzoquinone)$_3$(μ_3-4-tpt)][CF_3SO_3]$_6$ (**65**)

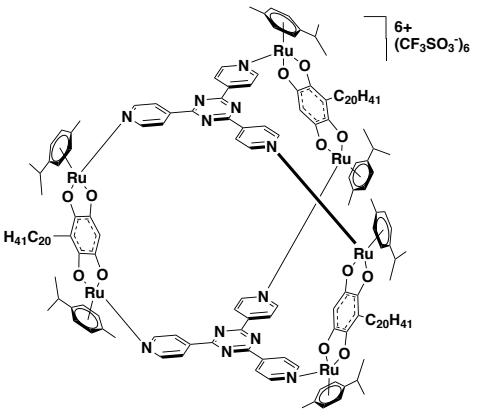

Molecular clip [(η^6-*p*-cymene)$_2$Ru$_2$(μ_4-3-icosyl-dihydroxybenzoquinone]Cl_2 (**59**) (50.0 mg, 52.0 μmol, 1.0 eq) was suspended in MeOH (20 mL), and $AgCF_3SO_3$ (26.7 mg, 104 μmol, 2.0 eq) was added and the mixture was stirred at RT for 3 h. AgCl was filtered off and 4-tpt (10.7 mg, 34.3 μmol, 0.66 eq) was added, and the mixture heated to 60 °C. The reaction was stirred for 30 h until the ^{1}H-NMR spectrum showed full conversion of the starting material. The reaction was allowed to cool to RT, the solvent was removed under reduced pressure, and the crude product was dried overnight. CH_2Cl_2 (1 mL) was added to dissolve the solid, and pentane (50 mL) was added to induce precipitation. The dark-red solid was filtered and dried under vacuum to obtain the desired hexa-nuclear prism **65** as a red solid (56.7 mg, 60%). **^{1}H-NMR** ($CDCl_3$, 400 MHz) δ/ppm: 8.75 (s, 12 H, C*H*, 4-tpt), 8.49 (s, 12H, C*H*, 4-tpt), 5.88 - 5.68 (m, 27 H, C*H*, *p*-cymene, dhbq), 2.85 (m, 6H, C*H*, *p*-cymene), 2.28 - 2.17 (m, 36H, CH_2, icosyl$_{chain}$; CH_3, *p*-cymene), 1.37 - 1.27 (132H, CH_2, icosyl$_{chain}$; (CH_3)$_2$, *p*-cymene), 0.88 (m, 9H, CH_3, icosyl$_{chain}$). **^{13}C-NMR** ($CDCl_3$, 101 MHz) δ/ppm: 184.0 (O*C*C$C_{20}H_{41}$, dhbq), 181.7 (O*C*CH_4, dhbq), 169.7 (NC_{quart}N, 4-tpt), 154.2 (N*C*H, 4-tpt), 144.3 (CC_{quart}C, 4-tpt), 125.6 (C*C*H, 4-tpt), 122.4 (*C*C$_{20}H_{41}$, dhbq), 119.2 (*C*C$_{20}H_{41}$, dhbq), 104.4 (*C*CH(CH_3)$_2$, *p*-cymene), 101.4 (*C*H, dhbq), 99.1 (*C*CH_3, *p*-cymene), 84.1 (*C*H, *p*-cymene), 83.5 (*C*H, *p*-cymene), 83.3 (*C*H, *p*-cymene), 82.4 (*C*H, *p*-cymene), 32.1 (*C*H$_2$, icosyl$_{chain}$), 31.5 (*C*H, *p*-cymene), 30.2 (*C*H$_2$, icosyl$_{chain}$), 30.1 (*C*H$_2$, icosyl$_{chain}$), 30.1 (*C*H$_2$, icosyl$_{chain}$), 30.0 (*C*H$_2$, icosyl$_{chain}$), 30.0 (*C*H$_2$, icosyl$_{chain}$), 29.9 (*C*H$_2$, icosyl$_{chain}$), 29.8 (*C*H$_2$, icosyl$_{chain}$), 29.5 (*C*H$_2$, icosyl$_{chain}$), 22.8 (*C*H$_2$, icosyl$_{chain}$), 22.5 (*C*H$_2$, icosyl$_{chain}$), 22.4 ((*C*H$_3$)$_2$, *p*-cymene), 22.4 ((*C*H$_3$)$_2$, *p*-cymene), 18.2 (*C*H$_3$, *p*-cymene), 14.3 (*C*H$_3$, icosyl$_{chain}$). **IR** (cm^{-1}): 2924 (w), 2852 (w), 1575 (w), 1514 (m), 1367 (m), 1278 (m), 1243 (m), 1224 (m), 1156 (m), 1058 (w), 1027 (m), 870 (w), 810 (w), 800 (w), 759 (w), 671 (w), 667 (w), 635 (w), 487 (w), 472 (w), 464 (w), 453 (w). **ESI-MS$^+$** Calcd for $C_{177}H_{234}F_9N_{12}O_{21}Ru_6S_3$ ([M - $3CF_3SO_3$]$^{3+}$): m/*z* 1246.7. Found: m/*z* 1246.7. Calcd for $C_{178}H_{234}F_{12}N_{12}O_{24}Ru_6S_4$ ([M - $2CF_3SO_3$]$^{2+}$): m/*z* 1944.5.

Found: m/*z* 1945.1. **UV-VIS** (1.0 × 10^{-5} M, CH_2Cl_2): λ_{max} 245 nm (ε = 7.8 × 10^4 M^{-1} cm^{-1}); λ_{max} 304 nm (ε = 4.3 × 10^4 M^{-1} cm^{-1}); λ_{max} 494 nm (ε = 2.8 × 10^4 M^{-1} cm^{-1}). **EA**: Calcd for $C_{180}H_{236}F_{18}N_{18}O_{30}Ru_6S_6 \cdot 3CH_2Cl_2$ (4191.0 + 254.8): C, 49.49; H, 5.45; N, 3.78. Found: C, 49.50; H, 5.88; N, 3.39.

8.25. Syntheses of Metalla-Cube [(η^6-p-cymene)$_8$Ru$_8$(μ_4-N^1,N^2-dihexyloxalamide)$_3$(μ_4-tpp)][CF_3SO_3]$_8$ (**66**)

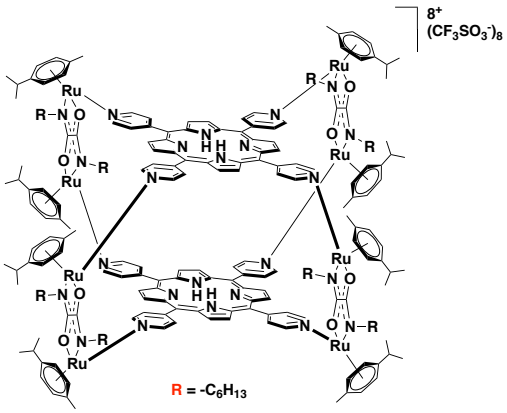

Molecular clip [(η^6-*p*-cymene)$_2$Ru$_2$(μ_4-N^1,N^2-dihexyloxalamide)Cl$_2$] (**50**) (50.0 mg, 62.8 μmol, 1.0 eq) was dissolved in MeCN (5 mL), $AgCF_3SO_3$ (32.3 mg, 126 μmol, 2.0 eq) was added and the suspension was stirred at RT. After 3 h AgCl was filtered off, tpp (40.0 mg, 62.8 μmol, 1 eq) was added and the reaction was stirred at 80 °C for 3 days. The reaction was allowed to cool to RT and was then concentrated. DCM (2 mL) was added to the mixture and pentane was added to induce precipitation to afford the desired octa-nuclear cube **66** as a dark brown solid (59.9 mg, 73%). **^{1}H-NMR** (CD_3NO_2, 600 MHz, 65°C) δ/ppm: 9.33 - 8.31 (m, 52H, tpp), 6.23 - 5-70 (m, 32H, *p*-cymene), 4.17 - 4.06 (m, 8H, C*H*H, hexyl$_{chain}$), 3.21 - 3.05 (m, 8H, CH*H*, hexyl$_{chain}$), 2.36 - 2.19 (C*H*, 8H, *p*-cymene; C*H*$_3$, 24H, *p*-cymene), 2.19 - 1.60 (m, C*H*$_2$, hexyl$_{chain}$), 1.59 - 1.56 (m, 24H, (C*H*$_3$)$_2$, *p*-cymene), 1.53 - 1.48 (m, 24H, (C*H*$_3$)$_2$, *p*-cymene), 1.13 - 1.04 (m, C*H*$_3$, hexyl$_{chain}$). **^{13}C-NMR** (CD_3NO_2, 151 MHz, 65 °C) δ/ppm: 167.8 (*C*O, oxalamide), 152.3 (tpp), 133.2 (tpp), 130.4 (tpp), 127.7 (tpp), 126.0 (tpp), 123.9 (tpp), 121.8 (tpp), 119.7 (tpp), 116.5 (tpp), 86.3 (*p*-cymene), 84.7 (*p*-cymene), 84.6 (*p*-cymene), 54.8 (N*C*H$_2$, hexyl$_{chain}$), 33.3 (*C*H$_2$, hexyl$_{chain}$), 33.2 (*C*H$_2$, hexyl$_{chain}$), 33.0 (*C*H$_2$, hexyl$_{chain}$), 31.7 (*C*H, *p*-cymene), 28.92 (*C*H$_2$, hexyl$_{chain}$ or (*C*H$_3$)$_2$, *p*-cymene), 28.86 (*C*H$_2$, hexyl$_{chain}$ or (*C*H$_3$)$_2$, *p*-cymene), 24.1 (*C*H$_2$, hexyl$_{chain}$ or (*C*H$_3$)$_2$, *p*-cymene), 24.0 (*C*H$_2$, hexyl$_{chain}$ or (*C*H$_3$)$_2$, *p*-cymene), 23.9 (*C*H$_2$, hexyl$_{chain}$ or (*C*H$_3$)$_2$, *p*-cymene), 23.2 (*C*H$_2$, hexyl$_{chain}$ or (*C*H$_3$)$_2$, *p*-cymene), 18.6 (*C*H$_3$, *p*-cymene), 14.80 (*C*H$_3$, hexyl$_{chain}$), 14.75 (*C*H$_3$, hexyl$_{chain}$). **IR** (cm^{-1}): 2961 (w), 2931 (w), 2869 (w), 2359 (w), 1597 (s), 1468 (w), 1418 (w), 1334 (w), 1258 (s), 1221 (m), 1152 (s), 1090 (w), 1062 (w), 1029 (s), 999 (w), 981 (w), 969 (w), 883 (w), 803 (m), 754 (w), 746 (w), 721 (w), 684 (w), 636 (s), 573 (w), 435 (m), 412 (s). **ESI-MS$^+$** Calcd for $C_{220}H_{268}F_{12}N_{24}O_{20}Ru_8S_4$ ([M - 4CF_3SO_3]$^{4+}$): m/*z* 1184.3. Found m/*z* 1184.8. Calcd for $C_{221}H_{268}F_{15}N_{24}O_{23}Ru_8S_5$ ([M - 3CF_3SO_3]$^{3+}$): m/*z* 1628.7.

Found: m/*z* 1628.3. Calcd for $C_{35}H_{54}F_3N_2O_5Ru_2S$ ([Clip - 2Cl + CF_3SO_3]$^+$): m/*z* 875.2. Found: 875.7. **UV-VIS** (3.33 × 10^{-6} M, $MeNO_2$): λ_{max} 414 nm (ε = 3.27 × 10^5 M^{-1} cm^{-1}). **EA**: Calcd for $C_{224}H_{268}F_{24}N_{24}O_{32}Ru_8S_8$ (5329.8): C, 50.48; H, 5.07; N, 6.31. Found: C, 52.31; H, 4.87; N, 8.23.

8.26. Syntheses of Metalla-Cube [(η^6-p-cymene)$_8$Ru$_8$(μ_4-N^1,N^2-dioctyloxalamide)$_3$(μ_4-tpp)][CF_3SO_3]$_8$ (**67**)

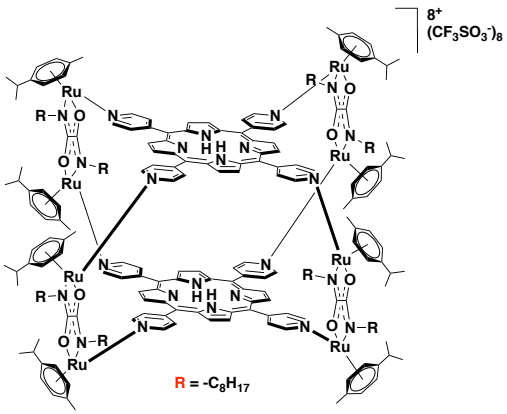

Molecular clip [(η^6-*p*-cymene)$_2$Ru$_2$(μ_4- N^1,N^2-dioctyloxalamide)Cl_2] (**51**) (50.0 mg, 58.7 μmol, 1.0 eq) was dissolved in MeCN (5 mL), $AgCF_3SO_3$ (30.2 mg, 117 μmol, 2.0 eq) was added and the suspension was stirred at RT. After 3 h AgCl was filtered off, tpp (36.3 mg, 58.7 μmol, 1 eq) was added and the reaction was stirred at 80 °C for 3 days. The reaction was allowed to cool to RT and was then concentrated. DCM (2 mL) was added to the mixture and pentane was added to induce precipitation to afford the desired octa-nuclear cube **67** as a dark brown solid (58.0 mg, 71%). **^{1}H-NMR** (CD_3NO_2, 600 MHz, 65 °C) δ/ppm: 9.44 - 7.81 (m, 52H, tpp), 6.22 - 5.65 (m, 32H, *p*-cymene), 4.17 - 4.01 (m, 8H, C*H*H, octyl$_{chain}$), 3.23 - 2.99 (m, 8H, CH*H*, octyl$_{chain}$), 2.35 - 2.19 (m, C*H*, 8H, *p*-cymene; CH_3, 24H, *p*-cymene), 2.00 - 1.27 (m, CH_2, octyl$_{chain}$; (CH_3)$_2$, *p*-cymene), 1.02 - 0.85 (m, CH_3, octyl$_{chain}$). **^{13}C-NMR** (CD_3NO_2, 151 MHz, 65 °C) δ/ppm: 130.4 (tpp), 127.7 (tpp), 33.3 (*C*H$_2$, octyl$_{chain}$ or *C*H$_3$, *p*-cymene or (*C*H$_3$)$_2$, *p*-cymene), 33.0 (*C*H$_2$, octyl$_{chain}$ or *C*H$_3$, *p*-cymene or (*C*H$_3$)$_2$, *p*-cymene), 31.7 (*C*H$_2$, octyl$_{chain}$ or *C*H$_3$, *p*-cymene or (*C*H$_3$)$_2$, *p*-cymene), 31.0 (*C*H$_2$, octyl$_{chain}$ or *C*H$_3$, *p*-cymene or (*C*H$_3$)$_2$, *p*-cymene), 30.8 (*C*H$_2$, octyl$_{chain}$ or *C*H$_3$, *p*-cymene or (*C*H$_3$)$_2$, *p*-cymene), 29.3 (*C*H$_2$, octyl$_{chain}$ or *C*H$_3$, *p*-cymene or (*C*H$_3$)$_2$, *p*-cymene), 24.6 (*C*H$_2$, octyl$_{chain}$ or *C*H$_3$, *p*-cymene or (*C*H$_3$)$_2$, *p*-cymene), 24.0 (*C*H$_2$, octyl$_{chain}$ or *C*H$_3$, *p*-cymene or (*C*H$_3$)$_2$, *p*-cymene), 24.0 (*C*H$_2$, octyl$_{chain}$ or *C*H$_3$, *p*-cymene or (*C*H$_3$)$_2$, *p*-cymene), 23.2 (*C*H$_2$, octyl$_{chain}$ or *C*H$_3$, *p*-cymene or (*C*H$_3$)$_2$, *p*-cymene), 18.3 (*C*H$_3$, *p*-cymene), 14.3 (*C*H$_3$, octyl$_{chain}$). **IR** (cm^{-1}): 2962 (w), 2931 (w), 2862 (w), 2360 (w), 1599 (s), 1468 (w), 1333 (w), 1275 (s), 1257 (s), 1223 (s), 1156 (s), 1066 (w), 1029 (s), 970 (w), 882 (w), 856 (w), 799 (m), 719 (m), 676 (w), 636 (s), 573 (w), 510 (w), 470 (w), 420 (s). **ESI-MS$^+$** Calcd for $C_{236}H_{300}F_{12}N_{24}O_{20}Ru_8S_4$ ([M - 4CF_3SO_3]$^{4+}$): m/*z* 1240.4. Found m/*z* 1240.5. Calcd for $C_{237}H_{300}F_{15}N_{24}O_{23}Ru_8S_5$ ([M - 3CF_3SO_3]$^{4+}$): m/*z* 1703.5. Found: 1702.7. Calcd for

$C_{39}H_{62}F_3N_2O_5Ru_2S$ ([Clip - 2Cl + CF_3SO_3]$^+$): m/*z* 931.2. Found: 931.1. **UV-VIS** (3.33×10^{-6} M, $MeNO_2$) λ_{max} 422 nm ($\varepsilon = 3.61 \times 10^5$ M^{-1} cm^{-1}). **EA**: Calcd for $C_{240}H_{300}F_{24}N_{24}O_{32}Ru_8S_8$ (5554.2): C, 51.90; H, 5.44; N, 6.05. Found: C, 50.96; H, 4.88; N, 8.20.

9. REFERENCES

(1) WHO | Cancer http://www.who.int/mediacentre/factsheets/fs297/en/ (accessed August 23, 2017).

(2) Cooper, G. M.; *The Cell: A Molecular Approach*, 2. ed.; American Society of Microbiology. Washington, DC, 2000, pp. 720 - 721.

(3) WHO | Cancer http://www.who.int/mediacentre/factsheets/fs297/en/ (accessed September 12, 2018).

(4) Furth, J.; Kahn, M. C. The Transmission of Leukemia of Mice with a Single Cell. *Cancer* **1937**, *31*, 276 - 282.

(5) NCI | Hyperplasia https://www.cancer.gov/publications/dictionaries/cancer-terms/def/hyperplasia (accessed Semptember 26, 2018).

(6) NCI | Carcinoma *in situ* https://www.cancer.gov/publications/dictionaries/cancer-terms/def/carcinoma-in-situ (accessed September 26, 2018).

(7) NCI | Invasive Carcinoma https://www.cancer.gov/publications/dictionaries/cancer-terms/def/invasive-cancer (accessed September 26, 2018).

(8) Yamaguchi, H.; Wyckoff, J.; Condeelis, J. Cell Migration in Tumors. *Current Opinion in Cell Biology* **2005**, *17*, 559 - 564.

(9) Strilic, B.; Offermanns, S. Intravascular Survival and Extravasation of Tumor Cells. *Cancer Cell* **2017**, *32*, 282 - 293.

(10) Gao, X.; Zhang, M.; Tang, Y.; Liang, X. Cancer Cell Dormancy: Mechanisms and Implications of Cancer Recurrence and Metastasis. *OncoTargets and Therapy* **2017**, *10*, 5219 - 5228.

(11) Aguirre-Ghiso, J. A. Models, Mechanisms and Clinical Evidence for Cancer Dormancy. *Nature Reviews Cancer* **2007**, *7*, 834 - 846.

(12) Sever, R.; Brugge, J. S. Signal Transduction in Cancer. *Cold Spring Harbor Perspectives in Medicine* **2015**, *5*, 1 - 20.

(13) Goel, G.; Makkar, H. P. S.; Francis, G.; Becker, K. Phorbol Esters: Structure, Biological Activity, and Toxicity in Animals. *International Journal of Toxicology* **2007**, *26*, 279 - 288.

(14) Emerit, I.; Cerutti, P. A. Tumor Promoter Phorbol-12-myristate-13-acetate Induces Chromosomal Damage *via* Indirect Action. *Nature* **1981**, *293*, 144 - 146.

(15) What When How | Tumor Promoters (Molecular Biology) http://what-when-how.com/molecular-biology/tumor-promoters-molecular-biology/ (accessed October

1, 2018).

(16) Sawyers, C. Targeted Cancer Therapy. *Nature* **2004**, *432*, 294 - 297.

(17) Shaw, R. J.; Cantley, L. C. Ras, PI(3)K and mTOR Signalling Controls Tumour Cell Growth. *Nature* **2006**, *441*, 424 - 430.

(18) Komiya, Y.; Habas, R. Wnt Signal Transduction Pathways. *Organogenesis* **2008**, *4*, 68 - 75.

(19) Cell Signaling | Protein and Pathway Abbreviations https://www.cellsignal.com/contents/resources/protein-and-pathway-abbreviations/pathway-abbreviations (accessed September 27, 2018).

(20) Kudo, M. Signaling Pathway/Molecular Targets and New Targeted Agents under Development in Hepatocellular Carcinoma. *World Journal of Gastroenterology* **2012**, *18*, 6005 - 6017.

(21) NCI | Cancer Treatment https://www.cancer.gov/about-cancer/treatment (accessed March 16, 2018).

(22) NCI | Surgery to Treat Cancer https://www.cancer.gov/about-cancer/treatment/types/surgery (accessed March 16, 2018).

(23) Singletray, S. E.; Walsh, G.; Vauthey, J - N.; Curley, S.; Sawaya, R.; Weber, K. L.; Meric, F.; Hortobagyi, G. N. A Role for Curative Surgery in the Treatment of Selected Patients with Metastatic Breast Cancer. *The Oncologist* **2003**, *8*, 241 - 251.

(24) NCI | Cryosurgery in Cancer Treatment https://www.cancer.gov/about-cancer/treatment/types/surgery/cryosurgery-fact-sheet (accessed March 16, 2018).

(25) NCI | Lasers in Cancer Treatment https://www.cancer.gov/about-cancer/treatment/types/surgery/lasers-fact-sheet (accessed March 16, 2018).

(26) NCI | Hyperthermia in Cancer Treatment https://www.cancer.gov/about-cancer/treatment/types/surgery/hyperthermia-fact-sheet (accessed March 16, 2018).

(27) NCI | Photodynamic Therapy for Cancer https://www.cancer.gov/about-cancer/treatment/types/surgery/photodynamic-fact-sheet (accessed March 16, 2018).

(28) NCI | Radiation Therapy to Treat Cancer https://www.cancer.gov/about-cancer/treatment/types/radiation-therapy (accessed March 17, 2018).

(29) NCI | Immunotherapy to Treat Cancer https://www.cancer.gov/about-cancer/treatment/types/immunotherapy (accessed March 17, 2018).

(30) Marone, R.; Cmiljanovic, V.; Giese, B.; Wymann, M. P. Targeting Phosphoinositide 3-Kinase - Moving towards Therapy. *Biochimica et Biophysica* **2008**, *1784*, 159 - 185.

(31) NCI | Targeted Therapy to Treat Cancer https://www.cancer.gov/about-

cancer/treatment/types/targeted-therapies (accessed March 17, 2018).

(32) NCI | Hormone Therapy to Treat Cancer https://www.cancer.gov/about-cancer/treatment/types/hormone-therapy (accessed March 17, 2018).

(33) NCI | Stem Cell Transplants in Cancer Treatment https://www.cancer.gov/about-cancer/treatment/types/stem-cell-transplant (accessed March 17, 2018).

(34) NCI | Precision Medicine in Cancer Treatment https://www.cancer.gov/about-cancer/treatment/types/precision-medicine (accessed March 17, 2018).

(35) NCI | Chemotherapy to Treat Cancer https://www.cancer.gov/about-cancer/treatment/types/chemotherapy (accessed March 17, 2018).

(36) Papac, R. J. Origins of Cancer Therapy. *Yale Journal of Biology and Medicine* **2001**, *74*, 391 - 398.

(37) Chabner, B. A.; Roberts, T. G. Chemotherapy and the War on Cancer. *Nature Reviews Cancer* **2005**, *5*, 65 - 72.

(38) Gilman, A. The Initial Clinical Trial of Nitrogen Mustard. The *American Journal of Surgery* **1963**, *105*, 574 - 578.

(39) Li, M - C.; Hertz, R.; Bergenstal, D. M. Therapy of Choricocarcinoma and Related Trophoblastic Tumors with Folic Acid and Purine Antagonists. *The New England Journal of Medicine* **1958**, *259*, 66 - 74.

(40) Jaffe, N.; Frei, E.; Traggis, D.; Bishop, Y. Adjuvant Methotrexate and Citrovorum-Factor Treatment of Osteogenic Sarcoma. *The New England Journal of Medicine* **1974**, *291*, 994 - 997.

(41) Osborn, M. J.; Huennekens, F. M. Enzymatic Reduction of Dihydrofolic Acid. *The Journal of Biological Chemistry* **1958**, *233*, 969 - 974.

(42) Jolivet, J.; Cowan, K. H.; Curt, G. A.; Clendeninn, N. J.; Chabner, B. A. The Pharmacology and Clinical Use of Methotrexate. *The New England Journal of Medicine* **1983**, *309*, 1094 - 1104.

(43) Stoller. R. G.; Hande, K. R.; Jacobs, S. A.; Rosenberg, S. A.; Chabner, B. A. Use of Plasma Pharmacokinetics to Predict and Prevent Methotrexate Toxicity. *The New England Journal of Medicine* **1977**, *297*, 630 - 634.

(44) Rodriguez, V.; Hart, J. S.; Freireich, E. J.; Bodey, G. P.; McCredie, K. B.; Whitecar, J. P.; Coltman, C. A. POMP Combination Chemotherapy of Adult Acute Leukemia. *Cancer* **1973**, *32*, 69 - 75.

(45) Skipper, H. E.; Thomson, J. R.; Elion, G. B.; Hitchings, G. H. Observations on the Anticancer Activity of 6-Mercaptopurine. *Cancer Research* **1954**, *14*, 294 - 298.

(46) Hitchings, G. H.; Elion, G. B. The Chemistry and Biochemistry of Purine Analogs. *Annals of the New York Academy of Sciences.* **1954**, *60*, 195 - 199.

(47) Johnson, I. S.; Armstrong, J. G.; Gorman, M.; Burnett, J. P. Jr. The Vinca Alkaloids: A New Class of Oncolytic Agents. *Cancer Research* **1963**, *23*, 1390 - 1427.

(48) Bensch, K. G.; Malawista, S. E. Microtubule Crystals: A New Biophysical Phenomenon Induced by Vinca Alkaloids. *Nature* **1968**, *218*, 1176 - 1177

(49) Gordon, C. The National Program for Cancer Chemotherapy. *Journal of the American Medical Association* **1972**, *222*, 1161 - 1162.

(50) Rosenberg, B.; van Camp, L.; Krigas, T. Inhibition of Cell Division in Escherichia Coli by Electrolysis Products from a Platinum Electrode. *Nature* **1965**, *205*, 698 - 699.

(51) Woloschuk, D. M. M.; Pruemer, J. M.; Cluxton, R. J. Jr. Carboplatin: A New Cisplatin Analog. *Drug intelligence and clinical pharmacy* **1988**, *22*, 843 - 849.

(52) Fewer, D.; Wilson, C. B.; Boldrey, E. B.; Enot, K. J.; Powell, M. R. The Chemotherapy of Brain Tumors: Clinical Experience with Carmustine (BCNU) and Vincristine. *Journal of the American Medical Association* **1972**, *222*, 549 - 552.

(53) Barabas, K.; Milner, R.; Lurie, D.; Adin, C. Cisplatin: A Review of Toxicities and Therapeutic Applications. *Veterinary and Comparative Oncology* **2008**, *6*, 1 - 18.

(54) Hanahan, D.; Weinberg, R. A. The Hallmarks of Cancer. *Cell* **2000**, *100*, 57 - 70.

(55) Åqvist, J.; Medina, C.; Samuelsson, J - E. A New Method for Predicting Binding Affinity in Computer-Aided Drug Design. *Protein Engineering* **1994**, *7*, 385 - 391.

(56) Goldman, J. M.; Melo, J. V. BCR-ABL in Chronic Myelogenous Leukemia - How Does It Work? *Acta Haematologica* **2008**, *119*, 212 - 217.

(57) Sihto, H.; Sarlomo-Rikala, M.; Tynninen, O.; Tanner, M.; Andersson, L. C.; Franssila, K.; Nupponen, N. N.; Joensuu, H. *KIT* and Platelet-Derived Growth Factor Receptor Alpha Tyrosine Kinase Gene Mutations and *KIT* Amplifications in Human Solid Tumors. *Journal of Clinical Oncology* **2005**, *23*, 49 - 57.

(58) Kris, M. G.; Natale, R. B.; Herbst, R. S.; Lynch, T. J. Jr.; Prager, D.; Belani, C. P.; Schiller, J. H.; Kelly, K.; Spiridonidis, H.; Sandler, A.; Albain, K. S., Cella, D.; Wolf, M. K.; Averbuch, S. D.; Ochs, J. J.; Kay, A. C. Efficacy of Gefitinib, an Inhibitor of the Epidermal Growth Factor Receptor Tyrosine Kinase, in Symptomatic Patients with Non-Small Cell Lung Cancer: A Randomized Trial. *Journal of the American Medical Association* **2003**, *290*, 2149 - 2158.

(59) Wang, C.; Huang, S. Drug Development Against Metastatic Cancers. *Yale Journal of Biology and Medicine* **2017**, *90*, 119 - 123.

(60) DSMZ | Tumor-Zelllinien bestehen deutlich häufiger als gedacht aus Subklonen https://www.dsmz.de/home/details/entry/tumor-zelllinien-bes.html (accessed June 13, 2018).

(61) Maeda, H.; Wu, J.; Sawa, T.; Matsumura, Y.; Hori, K. Tumor Vascular Permeability and the EPR Effect in Macromolecular Therapeutics: A Review. *Journal of Controlled Release* **2000**, *65*, 271 - 284.

(62) Maeda, H.; Tsukigawa, K.; Fang, J. A Retrospective 30 Years After Discovery of the Enhanced Permeability and Retention Effect of Solid Tumors: Next-Generation Chemotherapeutics and Photodynamic Therapy-Problems, Solutions, and Prospects. *Microcirculation* **2016**, *23*, 173 - 182.

(63) Matsumura, Y.; Maeda, H. A New Concept for Macromolecular Therapeutics in Cancer Chemotherapy: Mechanism of Tumoritropic Accumulation of Proteins and the Antitumor Agent Smancs. *Cancer Research* **1986**, *46*, 6387 - 6392.

(64) Satchi-Fainaro, R. Targeting Tumor Vasculature: Reality or a Dream? *Journal of Drug Targeting* **2002**, *10*, 529 - 533.

(65) Yin, H.; Liao, L.; Jun, F. Enhanced Permeability and Retention (EPR) Effect Based Tumor Targeting: The Concept, Application and Prospect. *JSM Clinical Oncology and Research* **2014**, *2*, 1 - 5.

(66) Folkman, J. Tumor Angiogenesis: Therapeutic Implications. *The New England Journal of Medicine* **1971**, *285*, 1182 - 1186.

(67) Nasu, R.; Kimura, H.; Akagi, K.; Murata, T.; Tanaka, Y. Blood Flow Influences Vascular Growth during Tumour Angiogenesis. *British Journal of Cancer* **1999**, *79*, 780 - 786.

(68) McDonald, D. M.; Baluk, P. Significance of Blood Vessel Leakiness in Cancer. *Cancer Research* **2002**, *62*, 5381 - 5385.

(69) Freitas, R. A. *Nanomedicine, Volume I: Basic Capabilities*; Landes Bioscience, Austin, TX, 1999, pp. 211.

(70) Wang, J.; Lu, Z.; Gao, Y.; Wientjes, M. G.; Au, J. L - S. Improving Delivery and Efficacy of Nanomedicines in Solid Tumors: Role of Tumor Priming. *Nanomedicine* **2011**, *6*, 1605 - 1620.

(71) Kobayashi, S.; Hori, M.; Wang, G. X.; Hirama, M. Formal Total Synthesis of Neocarzinostatin Chromophore. *The Journal of Organic Chemistry* **2006**, *71*, 636 - 644.

(72) Maeda, H.; Takeshita, J.; Kanamaru, R. A Lipophilic Derivative of Neocarzinostatin: A Polymer Conjugation of an Antitumor Protein Antibiotic. *International Journal of*

Peptide and Protein Research **1979**, *14*, 81 - 87.

(73) Maeda, H. SMANCS and Polymer-Conjugated Macromolecular Drugs: Advantages in Cancer Chemotherapy. *Advanced Drug Delivery Reviews* **2001**, *46*, 169 -185.

(74) Maeda, H. The Link between Infection and Cancer: Tumor Vasculature, Free Radicals, and Drug Delivery to Tumors *via* the EPR Effect. *Cancer Science* **2013**, *104*, 779 - 789.

(75) Kobayashi, A.; Oda, T.; Maeda, H. Protein Binding of Macromolecular Anticancer Agent SMANCS: Characterization of Poly(styrene-co-maleic acid) Derivatives as an Albumin Binding Ligand. *Journal of Bioactive and Compatible Polymers* **1988**, *3*, 319 - 333.

(76) Maeda, H. Toward a Full Understanding of the EPR Effect in Primary and Metastatic Tumors as Well as Issues Related to Its Heterogeneity. *Advanced Drug Delivery Reviews* **2015**, *91*, 3 - 6.

(77) Duncan, R. Polymer Conjugates as Anticancer Nanomedicines. *Nature Reviews Cancer* **2006**, *6*, 688 - 701.

(78) Yuan, F.; Dellian, M.; Fukumura, D.; Leunig, M.; Berk, D. A.; Torchilin, V. P.; Jain, R. K. Vascular Permeability in a Human Tumor Xenograft: Molecular Size Dependence and Cutoff Size. *Cancer Research* **1995**, *55*, 3752 - 3756.

(79) Fang, J.; Nakamura, H.; Maeda, H. The EPR Effect: Unique Features of Tumor Blood Vessels for Drug Delivery, Factors Involved, and Limitations and Augmentation of the Effect. *Advanced Drug Delivery Reviews* **2011**, *63*, 136 - 151.

(80) Maeda, H.; Bharate, G. Y.; Daruwalla, J. Polymeric Drugs for Efficient Tumor-Targeted Drug Delivery Based on EPR-Effect. *European Journal of Pharmaceutics and Biopharmaceutics* **2009**, *71*, 409 - 419.

(81) Haag, R.; Kratz, F. Polymer Therapeutics: Concepts und Applications. *Angewandte Chemie International Edition* **2006**, *45*, 1198 - 1215.

(82) Kobayashi, H.; Watanabe, R.; Choyke, P. L. Improving Conventional Enhanced Permeability and Retention (EPR) Effects; What Is the Appropriate Target? *Theranostics* **2014**, *4*, 81 - 89.

(83) Caliceti, P.; Veronese, F. M. Pharmacokinetic and Biodistribution Properties of Poly(ethylene glycol) - Protein Conjugates. *Advanced Drug Delivery Reviews* **2003**, *55*, 1261 - 1277.

(84) Lee, J. H.; Park, G.; Hong, G. H.; Choi, J.; Choi, H. S. Design Considerations for Targeted Optical Contrast Agents. *Quantitative Imaging in Medicine and Surgery* **2012**, *2*, 266 - 273.

(85) Lipfert, J.; Doniach, S.; Das, R.; Herschlag, D. Understanding Nucleic Acid-Ion Interactions. *Annual Review of Biochemistry* **2014**, *83*, 813 - 841.

(86) Perry, S. W.; Norman, J. P.; Barbieri, J.; Brown, E. B.; Gelbard, H. A. Mitochondrial Membrane Potential Probes and the Proton Gradient: A Practical Usage Guide. *BioTechniques* **2011**, *50*, 98 - 115.

(87) Mannancherril, V.; Therrien, B. Strategies toward the Enhanced Permeability and Retention Effect by Increasing the Molecular Weight of Arene Ruthenium Metallaassemblies. *Inorganic Chemistry* **2018**, *57*, 3626 - 3633.

(88) Sandoo, A.; van Zanten, V.; Metsios, G. S.; Carroll, D.; Kitas, G. D. The Endothelium and Its Role in Regulating Vascular Tone. *The Open Cardiovascular Medicine Journal* **2010**, *4*, 302 - 312.

(89) Fassas, A.; Anagnostopoulos, A. The Use of Liposomal Daunorubicin (DaunoXome) in Acute Myeloid Leukemia. *Leukemia and Lymphoma* **2005**, *46*, 795 - 802.

(90) EMA | Abraxane http://www.ema.europa.eu/docs/de_DE/document_library/EPAR_-_Summary_for_the_public/human/000778/WC500020431.pdf (accessed August 23, 2017).

(91) EMA | Depocyte http://www.ema.europa.eu/docs/en_GB/document_library/EPAR_-_Scientific_Discussion/human/000317/WC500035646.pdf (accessed August 24, 2017).

(92) Barenholz, Y. (C). Doxil® - The First FDA-Approved Nano-Drug: Lessons Learned. *Journal of Controlled Release* **2012**, *160*, 117 - 134.

(93) EMA | Myocet http://www.ema.europa.eu/docs/de_DE/document_library/EPAR_-_Summary_for_the_public/human/000297/WC500031806.pdf (accessed August 23, 2017).

(94) NCI | paclitaxel polymeric micelle formulation NANT-008 https://www.cancer.gov/publications/dictionaries/cancer-drug?cdrid=434427 (accessed August 24, 2017).

(95) NCI | Oncaspar https://www.cancer.gov/publications/dictionaries/cancer-drug?search=oncaspar (accessed August 24, 2017).

(96) Eliason, J. F. PEGylated Proteins in Immunotherapy of Cancer. *Delivery of Protein and Peptide Drugs in Cancer* **2006**, *6*, 111 - 126.

(97) Jain, R. K.; Stylianopoulos, T. Delivering Nanomedicine to Solid Tumors. *Nature Reviews Clinical Oncology* **2010**, *7*, 653 - 664.

(98) Suzuki, M.; Hori, K.; Abe, I.; Saito, S.; Sato, H. A New Approach to Cancer Chemotherapy: Selective Enhancement of Tumor Blood Flow with Angiotensin II.

Journal of the National Cancer Institute **1981**, *67*, 663 - 669.

(99) Danhier, F. To Exploit the Tumor Microenvironment: Since the EPR Effect Fails in the Clinic, what Is the Future of Nanomedicine? *Journal of Controlled Release* **2016**, *244*, 108 - 121.

(100) Wong, E.; Giandomenico, C. M. Current Status of Platinum-Based Antitumor Drugs. *Chemical Reviews* **1999**, *99*, 2451 - 2466.

(101) Jakupec, M. A.; Galanski, M.; Arion, V. B.; Hartinger, C. G.; Keppler, B. K. Antitumour Metal Compounds: More than Theme and Variations. *Dalton Transactions* **2007**, *2*, 183 - 194.

(102) Page, S. Ruthenium Compounds as Anticancer Agents. *The Royal Society of Chemistry Education in Chemistry* **2012**, *49*, 26 - 29.

(103) Pitchkov, V. N. The Discovery of Ruthenium. *Platinum Metals Review* **1996**, *40*, 181 - 188.

(104) Kupffer, A. Th. "Voyage dans l'Ural' entreprie en 1828", Paris, **1833**.

(105) Powell, A. R. The Platinum Metals in the Periodic System. *Platinum Metals Review* **1960**, *4*, 144 - 149.

(106) Kaji, M. Mendeleev's Discovery of the Periodic Law: The Origin and the Reception. *Foundations of Chemistry* **2003**, *5*, 189 - 214.

(107) reddit | Platinum Group Metals [Ruthenium, Rhodium, Palladium, Osmium, Iridium, Platinum] (Part 1) https://goo.gl/images/v8ga2s. (September 17, 2018).

(108) Renner, H.; Schlamp, G.; Kleinwächter, I.; Drost, E.; Lüschow, H. M.; Tews, P.; Panster, P.; Diehl, M.; Lang, J.; Kreuzer, T.; Knödler, A.; Starz, K. A.; Dermann, K.; Rothaut, J.; Drieselmann, R.; Peter, C.; Schiele, R. *Platinum Group Metals and Compounds*; Wiley-VCH Verlag GmbH & Co. KGaA, Weinheim, Germany, 2001, pp. 322 - 323.

(109) Chen, C - Y.; Wang, M.; Li, J - Y.; Pootrakulchote, N.; Alibabaei, L.; Ngoc-le, C.; Decoppet, J - D.; Tsai, J - H.; Grätzel, C.; Wu, C - G.; Zakeeruddin, S. M.; Grätzel, M. Highly Efficient Light-Harvesting Ruthenium Sensitizer for Thin-Film Dye-Sensitized Solar Cells. *American Chemical Society Nano* **2009**, *3*, 3103 - 3109.

(110) Umicore | Ruthenium https://www.umicore.com/en/about/elements/ruthenium/ (accessed October 9, 2018).

(111) Love, J. A.; Morgan, J. P.; Trnka, T. M.; Grubbs, R. H. A Practical and Highly Active Ruthenium-Based Catalyst That Effects the Cross Metathesis of Acrylonitrile. *Angewandte Chemie International Edition* **2002**, *41*, 4035 - 4037.

(112) Dasari, S.; Tchounwou, P. B. Cisplatin in Cancer Therapy: Molecular Mechanisms of Action. *European Journal of Pharmacology* **2014**, *740*, 364 - 378.

(113) Rosenberg, B.; VanCamp, L. The Successful Regression of Large Solid Sarcoma 180 Tumors by Platinum Compounds. *Cancer Research* **1970**, *30*, 1799 - 1802.

(114) Leo, M. **2015**, *Neurotoxische und neuroprotektive Mechanismen Cisplatin-induzierter Polyneuropathien.* (Doctoral dissertation). Fakultät für Biologie an der Universität Duisburg-Essen. pp. 16.

(115) Johnstone, T. C.; Alexander, S. M.; Wilson, J. J.; Lippard, S. J. Oxidative Halogenation of Cisplatin and Carboplatin: Synthesis, Spectroscopy, and Crystal and Molecular Structures of Pt(IV) Prodrugs. *Dalton Transactions* **2015**, *44*, 119 - 129.

(116) Han Ang, W. H.; Dyson, P. J. Classical and Non-Classical Ruthenium-Based Anticancer Drugs: Towards Targeted Chemotherapy. *European Journal of Inorganic Chemistry* **2006**, *2006*, 4003 - 4018.

(117) Auzias, M.; Gueniat, J.; Therrien, B.; Süss-Fink, G.; Renfrew, A. K.; Dyson, P. J. Arene-Ruthenium Complexes with Ferrocene-Derived Ligands: Synthesis and Characterization of Complexes of the Type $[Ru(\eta^6\text{-Arene})(NC_5H_4CH_2NHOC\text{-}C_5H_4FeC_5H_5)Cl_2]$ and $[Ru(\eta^6\text{-Arene})(NC_3H_3N(CH_2)_2O_2C\text{-}C_5H_4FeC_5H_5)Cl_2]$. *Organometallic Chemistry* **2009**, *694*, 855 - 861.

(118) Kratz, F.; Hartmann, M.; Keppler, B.; Messori, L. The Binding Properties of Two Antitumor Ruthenium(III) Complexes to Apotransferrin. *Journal of Biological Chemistry* **1994**, *269*, 2581 - 2588.

(119) Klajner, M.; Hebraud, P.; Sirlin, C.; Gaiddon, C.; Harlepp, S. DNA Binding to an Anticancer Organo-Ruthenium Complex. *The Journal of Physical Chemistry B* **2010**, *114*, 14041 - 14047.

(120) Chatterjee, S.; Kundu, S.; Bhattacharyya, A.; Hartinger, C. G.; Dyson, P. J. The Ruthenium(II)-Arene Compound RAPTA-C Induces Apoptosis in EAC Cells through Mitochondrial and P53-JNK Pathways. *Journal of Biological Inorganic Chemistry* **2008**, *13*, 1149 - 1155.

(121) Antonarakis, E. S.; Emadi, A. Ruthenium-Based Chemotherapeutics: Are They Ready for Prime Time? *Cancer Chemotherapy and Pharmacology* **2010**, *66*, 1 - 9.

(122) Richter, S.; Singh, S.; Draca, D.; Kate, A.; Kumbhar, A.; Kumbhar, A. S.; Maksimovic-Ivanic, D.; Mijatovic, S.; Lönnecke, P.; Hey-Hawkins, E. Antiproliferative Activity of Ruthenium(II) Arene Complexes with Mono- and Bidentate Pyridine-Based Ligands. *Dalton Transactions* **2016**, *45*, 13114 - 13125.

(123) Alessio, A.; Messori, L. The Deceptively Similar Ruthenium(III) Drug Candidates KP1019 and NAMI-A Have Different Actions. What Did We Learn in the Past 30 Years? *Metal Ions in Life Science* **2018**, *18*, 141 - 170.

(124) Allardyce, C. S.; Dyson, P. J.; Ellis, D. J.; Heath, S. L. [Ru(η^6-*p*-cymene)Cl_2(pta)] (pta = 1,3,5-triaza-7-phosphatricyclo[3.3.1.1]decane): A Water Soluble Compound that Exhibits pH Dependent DNA Binding Providing Selectivity for Diseased Cells. *Chemical Communications* **2001**, *0*, 1396 - 1397.

(125) Levi, S.; Rovida, E. The Role of Iron in Mitochondrial Function. *Biochimica et Biophysica Acta (BBA) - General Subjects* **2009**, *1790*, 629 - 636.

(126) Stevens, S. K.; Strehle, A. P.; Miller, R. L.; Gammons, S. H.; Hoffman, K. J.; McCarty, J. T.; Miller, M. E.; Stultz, L. K.; Hanson, P. K. The Anticancer Ruthenium Complex KP1019 Induces DNA Damage, Leading to Cell Cycle Delay and Cell Death in Saccharomyces Cerevisiae. *Molecular Pharmacology* **2013**, *83*, 225 - 234.

(127) Paul, B. T.; Manz, D. H.; Torti, F. M.; Torti, S. V. Mitochondria and Iron: Current Questions. *Expert Review of Hematology* **2017**, *10*, 65 - 79.

(128) Biochemden | Heme Synthesis: Synthesis of Porphyrin Molecule. https://www.biochemden.com/heme-synthesis/ (accessed October 3, 2018).

(129) Gao, G.; Chang, Y - Z. Mitochondrial Ferritin in the Regulation of Brain Iron Homeostasis and Neurodegenerative Diseases. *Frontiers in Pharmacology* **2014**, *5*, 1 - 7.

(130) Coverdale, J. P. C.; Laroiya-McCarron, T.; Romero-Canelon, I. Designing Ruthenium Anticancer Drugs: What Have We Learnt from the Key Drug Candidates? *Inorganics*, **2019**, *7*, 1 - 15.

(131) IUPAC Compendium of Chemical Terminology, *Gold Book*, Version 2.3.3, 2014, pp 108.

(132) Didier Astruc. *Organometallic Chemistry and Catalysis*; Springer, Berlin Heidelberg, 2007, pp 42.

(133) The University of Tokyo | Hartwig, http://www.f.u-tokyo.ac.jp/~kanai/seminar/om/Hartwig2.pdf (accessed October 17, 2018).

(134) Therrien, B. Arene Ruthenium Cages: Boxes Full of Surprises. *European Journal of Inorganic Chemistry* **2009**, *2009*, 2445 - 2453.

(135) 1stdibs | Piano stool, https://www.1stdibs.com/furniture/seating/stools/walnut-adjustable-piano-stool/id-f_11469123/ (accessed October 15, 2018).

(136) Sheldrick, W. S.; Heeb, S. Synthesis and Structural Characterization of η^6-Arene-

Ruthenium(II) Complexes of Alanine and Guanine Derivatives. *Inorganica Chimica Acta* **1990**, *168*, 93 - 100.

(137) Peacock, A. F. A.; Sadler, P. J. Medicinal Organometallic Chemistry: Designing Metal Arene Complexes as Anticancer Agents. *Chemistry - An Asian Journal* **2008**, *3*, 1890 - 1899.

(138) Dyson, P. J.; Sava, G. Metal-Based Antitumour Drugs in the Post Genomic Era. *Dalton Transactions* **2006**, *16*, 1929 - 1933.

(139) Maverick, A. W.; Klavetter, F. E. Cofacial Binuclear Copper Complexes of a Bis(*β*-diketone) Ligand'. *Inorganic chemistry*, **1984**, 4129 - 4130.

(140) Maverick, A. W.; Buckingham, S. C.; Yao, Q.; Bradbury, J. R.; Stanley, G. G. Intramolecular Coordination of Bidentate Lewis Bases to a Cofacial Binuclear Copper(II) Complex. *Journal of the American Chemical Society* **1986**, *108*, 7430 - 7431.

(141) Fujita, M.; Yazaki, J.; Ogura, K. Preparation of a Macrocyclic Polynuclear Complex, $[(en)Pd(4,4'\text{-}bpy)]_4(NO_3)_8$, which Recognizes an Organic Molecule in Aqueous Media. *Journal of the American Chemical Society* **1990**, *112*, 5645 - 5647.

(142) Kuehl, C. J.; Huang, S. D.; Stang, P. J. Self-Assembly with Postmodification: Kinetically Stabilized Metalla-Supramolecular Rectangles. *Journal of the American Chemical Society* **2001**, *123*, 9634 - 9641.

(143) Moriuchi, T.; Miyaishi, M.; Hirao, T. Conjugated Complexes Composed of Quinonediimine and Palladium: Controlled Formation of a Conjugated Trimetallic Macrocycle. *Angewandte Chemie International Edition* **2001**, *40*, 3042 - 3045.

(144) Das, N.; Mukherjee, P. S.; Arif, A. M.; Stang, P. J. Facile Self-Assembly of Predesigned Neutral 2D Pt-Macrocycles *via* a New Class of Rigid Oxygen Donor Linkers. *Journal of the American Chemical Society* **2003**, *125*, 13950 - 13951.

(145) Mukherjee, P. S.; Das, N.; Kryschenko, Y. K.; Arif, A. M.; Stang, P. J. Design, Synthesis, and Crystallographic Studies of Neutral Platinum-Based Macrocycles Formed *via* Self-Assembly. *Journal of the American Chemical Society* **2004**, *126*, 2464 - 2473.

(146) Caskey, D. C.; Shoemaker, R. K.; Michl, J. Toward Self-Assembled Surface-Mounted Prismatic Altitudinal Rotors. A Test Case: Molecular Rectangle. *Organic Letters* **2004**, *6*, 2093 - 2096.

(147) Yoshizawa, M.; Nagao, M.; Kumazawa, K.; Fujita, M. Side Chain-Directed Complementary *cis*-Coordination of Two Pyridines on Pd(II): Selective Multicomponent Assembly of Square-, Rectangular-, and Trigonal Prism-Shaped

Molecules. *Journal of Organometallic Chemistry* **2005**, *690*, 5383 - 5388.

(148) Kim, D.; Paek, J. H.; Jun, M - J.; Lee, J. Y.; Kang, S. O.; Ko, J. Self-Assembly of Rectangles and Prisms *via* a Molecular "Clip." *Inorganic Chemistry* **2005**, *44*, 7886 - 7894.

(149) Yan, H.; Süss-Fink, G.; Neels, A.; Stoeckli-Evans, H. Mono-, Di-and Tetra-Nuclear *p*-Cymeneruthenium Complexes Containing Oxalato Ligands. *Journal of the Chemical Society, Dalton Transactions* **1997**, *0*, 4345 - 4350.

(150) Mendoza-Ferri, M - G.; Hartinger, C. G.; Eichinger, R. E.; Stolyarova, N.; Severin, K.; Jakupec, M. A.; Nazarov, A. A.; Keppler, B. K. Influence of the Spacer Length on the *in Vitro* Anticancer Activity of Dinuclear Ruthenium - Arene Compounds. *Organometallics* **2008**, *27*, 2405 - 2407.

(151) Mendoza-Ferri, M. G.; Hartinger, C. G.; Mendoza, M. A.; Groessl, M.; Egger, A. E.; Eichinger, R. E.; Mangrum, J. B.; Farrell, N. P.; Maruszak, M.; Bednarski, P. J.; Klein, F.; Jakupec, M. A.; Nazarov, A. A.; Severin, K.; Keppler, B. K. Transferring the Concept of Multinuclearity to Ruthenium Complexes for Improvement of Anticancer Activity. *Journal of Medicinal Chemistry* **2009**, *52*, 916 - 925.

(152) Barry, N. P. E.; Furrer, J.; Freudenreich, J.; Süss-Fink, G.; Therrien, B. Designing the Host-Guest Properties of Tetranuclear Arene Ruthenium Metalla-Rectangles to Accommodate a Pyrene Molecule. *European Journal of Inorganic Chemistry* **2010**, *2010*, 725 - 728.

(153) Therrien, B.; Furrer, J. The Biological Side of Water-Soluble Arene Ruthenium Assemblies. *Advances in Chemistry* **2014**, *2014*, 1 - 20.

(154) Therrien, B. Coordination Chemistry of 2,4,6-Tri(pyridyl)-1,3,5-triazine Ligands. *Journal of Organometallic Chemistry* **2011**, *696*, 637 - 651.

(155) Leenders, S. H. A. M.; Becker, R.; Kumpulainen, T.; de Bruin, B.; Sawada, T.; Kato, T.; Fujita, M.; Reek, J. N. H. Selective Co-Encapsulation Inside an M_6L_4 Cage. *Chemistry - A European Journal* **2016**, *22*, 15468 - 15474.

(156) Kaminker, R.; Popovitz-Biro, R.; van der Boom, M. E. Coordination-Polymer Nanotubes and Spheres: A Ligand-Structure Effect. *Angewandte Chemie International Edition* **2011**, *50*, 3224 - 3226.

(157) Kobayashi, N.; Kijima, M. 1,3,5-Tris(functionalised-phenylethynyl)benzene - Metal Complexes: Synthetic Survey of Mesoporous Coordination Polymers and Investigation of Their Carbonisation. *Journal of Materials Chemistry* **2008**, *18*, 1037 - 1045.

(158) Wang, L.; Tao, X - T.; Yang, J - X.; Yu, W - T.; Ren, Y.; Xin, Q.; Liu, Z.; Jiang, M - H.

Synthesis, Structure and Two-Photon Absorption Properties of a New Multi-Branched Compound, 1,2,4,5-Tetrakis(4-pyridylvinyl)benzene. *Journal of Solid State Chemistry* **2004**, *177*, 4293 - 4299.

(159) Caskey, D. C.; Yamamoto, T.; Addicott, C.; Shoemaker, R. K.; Vacek, J.; Hawkridge, A. M.; Muddiman, D. C.; Kottas, G. S.; Michl, J.; Stang, P. J. Coordination-Driven Face-Directed Self-Assembly of Trigonal Prisms. Face-Based Conformational Chirality. *Journal of the American Chemical Society* **2008**, *130*, 7620 - 7628.

(160) Adler, A. D.; Longo, F. R.; Shergalis, W. Mechanistic Investigations of Porphyrin Syntheses. I. Preliminary Studies on *ms*-Tetraphenylporphin. *Journal of the American Chemical Society* **1964**, *86*, 3145 - 3149.

(161) Rothemund, P. Formation of Porphyrins from Pyrrole and Aldehydes. *Journal of the American Chemical Society* **1935**, *57*, 2010 - 2011.

(162) Garci, A.; Dobrov, A. A.; Riedel, T.; Orhan, E.; Dyson, P. J.; Arion, V. B.; Therrien, B. Strategy to Optimize the Biological Activity of Arene Ruthenium Metalla-Assemblies. *Organometallics* **2014**, *33*, 3813 - 3822.

(163) Lu, S.; Drees, M.; Yao, Y.; Boudinet, D.; Yan, H.; Pan, H.; Wang, J.; Li, Y.; Usta, H.; Facchetti, A. 3,6-Dithiophen-2-yl-diketopyrrolo[3,2- *b*]pyrrole (IsoDPPT) as an Acceptor Building Block for Organic Opto-Electronics. *Macromolecules* **2013**, *46*, 3895 - 3906.

(164) Hornung, R.; Fehr, M. K.; Monti-Frayne, J.; Krasieva, T. B.; Tromberg, B. J.; Berns, M. W.; Tadir, Y. Highly Selective Targeting of Ovarian Cancer with the Photosensitizer PEG-m-THPC in a Rat Model. *Photochemistry Photobiology* **1999**, *70*, 624 - 629.

(165) Rovers, J. P.; Saarnak, A. E.; de Jode, M.; Sterenborg, H. J. C. M.; Terpstra, O. T.; Grahn, M. F. Biodistribution and Bioactivity of Tetra-Pegylated Meta-tetra(hydroxyphenyl)chlorin Compared to Native Meta-tetra(hydroxyphenyl)chlorin in a Rat Liver Tumor Model. *Photochemistry and Photobiology* **2000**, *71*, 211 - 217.

(166) Tabatadze, D.; Zamecnik, P.; Yanachkov, I.; Wright, G.; Pierson, K.; Zhang, S.; Bogdanov, A.; Metelev, V. A Novel Thymidine Phosphoramidite Synthon for Incorporation of Internucleoside Phosphate Linkers During Automated Oligodeoxynucleotide Synthesis. *Nucleosides Nucleotides Nucleic Acids* **2008**, *27*, 157 - 172.

(167) Zuo, Y - J.; Qu, J. How Does Aqueous Solubility of Organic Reactant Affect a Water-Promoted Reaction? *The Journal Organic Chemistry* **2014**, *79*, 6832 - 6839.

(168) Holden, D. A. Synthesis and Spreading Behaviour of Some Reactive Derivatives of

Long-Chain Alcohols and Carboxylic Acids. *Canadian Journal of Chemistry* **1984**, *62*, 574 - 579.

(169) Sumiyoshi, T.; Nishimura, K.; Nakano, M.; Handa, T.; Miwa, Y.; Tomioka, K. Molecular Assembly of C_2-Symmetric Bis-(2*S*)-2-methyldodecanoylamides of α,ω-Alkylidenediamines into Coiled Coil and Twisted Ribbon Aggregates. *Journal of the American Chemical Society* **2003**, *125*, 12137 - 12142.

(170) Billera, C. F.; Dunn, T. B.; Barry, D. A.; Engel, P. S. Thermolysis of Acylazo *O*-Trimethylsilyl Cyanohydrins: Azoalkanes Yielding Captodatively Substituted Radicals. *The Journal of Organic Chemistry* **1998**, *63*, 9763 - 9768.

(171) Wu, D - Y.; Herbst, R. M. Substituted Phenyltetrazoles. Alkoxynitrophenyl-Tetrazoles and Alkoxyaminophenyltetrazoles. *The Journal of Organic Chemistry* **1952**, *17*, 1216 - 1227.

(172) Garci, A.; Mbakidi, J - P.; Chaleix, V.; Sol, V.; Orhan, E.; Therrien, B. Tunable Arene Ruthenium Metallaprisms to Transport, Shield, and Release Porphin in Cancer Cells. *Organometallics* **2015**, *34*, 4138 - 4146.

(173) Gan, X.; Jiang, W.; Wang, W.; Hu, L. An Approach to 3,6-Disubstituted 2,5-Dioxybenzoquinones *via* Two Sequential Suzuki Couplings. Three-Step Synthesis of Leucomelone. *Organic Letters* **2009**, *11*, 589 - 592.

(174) Viault, G.; Grée, D.; Das, S.; Yadav, J. S.; Grée, R. Synthesis of a Focused Chemical Library Based on Derivatives of Embelin, a Natural Product with Proapoptotic and Anticancer Properties. *European Journal of Organic Chemistry* **2011**, *2011*, 1233 - 1241.

(175) Koizumi, M.; Dietrich-Buchecker, C.; Sauvage, J - P. A [2]Catenane Containing 1,1′-Binaphthyl Units and 1,10-Phenanthroline Fragments: Synthesis and Intermolecular Energy Transfer Processes. *European Journal of Organic Chemistry* **2004**, *2004*, 770 - 775.

(176) Gillet, L. C. J.; Namoto, K.; Ruchti, A.; Hoving, S.; Boesch, D.; Inverardi, B.; Mueller, D.; Coulot, M.; Schindler, P.; Schweigler, P.; Bernardi, A.; Gil-Parrado, S. In-Cell Selectivity Profiling of Serine Protease Inhibitors by Activity-Based Proteomics. *Molecular & Cellular Proteomics* **2008**, *7*, 1241 - 1253.

(177) Gudipati, V.; Curran, D. P.; Wilcox, C. S. Solution-Phase Parallel Synthesis with Oligoethylene Glycol Sorting Tags. Preparation of All Four Stereoisomers of the Hydroxybutenolide Fragment of Murisolin and Related Acetogenins. *The Journal of Organic Chemistry* **2006**, *71*, 3599 - 3607.

(178) Bailey, J. M.; Bruton, G.; Huxley, A.; Milner, P. H.; Orlek, B. S. Substituted Piperidines as Histamine H3 Receptor Ligands. From PCT Int. Appl.; **WO**2005014571A1, **2005**.

(179) Bao, R.; Lai, C.; Qian, C. Treatment of Cancers Having K-Ras Mutations. From PCT Int. Appl.; **WO**2011130628A1, **2005**.

(180) Gupta, O. P.; Ali, M. M.; Ghatak, B. J. R.; Atal, C. K. Some Pharmacological Investigations of Embelin and Its Semisynthetic Derivatives. *Indian Journal of Physiology and Pharmacology* **1977**, *21*, 31 - 39.

(181) Chitra, M.; Sukumar, E.; Suja, V.; Shyamala Devi, C. S. Antitumor, Anti-Inflammatory and Anagesic Property of Embeline, a Plant Product. *Chemotherapy* **1994**, *40*, 109 - 113.

(182) Reuter, S.; Prasad, S.; Phromnoi, K.; Kannappan, R.; Yadav, V. R.; Aggarwal, B. B. Embelin Suppresses Osteoclastogenesis Induced by Receptor Activator of NF-*κ*B Ligand and Tumor Cells *In Vitro* through Inhibition of the NF-*κ*B Cell Signaling Pathway. *Molecular Cancer Research* **2010**, *8*, 1425 - 1436.

(183) Taghiyev, A.; Sun, D.; Gao, Z. M.; Liang, R.; Wang, L. Embelin-Induced Apoptosis of HepG2 Human Hepatocellular Carcinoma Cells and Blockade of HepG2 Cells in the G2/M Phase *via* the Mitochondrial Pathway. *Experimental and Therapeutic Medicine* **2012**, *4*, 649 - 654.

(184) Hu, R.; Zhu, K.; Li, Y.; Yao, K.; Zhang, R.; Wang, H.; Yang, W.; Liu, Z. Embelin Induces Apoptosis through Down-Regulation of XIAP in Human Leukemia Cells. *Medical Oncology* **2011**, *28*, 1584 - 1588.

(185) Mori, T.; Doi, R.; Kida, A.; Nagai, K.; Kami, K.; Ito, D.; Toyoda, E.; Kawaguchi, Y.; Uemoto, S. Effect of the XIAP Inhibitor Embelin on TRAIL-Induced Apoptosis of Pancreatic Cancer Cells. *Journal of Surgical Research* **2007**, *142*, 281 - 286.

(186) Chen, F.; Zhang, G.; Hong, Z.; Lin, Z.; Lei, M.; Huang, M.; Hu, L. Design, Synthesis, and SAR of Embelin Analogues as the Inhibitors of PAI-1 (Plasminogen Activator Inhibitor-1). *Bioorganic and Medicinal Chemistry Letters* **2014**, *24*, 2379 - 2382.

(187) Filosa, R.; Peduto, A.; Schaible, A. M.; Krauth, V.; Weinigel, C.; Barz, D.; Petronzi, C.; Bruno, F.; Roviezzo, F.; Spaziano, G.; D'Agostino, B.; De Rosa, M.; Werz, O. Novel Series of Benzoquinones with High Potency against 5-Lipoxygenase in Human Polymorphonuclear Leukocytes. *European Journal of Medicinal Chemistry* **2015**, *94*, 132 - 139.

(188) Green, M. D.; Choi, J - H.; Winey, K. I.; Long, T. E. Synthesis of Imidazolium-Containing ABA Triblock Copolymers: Role of Charge Placement, Charge Density, and

Ionic Liquid Incorporation. *Macromolecules* **2012**, *45*, 4749 - 4757.

(189) Sugandhi, E. W.; Macri, R. V.; Williams, A. A.; Kite, B. L.; Slebodnick, C.; Falkinham, J. O.; Esker, A. R.; Gandour, R. D. Synthesis, Critical Micelle Concentrations, and Antimycobacterial Properties of Homologous, Dendritic Amphiphiles. Probing Intrinsic Activity and the "Cutoff" Effect. *Journal of Medicinal Chemistry* **2007**, *50*, 1645 - 1650.

(190) Mathison, I. W.; Gueldner, R. C.; Carroll, D. M. Application of *n*-Butyl Lithium in the Synthesis of Some Methoxy-Substituted Aromatic Carboxylic Acids. *Journal of Pharmaceutical Sciences* **1968**, *57*, 1820 - 1821.

(191) Leggio, A.; Belsito, E. L.; De Luca, G.; Di Gioia, M. L.; Leotta, V.; Romio, E.; Siciliano, C.; Liguori, A. One-Pot Synthesis of Amides from Carboxylic Acids Activated Using Thionyl Chloride. *Royal Society of Chemistry Advances* **2016**, *6*, 34468 - 34475.

(192) Bentley, M. D.; Zhao, X. Hydrolytically Degradable Carbamate Derivatives of Poly(ethylene glycol). From PCT Int. Appl.; **WO**0147562A2, **2001**.

(193) Bamborough, P.; Barnett, H. A.; Becher, I.; Bird, M. J.; Chung, C; Craggs, P. D.; Demont, E. H.; Diallo, H.; Fallon, D. J.; Gordon, L. J.; Grandi, P.; Hobbs, C. I.; Hooper-Greenhill, E.; Jones, E. J.; Law, R. P.; Le Gall, A.; Lugo, D.; Michon, A - M.; Mitchell, D. J.; Prinjha, R. K.; Sheppard, R. J.; Watson, A. J. B.; Watson, R. J. GSK6853, a Chemical Probe for Inhibition of the BRPF1 Bromodomain. *American Chemical Society Medicinal Chemistry Letters* **2016**, *7*, 552 - 557.

(194) Ihre, H.; Hult, A.; Fréchet, J. M. J.; Gitsov, I. Double-Stage Convergent Approach for the Synthesis of Functionalized Dendritic Aliphatic Polyesters Based on 2,2-Bis(hydroxymethyl)propionic Acid. *Macromolecules* **1998**, *31*, 4061 - 4068.

(195) Boden, E. P.; Keck, G. E. Proton-Transfer Steps in Steglich Esterification: A Very Practical New Method for Macrolactonization. *The Journal of Organic Chemistry* **1985**, *50*, 2394 - 2395.

(196) Jeon, J.; Kang, J. A.; Shim, H. E.; Nam, Y. R.; Yoon, S.; Kim, H. R.; Lee, D. E.; Park, S. H. Efficient Method for Iodine Radioisotope Labeling of Cyclooctyne-Containing Molecules Using Strain-Promoted Copper-Free Click Reaction. *Bioorganic and Medicinal Chemistry* **2015**, *23*, 3303 - 3308.

(197) Sigma-Aldrich | https://www.sigmaaldrich.com/technical-documents/articles/biology/ir-spectrum-table.html (accessed December 9, 2018).

(198) Barry, N. P. E.; Therrien, B. Host-Guest Chemistry in the Hexanuclear (Arene)Ruthenium Metalla-Prismatic Cage $[Ru_6(p\text{-cymene})_6(tpt)_2(dhnq)_3]^{6+}$. *European Journal of Inorganic Chemistry* **2009**, *2009*, 4695 - 4700.

(199) Vieille-Petit, L.; Therrien, B.; Süss-Fink, G. Synthesis and Molecular Structure of the Trinuclear Ruthenium Cluster Cations $[H_3Ru_3\{C_6H_5(CH_2)_2OC(O)C_6H_5\}(C_6Me_6)_2(O)]^+$ and $[H_3Ru_3\{C_6H_5(CH_2)_2OC(O)(CH_2)_3C_6H_5\}(C_6Me_6)_2(O)]^+$. *Inorganica Chimica Acta* **2004**, *357*, 3437 - 3442.

(200) Morris, K. F.; Johnson, C. S. Diffusion-Ordered Two-Dimensional Nuclear Magnetic Resonance Spectroscopy. *Journal of the American Chemical Society* **1992**, *114*, 3139 - 3141.

(201) Barry, N. P. E.; Govindaswamy, P.; Furrer, J.; Süss-Fink, G.; Therrien, B. Organometallic Boxes Built from 5,10,15,20-Tetra(4-pyridyl)porphyrin Panels and Hydroxyquinonato-Bridged Diruthenium Clips. *Inorganic Chemistry Communications* **2008**, *11*, 1300 - 1303.

(202) Ma, X.; Zhao, Y. Biomedical Applications of Supramolecular Systems Based on Host-Guest Interactions. *Chemical Reviews* **2015**, *115*, 7794 - 7839.

(203) Barry, N. P. E.; Furrer, J.; Therrien, B. In- and Out-of-Cavity Interactions by Modulating the Size of Ruthenium Metallarectangles. *Helvetica Chimica Acta* **2010**, *93*, 1313 - 1328.

(204) Govindaswamy, P.; Furrer, J.; Süss-Fink, G.; Therrien, B. Encapsulation of Triphenylene Derivatives in the Hexanuclear Arene Ruthenium Metallo-Prismatic Cage $[Ru_6(p\text{-}Pr^iC_6H_4Me)_6(tpt)_2(dhbq)_3]^{6+}$ (tpt = 2,4,6-tri(pyridin-4-yl)-1,3,5-triazine, dhbq = 2,5-dihydroxy-1,4-benzoquinonato). *Zeitschrift für anorganische und allgemeine Chemie.* **2008**, *634*, 1349 - 1352.

(205) Freudenreich, J.; Dalvit, C.; Süss-Fink, G.; Therrien, B. Encapsulation of Photosensitizers in Hexa- and Octanuclear Organometallic Cages: Synthesis and Characterization of Carceplex and Host - Guest Systems in Solution. *Organometallics* **2013**, *32*, 3018 - 3033.

(206) Freudenreich, J. **2012**, *Complexes arène-ruthénium multinucléaires: Véhicules pour le transport intracellulaire de molécules cytotoxique et photosensibilisantes*. (Doctoral dissertation). Chimie macromoléculaire, Université de Neuchâtel. pp. 100.

(207) Mosmann, T. Rapid Colorimetric Assay for Cellular Growth and Survival: Application to Proliferation and Cytotoxicity Assays. *Journal of Immunological Methods* **1983**, *65*, 55 - 63.

(208) Rickhaus, M.; Jentzsch, A. V.; Tejerina, L.; Grübner, I.; Jirasek, M.; Claridge, T. D. W.; Anderson, H. L. Single-Acetylen Linked Porphyrin Nanorings. *Journal of the American Chemical Society* **2017**, *139*, 16502 - 16505.

(209) Tanaka, T.; Osuka, A. Conjugated porphyrin arrays: synthesis, properties and applications for functional materials. *Chemical Society Reviews* **2015**, *44*, 943 - 969.

(210) Tsuda, A.; Osuka A. Fully Conjugated Porphyrin Tapes with Electronic Absorption Bands That Reach into Infrared. *Science* **2001**, *293*, 79 - 82.

(211) Aratani, N.; Osuka, A.; Kim, Y. H.; Jeong, D. H.; Kim, D. Extremely Long, Discrete *meso* - *meso*-Coupled Porphyrin Arrays. *Angewandte Chemie International Edition* **2000**, *39*, 1458 - 1462.

(212) Osuka, A.; Shimidzu, H. *meso,meso*-Linked Porphyrin Arrays. *Angewandte Chemie International Edition in English* **1997**, *36*, 135 - 137.

(213) Gonçalves D. P. N.; Ladame, S.; Balasubramaniam, S.; Sanders, J. K. M. Synthesis and G-quadruplex binding studies of new 4-N-methylpyridinium porphyrins. *Organic and Biomolecular Chemistry* **2006**, *4*, 3337 - 3342.

(214) Fulmer, G. R.; Miller, A. J. M.; Sherden, N. H.; Gottlieb, H. E.; Nudelman, A.; Stoltz, B. M.; Bercaw, J. E.; Goldberg, K. I. NMR Chemical Shifts of Trace Impurities: Common Laboratory Solvents, Organics, and Gases in Deuterated Solvents Relevant to the Organometallic Chemist. *Organometallics* **2010**, *29*, 2176 - 2179.

(215) Science and Fun | Nitromethane-d_3 http://www.science-and-fun.de/tools/solvents/cd3no2.htm (accessed December 19, 2018).

(216) Bennett, M. A.; Huang, T - N.; Matheson, T. W.; Smith, A. K. *Inorganic Syntheses* **1982**, *21*, 74 - 78.

10. LIST OF STRUCTURES

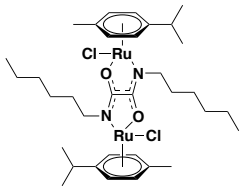

50

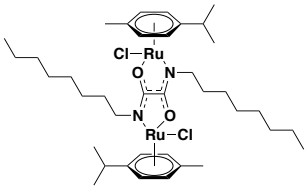

51

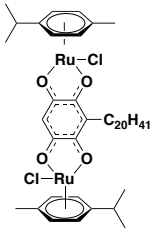

59

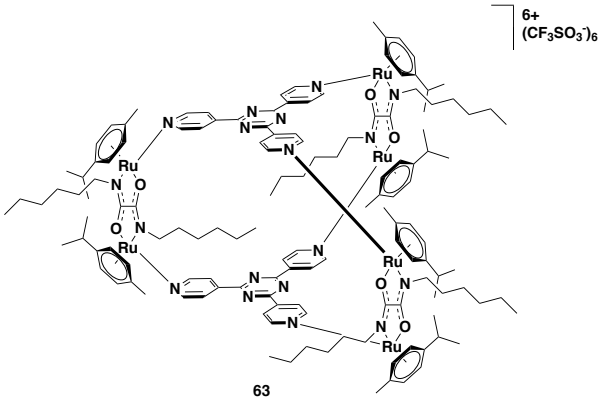

63

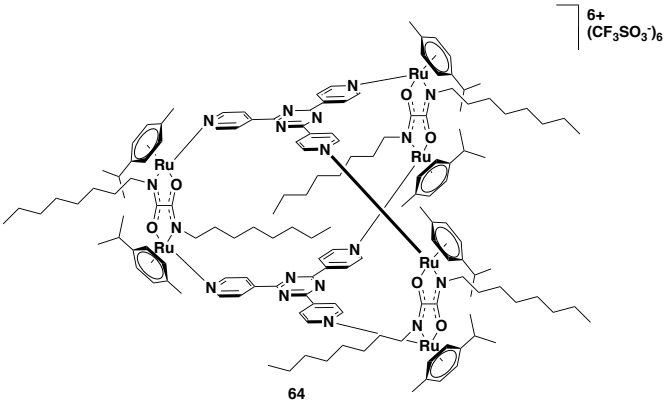

64

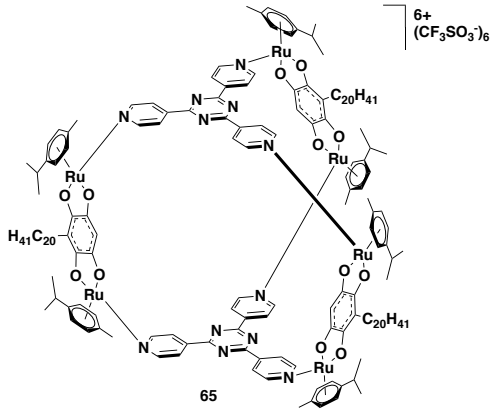

65

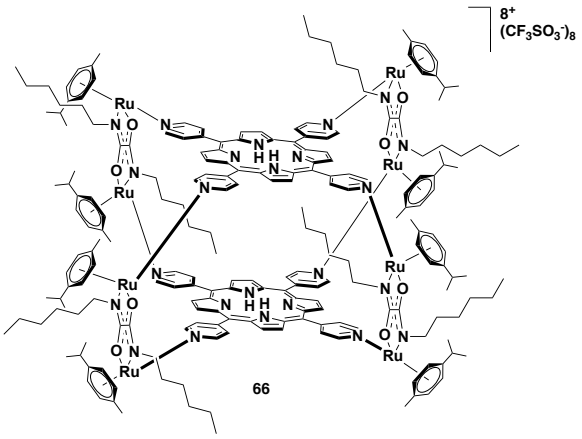

66

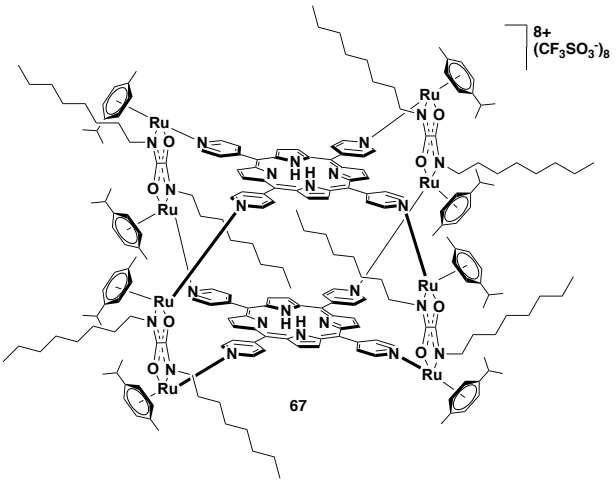

67

11. LIST OF FIGURES

12. LIST OF SCHEMES

13. LIST OF TABLES

14. LIST OF PUBLICATIONS

14.1. PUBLICATION DURING THE PH.D. STUDIES

(1) Mannancherril, V.; Therrien, B. Strategies toward the Enhanced Permeability and Retention Effect by Increasing the Molecular Weight of Arene Ruthenium Metallaassemblies. *Inorg. Chem.* **2017**, *57*, 3626.

14.2. CONFERENCE AND SYMPOSIUM CONTRIBUTIONS

(1) SCS Fall Meeting 2018, Lausanne, Switzerland, September 7th, 2018, Poster.
(2) SCS Spring Meeting 2018, Neuchâtel, Switzerland, April 4th, 2018, Poster.
(3) SCS Fall Meeting 2017, Bern, Switzerland, August 21st - 22nd, 2017, Poster.
(4) ICREA Conference of Functional Nanocontainers 2016, Tarragona, Spain, October 17th - 20th, 2016, Poster.
(5) SCS Fall Meeting 2016, Zurich Switzerland, September 15th, 2016, Poster.
(6) Graduate Student Symposium 2016, Bern, Switzerland, September 12th, 2016, Presentation.

15. APPENDICES

15.1. INORGANIC CHEMISTRY PUBLICATION

Strategies towards the EPR-Effect by Increasing the Molecular Weight of Arene Ruthenium Metalla-Assemblies

Vidya Mannancherril and Bruno Therrien*

Institut de Chimie, Université de Neuchâtel, Avenue de Bellevaux 51, 2000 Neuchâtel, Switzerland.

KEYWORDS: Enhanced Permeability and Retention Effect; Arene Ruthenium; Metalla-Assemblies; Supramolecular Chemistry; Tumor Targeting

ABSTRACT: The enhanced permeability and retention (EPR) effect is an attractive avenue to target tumors: The size of the drug being the key to accumulate predominantly in tumors. Therefore, to increase the molecular weight of arene ruthenium metalla-assemblies, several strategies can be adopted, and we present here our first step in the design of larger and heavier discrete arene ruthenium metalla-assemblies to dfreach an EPR-size dimension.

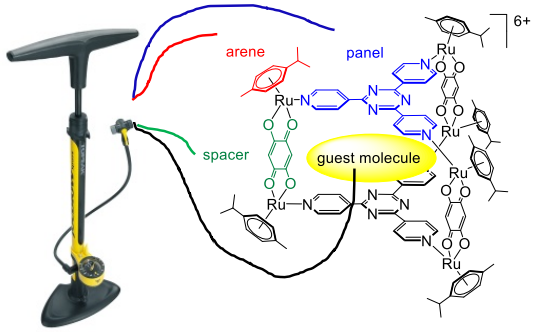

Introduction

Most solid and metastatic tumors show unique characteristics which are not observed in healthy tissues and organs, such as increased production of vascular permeability mediators, defective vascular architecture, impaired lymphatic drainage and impaired recovery system, as well as an extensive angiogenesis leading to hypervasculature. All these features compose the enhanced permeability and retention effect (EPR-effect).[1,2] Currently, only a small number of drugs are effective against metastatic cancers, therefore the EPR-effect offers great perspectives in nanomedicine therapy.

The EPR-effect was first described in 1986 by Maeda and it remains a popular strategy for cancer-selective drug delivery,[1,2] despite recent indication that the EPR-effect might not be valid in humans.[3] Nevertheless, rapid and chaotic angiogenesis coupled to excessive production of vascular mediators generate poorly defined blood vessels, showing gaps between endothelial cells.[1-4] Tumor blood vessels do not have a fixed and compact structure like healthy tissues, but a

very dynamic system with large openings between endothelial cells, which make them leaky and permeable. The size of those gaps can vary from 100 nm to approximately 1 µm, whereas in normal tissues the gaps are < 6 nm (continuous endothelial cells in striated muscles), 10 - 100 nm in diameter (fenestrated endothelial cells in renal medulla, endocrine glands, renal glomerulus, choroid plexus in the brain, intestinal villus) and even larger (discontinuous endothelial cells in sinusoid vessels, liver, spleen, bone marrow, extraneous particles from the blood).[5-7]

High molecular weight compounds such as nanoparticles, macromolecular drugs, polymeric drugs and lipid particles enter predominantly into tumor tissues rather than into normal tissues (enhanced permeability) and will remain in the tumor tissues for a prolonged period of time (retention). In Figure 1, the upper part shows healthy tissues where the cellular structure is well defined, and where small molecules are able to pass the endothelial cells to enter, and are subsequently removed by the lymphatic drainage. The lower part shows cancerous tissues with large gaps between cells, where not only small molecules but also macromolecules can enter. Furthermore, large molecules (drugs) will accumulate due to a defective lymphatic drainage.

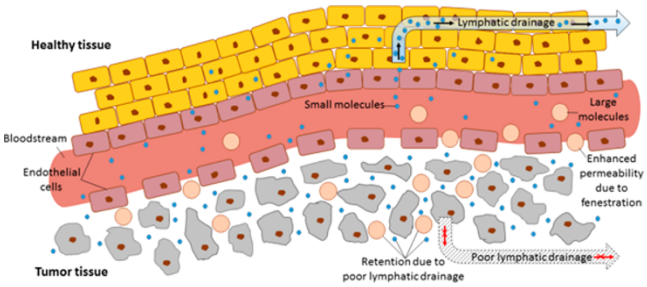

Figure1. Illustration of the EPR-effect (top = healthy tissue; bottom = tumor tissue).

A key mechanism of the EPR-effect is the retention of high-molecular weight substances in the tumor environment, whereas low molecular weight substances are returned to the blood circulatory system by diffusion.[1] Retention is caused by the impaired lymphatic drainage. An intact lymphatic drainage ensures that ectopic substances are removed from tissues. However, in a damaged lymphatic system, only low-molecular weight substances are removed and high-molecular weight substances are retained. After administration of such high-molecular weight compounds it was shown that their concentration are 10 - 200 times higher in tumors than in normal tissues,[5] and this phenomenon can be used to our benefit.

However, great diversities exist among tumors and the grade of EPR-effect observed can differ tremendously. Some tumors show a strong EPR-effect whereas others only a limited or even no effect, which can be demonstrated by arterial angiography using an X-ray lipid contrast agent.[2] Vascular permeability and the grade of EPR-effect may also depend on tumor type and may increase with tumor size and growth rate, and it might be higher in the periphery than in the central region of tumors.[8] Therefore, there is no uniform treatment of solid cancers exploiting the EPR-effect, which ensures sufficient drug delivery to all tumor regions.[9]

The over production of vascular mediators such as bradykinin, nitric oxide (NO), vascular endothelial growth factor (VEGF) and carbon monoxide (CO), further enhance the permeability of tumors. This can be used for the augmentation of EPR-based tumor targeting, achieving more tumor accumulation of macromolecular drugs.[5] NO production is inevitable

Table 1. Examples of macromolecular anti-cancer drugs that have passed clinical or preclinical trials.

drug	active component	conjugate	mode of action
DaunoXome	daunorubicin (anthracycline)	daunorubicin citrate liposome	prevention of DNA replication, inhibition of protein synthesis, and conjugate decreases side effects[13]
Abraxane	paclitaxel (taxanes)	paclitaxel bound to albumin	blocks mitosis and one stade of cell division[14]
Genexol-PM	paclitaxel	paclilaxel-loaded polymeric micelle	antineoplastic activity, interferes with mitosis, and conjugate increases water solubility[15]
DepoCyte	cytarabine	cytarabine encapsulated in multivesicular lipid particles for sustained release (Depofaom)	antimetabolites that are similar to normal substances in the cell (when they are incorporated into the cellular metabolism, the cells are unable to divide[16])
Doxil	doxorubicin (anthracycline)	PEGylated liposomal doxorubicin hydrochloride	prevention of DNA replication, inhibition of protein synthesis, and conjugate improves drug penetration into tumors and decreases drug clearance[17]
Myocet	doxorubicin (anthracycline)	doxorubicin–hydrochlorid packed in liposomes	prevention of DNA replication, inhibition of protein synthesis, and conjugate decreases side effects[18]
Oncaspar Pegaspargase	L-asparaginase	PEG conjugated with L-asparginase	L-asparagine depletion blocks protein synthesis and cell proliferation[12,19]
Oncaspar Calaspargase Pegol	L-asparaginase	*E. coli*-derived L-asparagine II conjugated with succinimidyl carbonate monoethylene glycol	antineoplastic activity, L-asparagine depletion blocks protein synthesis and cell proliferation[12,19]

during tumor growth to maintain the supply of nutrients and oxygen. In the presence of NO-scavengers the extravasation is significantly inhibited. CO is involved in many biological functions including vascular regulation, anti-apoptosis, anti-inflammation and angiogenesis. CO is also found to increase vascular permeability, blood flow and augment the EPR-effect. Furthermore, the usage of CO donors can increase the grade of the EPR-effect.[5] Another strategy to enhance the EPR-effect is the elevation of systolic blood pressure via slow angiotensin II infusion.[10] Infusion of angiotensin II, a peptide hormone, leads to a tremendous increase of the blood flow in tumor tissue without increasing blood flow in normal tissue.[11]

In this regard, many macromolecular compounds containing clinically approved small molecular drug linked to biologically relevant enzymes or proteins have been developed to exploit the EPR-effect. In addition, polymer-conjugates can increase the water solubility of those drugs and therefore the effectiveness can also be enhanced. Polymer conjugation alters the bio-distribution of low molecular weight drugs, thus enabling tumor-specific targeting.[12] Examples of EPR-targeting compounds under clinical trials or being clinically approved are presented in Table 1.

In the case of Oncaspar® (Pegaspargase) the active component is the already large enzyme L-asparaginase which causes an L-asparagine depletion that prevents protein synthesis and cell proliferation. The drug was further modified by PEGylation (Calaspargase Pegol) which is an important tool in the development of anti-cancer conjugates. PEGylation has proven to be useful for a variety of reasons:[12]

-increases protein solubility and stability and reduces protein immunogenicity

-prevents the rapid clearance of small proteins

-is non-toxic and non-immunogenic

-increases plasma residence of the drug-conjugate

-can increase the therapeutic index in order to elevate the dose without causing toxicity

-its high degree of hydration provides a water shell to mask the active core

Overall, these commercial examples confirm that designing large conjugates to treat cancers is a suitable strategy.

Nevertheless, researchers disagree about the perfect size (20-200 nm)[3] or weight (25-160 kDa) for an EPR-effective drug. In the year 2000 Maeda stated that the EPR-effect was observed at a molecular weight of 60

kDa, whereas later he stated that accumulation was observed already at a weight of 40 kDa.[1,2,10,20] In 2006 Haag and Kratz observed an EPR-effect at a molecular weight of 20 kDa, but they also stated that the renal clearance occurs at a molecular weight of 30 - 50 kDa.[21] In 2014 Kobayashi estimated a desired size of over 6 nm in diameter, which is approximately the pore size of a glomerulus of the kidney, to avoid excretion.[22] Caliceti and Veronese stated in 2003 that renal clearance can be avoided from a molecular weight of 70 kDa, but molecules that exceed this size can be eliminated from the body by other pathways, such as liver uptake, proteolytic digestion, and clearance by the immune system.[23] However one thing is certain: As molecular size increases, systematic clearance decreases.

To investigate the molecular size dependence of drugs, Jain and coworkers have examined compounds between 25 and 160 kDa in a mice transplanted human colon adenocarcinoma model using intravital fluorescence microscopy technique.[8] The permeability increased by a factor of two from 25 to 160 kDa. The transport of macromolecular compounds appears to occur by diffusion through the porous structure. Experiments with liposomes performed by the same group suggest that the cutoff size of the pores lies between 400 and 600 nm in diameter.[8]

According to these studies, arene ruthenium metalla-assemblies, if they are big enough, could in principle exploit the EPR-effect. For many years, we[24-27] as well as others[28-30] have synthesized numerous tetranuclear, hexanuclear and octanuclear arene ruthenium metalla-assemblies, and the first example of a biologically active system was published in 2008.[31] The complex-in-a-complex system $[(acac)_2Pt\subset Ru_6(p\text{-cymene})_6(tpt)_2(dhbq)_3]^{6+}$ was able to carry platinum acetylacetonate to cancer cells. This supramolecular system possesses several components (Figure 2) and has a molecular weight of approximately 4 kDa. The components are: The arene ligands that can protect and stabilize the ruthenium atom in a 2+ oxidation state;[32] Multidentate anionic spacers that can modulate the size of the cavity;[33] Multidentate N-donor panels that can dictate the shape and geometry of the assembly.[34] All components can therefore be used to increase upon functionalization the molecular weight and size of the arene ruthenium metalla-assemblies, including also the guest molecule.

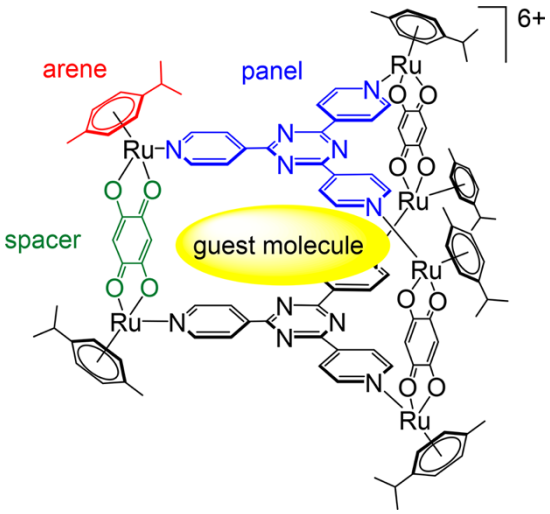

Figure 2. Components of a typical arene ruthenium metalla-assembly.

Indeed, several pyrenyl-functionalized compounds have been used as guest molecules to increase the molecular weight of arene ruthenium metalla-assemblies.[35-36] The pyrenyl group fits perfectly in the cavity of the metalla-assemblies, while the remaining part sits outside (Figure 3). The hydrophobicity of pyrene coupled to the ideal shape of the cavity allows

the formation of highly stable host-guest systems. As illustrated in Figure 3, when a large pyrenyl-functionalized guest is used, the arene ruthenium metalla-assembly provides a cationic and hydrophilic head to the system. The largest host-guest system obtained so far has a combined (host-guest) molecular weight of 5.5 kDa.[37]

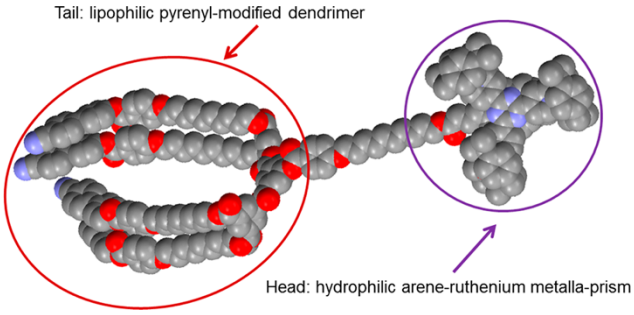

Figure 3. Pyrenyl-functionalized dendrimer encapsulated in an arene ruthenium metalla-prism.

Until now, our efforts to increase the molecular weight of arene ruthenium metalla-assemblies have mainly focused on the guest molecules. We want now to explore other possibilities such as the arenes, the panels and the spacers. Herein, as a proof of concept, we present our preliminary study dealing with functionalized spacers, in which alkyl chains of different lengths were attached.

Results and Discussion

To increase the molecular weight of arene ruthenium metalla-assemblies, we have first focused our attention to the insertion of alkyl chains to the spacer-components. Two types of spacers were chosen, dialkyloxalamide and 2,5-dihydroxy-3-alkyl-2,5-diene-1,4-dione (Figure 4). Synthetic strategies to prepare such compounds are already available in the literature. The dihexyloxalamide (H_2L^a) and dioctyloxalamide (H_2L^b) were obtained following the strategy developed by Lu and Facchetti,[38] while the 2,5-dihydroxy-3-icosyl-2,5-diene-1,4-dione (H_2L^c) was prepared according to the method developed by Huang and Hu,[39] by replacing a $C_{11}H_{23}$ alkyl chain with a $C_{20}H_{41}$ chain (see exp. part). All compounds show the expected spectroscopic data, and were used without further purification to synthesize the corresponding dinuclear arene ruthenium clip.

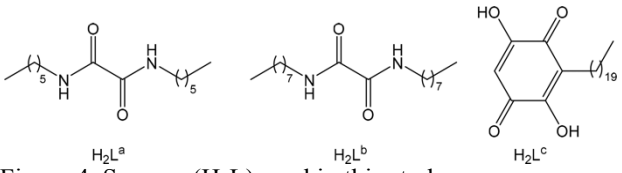

Figure 4. Spacers (H_2L) used in this study.

The dinuclear arene ruthenium metalla-clips **1a** and **1b** are obtained in moderate yield by reacting first the alkyloxalamide (H_2L^a, H_2L^b) with two equivalents of *N,N*-diisopropylethylamine (DIPEA), followed by the addition of $[(\eta^6\text{-}p\text{-cymene})_2Ru_2(\mu_2\text{-}Cl)_2Cl_2]$. The metalla-clip **1c** is prepared in good yield in a similar fashion, using $NaCOOCH_3$ as the base. All dinuclear complexes show in their ^1H NMR spectrum diastereotopic protons due to the coordination of the arene ruthenium units to the spacers; the ruthenium atoms being chiral-at-the-metal in these complexes.

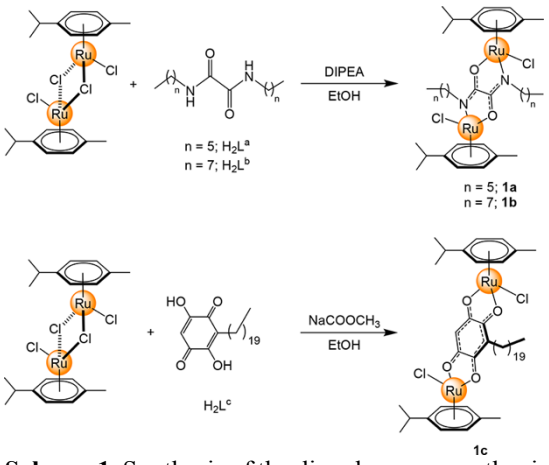

Scheme 1. Synthesis of the dinuclear arene ruthenium clips (**1a-1c**).

Once the dinuclear clips have been prepared and purified, the synthesis of the larger metalla-assemblies was performed. A series of metalla-prisms was obtained by reacting the dinuclear clips (**1**) with silver triflate, followed by addition of 2,4,6-tri(pyridin-4-yl)-1,3,5-triazine (4-tpt). These metalla-prisms are isolated in good yields as dark green (**2a** and **2b**) or dark red (**2c**) solids (Figure 5). They are non-hygroscopic and stable in solution (DMSO, CH_2Cl_2, $CHCl_3$, CH_3CN) for several days.

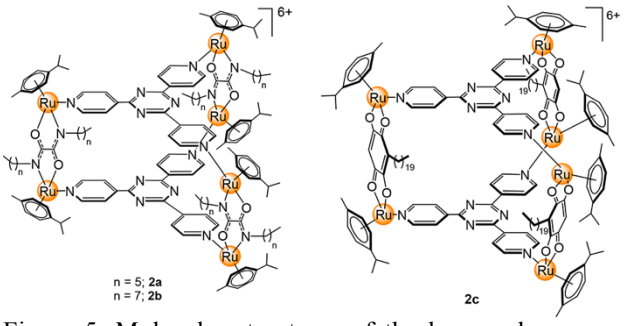

Figure 5. Molecular structures of the hexanuclear arene ruthenium metalla-prisms (**2a**-**2c**).

The molecular structure of the metalla-prisms was confirmed by a combination of NMR spectroscopy and mass spectrometry. Upon formation of the metalla-prisms, the ^{1}H NMR signals assigned to the metalla-clips are slightly shifted and become broad, while new signals associated to the 4-tpt panels appear (Figure 6). These observations are consistent with the formation of the metalla-prisms **2a**-**2c**, in which the alkyl chains are either pointing away or towards the cavity and the components of the assemblies, thus generating large and broad signals.[40] Moreover, the nature of the metalla-clips (**1a**-**1c**) generates two isomers for each metalla-prism,[41] in which the orientation of the μ_4-L spacers are either all the same or mixed.

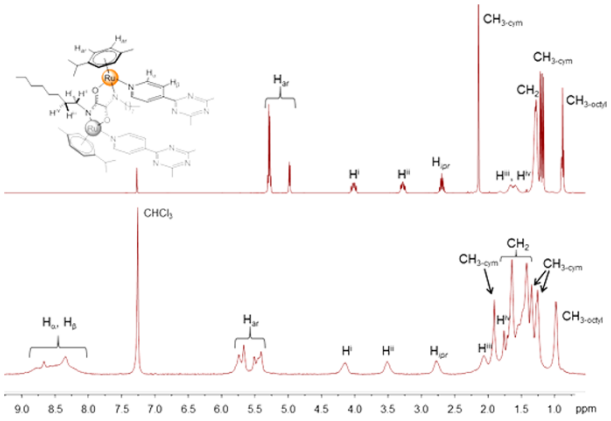

Figure 6. ^{1}H NMR spectra of **1b** (top) and **2b** (bottom).

The ESI mass spectra of the metalla-prisms show characteristic dicationic ($[\mathbf{2} - 2\ CF_3SO_3^-]^{2+}$) and tricationic ($[\mathbf{2} - 3\ CF_3SO_3^-]^{3+}$) peaks, corresponding to the intact metalla-prism plus four triflate and three triflate anions respectively (Figure 7). Moreover, the dinuclear arene ruthenium clips show a single parent mass peak corresponding to $[\mathbf{1} - Cl]^+$; a peak not observed in the mass spectra of the metalla-prims. However, fragments corresponding to $[(p\text{-cymene})_2Ru_2(\mu_4\text{-L})]^{2+}$ and $[(p\text{-cymene})_2Ru_2(\mu_4\text{-L}) + CF_3SO_3]^+$ are observed in the mass spectra of **2** and confirmed the presence of the metalla-clips in the metalla-prisms. To illustrate this behavior, the mass spectra of **1b** and **2b** are presented in Figure 7.

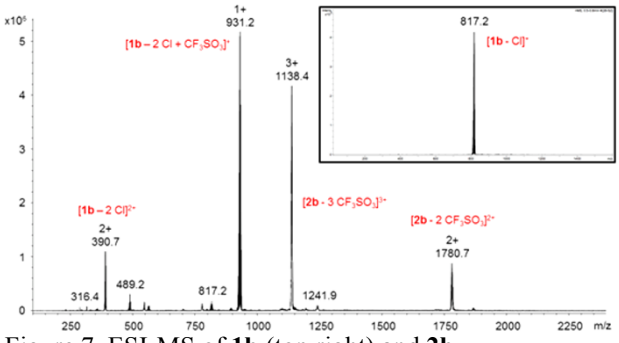

Figure 7. ESI-MS of **1b** (top right) and **2b**.

Thus far in this project three prisms were synthesized. The molecular weight of the prisms amounts 3692.6 g·mol^{-1} (**2a**), 3864.8 g·mol^{-1} (**2b**) and 4191.0 g·mol^{-1} (**2c**), still remaining relatively small to fully exploit the EPR-effect. However, by introducing octyl chains on the oxalamide spacer, an additional mass of 589 g·mol^{-1} was added to the metalla-prism **2b**, in comparison to a dimethyloxalamide analogue. Unfortunately, attempts to introduce longer alkyl chains to the oxalamide moiety were unsuccessful, generating only insoluble materials. Nevertheless, by simply adding one icosyl chain to a dihydroxy benzoquinone spacer, a mass of nearly 1 kDa was added to the metalla-prism, representing an increase of about 20% when compare to the non-functionalized dihydroxybenzoquinone metalla-prism (Figure 2).

As demonstrated here, insertion of alkyl chains to organic spacers remains easy synthetically but reduces the solubility of the compounds. Therefore, to facilitate solubility whilst still increasing the molecular weight of the metalla-assemblies, we are now shifting our attention to pegylated chains, and instead of dealing with mono-functionalized hydroxybenzoquinone spacers, we are preparing bis-functionalized derivatives.[42]

Conclusion

The EPR-effect represents an important discovery which occurs in most solid cancers. This phenomenon is based on the cellular structure of solid cancers and on a defective lymphatic drainage. Macromolecular compounds can be administered in order to accumulate on tumor sites and to operate locally via the EPR-effect. However to date, no ruthenium containing drugs are known to operate via the EPR-effect, and studies have showed that the EPR-effect is questionable when dealing with humans.[3]

Therefore, if reaching an EPR-effect is no more a goal, these functionalized arene ruthenium metalla-assemblies can still found other applications, such as drug delivery vectors. Indeed, the use of metalla-cages as drug delivery vectors and as anticancer agents is becoming a new field of research, showing great promises.[43-45] Then, like in arene ruthenium metalla-assemblies, the introduction of tumor targeting agents at the periphery of the metalla-assembly can in principle increase the selectivity and efficacy of these abiological systems.[46]

For these reasons, we want in the future to use similar synthetic strategies to functionalize as well the arenes and the panels, not only the spacers and the guest molecules. We also want to use other metals (iridium or osmium) and introduce specific functional-groups (targeting agents, hydrophilic or hydrophobic groups, peptidic chains, etc…) to fine tune the biological activity, and to ultimately, generate metalla-assemblies with higher and better therapeutic properties (Figure 8).

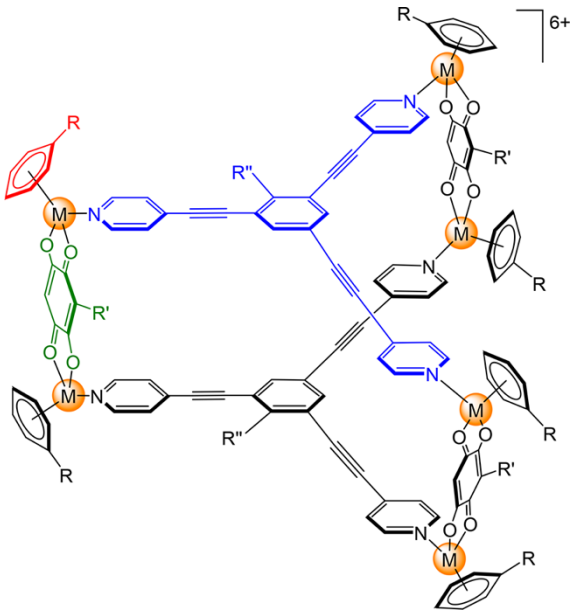

Figure 8. Highly functionalized metalla-assemblies.

ASSOCIATED CONTENT

Experimental Part

Materials and Methods: All solvents were dried before use according to standard procedures, and all reactions were performed under an inert atmosphere. All other reagents were commercially available and used as received. NMR spectra were recorded with a Bruker Avance II 400 spectrometer. UV/VIS absorption spectra were recorded with a Perkin–Elmer UV/Vis spectrophotometer. Infrared spectra were recorded with a Nicolet iS5 from Thermo scientific spectrometer. Electrospray mass spectra were obtained in positive or negative mode with a LCQ Finnigan mass spectrometer. Microanalyses were carried out by the Mikroelementaranalytisches Laboratorium, ETH Zürich (Switzerland). The ruthenium precursor [(η^6-*p*-cymene)$_2$Ru$_2$(μ_2-Cl)$_2$Cl$_2$],[47] the spacers dihexyloxalamide (H_2L^a)[38] and dioctyloxalamide (H_2L^b)[38] and the panel ligand 2,4,6-tri(pyridin-4-yl)-1,3,5-triazine[48] were prepared according to published methods.

Synthesis of 3-Icosyl-1,2,4,5-tetramethoxybenzene

1,2,3,4-Tetramethoxybenzene, (430 mg, 2.20 mol, 1.0 eq) was dissolved in THF (10 mL) and the solution was cooled to -10 °C. The flask was flushed with N_2 and *n*-BuLi (2.5 M in hexane, 1 mL, 2.42 mmol, 1.1 eq) was slowly added under a N_2 atmosphere. The mixture was stirred at -10 °C for 30 min and 1-bromo-icosane (904 mg, 2.42 mmol, 1.1 eq) was slowly added. The mixture was stirred at -10 °C for 10 min and then allowed to warm to RT overnight. After completion of the reaction aqueous saturated NH_4Cl (2 mL) was added to the solution and the mixture was extracted with Et_2O (3 x 50 mL), washed with brine (1 x 50 mL), dried over $MgSO_4$ and concentrated under reduced pressure. The crude product was purified by flash column chromatography (SiO_2, pentane/EtOAc 40:1) to yield the desired product as a colorless solid. (710 mg, 68%). **^{1}H-NMR** ($CDCl_3$, 400 MHz) δ/ppm: 6.41 (s, 1H, C*H*), 3.84 (s, 6H, OC*H*$_3$), 3.76 (s, 6H, OC*H*$_3$), 2.62-2.59 (m, 2H, C*H*$_2$), 1.56-1.49 (m, 2H, C*H*$_2$), 1.37-1.35 (m, 2H, C*H*$_2$), 1.25 (s, 32H, C*H*$_2$), 0.88 (t, $^3J_{HH}$ = 6.2 Hz, 3H, C*H*$_3$). **^{13}C-NMR** ($CDCl_3$, 101 MHz) δ/ppm: 149.0 (2C, CH_3OC), 141.3 (2C, CH_3OC), 131.3 (1C, $CC_{20}H_{41}$), 96.9 (1C, *C*H), 61.1 (2C, O*C*H$_3$), 56.4 (2C, O*C*H$_3$), 32.1 (1C, *C*H$_2$), 30.9 (1C, *C*H$_2$), 30.2 (1C, *C*H$_2$), 29.9 (10C, *C*H$_2$), 29.8 (1C, *C*H$_2$), 29.7 (1C, *C*H$_2$), 29.6 (1C, *C*H$_2$), 29.5 (1C, *C*H$_2$), 24.8 (1C, *C*H$_2$), 22.8 (1C, *C*H$_2$), 14.3 (1C, *C*H$_3$). **IR** (cm^{-1}): 2957 (w), 2916 (m), 2849 (m), 1594 (w), 1467 (m), 1408 (m), 1367 (w), 1343 (w), 1306 (w), 1244 (w), 1203 (w), 1117 (m), 1066 (w), 1044 (m), 1024 (w), 954 (m), 899 (w), 868 (w), 854 (w), 831 (W), 811 (w), 721 (w), 639 (w). **MS** (ESI+, m/*z*): calculated for $C_{30}H_{54}O_4Na$ $[M + Na]^+$ 501.4; found: 501.4 $[M + Na]^+$. **UV-VIS** (1.0 x 10^{-4}, CH_2Cl_2): λ_{max} 229 (ε = 0.7 x 10^3 M^{-1}cm^{-1}), λ_{max} 284 (ε = 1.7 x 10^3 M^{-1}cm^{-1}). **EA:** Anal. calc. for $C_{30}H_{54}O_4$ (478.4) C 75.26; H 11.37; Found: C 75.40; H 11.39.

Synthesis of 3-Icosyl-2,5-dimethoxycyclohexa-2,5-diene-1,4-dione

3-Icosyl-1,2,4,5-tetramethoxybenzene (177 mg, 370 µmol, 1.0 eq) was suspended in MeCN (3 mL) and ceric ammonium nitrate (510 mg, 930 µmol, 2.51 eq) was added and the yellow suspension turned into an orange suspension. The mixture was stirred at RT for 2 h. After

completion of the reaction, the mixture was extracted with EtOAc (3 x 15 mL). The combined organic layers were washed with brine (1 x 20 mL), dried over $MgSO_4$, filtered and concentrated. The crude product was purified by flash column chromatography (SiO_2, pentane/EtOAc 20:1) to yield the desired product as a colorless solid (80.2 mg, 48%). **^{1}H-NMR** ($CDCl_3$, 400 MHz) δ/ppm: 5.72 (s, 1H, C*H*), 4.04 (s, 3H, OC*H*$_3$), 3.80 (s, 3H, OC*H*$_3$), 2.42 (t, $^3J_{HH}$ = 7.5 Hz, 2H, C*H*$_2$), 1.41-1.35 (m, 2H, C*H*$_2$), 1.25 (s, 34 H, C*H*$_2$), 0.88 (t, $^3J_{HH}$ = 6.6 Hz, 3H, C*H*$_3$). **^{13}C-NMR** ($CDCl_3$, 101 MHz) δ/ppm: 183.7 (1C, *C*O), 182.6 (1C, *C*O), 158.9 (1C, CH_3O*C*), 156.0 (1C, CH_3O*C*), 130.9 (1C, *C*$C_{20}H_{41}$), 105.5 (1C, *C*H), 61.5 (1C, O*C*H$_3$), 56.5 (1C, O*C*H$_3$), 32.1 (1C, *C*H$_2$), 29.8 (8C, *C*H$_2$), 29.75 (4C, *C*H$_2$), 29.68 (1C, *C*H$_2$), 29.55 (1C, *C*H$_2$), 29.51 (1C, *C*H$_2$), 28.82 (1C, *C*H$_2$), 23.2 (1C, *C*H$_2$), 22.8 (1C, *C*H$_2$), 14.3 (1C, *C*H$_3$). **IR** (cm^{-1}): 2916 (m), 2849 (m), 1649 (w), 1597 (w), 1467 (w), 1324 (w), 1206 (w), 1154 (w), 1046 (w), 928 (w), 835 (w), 797 (w), 720 (w), 500 (w), 483 (w), 469 (w), 401 (w), 453 (w), 433 (w), 429 (w). **MS** (ESI+, m/*z*): calculated for $C_{28}H_{48}O_4Na$ $[M + Na]^+$ 471.4; found: 471.3 $[M + Na]^+$. **UV-VIS** (1.0 x 10^{-4}, CH_2Cl_2): λ_{max} 286 (ε = 8.2 x 10^3 M^{-1}cm^{-1}). **EA:** Anal. calc. for $C_{28}H_{48}O_4$ (448.4) C 74.95; H 10.78; Found: C 75.21; H 10.85.

Synthesis of 2,5-dihydroxy-3-icosylcyclohexa-2,5-diene-1,4-dione (H_2L^c)

3-Icosyl-2,5-dimethoxycyclohexa-2,5-diene-1,4-dione (116 mg, 259 μmol, 1.0 eq) and EtOH (10 mL) was mixed to give an orange suspension. NaOH (2 M, 5 mL) was added and the suspension turned into a violet solution. The solution was heated to 70 °C and stirred until TLC showed full conversion of the starting material. The reaction was allowed to cool to RT and HCl (2 M, 25 mL) was added, and the solution turned into an orange suspension. The mixture was extracted with EtOAc (3 x 30 mL). The combined organic layers were dried over $MgSO_4$, filtered, concentrated and dried under high vacuum to yield the desired product as a brown solid which was used without further purification (73 mg, 72%). **^{1}H-NMR** ($SO(CD_3)_2$, 400 MHz) δ/ppm: 11.17 (s, 2H, O*H*), 5.77 (s, 1H, C*H*), 2.27 (t, $^3J_{HH}$ = 7.5 Hz, 2H, C*H*$_2$), 1.34 (m, 2H, C*H*$_2$), 1.22 (m, 34H, C*H*$_2$), 0.84 (t, $^3J_{HH}$ = 6.6 Hz, 3H, C*H*$_3$). **IR** (cm^{-1}): 3304 (m), 2917 (m), 2847 (m), 1612 (m), 1462 (w), 1325 (m), 1187 (m), 860 (w), 768 (w), 708 (w). **MS** (ESI-, m/*z*): calculated for $C_{26}H_{43}O_4$ $[M - H]^-$ 419.3; found: 419.3 $[M - H]^-$. **UV-VIS** (1.0 x 10^{-4}, CH_2Cl_2): λ_{max} 282 (ε = 1.4 x 10^4 M^{-1}cm^{-1}), λ_{max} 290 (ε = 1.4 x 10^4 M^{-1}cm^{-1}).

Synthesis of Metalla-Clip [(η^6-p-Cymene)$_2$Ru$_2$(μ_4-L^a)Cl$_2$] (1a)

Dihexyloxalamide (H_2L^a) (200 mg, 780 μmol, 1.0 eq) was suspended in EtOH (15 mL) and DIPEA (0.3 mL, 1.73 mmol, 2.2 eq) was added dropwise at RT. The mixture was heated to 50 °C until the solid was dissolved, and the solution stirred at that temperature for 30 min. The dinuclear complex [(η^6-*p*-cymene)$_2$Ru$_2$(μ_2-Cl)$_2$Cl$_2$] (500 mg, 0.816 mmol, 1.05 eq) was added and the mixture was heated at 80 °C overnight. The mixture was allowed to cool to RT and was filtered and washed with EtOH, acetone, H_2O, Et_2O and pentane then dissolved in CH_2Cl_2, before being filtered over celite and concentrated to yield the desired product as an orange solid (156 mg, 25%). **^{1}H-NMR** ($CDCl_3$, 400 MHz) δ/ppm: 5.31-5.26 (m, 6H, C*H*), 4.99 (d, $^3J_{HH}$ = 5.9 Hz, 2H, C*H*), 4.06-3.99 (m, 2H, C*H*H), 3.32-3.26 (m, 2H, C*H*H), 2.69 (sept, $^3J_{HH}$ = 6.9 Hz, 2H, C*H*), 2.15 (s, 6H, C*H*$_3$), 1.71-1.56 (m, 4H, C*H*$_2$), 1.38-1.27 (m, 12H, C*H*$_2$), 1.22 (d, $^3J_{HH}$ = 6.9 Hz, 6H, C*H*$_3$), 1.18 (d, $^3J_{HH}$ = 6.9 Hz, 6H, C*H*$_3$), 0.92-0.87 (m, 6H, C*H*$_3$). **^{13}C-NMR**

($CDCl_3$, 101 MHz) δ/ppm: 170.2 (2C, *C*O), 100.7 (2C, *C*CH(CH_3)$_2$), 94.4 (2C, *C*CH_3), 82.6 (2C, *C*H), 81.2 (2C, *C*H), 79.8 (2C, *C*H), 79.6 (2C, *C*H), 51.7 (2C, H*C*(CH_3)$_2$), 31.9 (2C, *C*H_2), 30.9 (2C, *C*H_2), 29.4 (2C, *C*H_2), 27.6 (2C, *C*H_2), 22.9 (2C, *C*H_2), 22.6 (2C, HC(*C*H_3)$_2$), 22.2 (2C, HC(*C*H_3)$_2$), 18.6 (2C, *C*H_3), 14.3 (2C, *C*H_3). **IR** (cm^{-1}): 2923 (w), 1596 (s), 1458 (w), 1333 (m), 1051 (w), 872 (w), 532 (w), 524 (w), 511 (w), 501 (w), 494 (w), 485 (w), 475 (w), 467 (w), 458 (w), 450 (w), 441 (w), 433 (w). **MS** (ESI+, m/*z*): calculated for $C_{34}H_{54}ClN_2O_2Ru_2$ $[M - Cl]^+$ 761.2; found: 761.1 $[M - Cl]^+$. **UV-VIS** (1.0 x 10^{-5}, CH_2Cl_2): λ_{max} 231 (ε = 2.1 x 10^5 $M^{-1}cm^{-1}$). **EA:** Anal. calc. for $C_{34}H_{54}$ $Cl_2N_2O_2Ru_2$ (795.9) C 51.31; H 6.84; N 3.52; Found: C 51.32; H 6.85; N 3.72.

Synthesis of Metalla-Clip [(η^6-p-Cymene)$_2$Ru$_2$(μ_4-L^b)Cl$_2$] (1b)

Dioctyloxalamide (H_2L^b) (500 mg, 1.60 mmol, 1.0 eq) was suspended in EtOH (30 mL) and DIPEA (0.6 mL, 3.44 mmol, 2.1 eq) was added slowly and stirred at RT for 30 min. The dinuclear complex [(η^6-*p*-cymene)$_2$Ru$_2$(μ_2-Cl)$_2$Cl$_2$] (1.03g, 1.68 mmol, 1.05 eq) was added and the mixture was heated at 90 °C overnight. The reaction was allowed to cool to RT and the volume was reduced to its half and the mixture was stored in the fridge for 1 h. The orange residue was filtered and washed with EtOH, H_2O, acetone, Et_2O and pentane. The residue was dissolved in CH_2Cl_2 and filtered over celite and concentrated to yield the desired product as an orange solid (280 mg, 21%). **^{1}H-NMR** ($CDCl_3$, 400 MHz) δ/ppm: 5.30-5.25 (m, 6H, C*H*), 4.97 (d, $^3J_{HH}$ = 5.8 Hz, 2H, C*H*), 4.04-3.97 (m, 2H, C*H*H), 3.30-3.24 (m, 2H, C*H*H), 2.68 (sept, $^3J_{HH}$ = 6.9 Hz, 2H, C*H*), 2.12 (s, 6H, CH_3), 1.70-1.52 (m, 4H, CH_2), 1.33-1.25 (m, 20H, CH_2), 1.20 (d, $^3J_{HH}$ = 6.8 Hz, 6H, CH_3), 1.16 (d, $^3J_{HH}$ = 6.9 Hz, 6H, CH_3) 0.89-0.86 (m, 6H, CH_3). **^{13}C-NMR** ($CDCl_3$, 101 MHz) δ/ppm: 170.1 (2C, *C*O), 100.7 (2C, *C*CH(CH_3)$_2$), 94.4 (2C, *C*CH_3), 82.5 (2C, *C*H), 81.2 (2C, *C*H), 79.7 (2C, *C*H), 79.5 (2C, *C*H), 51.7 (2C, H*C*(CH_3)$_2$), 32.1 (2C, *C*H_2), 30.7 (2C, *C*H_2), 29.7 (2C, *C*H_2), 29.5 (2C, *C*H_2), 29.4 (2C, *C*H_2), 27.9 (2C, *C*H_2), 22.8 (2C, *C*H_2), 22.6 (2C, HC(*C*H_3)$_2$, 22.2 (2C, HC(*C*H_3)$_2$), 18.6 (2C, C*H*$_3$), 14.3 (2C, C*H*$_3$). **IR** (cm^{-1}): 3302 (w), 2954 (m), 2914 (m), 2849 (m), 1645 (w), 1604 (s), 1531 (w), 1510 (w), 1466 (w), 1373 (w), 1349 (w), 1324 (m), 1200 (w), 1153 (w), 1080 (w), 1055 (w), 1025 (w), 996 (w), 857 (m), 800 (m), 724 (m), 594 (w), 496 (w), 463 (w), 445 (w), 429 (w). **MS** (ESI+, m/*z*): calculated for $C_{38}H_{62}ClN_2O_2Ru_2$ $[M - Cl]^+$ 817.3; found: 817.2 $[M - Cl]^+$. **UV-VIS** (1.0 x 10^{-4}, CH_2Cl_2): λ_{max} 228 (ε = 2.33 x 10^4 $M^{-1}cm^{-1}$), λ_{max} 313 (ε = 1.6 x 10^4 $M^{-1}cm^{-1}$). **EA**: Anal. calc. for $C_{38}H_{62}N_2O_2Cl_2Ru_2$ (852.2) C 53.57; H 7.33; N 3.29; Found: C 53.61; H 7.48; N 3.24.

Synthesis of Metalla-Clip [(η^6-p-Cymene)$_2$Ru$_2$(μ_4-L^c]Cl$_2$ (1c)

2,5-Dihydroxy-3-icosylcyclohexa-2,5-diene-1,4-dione (H_2L^c) (158 mg, 375 µmol, 1.0 eq) was suspended in EtOH (50 mL) and $NaCOOCH_3$ (64.7 mg, 789 µmol, 2.1 eq) was added. The yellow suspension turned into a red solution. The mixture was allowed to stir for 1 hour at RT and then [(η^6-*p*-cymene)$_2$Ru$_2$(μ_2-Cl)$_2$Cl$_2$] (225 mg, 367 µmol, 0.98 eq) was added and the reaction was heated to 80 °C for 48 h. The reaction was allowed to cool to RT and the volume was reduced to its half and the mixture was stored in the fridge overnight. The

violet precipitate was filtered and washed with cold H_2O to obtain the desired product as a violet solid (267 mg, 77%). **^{1}H-NMR** ($CDCl_3$, 400 MHz) δ/ppm: 5.69 (s, 1H, C*H*), 5.63-5.59 (m, 4H, C*H*), 5.36 (d, $^3J_{HH}$ = 5.8 Hz, 4H, C*H*), 2.90 (sept, $^3J_{HH}$ = 6.9 Hz, 2H, C*H*), 2.36-2.32 (m, 2H, CH_2), 2.91 (s, 6H, CH_3), 1.36-1.33 (m, 12H, (CH_3)$_2$), 1.27-1.26 (m, 36H, CH_2) 0.89-0.86 (m, 3H, CH_3). **^{13}C-NMR** ($CDCl_3$, 101 MHz) δ/ppm: 184.4 (2C, *C*O), 181.8 (2C, *C*O), 115.5 (1C, *C*$C_{20}H_{41}$), 100.7 (1C, *C*H), 100.6 (2C, *C*CH(CH_3)$_2$), 96.4 (2C, *C*CH_3), 82.0 (1C, *C*H), 81.4 (1C, *C*H), 79.7 (1C, *C*H), 79.1 (1C, *C*H), 32.1 (1C, *C*H_2), 31.5 (1C, *C*H_2), 30.0 (1C, *C*H_2), 30.0 (2C, *C*H_2), 29.9 (2C, *C*H), 29.9 (2C, *C*H_2), 29.9 (2C, *C*H_2), 29.9 (4C, *C*H_2), 29.8 (1C, *C*H_2), 29.7 (1C, *C*H_2), 29.5 (1C, *C*H_2), 28.3 (1C, *C*H_2), 22.8 (1C, *C*H_2), 22.7 (2C, (*C*H_3)$_2$), 18.7 (1C, *C*H_3), 14.3 (1C, *C*H_3). **IR** (cm^{-1}): 2918 (m), 2849 (m), 1509 (s), 1495 (s), 1469 (m), 1363 (s), 1315 (w), 1236 (w), 1225 (w), 1165 (w), 1086 (w), 1030 (w), 874 (w), 834 (w), 805 (w), 788 (w), 722 (w), 502 (w), 487 (w), 464 (w), 453 (w), 449 (w), 445 (w), 433 (w), 430 (w). **MS** (ESI+, m/*z*): calculated for $C_{46}H_{70}ClO_4Ru_2$ $[M - Cl]^+$ 925.3; found: 925.3 $[M - Cl]^+$. **UV-VIS** (1.0×10^{-5}, CH_2Cl_2): λ_{max} 228 ($\varepsilon = 3.7 \times 10^4$ $M^{-1}cm^{-1}$), λ_{max} 317 ($\varepsilon = 1.5 \times 10^4$ $M^{-1}cm^{-1}$), λ_{max} 500 ($\varepsilon = 2.0 \times 10^4$ $M^{-1}cm^{-1}$). **EA:** Anal. calc. for $C_{46}H_{70}O_4Cl_{12}Ru_2$ (960.3) C 57.55; H 7.35; N 0.00: Found: C 58.08; H 7.56; N 0.01.

Syntheses of Metalla-Prism [(η^6-p-cymene)$_6$Ru$_6$(μ_4-L^a)$_3$(μ_3-4-tpt)$_2$][CF$_3$SO$_3$]$_6$ (2a)

Metalla-clip [(η^6-*p*-cymene)$_2$Ru$_2$(μ_4-L^a)Cl$_2$] (**1a**) (100 mg, 128 μmol, 1.0 eq) was dissolved in MeOH (20 mL) and $AgCF_3SO_3$ (64.0 mg, 249 μmol, 1.95 eq) was added. The mixture was stirred at RT for 3 h. AgCl was filtered off and 4-tpt (44.0 mg, 141 μmol, 1.1 eq) was added to the solution and the mixture was heated at 60 °C for 24 h. The reaction was allowed to cool to RT and the solvent was removed under reduced pressure. CH_2Cl_2 (2 mL) and pentane (100 mL) was added to induce precipitation. The dark green precipitate was filtered and washed with cold EtOH (3 x 20 mL) to yield the desired product as a dark green solid. (152 mg, 96%). **^{1}H-NMR** ($CDCl_3$, 400 MHz) δ/ppm: 8.99-8.20 (m, 24H, C*H*), 5.83-5.69 (m, 12H, C*H*), 5.56-5.44 (m, 12H, C*H*), 4.20-4.13 (m, 6H, CH_2), 3.62-3.55 (m, 6H, CH_2), 2.86-2.75 (m, 6H, CH_2), 2.14-2.07 (m, 6H, CH_2), 1.96 (s, 18H, CH_3), 1.82-1.66 (m, 22H, CH_2), 1.61-1.52 (m, 20H, CH_2), 1.40-1.37 (m, 18H, CH_3), 1.32-1.26 (m, 18H, CH_3), 1.07-1.03 (m, 18H, CH_3). **IR** (cm^{-1}): 2928 (w), 1596 (s), 1516 (s), 1371 (m), 1257 (s), 1222 (m), 1149 (m), 1056 (w), 1028 (s), 811 (m), 670 (w), 636 (s), 496 (w), 480 (w), 445 (w). **MS** (ESI+, m/*z*): calculated for $C_{141}H_{186}F_9N_{18}O_{15}Ru_6S_3$ $[M - 3\ CF_3SO_3]^{3+}$ 1083.3; found: 1082.4 $[M - 3\ CF_3SO_3]^{3+}$; calculated for $C_{142}H_{186}F_{12}N_{18}O_{18}Ru_6S_4$ $[M - 2\ CF_3SO_3]^{2+}$ 1699.4; found: 1697.3 $[M - 2\ CF_3SO_3]^{2+}$. **UV-VIS** (1.0×10^{-5}, CH_2Cl_2): λ_{max} 249 ($\varepsilon = 1.73 \times 10^5$ $M^{-1}cm^{-1}$). **EA:** Anal. calc. for $C_{144}H_{186}F_{18}N_{18}O_{24}Ru_6S_6$ (3692.6) C 46.82; H 5.08; N 6.83; Found: C 46.71; H 5.12; N 7.30.

Syntheses of Metalla-Prism [(η^6-p-cymene)$_6$Ru$_6$(μ_4-L^b)$_3$(μ_3-4-tpt)$_2$][CF$_3$SO$_3$]$_6$ (2b)

Metalla-clip [(*p*-cymene)$_2$Ru$_2$(μ_4-L^b)Cl$_2$] (**1b**) (150 mg, 176 μmol, 1.0 eq) was dissolved in MeOH (20 mL) and $AgCF_3SO_3$ (88.1 mg, 343 μmol, 1.95 eq) was added. The mixture was stirred at RT for 3 h. The AgCl was filtered off and 4-tpt (60.4 mg, 194 μmol, 1.1 eq) was added to the mixture and the solution heated at 60 °C for 24 h. The reaction was allowed to cool to RT and MeOH was removed. CH_2Cl_2 (2 mL) was added and pentane (100 mL) was added to induce precipitation. The dark green-black precipitation was filtered and washed with

EtOH (3 x 20 mL) to yield the desired product (129 mg, 60%). **^{1}H-NMR** ($CDCl_3$, 400 MHz) δ/ppm: 8.78-8.21 (m, 24H, C*H*), 5.77-5.65 (m, 12H, C*H*), 5.51-5.39 (m, 12H, C*H*), 4.26-4.07 (m, 6H, CH_2), 3.60-3.42 (m, 6H, CH_2), 2.85-2.69 (m, 6H, CH_2), 2.13-2.00 (m, 8H, CH_2), 1.96-1.86 (m, 18H, CH_3), 1.79-1.74 (m, 4H, CH_2), 1.70-1.60 (m, 30H, CH_2), 1.48-1.34 (m, 44H, CH_2; CH_3), 1.30-1.19 (m, 22H, CH_2; CH_3), 1.06-0.92 (m, 18H, CH_3). **IR** (cm^{-1}): 2926 (w), 1596 (s), 1517 (s), 1466 (w), 1371 (m), 1332 (w), 1257 (s), 1222 (m), 1149 (m), 1056 (w), 1028 (s), 871 (w), 811 (m), 753 (w), 670 (w), 658 (w), 635 (s), 572 (w), 487 (w), 467 (w), 439 (w). **MS** (ESI+, m/*z*): calculated for $C_{153}H_{210}F_9N_{18}O_{15}Ru_6S_3$ [M - 3 CF_3SO_3]$^{3+}$ 1139.3; found: 1138.4 [M - 3 CF_3SO_3]$^{3+}$; calculated for $C_{154}H_{210}F_{12}N_{18}O_{18}Ru_6S_4$ [M - 2 CF_3SO_3]$^{2+}$ 1782.5; found: 1780.7 [M - 2 CF_3SO_3]$^{2+}$. **UV-VIS** (1.0 x 10^{-5}, CH_2Cl_2): λ_{max} 251 (ε = 1.33 x 10^5 $M^{-1}cm^{-1}$). **EA**: Anal. calc. for $C_{156}H_{210}F_{18}F_{18}O_{24}Ru_6S_6$ (3864.8) C 48.51; H 5.48; N 6.53; Found: C 48.31; H 5.42; N 7.76.

Synthesis of Metalla-Prism [(η^6-p-cymene)$_6$Ru$_6$(μ_4-L^c)$_3$(μ_3-4-tpt)$_2$][CF_3SO_3]$_6$ (2c)

Metalla-clip [(η^6-*p*-cymene)$_2$Ru$_2$(μ_4-L^c]Cl_2 (**1c**) (50.0 mg, 52.0 μmol, 1.0 eq) was suspended in MeOH (20 mL), and $AgCF_3SO_3$ (26.7 mg, 104 μmol, 2.0 eq) was added. The solution turned red, and a white suspension was observed after 1 h. The reaction was stirred for an additional 3 hours at RT before filtering the suspension (AgCl). Then, to the red solution, 4-tpt (10.7 mg, 34.3 μmol, 0.66 eq) was added and the mixture was heated to 60 °C. The reaction was stirred for 30 h until the ^{1}H-NMR showed full conversion of the starting material. The reaction was allowed to cool to RT and the solvent was removed under reduced pressure and the crude product was dried overnight. CH_2Cl_2 (1 mL) was added to dissolve the solid and pentane (50 mL) was added to induce precipitation. The dark red solid was filtered and dried under vacuum (56.7 mg, 60%).**^{1}H-NMR** ($CDCl_3$, 400 MHz) δ/ppm: 8.75 (s, 12 H, C*H*), 8.49 (s, 12H, C*H*), 5.88-5.68 (m, 35 H, C*H*), 2.85 (m, 6H, C*H*), 2.28-2.17 (m, 36H, CH_3)$_2$), 1.37-1.27 (132H, CH_2; CH_3), 0.88 (m, 9H, CH_3). **^{13}C-NMR** ($CDCl_3$, 101 MHz) δ/ppm: 184.1 (6C, *C*O), 181.7 (6C, *C*O), 169.7, (6C, N*C*N), 154.2 (6C, C*C*C), 144.3 (12C, N*C*C), 125.6 (12C, C*C*C), 122.4 (3C, *C*C$_{20}$H$_{41}$), 119.2 (3C, *C*H), 104.4 (12C, *C*H), 99.1 (12C, *C*H), 84.1 (6C, *C*CH(CH$_3$)$_2$), 82.4 (6C, *C*CH$_3$), 32.1 (1C, *C*H$_2$), 31.5 (1C, *C*H$_2$), 30.2 (1C, *C*H$_2$), 30.1 (1C, *C*H), 30.1 (1C, *C*H$_2$), 30.0 (1C, *C*H$_2$), 30.0 (2C, *C*H$_2$), 29.9 (2C, *C*H$_2$), 29.8 (4C, *C*H$_2$), 29.5 (2C, *C*H$_2$), 22.8 (2C, (*C*H$_3$)$_2$), 22.9 (1C, *C*H$_2$), 22.5 (1C, *C*H$_2$), 22.4 (1C, *C*H$_2$), 18.2 (1C, *C*H$_3$), 14.3 (1C, *C*H$_3$). **IR** (cm^{-1}): 2924 (w), 2852 (w), 1575 (w), 1514 (m), 1367 (m), 1278 (m), 1243 (m), 1224 (m), 1156 (m), 1058 (w), 1027 (m), 870 (w), 810 (w), 800 (w), 759 (w), 671 (w), 667 (w), 635 (w), 487 (w), 472 (w), 464 (w), 453 (w). **UV-VIS** (1.0 x 10^{-5}, CH_2Cl_2): λ_{max} 245 (ε = 7.8 x 10^4 $M^{-1}cm^{-1}$), λ_{max} 304 (ε = 4.3 x 10^4 $M^{-1}cm^{-1}$), λ_{max} 494 (ε = 2.8 x 10^4 $M^{-1}cm^{-1}$). **MS** (ESI+, m/*z*): calculated for $C_{177}H_{234}F_9N_{12}O_{21}Ru_6S_3$ [M - 3 CF_3SO_3]$^{3+}$ 1246.7; found: 1246.7 [M - 3 CF_3SO_3]$^{3+}$; calculated for $C_{178}H_{234}F_{12}N_{12}O_{24}Ru_6S_4$ [M - 2 CF_3SO_3]$^{2+}$ 1944.5; found: 1945.1 [M - 2 CF_3SO_3]$^{2+}$. **EA:** Anal. calc. for $C_{180}H_{236}F_{18}N_{18}O_{30}Ru_6S_6$·[3 CH_2Cl_2] (4191.0 + 254.78) C 49.49; H 5.45; N 3.78; Found: C 49.50; H 5.88; N 3.39.

AUTHOR INFORMATION

Corresponding Author

bruno.therrien@unine.ch

Present Addresses

Institut de Chimie, Université de Neuchâtel, Avenue de Bellevaux 51, 2000 Neuchâtel, Switzerland.

ABBREVIATIONS

EPR-effect = enhanced permeability and retention effect, 4-tpt = 2,4,6-tri(pyridin-4-yl)-1,3,5-triazine, MeCN = acetonitrile, DCM = dichloromethane, THF = tetrahydrofuran, MeOH = methanol, EtOH = ethanol, DIPEA = diisopropylethylamine, RT = room temperature.

REFERENCES

(1) Maeda, H.; Wu, J.; Sawa, T.; Matsumura, Y.; Hori, K. Tumor vascular permeability and the EPR effect in macromolecular therapeutics: a review. *J. Control. Release* **2000**, *65*, 271-284.

(2) Maeda, H.; Tsukigawa, K.; Fang, J. A Retrospective 30 Years After Discovery of the Enhanced Permeability and Retention Effect of Solid Tumors: Next-Generation Chemotherapeutics and Photodynamic Therapy-Problems, Solutions, and Prospects. *Microcirculation* **2016**, *23*, 173-182.

(3) Danhier, F. To exploit the tumor microenvironment: Since the EPF effect fails in the clinic, what is the future of nanomedicine? *J. Control. Rel.* **2016**, *244*, 108-121.

(4) Nasu, R.; Kimura, H.; Akagi, K.; Murata, T.; Tanaka, Y. Blood flow influences vascular growth during tumour angiogenesis. *Br. J. Cancer* **1999**, *79*, 780-786.

(5) Yin, H.; Liao, L.; Jun, F. Enhanced Permeability and Retention (EPR) Effect Based Tumor Targeting: The Concept, Application and Prospect. *JSM Clin. Oncol. Res.* **2014**, *2*, 1010.

(6) Freitas, R.A. Nanomedicine; Landes Bioscience: Austin, TX, 1999.

(7) Wang, J.; Lu, Z.; Gao, Y.; Wientjes, M. G.; Au, J. L.-S. Improving delivery and efficacy of nanomedicines in solid tumors: role of tumor priming. *Nanomed*. **2011**, *6*, 1605-1620.

(8) Yuan, F.; Dellian, M.; Fukumura, D.; Leunig, M.; Berk, D.A.; Torchilin, V.P.; Jain, R.K. Vascular permeability in a human tumor xenograft: molecular size dependence and cutoff size. *Cancer Res.* **1995**, *55*, 3752-3756.

(9) Jain, R. K.; Stylianopoulos, T. Delivering nanomedicine to solid tumors. *Nat. Rev. Clin. Oncol.* **2010**, *7*, 653-664.

(10) Fang, J.; Nakamura, H.; Maeda, H. The EPR effect: Unique features of tumor blood vessels for drug delivery, factors involved, and limitations and augmentation of the effect. *Adv. Drug Deliv. Rev.* **2011**, *63*, 136-151.

(11) Suzuki, M.; Hori, K.; Abe, I.; Saito, S.; Sato, H. A New Approach to Cancer Chemotherapy: Selective Enhancement of Tumor Blood Flow With Angiotensin II. *J. Natl. Cancer Inst.* **1981**, *67*, 663-669.

(12) Duncan, R. Polymer conjugates as anticancer nanomedicines. *Nat. Rev. Cancer* **2006**, *6*, 688-701.

(13) Fassas, A.; Anagnostopoulos, A. The use of liposomal daunorubicin (DaunoXome) in acute myeloid leukemia. *Leuk. Lymphoma*, **2005**, *46*, 795-802.

(14) European Medicines Agency: Science Medicines Health. Zusammenfassung des EPAR für die Öffentlichkeit: Abraxane.

http://www.ema.europa.eu/docs/de_DE/document_library/EPAR_-_Summary_for_the_public/human/000778/WC500020431.pdf.

(15) National Cancer Institute: Paclitaxel-loaded polymeric micelle. https://www.cancer.gov/publications/dictionaries/cancer-drug?cdrid=434427.

(16) European Medicines Agency: Science Medicines, Health: Depocyte. http://www.ema.europa.eu/docs/en_GB/document_library/EPAR_-_Scientific_Discussion/human/000317/WC500035646.pdf.

(17) Barenholz, Y. *J. Control. Release*, **2012**, *160*, 117-134.

(18) European Medicines Agency: Science Medicines, Health: Zusammenfassung des EPAR für die Öffentlichkeit: Myocet. http://www.ema.europa.eu/docs/de_DE/document_library/EPAR_-_Summary_for_the_public/human/000297/WC500031806.pdf.

(19) National Cancer Institute: calaspargasse pegol and pegaspargase. https://www.cancer.gov/publications/dictionaries/cancer-drug?search=oncaspar.

(20) Maeda, H.; Bharate, G.Y.; Daruwalla, J. Polymeric drugs for efficient tumor-targeted drug delivery based on EPR-effect. *Eur. J. Pharm. Biopharm.* **2009**, *71*, 409-419.

(21) Haag, R.; Kratz, F. Polymer Therapeutics: Concepts and Applications. *Angew. Chem. Int. Ed.* **2006**, *45*, 1198-1215.

(22) Kobayashi, H.; Watanabe, R.; Choyke, P. L. Improving Conventional Enhanced Permeability and Retention (EPR) Effects; What Is the Appropriate Target? *Theranostics* **2014**, *4*, 81-89.

(23) Caliceti, P.; Veronese, F. M. Pharmacokinetic and biodistribution properties of poly (ethylene glycol)–protein conjugates. *Adv. Drug Deliv. Rev.* **2003**, *55*, 1261-1277.

(24) Therrien, B. Biologically relevant arene ruthenium metalla-assemblies. *CrystEngComm* **2015**, *17*, 484-491.

(25) Therrien, B. Transporting and Shielding Photosensitisers by Using Water-Soluble Organometallic Cages: A New Strategy in Drug Delivery and Photodynamic Therapy. *Chem. Eur. J.* **2013**, *19*, 8378-8386.

(26) Furrer, J.; Therrien, B. The biological side of water-soluble arene ruthenium assemblies. *Adv. Chem.* **2014**, ID 589686.

(27) Yan, H.; Süss-Fink, G.; Neels, A.; Stoeckli-Evans, H. Mono-, di-and tetra-nuclear p-cymeneruthenium complexes containing oxalato ligands. *J. Chem. Soc., Dalton Trans.* **1997**, *22*, 4345-4350.

(28) Singh, A. K.; Pandey, D. S.; Xu, Q.; Braunstein, P.; Recent Advances in Supramolecular and Biological Aspects of Arene Ruthenium(II) Complexes. *Coord. Chem. Rev.* **2014**, *270-271*, 31-56.

(29) Dubey, A.; Jeong, Y. J.; Jo, J. H.; Woo, S.; Kim, D. H.; Kim, H.; Kang, S. C.; Stang, P. J.; Chi, K.-W.

Anticancer Activity and Autophagy Involvement of Self-Assembled Arene-Ruthenium Metallacycles. *Organometallics* **2015**, *34*, 4507-4514.

(30) Mishra, A.; Kang, S.C.; Chi, K.-W. Coordination-Driven Self-Assembly of Arene-Ruthenium Compounds. *Eur. J. Inorg. Chem.* **2013**, 5222-5232.

(31) Therrien, B.; Süss-Fink, G.; Govindaswamy, P.; Renfrew, A.K.; Dyson, P.J. The "Complex-in-a-Complex" Cations $[(acac)_2M\subset Ru_6(p\text{-}i PrC_6H_4Me)_6(tpt)_2(dhbq)_3]^{6+}$: A Trojan Horse for Cancer Cells. *Angew. Chem. Int. Ed.* **2008**, *47*, 3773-3776.

(32) Therrien, B. Functionalised η^6-arene ruthenium complexes. *Coord. Chem. Rev.* **2009**, *253*, 493-519.

(33) Barry, N.P.E.; Furrer, J.; Freudenreich, J.; Süss-Fink, G.; Therrien, B. Designing the Host-Guest Properties of Tetranuclear Arene Ruthenium Metalla-Rectangles to Accommodate a Pyrene Molecule. *Eur. J. Inorg. Chem.* **2010**, *5*, 725-728.

(34) Schmitt, F.; Freudenreich, J.; Barry, N.P.E.; Juillerat-Jeanneret, L.; Süss-Fink, G.; Therrien, B. Organometallic Cages as Vehicles for Intracellular Release of Photosensitizers. *J. Am. Chem. Soc.* **2012**, *134*, 754-757.

(35) Yi, J.W.; Barry, N.P.E.; Furrer, M.A.; Zava, O.; Dyson, P.J.; Therrien, B.; Kim, B.H. Delivery of Floxuridine Derivatives to Cancer Cells by Water-Soluble Organometallic Cages. *Bioconjugate Chem.* **2012**, *23*, 461-471.

(36) Pitto-Barry, A.; Barry, N. P. E.; Zava, O.; Deschenaux, R.; Dyson, P.J.; Therrien, B. Double Targeting of Tumours with Pyrenyl-Modified Dendrimers Encapsulated in an Arene–Ruthenium Metallaprism. *Eur. J. Chem.* **2011**, *17*, 1966-1971.

(37) Pitto-Barry, A.; Barry, N.P.E.; Zava, O.; Deschenaux, R.; Therrien, B. Encapsulation of Pyrene-Functionalized Poly(benzyl ether) Dendrons into a Water-Soluble Organometallic Cage. *Chem. Asian. J.* **2011**, *6*, 1595-1603.

(38) Lu, S.; Drees, M.; Yao, Y.; Boudinet, D.; Yan, H.; Pan, H.; Wang, J.; Li, Y.; Usta, H.; Facchetti, A. 3,6-Dithiophen-2-yl-diketopyrrolo[3,2-*b*]pyrrole (isoDPPT) as an Acceptor Building Block for Organic Opto-Electronics. *Macromolecules* **2013**, *46*, 3895-3906.

(39) Chen, F.; Zhang, G.; Hong, Z.; Lin, Z.; Lei, M.; Huang, M.; Hu, Lu. Design, synthesis, and SAR of embelin analogues as the inhibitors of PAI-1 (plasminogen activator inhibitor-1). *Bioorg. Med. Chem. Lett.* **2014**, *24*, 2379–2382.

(40) Furrer, M.A.; Furrer, J.; Therrien, B. Physical and physicochemical stimuli-responsive arene ruthenium metallaprism. *Organometallics* **2012**, *31*, 3149-3154.

(41) Garci, A.; Dobrov, A.A.; Riedel, T.; Orhan, E.; Dyson, P.J.; Arion, V.B.; Therrien, B. Strategy to Optimize the Biological Activity of Arene Ruthenium Metalla-Assemblies. *Organometallics* **2014**, *33*, 3813-3822.

(42) Garci, A.; Mbakidi, J.-P.; Chaleix, V.; Sol, V.; Orhan, E.; Therrien, B. Tunable Arene Ruthenium Metallaprisms to Transport, Shield, and Release Porphin in Cancer Cells. *Organometallics* **2015**, *34*, 4138-4146.

(43) Lewis, J.E.M.; Gavey, E.L.; Cameron, S.A.; Crowley, J.D. Stimuli-responsive Pd_2L_4 metallosupramolecular cages: towards targeted cisplatin drug delivery *Chem. Sci.* **2012**, *3*, 778-784.

(44) Schmidt, A.; Molano, V.; Hollering, M.; Pöthig, A.; Casini, A.; Kühn, F.E. Evaluation of new palladium

cages as potential delivery systems for the anticancer drug cisplatin *Chem. Eur. J.* **2016**, *22*, 2253-2256.

(45) Zheng, Y.-R.; Suntharalingam, K.; Johnstone, T.C.; Lippard, S. J. Encapsulation of Pt(IV) prodrugs within a Pt(II) cage for drug delivery *Chem. Sci.* **2015**, *6*, 1189-1193.

(46) Stang, P.J. Abiological self-assembly via coordination: Formation of 2D metallacycles and 3D metallacages with well-defined shapes and sizes and their chemistry. *J. Am. Chem. Soc.* **2012**, *134*, 11829-11830.

(47) Bennett, M.A.; Huang, T.N.; Matheson, T.W.; Smith, A.K. (η^6-Hexamethylbenzene)Ruthenium Complexes. *Inorg. Synth.* **1982**, *21*, 74-78.

(48) Anderson, H.L.; Anderson, S.; Sanders, J.K.M. Ligand binding by butadiyne-linked porphyrin dimers, trimers and tetramers. *J. Chem. Soc., Perkin Trans. 1* **1995**, 2231-2246.